Suez Canal University
Faculty of Petroleum & Mining Engineering
Engineering Science Department

# STUDY OF WATER DESALINATION BY SOLAR ENERGY USING MULTI-STAGE FLASH (MSF) PROCESS

A thesis
Submitted in partial fulfillment of the requirements for the Master degree of science in
Thermal and Energy Systems Engineering

BY

## MOHAMED ABDEL WAHAB SHARAF EL-DEAN

Mach. Power Eng. Dept. Arab Academy for Science and Technology, Alex.

SUPERVISORS

PROF. DR. MANSOUR AWAD
MOHAMAD
Energy Department
National Research Center
Cairo

DR. SAYED O. EL-HELALY
Head of Eng. Sc. Depart.
Faculty of Pet. and Min. Eng.
Suez Canal University

DR. AHMED SAFWAT M. T. NADA
Lecturer, Engineering Science Dep.
Faculty of Pet. and Min. Eng.
Suez Canal University

2007

**Suez Canal University**
**Faculty of Petroleum & Mining Engineering**
**Engineering Science Department**

# STUDY OF WATER DESALINATION BY SOLAR ENERGY USING MULTI-STAGE FLASH (MSF) PROCESS

A thesis
Submitted in partial fulfillment of the requirements for the Master degree of Science in Thermal and Energy Systems Engineering

**BY**

## MOHAMED ABDEL WAHAB SHARAF EL-DEAN

(B. SC., Mech. Power Eng. Dept, Arab Academy for Science and Technology, Alex, 1999)

**SUPERVISORS**

PROF. DR. MANSOUR AWAD MOHAMAD

Solar Energy Department
National Research Center
Cairo

DR. SAYED O. EL-HELABY

Head of Eng. Sc. Depart.
Faculty of Pet. and Min. Eng.
Suez Canal University

DR. AHMED SAFWAT M. T. NAFEY
Lecturer, Engineering. Science Dept.
Faculty of Pet. and Min. Eng.
Suez Canal University

**2007**

# APPROVAL SHEET


# STUDY OF WATER DESALINATION BY SOLAR ENERGY USING MULTI-STAGE FLASH (MSF) PROCESS
(M. Sc. Thesis)


## BY


# MOHAMED ABDEL WAHAB SHARAF EL-DEAN

(B. SC., Mech. Power Eng. Dept, Arab Academy for Science and Technology, Alex, 1999)


**Has been approved by the following examination committee:**

| Name | Signature |
| --- | --- |
| 1. Prof. Dr. Mansour Awad Mohamad-Solar Energy Dept. National Research center, Cairo. | |
| 2. Dr. Ahmed Safwat M. T. Nafey-Engineering Science Dept. Faculty of Petroleum & Mining Engineering, Suez. | |
| 3. Prof. Dr. Hassan El-Banah Saad Fath-Mechanical Power Engineering Dept. Alexandria University. | |
| 4. Prof. Dr. Mohamed Reda Abdel Kader-Mechanical Power Engineering Dept. Faculty of Engineering, Port Saied. | |

# Acknowledgment

*First of all, I thank ALLAH the merciful, for helping me to complete this work.*

*Thanks a lot to…*

    *Prof. Dr. Mansour Awad Mohamad,*

    *Prof. Sayed Othman EL-Helaby*

   *Dr. Ahmed Safwat Nafey,*

*To my Parents…*

     *To my wife…*

      *To my child, Reem...*

بسم الله الرحمن الرحيم

أَوَلَمْ يَرَ الَّذِينَ كَفَرُوا أَنَّ السَّمَاوَاتِ وَالْأَرْضَ كَانَتَا رَتْقاً

فَفَتَقْنَاهُمَا وَجَعَلْنَا مِنَ الْمَاءِ كُلَّ شَيْءٍ حَيٍّ أَفَلَا يُؤْمِنُونَ

الأنبياء (30)

# ABSTRACT

Global resources of fresh water are scarce, unevenly distributed and, in many cases, may require some form of treatment and handling. These limited resources have resulted in water shortages in 88 developing countries across the world containing 50% of the world's population. Need for purification of saline water is increasing due to an increase of population and limited supply of potable water. The standard techniques like multi stage flash, multi effect distillation, vapor compression and reverse osmosis are reliable for large capacity range of (100-50,000) m$^3$/day of fresh water production. However, these technologies are expensive for small amounts of fresh water. Moreover, they can not be used in locations where there are limited maintenance facilities. In addition, the use of conventional energy sources to drive these technologies has a negative impact on environment. Using solar energy is a practical method for obtaining small amounts of fresh water from saline water. Solar water distillation has been a subject of great interest for several decades.

Solar desalination techniques are considered to be clean operations for producing clean water from the saline water. Egypt is considered to be one of the high insolation countries of the world. The sunshine hours are estimated to be 3600 hours/year. Also Suez-Gulf region is considered to be one of the highest insolation regions in Egypt hence the world. The average total insolation that hits this region is found to be range as 3.5 to 7.2 kWhr/m$^2$ and this is during the year. That for some geographically reasons like nearest from the sea level, the seasonal rainfall hours almost low and the weather is always hot and dry. So it is very important to utilize this present huge energy in Egypt (Suez-Gulf) in desalination technologies (small and large sizes).

In the present work a small size of flash unit coupled with flat plate solar collector has been designed and tested in many ways, especially for producing a small amount of potable water for small groups of people. The system is designed and investigated at the Faculty of Petroleum and Mining Engineering at Suez-Egypt. The system is operated and investigated under real environmental conditions during winter and summer seasons. The theoretical study is performed to achieve some targets like:

1- Determining best configuration (based on exergetic analysis) of the examined process.
2- Investigating the system productivity and performance under real operating conditions.
3- Developing a simulation program using Mat-Lab to predict the process behavior under a wide range of operating conditions and design parameters. Deferent solar intensity models are examined, and the most reasonable one for the considered location is determined. Also the performance of multi stages (two and three stages) is developed by the simulation program.
4- Examining the system productivity enhancement using different dosages of surfactant material.

i

# CONTENTS

iii

# LIST OF FIGUERS

v

# LIST OF TABLES

# NOMENCLATURE

| | |
|---|---|
| $A$ | The apparent solar irradiance at air mass zero (ASHREA model), and equal to 0.709 in (S.C.S.G model) |
| | Tends to area in $m^2$, or a parameter used in chapter 3 |
| $A_1$ | Condenser heat transfer area ($m^2$) |
| $A_c$ | The collector heat transfer area ($m^2$) |
| $A_e$ | The collector effective area ($m^2$) |
| $A_p$ | The collector absorber area ($m^2$) |
| $A_{1,2}$ | Nonflow availability |
| $A_f$ | Flow availability |
| $A_q$ | Heat availability transfer |
| $A_w$ | Work availability transfer |
| $a_{1:5}$ | Correlations by HOYT |
| $a_i$ | Absorptance parameters defined by HOYT |
| $a_{co}$ | Carbon dioxide absorptance |
| $a_{ox}$ | Oxygen absorptance |
| $a_w$ | Water vapor Absorptance |
| $a_f$ | Flow availability |
| $B$ | Is the atmosphere extinction coefficient (ASHREA) |
| $B_a$ | Ratio of the forward-scattered irradiance to the total scattered irradiance due to aerosols, =1, 0.5 and 0 for forward, isotropic and backward scattering respectively |
| $B$ | Tends to the brine, or a parameter used in chapter 3 |
| $B_o$ | Mass flow rate of the brine entering the flash unit (kg/s) |
| $B_1$ | Mass flow rate of the brine exiting from the 1st flash unit (kg/s) |
| BPR | Boiling point elevation of saline water parameter |
| $B^{\cdot}$ | Brine flow rate( kg/s) |
| $b$ | The thickness of the bond (m) |
| $C$ | Is the diffuse radiation factor (ASHREA),or surfactant concentration (ppm), or the parameter used in chapter 5 or the collector heat capacity |
| C.O.P | Coefficient of performance |
| $C_{season}$ | The season coefficient (S.C.S.G model) |
| $C_p$ | Bond conductance or specific heat capacity of saline water (kJ/kgK) |
| $C_h$ | Collector height (m) |
| $C_L$ | Collector length (m) |
| $C_W$ | Collector width (m) |
| $C_{pb}$ | Specific heat at constant pressure for the brine (kJ/kg k) |
| $C_{pd}$ | Specific heat at constant pressure for the distillate( kJ/kg K) |
| $C_{pl}$ | Specific heat at constant pressure for the liquid( kJ/kg K) |

| | |
|---|---|
| $D$ | Tends to distillate or parameter used in chapter 3 |
| $DP$ | Distillate product( kg/hr) |
| $D_1$ | Distillate product from the $1^{st}$ stage (kg/s) |
| $d$ | Collector tube outer diameter (m) |
| $d_i$ | The inside diameter (m) |
| $d_o$ | The outside diameter (m) |
| $E$ | Parameter used in chapter 3 |
| $Epower$ | Electric (equivalent) power input (watt) |
| $E_d$ | Exergy destruction term kJ/kg distillate |
| $E_x$ | Specific exergy (kJ/kg) |
| $E_c$ | The collector effectiveness |
| $\dot{F}$ | Feed water flow rate( kg/s) |
| $F$ | Fin efficiency |
| $F_{i,o}$ | Inlet and outlet feed water to the condenser (kg/s) |
| $FPC$ | Flat plate collector |
| $FF$ | Flooding factor |
| $F'$ | Efficiency factor for solar collector |
| $F_R$ | Heat removal factor |
| $F_S$ | Feed water system (kg/s) |
| $G$ | Overall specific mass flow rate |
| $G_{bn}$ | The global normal beam (ASHREA) |
| $G_d$ | The global diffuse (ASHREA) ($W/m^2$) |
| $H_v$ | Latent heat of condensation (kJ/kg) |
| $H_{v1}$ | Latent heat of vaporization of water (kJ/kg) |
| $h_f$ | Fluid heat transfer coefficient ($W/m^2K$) |
| $h_o$ | Enthalpy stream of the inlet brine to the stage ($W/m^2K$) |
| $h_{b1}$ | Enthalpy stream of the outlet brine from the stage (kJ/kg) |
| $h_{D1}$ | Enthalpy stream of the distillate product (kJ/kg) |
| $h_{Fi,o}$ | Enthalpy stream of the inlet and outlet feed water to the condenser (kJ/kg) |
| $h_w$ | Convection heat transfer coefficient  ($W/m^2K$) |
| $I$ | Internal irreversibility( kJ), Current (A) |
| $I_{as}$ | Solar irradiance on a horizontal surface from atmospheric scattering($W/m^2$) |
| $I_d$ | Direct solar irradiance on a horizontal surface ($W/m^2$) |
| $I_G$ | Solar irradiance on a horizontal surface from  multiple reflections between the ground and sky ($W/m^2$) |
| $I_s$ | Solar irradiance on a horizontal surface from scattered light ($I_{as}+I_G$) |
| $I_T$ | Total (global) Solar irradiance on a horizontal surface ($W/m^2$) |
| $It1,2,3,4,5,6,7,8$ | Total (global) Solar irradiance on a horizontal surface for ASHREA, ATWATER&BALL, BIRD, DAVIES&HAY, HOYT, LACIS&HANSEN, SPICTRAL2 and S.C.S.G models respectively ($W/m^2$) |
| $i$ | Initial value |
| $I_0$ | Extraterrestrial Solar irradiance =1367 $W/m^2$ |
| $ID_1$ | Inner diameter of the condenser tubes ($m^2$) |
| $K$ | Aerosol transmittance for Davies and Hay |
| $K_1$ | Constant used in Bird model associated with Aerosol absorptance |
| $K$ | Factor derived and is approximately = 0.5 |

| | |
|---|---|
| $k_b$ | Back insolation conductivity (W/mK) |
| $k_e$ | Edge insolation conductivity (W/mK) |
| $k$ | Thermal conductivity (W/mK) |
| $L$ | Length (m) |
| $l_b$ | Back insolation thickness (m) |
| $l_e$ | Edge insolation thickness (m) |
| $M$ | Air mass |
| $MBE$ | Mean bias error (W/m$^2$) |
| $MPE$ | Mean percentage error (%) |
| $MSF$ | Multi stage flash |
| $M^{\cdot}$ | Pressure-corrected air mass |
| $m^{\cdot}$ | Mass flow rate (kg/s) |
| $m_{Fi,o}$ | Mass flow rate in and out of the condenser (kg/s) |
| $NEA$ | Non equilibrium allowance |
| $NG$ | No. of glass covers of the collector |
| $NTU_1$ | No. of transfer unit parameter |
| $N$ | Iteration number, considered day light hours |
| $N_s$ | Minimum number of entropy generation |
| $N_{tubes}$ | Numbers of tubes through the collector |
| $n$ | Julian day number |
| $OD_o$ | Outer diameter of the condenser tubes (m) |
| $P$ | Tends to the pressure (kPa) |
| $PF_H$ | Electric heater power factor |
| $PR$ | Unit performance ratio |
| $P_{bo}$ | Pressure stream of the inlet brine to the flash stage (kPa) |
| $P_{b1}$ | Pressure stream of the outlet brine from the flash stage (kPa) |
| $P_{d1}$ | Pressure stream of the distillate (kPa) |
| $P_{Fi,o}$ | Pressure stream of the condenser (kPa) |
| $P_r$ | Prandtl number |
| $P$ | Surface Pressure (mbars) |
| $PM$ | Pressure (mbars) |
| $Q_1$ | Thermal energy of the condenser in steady state (Watt) |
| $Q_u$ | Useful energy from the collector (Watt) |
| $Q_{loss}$ | Energy loss from the collector (Watt) |
| $Q_{stg}$ | Energy stored in the collector (Watt) |
| $Q^*$ | Rate of solar radiation from the sun (W/m$^2$) |
| $Q_j$ | Rate of energy transferred at portion of the boundary |
| $Q_{loss}$ | Rate of energy loss |
| $R^{\cdot}$ | Brine recycle flow rate (kg/s) |
| $RMSE$ | Root mean square error (W/m$^2$) |
| $R_F$ | Stage fouling factor |
| $r_g$ | Ground albedo |
| $r_s$ | Sky, or atmospheric, albedo |
| $r_S^{'}$ | Correlation by LACIS&HANSEN |
| $R_a$ | Rayleigh number |
| $R_e$ | Reynolds number |
| $R_t$ | Total thermal resistance |

| | |
|---|---|
| $S_{gen}$ | *Entropy generation* |
| $S_t$ | *Tube spacing (m)* |
| *SNTU* | *Solar number of transfer units* |
| $s$ | *Specific entropy ( kJ/kg K)* |
| *TBT* | *Top brine temperature ($^oC$)* |
| $T_o$ | *Top brine temperature ($^oC$)* |
| $T_{amb}$ | *Ambient temperature ($^oC$)* |
| $T_{bo}$ | *Inlet brine stream temperature to the flash stage ($^oC$)* |
| $T_{b1}$ | *Outlet brine stream temperature from the flash stage ($^oC$)* |
| $T_{i,ocol}$ | *Inlet and outlet brine stream temperature to the collector ($^oC$)* |
| $T_{D1,d1}$ | *Distillate product stream temperature ($^oC$)* |
| $T_{Fi,o}$ | *Inlet and outlet feed temperature of the condenser ($^oC$)* |
| $T_g$ | *Collector glass cover temperature ($^oC$)* |
| $T_{ins}$ | *Collector insulation temperature ($^oC$)* |
| $T_{lm1}$ | *Logarithmic mean temperature ($^oC$)* |
| $T_{mp}$ | *Mean plate temperature of the collector ($^oC$)* |
| $T_p$ | *Plate temperature of the collector ($^oC$)* |
| $T_{v1}$ | *Vapor temperature ($^oC$)* |
| $T$ | *Surface temperature (K)* |
| $T_A$ | *Transmittance of aerosol absorptance and scattering* |
| $T_{AA}$ | *Transmittance of aerosol absorptance* |
| $T_M$ | *Global Transmittance of all molecular effects except water vapor for Atwater* |
| $T_{Md}$ | *Direct transmittance of all molecular effects except water vapor for Atwater* |
| $T_0$ | *Transmittance of ozone absorptance* |
| $T_R$ | *Transmittance of Rayleigh scattering* |
| $T_{sun}$ | *Sun temperature ($^oK$)* |
| $T_{stage}$ | *The flash stage temperature drop ($^oC$)* |
| $T_{ws}$ | *Transmittance of water vapor scattering* |
| $t_c$ | *the collector time constant in min* |
| $T^*$ | *Sun temperature K* |
| $T_{bout}$ | *Wasted brine temperature ($^oC$).* |
| $T_{Fi}$ | *Inlet feed water to the collector ($^oC$).* |
| $T_{icol}$ | *Inlet feed water to the collector ($^oC$).* |
| $T_{Fo}$ | *Outlet feed water from the collector ($^oC$).* |
| $U_0$ | *Amount of ozone in a vertical column from surface (cm)* |
| $U_1$ | *Overall heat loss of the stage($W/m^2K$)* |
| $U_t$ | *Overall top loss in the collector ($W/m^2K$)* |
| $U_l$ | *Overall losses in the collector ($W/m^2K$)* |
| $V$ | *Volume ( kg), Voltage (Volt)* |
| $V_w$ | *Wind speed (m/s)* |
| $W_{b1}$ | *Flow rate of water in the brine (kg/s)* |
| $W_e$ | *The effective tube spacing (m)* |
| $X$ | *Salt concentration* |
| $X_{b1}$ | *Flow rate of salt in the brine (kg/s)* |
| $X_O$ | *Total amount of ozone in slanted path (cm)* |

| | |
|---|---|
| $X_W$ | Coefficient used by LACIS&HANSEN model (cm) |
| $Y$ | Glass cover thickness (m) |
| $z$ | Zenith angle (degree) |

**Greek**

| | |
|---|---|
| $\eta_{thc}$ | Collector thermal efficiency |
| $\eta_{ex}$ | Exergetic efficiency |
| $\sum$ | Summation |
| $\phi$ | Tube side brine velocity (m/s) |
| $\phi_c$ | The flow parameter |
| $\varepsilon_c$ | The collector effectiveness as a function of efficiency factor |
| $\varepsilon_p$ | The emissivity of the absorber plate |
| $\varepsilon_g$ | The emissivity of the glass cover |
| E | Effectiveness defined by Edwards and Phillips |
| $\psi$ | Design parameter= $N_{tubes}F^*A_p / A_r$ |
| $\delta$ | Fin thickness |
| $\beta$ | Collector tilt angle=$45^o$ |
| $\tau_A$ | Broad band turbidity |
| $\tau_{A:0.5,0.38}$ | Optical depth at wave length 0.5 and 0.38 $\mu m$ respectively |
| $\sigma$ | Boltzmann constant |
| $\theta$ | Incident angle (degree) |

**Subscripts**

| | |
|---|---|
| 0 | Dead state |
| 1,2 | State one, two |
| b | Brine |
| col | Collector |
| cv | Control volume |
| cw | Cooling water |
| d | Distillate |
| e | Exit state |
| ex | Exergy |
| f | Flow |
| fch | Flash chamber |
| fu | Flash unit |
| H | Heater |
| i | Inlet state |
| j | Portion of the boundary |
| l | Liquid |
| n | Number |
| t | Total |
| $w_{i,e}$ | Water in or exit |
| xout | Exergy out |
| xin | Exergy in |

# CHAPTER 1

# INTRODUCTION

## 1.1 WATER SHORTAGE

Water and its natural resources considered very important part for living on the earth. Water is very important for the proceeding of the all life needs and in all life fields like agricultures needs, human needs and artificial needs. But at the last few decades water shortage problems appear at many countries especially developing countries. Many remote areas of the world such as coastal desert areas in the Middle East or some Mediterranean and Caribbean islands are suffering from acute shortage of drinking water [1]. By 2020, the demand for water is expected to increase by 40 per cent, and 17 per cent more water will be needed to irrigate the crops that will have to be cultivated to feed a growing population. Yet already in the world today, nearly 20 per cent of the world's population do not have ready access to drinking water, while 40 per cent lack adequate sanitation [3].

North Africa increased from 49.5 million in 1955 to 118.1 million in 1990 and it is expected to exceed 188 million by the year 2025. The total annual renewable fresh water supply available in the region has been estimated at the fixed rate of 113.1 $Km^3$/yr. According to this, the regional annual average per capita water availability has been reduced from 2285 $m^3$ in 1955 to 958 $m^3$ in 1990 and is expected to reach 602 $m^3$ by the year 2025. Thus the whole region is already experiencing water scarcity that is getting more severe with time. The problem occurs by many causes like population increasing and the pollution increasing for the natural water resources. Problems are bound to worsen. Already many countries do not have enough water to meet domestic demands for food, creating a source of potential political instability. Water-short countries are increasingly turning to the world grain market. But for trying to backup and solve this important problem of water natural resources; many of the new and different techniques have been developed.

Desalination of sea water considered the most important method to free water from salt and simply makes it ready to be used in the human needs. One of these important techniques and famous called Multi Stage Flash evaporation processes (MSF) [7]. This evaporation method considered a kind of desalination of sea water by distillation process. Simply distillation process is to boil sea water till become vapor and then condensate it. MSF plants are globally used for the artificial needs. At last few decades MSF process is coupled with solar energy to give what called solar desalination processes [5].

The use of solar energy as an economic source for the realisation of large-scale industrial seawater desalination is still unattainable [2]. Actually this technique or this branch of desalination needs some terms to be achieved like the good presence of the sun.

For Middle East countries sun has a good presence beside a huge area of the desert. Sun is considered one of the most important natural, renewable and clean sources of thermal energy and considered very important for the proceeding of the life. The idea of using solar energy systems with desalinating plants is considerably helpful and good from the side of pollution.


## 1.2 WATER DESALINATION TECHNOLOGIES IN EGYPT

Historically, multi-stage flash (MSF) and multi-effect evaporation and vapor compression desalination technologies were among the oldest methods applied in Egypt. These were usually found on the Red Sea coastal areas for the oil refineries and small settlements. One of the largest thermal MSF plants is located on the northern coast in Mersa Matrouh with typically a production rate of 2,000 $m^3$/day. With recent developments and the changing economical determining factors, emphasis has also been placed on the use of reverse osmosis desalination units for seawater rather than the conventionally used brackish water [2].


## 1.3 IMPORTANCE OF SOLAR DESALINATION IN EGYPT

The desert in Egypt represents 96 % of its all area and most of Egypt populations live in the limited area of the Nile Valley. So it is very important to create new society faraway sites from the Nile Valley to face the problem of such crowd population. Potable water shortage in Egyptian dessert represents the main factor that retards its development. Besides, Nile water is not adequate for such projects due to the high water transportation cost from the Nile Valley to such remote arid area. The conventional water resources from the River Nile and the available wells are barely able to cover the increasing demand in the valley and in the Red Sea areas [2]. On other hand most of projects sites are either near to seashore or its underground has a natural reservoir of brackish water. So the desalination represent one of the optimum solutions of water shortage problem in desert and to face the future demands for water in Egypt, see illustration in Table (1-1) [3]. The table shows that by 2025 the minimum of portion human per year will become 637 $m^3$/year. Different desalinating technologies are currently in use in Egypt. Due to water shortage in many areas in the country, Egypt has 230 units can give (174:640) $m^3$/day [3].

Table (1-1) The future demands for water in Egypt [3]

| The year | Number of people | The source of water | | | | | The water demand | | | | Potion of 1 m³/year | The gap of water demand | |
| | | Conventional | | Non conventional | | | | | | | | | |
| | | Surface | Under ground | desalination | treatment | total | drink | industrial | irrigation | Total | | A | B |
|---|---|---|---|---|---|---|---|---|---|---|---|---|---|
| 1990 | 52 | 55.5 | 3.1 | 0.02 | 4.9 | 63.5 | 3.1 | 4.6 | 49.7 | 57.4 | 1221 | + 6.1 | + 19.5 |
| 2000 | 62 | 75.5 | 7.4 | 0.05 | 9.1 | 74.05 | 4.5 | 6.1 | 59.9 | 70.5 | 1194 | + 3.55 | + 12.05 |
| 2025 | 86 | 57.5 | 7.4 | 0.07 | 9.1 | 74.07 | 8 | 9.85 | 85.4 | 103.25 | 637 | - 29.20 | - 11.95 |
| 2051 | 120 | 57.5 | 7.4 | 0.09 | 9.1 | 74.09 | 10.6 | 13.7 | 111.92 | 136.31 | 617 | - 62.26 | - 45.95 |

The gap A = the total source – the total demand
The gap B = portion of one – the minimum of portion human per year (1000 m³)

The cost of energy which using in desalination plant represent (60% - 80%) from capital cost. The rapid escalation in cost of fuels has made the solar energy more attractive alternative, especially in remote arid regions. Solar energy is one of renewable energy source that can be appropriately exploited for providing part of energy demand. In fact, the use of alternative energy source is of particular interest since in areas where the wind potential is low, most often the solar potential is high [4].

Fortunately, solar energy is available in Egypt with relatively high intensity in most of the year. Some of the remote areas are blessed with abundant solar radiation which can be used as an energy source for small desalination units to provide a reliable drinking water supply for the inhabitants of the remote areas. Recently, considerable attention has been given to the use of solar energy as an energy source for desalination because of the high cost of fossil fuel in remote areas, difficulties in obtaining it, interest in reducing air pollution and the lack of an electrical power source in remote areas [1]. Figure (1.1) shows the irradiation map for Egypt and Middle East countries. The dark area on the map represents the region that has the highest solar flux. The gray areas represent the lower and so on. Although the figure show that a higher aspects for solar energy at this region, but this region already suffering from water shortage. So it is very important and vital to combined and utilize this clean energy with desalination technologies.
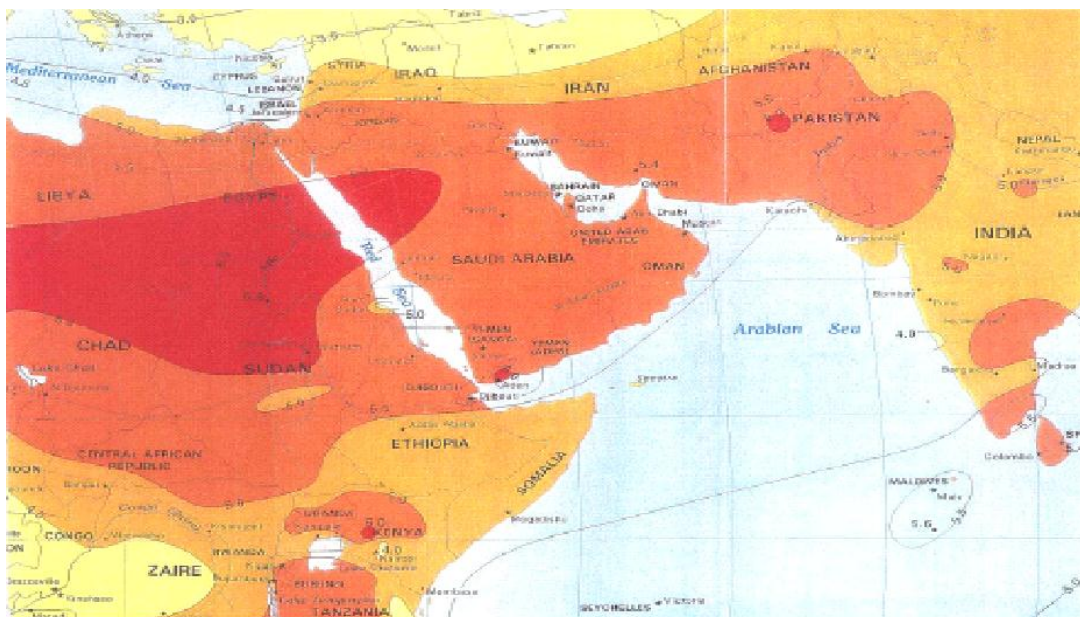
Figure (1.1) The solar irradiation map for middle east area

Egypt is considered a high insolation country. The number of sunshine hours amounts almost to 3600hr/year. It's very important and valuable to use this energy in desalinating technology in Egypt. Solar energy could be use as the main source of heat in MSF plants or the main source of electricity or to drive the pump in RO plants [4]. Solar assisted multi-stage flash (MSF) distillation system is economically acceptable with a conventional energy MSF plant [5]. There are some benefits of using solar energy with distillation techniques like flash evaporation technique as; using solar energy as a clean energy. Solar energy has a negative impact on the environment. Not expensive, just initial and installations cost. Also, ease of maintenance and simplicity in design is considered.

## 1.4 WORK PROCEDURE AND OBJECTIVES

In this study one unit of flash evaporation process coupled with one unit of solar water heater to desalinate salt water is presented and examined experimentally as well as theoretically. This system is operated at the Faculty of Petroleum & Mining Engineering at Suez, Egypt.

The flash unit is designed vertically with its preheater/condenser; and the main source of heating the fluid is solar collector (flat plate solar collector FPC). Flat-plate collectors are the most common solar collector for solar water-heating systems in homes and solar space heating. Choosing flat plate collector type as an input power instead of other types of solar collectors refers to its collecting area and feed flow rate. In this work a review of solar desalination techniques is presented in Chapter 2. The mathematical model analysis

of all system components (Flash chamber and Flat Plate Collector (FPC)) is made and supported by a computer program (Chapter 3).

The analysis of solar aspects at the location of operation is performed to know precisely the amount of energy collected by the brine heater. For that purpose; BIRD, DAVIES&HAY models and a new correlation are found to be matched with the measured data from the sun. Developing a new correlation for solar flux or using a famous solar radiation model is important in case of absence of solar energy instruments. Chapter 4 is developed to predict and investigate the solar energy over Suez Gulf region (the location of operation).

Exergetic analysis is performed and introduced in Chapter 5 to know the location of real losses in the system and also to measure the real performance of the process. Also Exergetic analysis is made to decide the best configuration between three different configurations. After deciding and choosing the best configuration (exergy analysis).

Chapter 6 is developed to present the system setup and the instruments used. Results under different operating conditions are presented in Chapter 7. Also the enhancement of the system performance by surfactant additives is made and evaluated in Chapter 8. Conclusions and future work are introduced in Chapter 9.

# CHAPTER 2

# LITERATURE SURVEY

## 2.1 INTRODUCTION

Water shortage around the world increased rapidly and the demand of new water resources to satisfy human, agricultural and industrial needs has increased substantially in the last few decades [6]. And, the global resources of freshwater are scarce, unevenly distributed and, in many cases, may require some form of treatment and handling. These limited resources have resulted in water shortages in 88 developing countries across the world containing 50% of the world's population. Water supplies in these countries cannot meet urban and industrial development needs as well as associated changes in life style. Moreover, common use of poor water in developing countries causes 80-90% of all diseases and 30% of all deaths.

The current water shortage extends to include underground water supplies, previously considered to be an unlimited resource in many countries. In this regard, several cases have been reported of well failure, decline of the water table and seawater intrusion into freshwater aquifers [7]. On the other hand the population explosion around the worldwide and the problem of pollution of the rivers, air, seas, and lakes caused by the industrial wastes made a great problem for the natural resources of the fresh water on the mother earth. Because of this, desalinated water has become a potential supplement to, and competitor with, natural freshwater resources. Desalination technologies are many like, distillation processes, distillation combined with solar or wind energies, reverse osmosis (RO), electro dialysis (ED), and ion exchange and freeze desalination. And there are several new concepts and/or variation on existing concepts that may have some potential. Among these are: hybrid desalination plants that optimize the use of capital and energy resources by combining various desalination processes (e. g., RO and distillation). Of the three commercially proven processes: distillation, reverse osmosis and electro dialysis, there is no one "best" method of desalination. Generally, distillation and reverse osmosis (RO) are used for seawater desalination, while reverse osmosis and electro dialysis are used for brackish water desalination. However, the selection and use of these processes can be very site-specific; they must be selected very carefully, especially in developing countries.

There are many considerations for the selection of the desalting method. One of the major considerations in the selection of a desalination process is its cost. However, desalination technology is still in developmental stage and considerable effort must be made to improve desalinating methods, reduce equipment cost, and reduce energy requirements [6]. There are many methods considered as a great new source to produce fresh water to overcome the water shortage around the world. Water distillation is one of the new of many methods, which can solve the water problems around the world. Distillation simply is to free saline water from its salt by condensation and make it ready to be easily used in the human needs as regarded above. The advantage of distillation over other desalting

processes is that it produces pure water independent of feed water quality like multi stage flash processes (MSF), solar stills, solar ponds, vapor compression; multiple effect evaporation processes (MEE) and reverse osmosis processes (RO). Currently, the opportunity to couple solar thermal power systems to desalination plants seems particularly attractive especially in Middle East area which is expected to be a significant market for desalination.

Countries like Egypt, Saudi Arabia, Kuwait and other major countries of the Arabian Gulf are typically desert areas with no permanent streams. Therefore, avoiding water shortages in these countries is of critical concern. Current industrial development and agricultural growth in these countries suffer from the shortage of freshwater [6]. Middle East countries have a good presence of solar energy in the whole world and also have a potential market in desalination technologies.

At the last few decades; desalination technologies are transferred to use solar energy with distillation processes. Solar desalination techniques are summarized into many branches like using solar energy with Multi Effect distillation (MED), Solar Still, Reverse Osmosis (RO), Humidification processes and also Flash Evaporation processes. In this work, surveys on solar distillations techniques are involved.

## 2.2 SOLAR DESALINATION TECHNIQUES

Techniques of solar desalination are many and varying according to the size of the demanding of fresh water and the size of solar energy presence. In this section; using solar energy with desalination techniques are involved. Figure (2.1) shows a simple classification of solar desalination techniques.
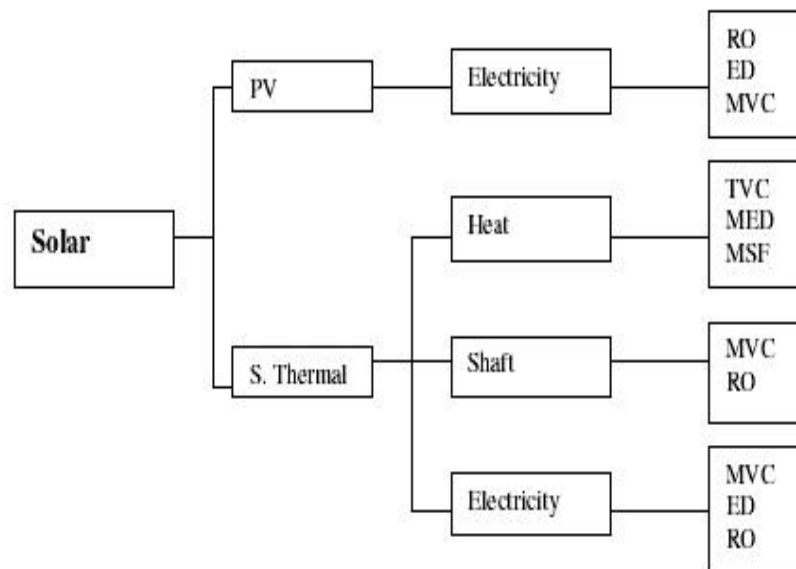


Figure (2.1) The flow chart of solar desalination category techniques

## 2.2.1 Solar Energy to Drive Reveres Osmosis (RO) Processes

Figure (2.2) shows a solar-assisted RO desalination plant that mainly consists of the membrane separation section (various membrane modules connected together), which is fed via a high pressure reciprocating pump and which is properly connected to a hydroturbine, for the recovery of energy by the brine stream leaving the process. The solar thermal subsystem provides the required shaft work to drive the high pressure pump of the desalination plant by means of a properly interconnected steam turbine [8].
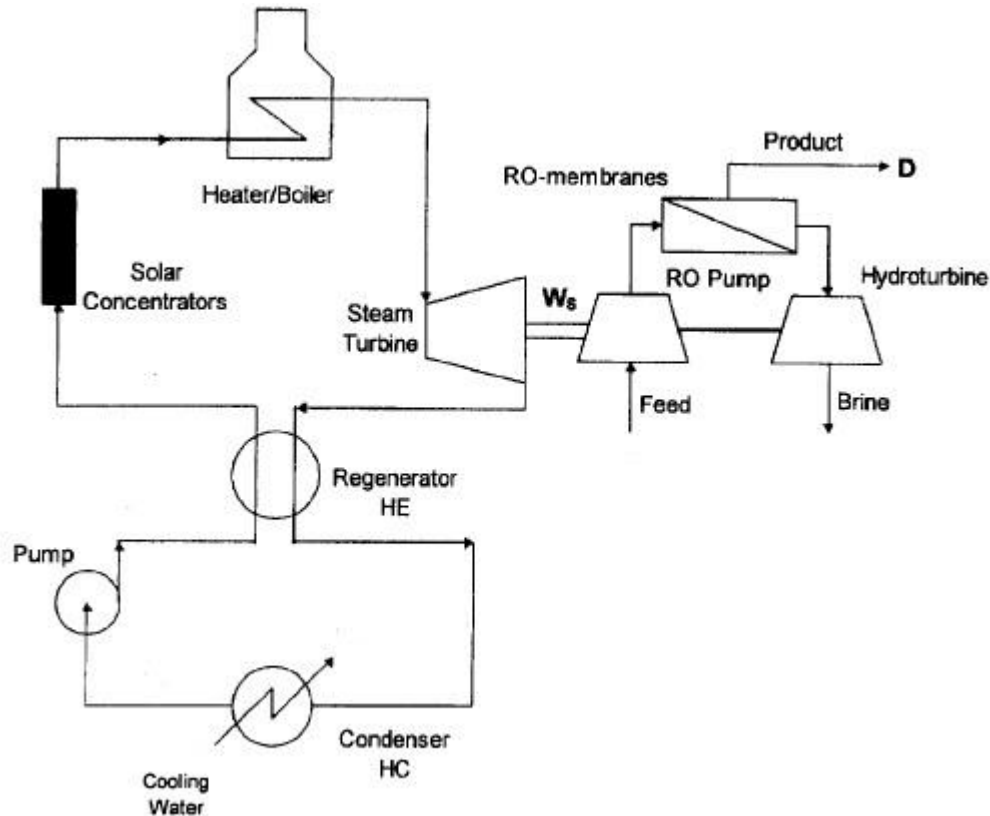


Figure (2.2) A flow sheet of solar-assisted RO desalination plant

## 2.2.2 Solar Energy to Drive Multi Effect Distillation (MED) Processes

Ali M. El-Nashar presents a small solar MED of seawater desalination processes for remote arid areas [1]. A solar stand-alone system consisting of a Multi-Effect Stack (MES) evaporator supplied by thermal energy from flat plate or evacuated tube collectors with pumping power supplied by a solar PV system as shown in Fig. (2.3).
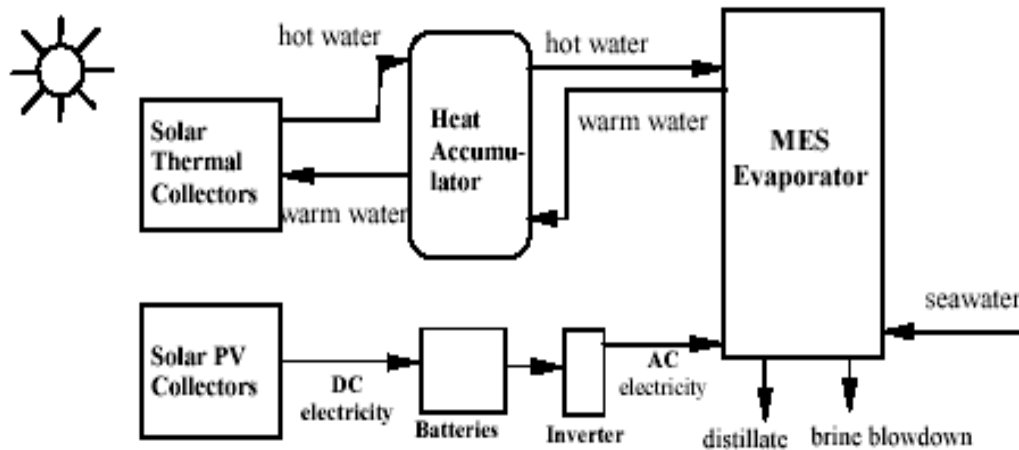
Figure (2.3) Schematic diagram of MED
system powered by solar energy

The system in the past figure utilizes solar energy to satisfy both thermal and electrical energy demands of the evaporator. However, the power requirement is supplied by an array of solar PV cells instead of a diesel generator. An inverter is used to change the DC output into AC electricity required by the pump motors. The thermal energy required by the MES evaporator can be supplied in the form of hot water generated by either flat plate or evacuated tube collectors. Double glazed, well designed flat plate collectors can produce hot water at about 80°C with reasonable efficiency while evacuated tube collectors can easily produce water at more than 95°C with good efficiency albeit higher collector cost. Lourdes Garcia-Rodriguez presented a preliminary design of different solar systems of seawater distillation processes [9].

The solar collectors are parabolic trough ones in which brine circulate as thermal fluid. Steam is directly obtained from circulating brine. The solar collector field could be connected to condenser/preheater heat exchangers; nevertheless, the system would have a low performance ratio. In addition, the solar collectors could be coupled to multi-stage flash or multi-effect distillation systems to continue the evaporation of the remaining brine. The steam generated by the solar field would drive the distillation plant. The solar MED plant describe above is schematically represented in Fig. (2.4). Steam is generated at the MED plant as well as at the solar PTC field. The condensation of the steam generated preheats the income seawater (1) before entering the solar field (3). Brine (4) and steam (5), leaving the solar field, pass through the MED plant, from the first cell to the last one.
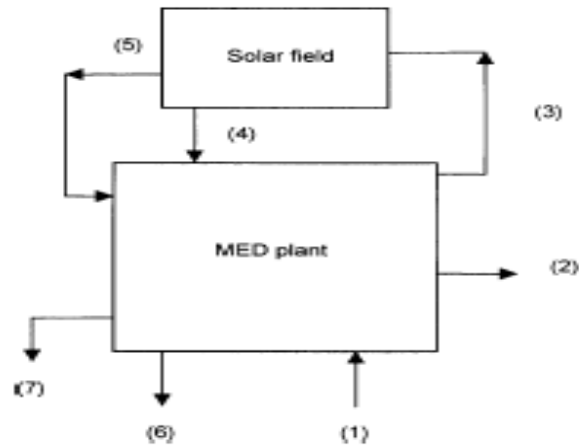
Figure (2.4) A solar multi-effect distillation plant. 1 seawater,
2 cooling seawater outlet, 3 preheated seawater, 4 brine,
5 steam, 6 fresh water, 7 blow down

Advantages of the system are as follows: First, since the system is modular, the capacity can be easily increased connecting in parallel additional collectors and/or heat exchangers. Second, the simple design arrangement makes the system suitable for remote areas if its reliability and technical feasibility is proved [9].

### 2.2.3 Solar Still Productivity for Remote Areas

The solar still consists of a body of water that captures solar radiation, causing vaporization and condensation on the inside of a sloped transparent sheet. This arrangement enables the condensed water droplets to run down and be collected in a catch basin. The efficiency of a single effect solar still is estimated between 35% to 50%. A. S. Nafey presented a small size of solar still unit that could be suitable for small groups of people [10]. In that work, four experimental still units of $0.25m^2$ each are constructed. The optimum accumulative productivity of the still/area was about 4 lit/day/1$m^2$. Figure (2.5) shows a simple unit of solar still configuration presented by [10]. So, solar still with its lower productivity, does not compete with other desalination techniques. However, when the demand of fresh water does not exceed a few cubic meters, the solar still is a viable option.

10
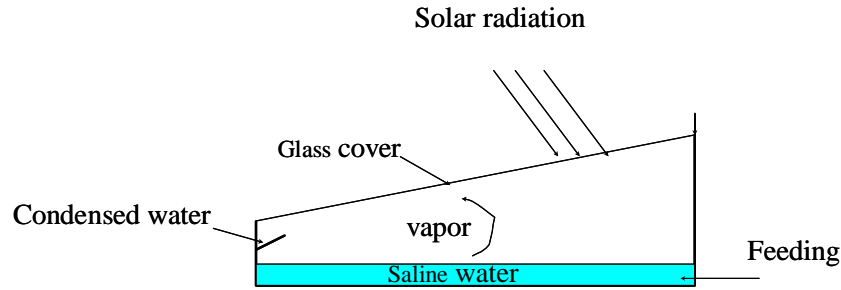
Figure (2.5) Schematic draw of a small unit of solar still unit

Also Badran [46] presented a flat plate solar collector coupled with solar still unit. The experimental investigation was made to study the effect of coupling a flat plate solar collector on the productivity of solar stills. It has been found that coupling of a solar collector with a still has increased the productivity by 36%. The still area was about $1m^2$ filled with brackish water supplied to it from a collector which preheats the water to act as an enhancer to the solar still. The flat plate collector area was found to be about 1.8m long and 0.6m width with 0.15m thickness. The system total productivity was found to give 3.25 kg/day/m$^2$ and found to be 36% more than that when the still was operated alone (2.24 kg/day/m$^2$). Figure (2.6) shows a schematic diagram showing the arrangement of the still-collector systems.
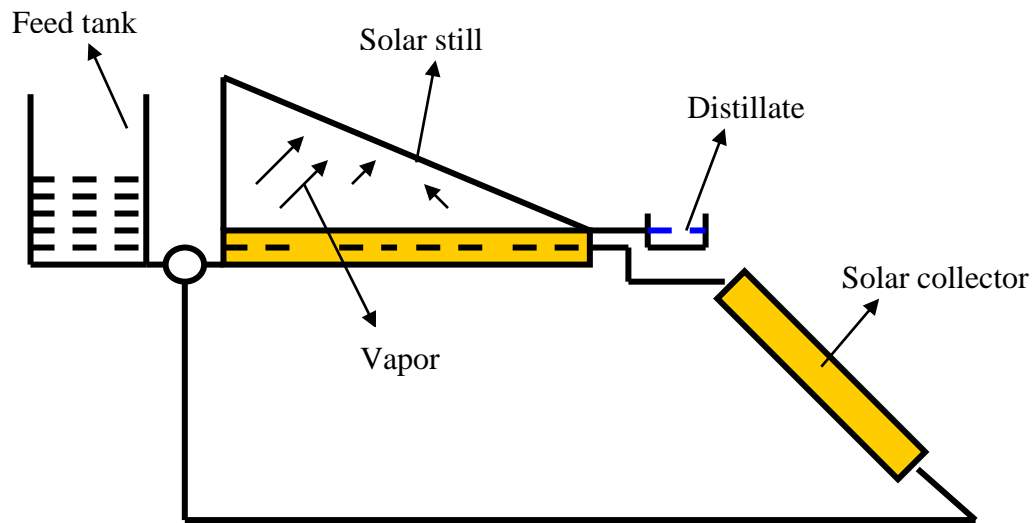


Figure (2.6) A schematic diagram showing the arrangement of the still-collector systems

## 2.2.4 Using Solar Energy with Humidification-Dehumidification Processes

HDD technique is one of the non-conventional water desalting processes. It can be visualized simply as a process of bringing warm unsaturated air into contact with warm saline water under such conditions that a desired humidity is reached, followed by stripping out the vapor from the humidified air by passing it through a condenser. A. S. Nafey and A. Soliman introduced a humidification dehumidification desalination system powered by solar collector [3]. The collector area was about 2.5m$^2$. The system total productivity was about 3.2kg/day/m$^2$. The system was suitable for remote zones. Figure (2.7) shows a schematic diagram of the system operation. That system is distinguished by low productivity and also the system consists of many components and that will lead to a problem while maintenance operations.
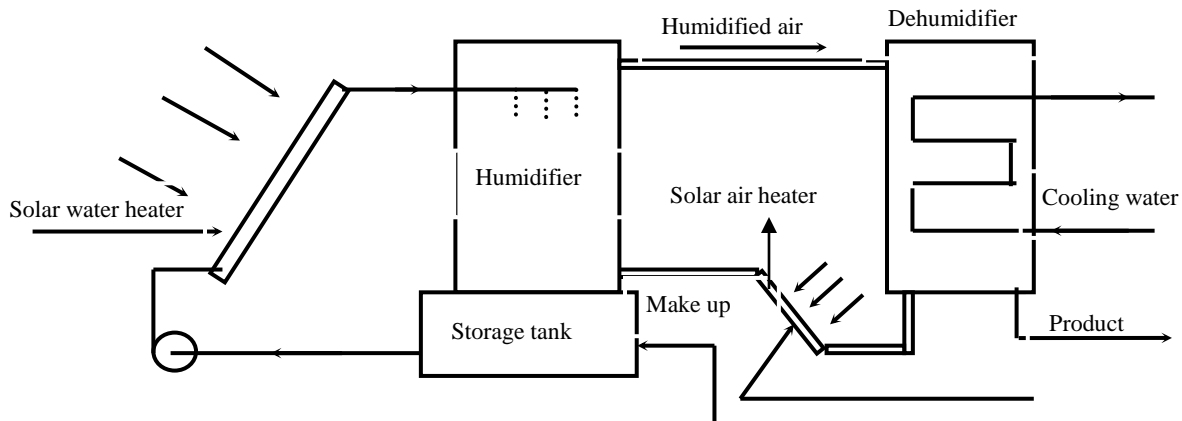


Figure (2.7) Scheme diagram of HDD process

## 2.2.5 Flash Evaporation Processes Powered by Solar Energy

First it is better to recognize what are the flashing processes. Multi stage flash desalination (MSF) is currently the workhorse of desalination industry with a market share close to 60% of the total world production capacity [9]. MSF distillation was developed in the late 1950s; the first commercial plant was built in 1957 in Kuwait [12]. Since the late 1960s MSF plants have dominated the commercial distillation market. Because of the significant economies of scale achieved by large capacity plants, and the extensive design and operational experience gained over the last three decades, MSF plants, found in 55 countries, now account for almost two-thirds of the world's desalination capacity, or about 2 billion gpd [12].

Individual units as large as 10 mgd are now being built. In fact, a MSF multi-plant complex with a total capacity of almost 300 mgd was completed in Saudi Arabia in the early 1980s. The MSF process has many attractive features, which distinguish it from other desalination configurations. The MSF system doesn't include moving parts, other

than conventional pumps. Construction of MSF plants is simple and involves a small number of connection tubes, which limits leakage problems and simplifies maintenance work. This method use low grade thermal energy which can be provided by a solar collector to evaporate water vapor from saline solution. The vapor produced in any flash chamber or stage in the MSF process is used to preheat the incoming sea water in that chamber. Figure (2.8) shows a flow sheet diagram of a common MSF processes.
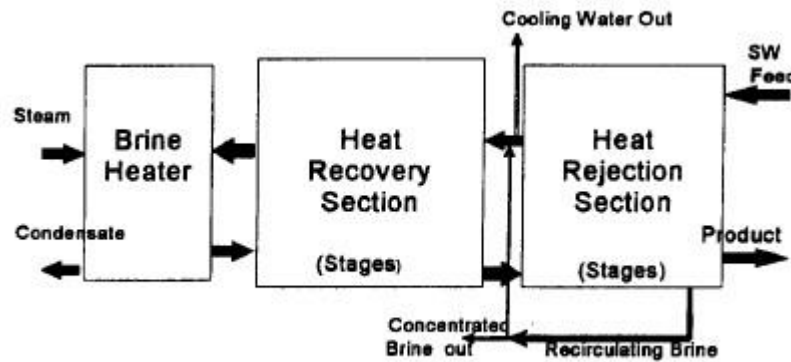


Figure (2.8) A flow sheet diagram of MSF processes (heat
rejection and heat recovery sections)

Figure (2.9) shows a schematic diagram of the MSF system. The system involves six main streams: intake seawater, rejected cooling seawater, distillate product, rejected brine, brine recycle and heating steam. The system contains flashing stages, a brine heater, pumping units, venting system, and a cooling water control loop. The flashing stages are divided into two sections: heat recovery and heat rejection. The number of flashing stages in the heat rejection section is commonly limited to three. On the other hand, the number of flashing stages in the heat recovery section varies between 21 and 40. The intake seawater is introduced into the inside of the preheater/condenser tubes of the last flashing stage in the heat rejection section. Similarly, the brine recycle stream is introduced into the inside of the preheater/condenser tubes of the last flashing stage in the heat recovery section. The flashing brine flows counter to the brine recycles from the first to the last flashing stage. The saturated heating steam with a temperature range of 97±117 °C drives the flashing process. The heating steam flows on the outside of the brine heater tubes and the brine stream flows on the inside of the tubes. As the heating steam condenses, the brine stream gains the latent heat of condensation and its temperature reaches the desired top brine temperature. This parameter, together with the flashing temperature in the last stage, defines the total flashing range. The hot brine enters the first stage, where a small amount of product vapor is formed. The flashing process reduces the temperature of the unevaporated brine. The temperature reduction across the flashing stages is associated with a drop in the stage pressure, where the highest stage pressure is found in the first stage after the brine heater and the lowest pressure is that of the last stage. The pressure drop across the stages allows for brine flow without the use of

13

interstage pumping units. In each stage, the flashed off vapor flows through the demister, which removes entrained droplets of unevaporated brine. The vapor then condenses on the outside surface of the preheater/condenser tubes. The condensed vapor collects over the distillate trays across the flashing stages to form the final product water, which is withdrawn from the last flashing stage. The condensation process releases the vapor latent heat, which is used to preheat the brine recycle stream in the heat recovery section. The same process takes place in the preheater/condenser tubes in the heat rejection section. This results in an increase in the seawater temperature to a higher value, equal to the temperature of the flashing brine, in the last stage of the heat rejection section. The intake seawater stream leaves the heat rejection section, where it splits into two streams. The first stream is the cooling seawater stream, which is rejected back to the sea, and the second is the feed seawater stream, which is mixed in the brine pool in the last flashing stage in the heat rejection section. Prior to the mixing location of the feed seawater stream, the rejected brine stream is withdrawn from the brine pool. On the other hand, the brine recycle is withdrawn from a location after the mixing point. The brine blow down is rejected to the sea and the brine recycle is introduced to the last stage in the heat recovery section. There are many types of MSF processes, Once-Through (MSF-OT) and Brine mixing type (MSF-M). Figure (2.10) shows the MSF-OT with its temperature profile. Figure (2.11) shows the MSF-M process with its temperature profile. Also Figure (2.12) shows a real schematic diagram of an existing MSF plant exists in Oman. The plant specification is presented in Table (2-1) [11].
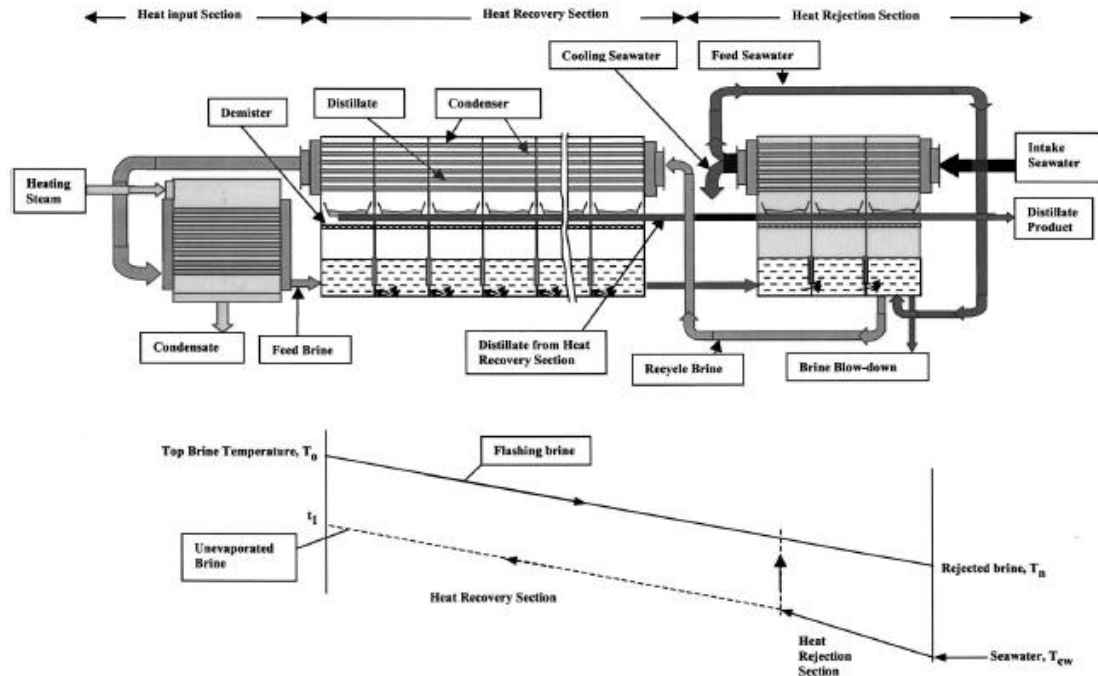


Figure (2.9) A schematic diagram of MSF brine recycle process

14
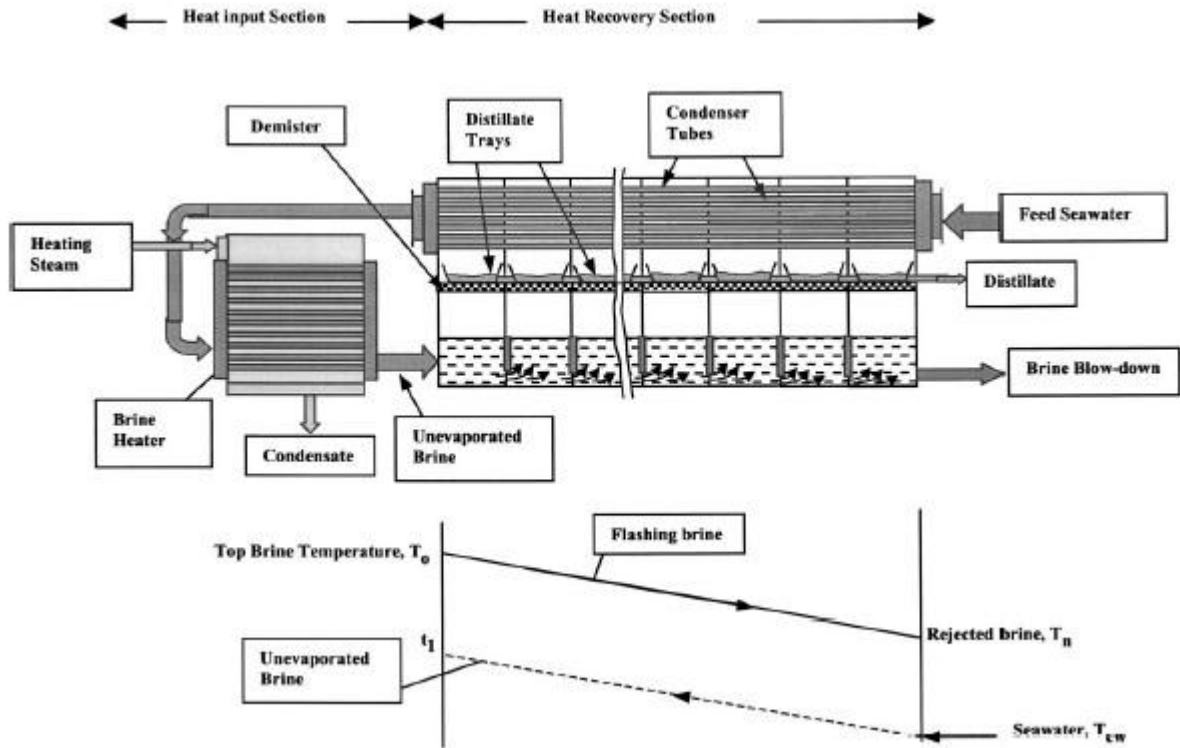
Figure (2.10) A schematic diagram of MSF-OT process
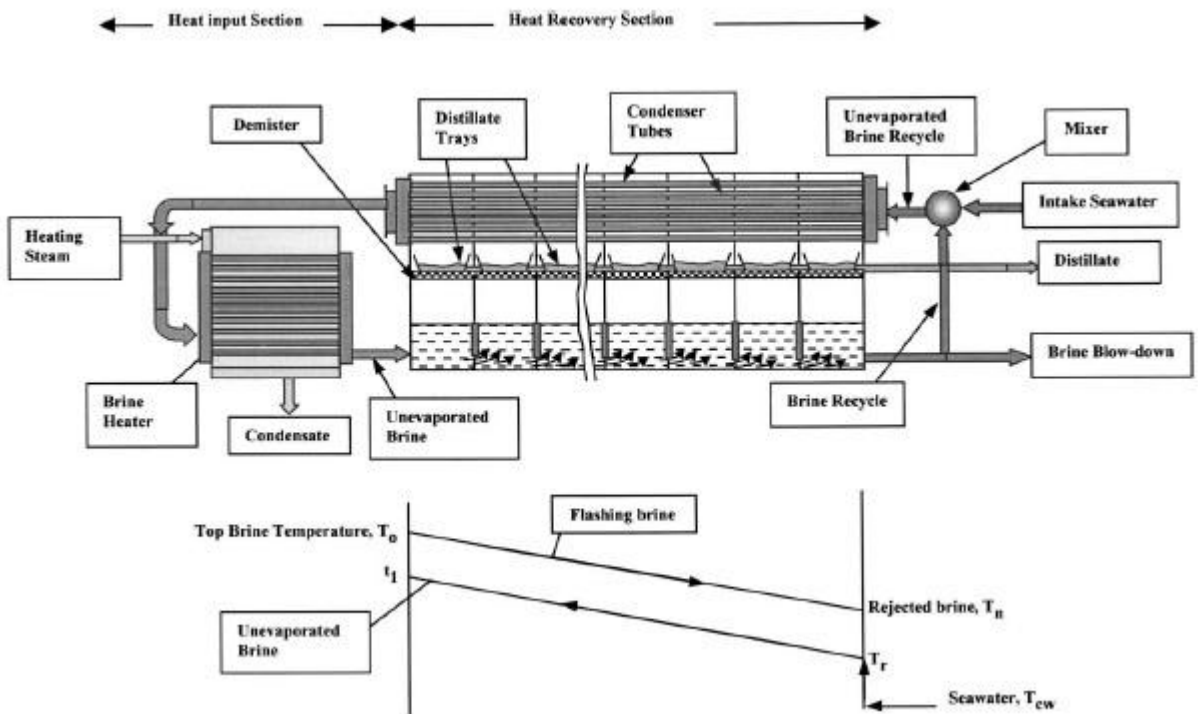

Figure (2.11) A schematic diagram of MSF-M process

Figure (2.12) shows a schematic diagram of a real MSF plant [11]

Table (2-1) A large MSF plant specification table

Process: - **MULTI-STAGE FLASH**
Client: - **MINISTRY OF ELECTRICITY AND WATER**
Country: - **OMAN**
Site: - **GHUBRAH POWER AND DESALINATION PLANT EXTENSION PHASE VI**
Contract Description: - **Design/Supply/Erection/Commissioning/Testing Turnkey Contract for 1 double deck Desalination Plant.**
Contract value: - **U.S.$ 50 million**
Contract Date: - **August 1999**
Capacity: - **31,822 m³ product per day**
Top Brine Temp: - **105ºC** Bottom Brine Temperature: - **42ºC**
Design Performance Ratio: - **7.0 : 1** Steam Req. (per unit): -_**18 bar (a) at a flow rate of 54.2 kgs/sec.**
Seawater TDS: - **39,255 ppm** Sea Water Req. (per unit): - **15,559 m³ / hr (Design Temp. 35ºC)**

Actually, a small range of top brine temperature beginning from 50 ºC can operate MSF processes. Solar stills, solar ponds and solar collectors can produce these small ranges of temperatures needed in flashing stages. An R&D partnership for development and implementation of solar desalination technology has been set up between the Swiss federal institute of technology, Atlantis Energy Ltd. and the Kuwait institute for scientific research a MSF plant operated by solar collectors (concentrating solar greenhouse collectors). R&D constructed a conventional 6 m³/day MSF plant with a brine maximum temperature of 120 ºC and coupled with a concentrating solar greenhouse collector and a hot water storage tank were used to run the plant [12]. The choosing of this type of solar collector was made to overcome the high price of ordinary solar collectors and by fixing it under the glass; it is protected against wind, ultraviolet rays and sand. Figure (2.13) shows the world's first MSF desalination plant, heated with solar collectors.
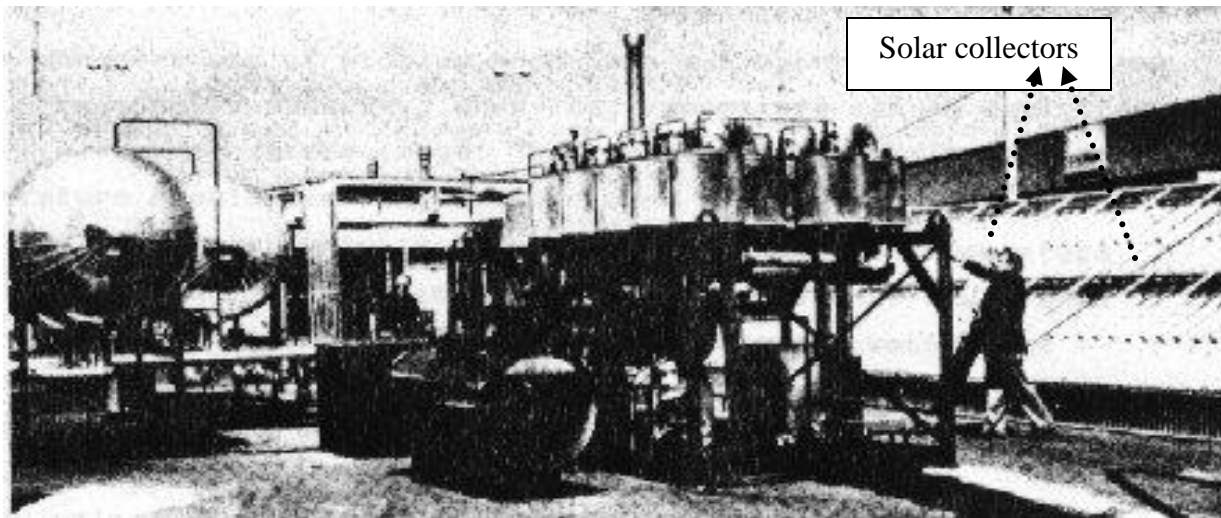


Figure (2.13) The worlds first MSF desalination plant,
heated with solar collectors [12]

For another example of using solar collectors with distillation processes (MSF), solar parabolic collectors' field could be connected to condenser/preheater heat exchangers. The steam generated by the solar field would drive the distillation plant. Figure (2.14) shows the design arrangement of the proposed solar MSF plant [9]. The preheated brine feed) leaves the condenser/preheater of the first cell (5). Then, the feed is separate in two different streams; the first one enters the brine heater (6) as the second one goes to the solar field (7). The brine streams that leave the solar field (11) and the brine heater (10) are mixed and sent to the first flash chamber to begin the multi-flash process (12). The steam generated by solar energy (8) condenses on the tube bundle of the brine heater. Therefore, the end temperature of the brine at the brine heater is lower than the end temperature of the brine at the solar field. Advantages of the system are as follows: First, since the system is modular, the capacity can be easily increased connecting in parallel

additional collectors and/or heat exchangers. Second, the simple design arrangement makes the system suitable for remote areas if its reliability and technical feasibility is proved. Finally, little auxiliary energy is required for control and pumping equipments.
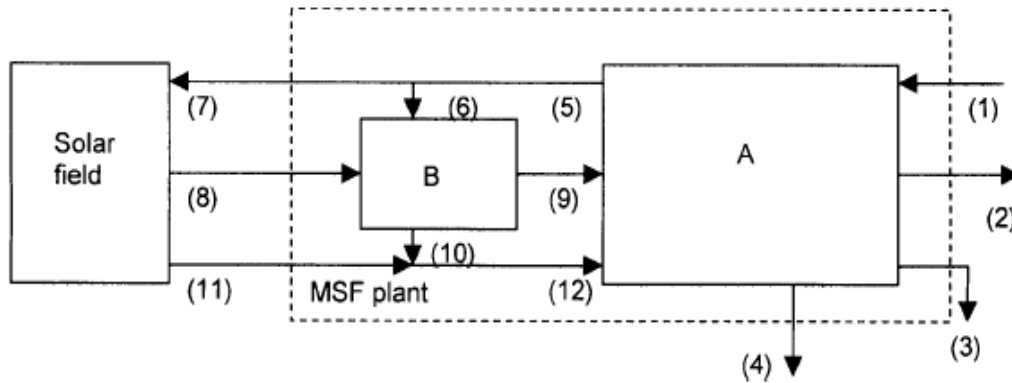


Figure (2.14) A solar multistage flash plant. B, brine heater; A, heat recovery and heat rejection sections. 1 seawater, 2 product, 3 blowdown, 4 cooling seawater outlet, 5–7 preheated brine, 8 steam, 9 condensed steam, 10–12 brine

For a larger use of solar energy operated with MSF plants, a scheme for large-scale desalination of seawater by solar energy was manufactured in Thar Desert of India [13]. The scheme has been using solar energy for the Thar Desert of India. The scheme has been designed to produce about $5.25 \times 10^7$ m$^3$/year of fresh water with 11.52 km$^2$ of collector area. The solar collectors are rectangular concrete tubes, half buried in the ground, through which seawater flows and is heated by solar energy. The heated seawater is then flash evaporated in MSF unit to yield fresh water. 415 wind turbines each of 200 kW capacity power pumping of the seawater to the site and through the MSF unit. Figure (2.15) shows the flow diagram of the MSF process and the solar field. The economic analysis that was made of this plant showed that it compares favorably with the existing fossil fuel fired desalination plants of the equivalent capacity.

18
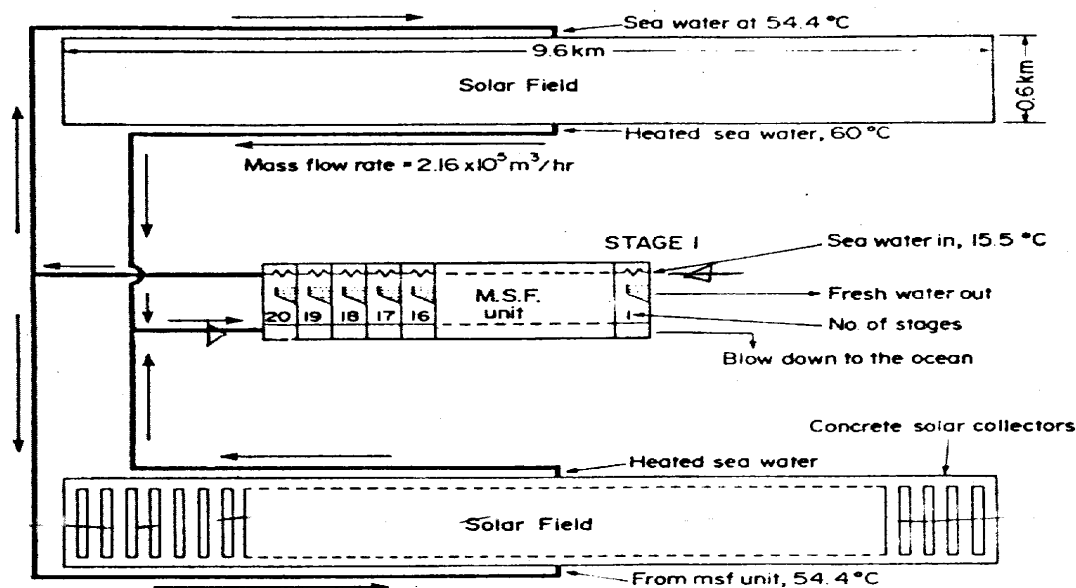
Figure (2.15) Flow diagram of the MSF process and the
solar field

Ziad M et al [14] investigated a small unit of MSF processes by solar collectors especially by flat plate solar collector type with a performance of a low temperature rang. In that work the boiler consisted of a double-glazed flat plate solar collector, a flash chamber, a water-cooled surface condenser, a circulating pump, and a temperature-controlled preheater to simulate constant temperature thermal storage. Data were obtained on this boiler from October 1980 to May 1981. During this period, the instantaneous total incident solar radiation at noon, as measured by a pyranometer in the plane of the collector ranged from 0.7 to 1.0 $kWm^{-1}$ and the diurnal total incident solar radiation ranged form 13 to 29 $MJ/m^2$.day. At these conditions the instantaneous efficiency of the collector ranged from 30 to 55 percent while the diurnal efficiency ranged from 20 to 44 percent. The advantages of that system represented as following: first, using solar flat plate collector is more favorable than solar still. Results indicates that the still area needed to produce one cubic meter per day on a yearly basis is about 400 $m^2$ and with the addition of about 100 $m^2$ for servicing the stills one can conclude that average figure of 500 $m^2$ of land area would be needed to produce one cubic meter of water per day. Second, the presence of the preheater is to manipulate a constant temperature after sunset. Third, the system is simple and not complicated and very easy at maintenance operations. Figure (2.16) shows the flow diagram of the system.
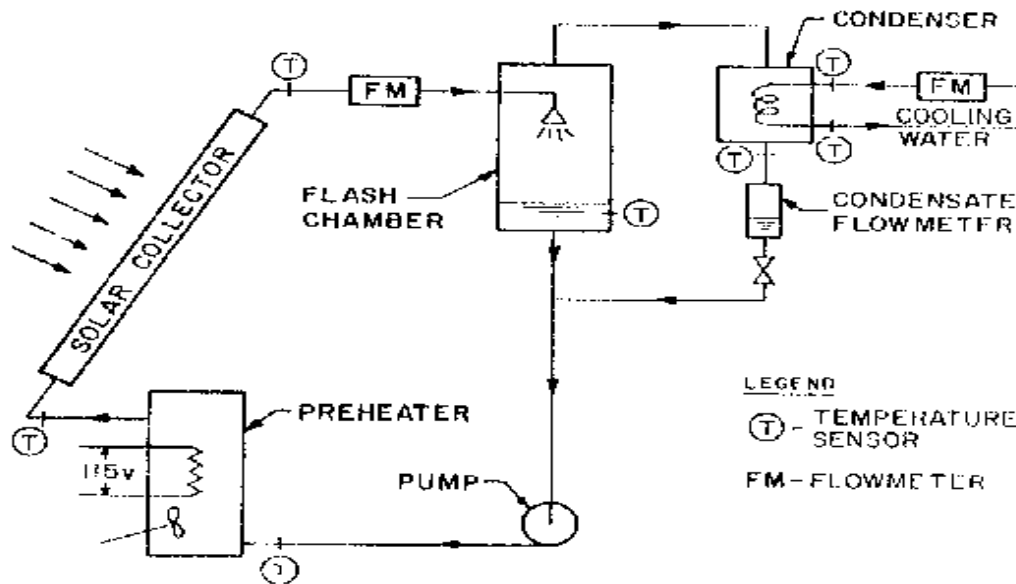
Figure (2.16) The flow diagram of the solar boiler
system

Figure (2.17) represents the design arrangement of the considered MSF system [5]. During daylight solar collectors heat the brine, and at nighttime a conventional energy supply drives the MSF plant. A control system chooses the operation mode, solar or fossil fuel, depending on the available solar irradiance. The fossil fuel mode is selected whenever the proper operation of the solar field is not possible, during the night or in cloudy periods. This system is completely complicated and the idea of using fossil fuel is not recommended for the ecology requirements.
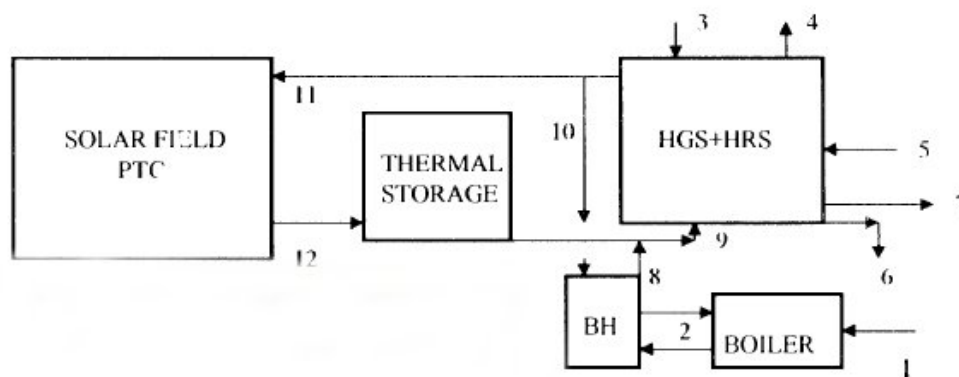


Figure (2.17) BH, brine heater; HGS, heat recovery section; HRS, heat
rejection section. 1 fossil fuel, 2 steam supply, 3, auxiliary
energy, 4 cooling seawater output, 5 seawater input,
6 blowdown, 7 fresh water, 8, 9 brine at its top temperature,
10, 11 preheated brine, 12 brine heated by the solar field

20

## 2.3 THE SUGGESTED CONFIGURATIONS OF FLASH PROCESSES USING SOLAR ENERGY

Different configurations can be obtained by combining the process units and streams. First; the idea description of the system is concluded as shown in Fig. (2.18). Simply the system is containing: solar water heater (FPC) (1) and flash evaporation unit (2) designed vertically and attached to the condenser/preheater unit (3). Feed water enters the condenser inlet point (4) at a known temperature then passing through the condenser tubes till out going from the outlet point (5) with a new temperature value caused by the heat transferred from the vapor that condensate across the outside tubes of the condenser unit. Then feed water enters the solar collector with its new temperature to gain the top brine temperature before entering the flash chamber. Then hot brine will enter the flash chamber by passing through the injector (6). This injector consists of 3 to 9 nozzles for spraying the feed. Each nozzle is operated at flow rate range between 4.5 to 10 kg/hr. The wasted brine then exits after releases its vapor (7) that will be condensate on the condenser tubes at the same time (8) to produce fresh water.
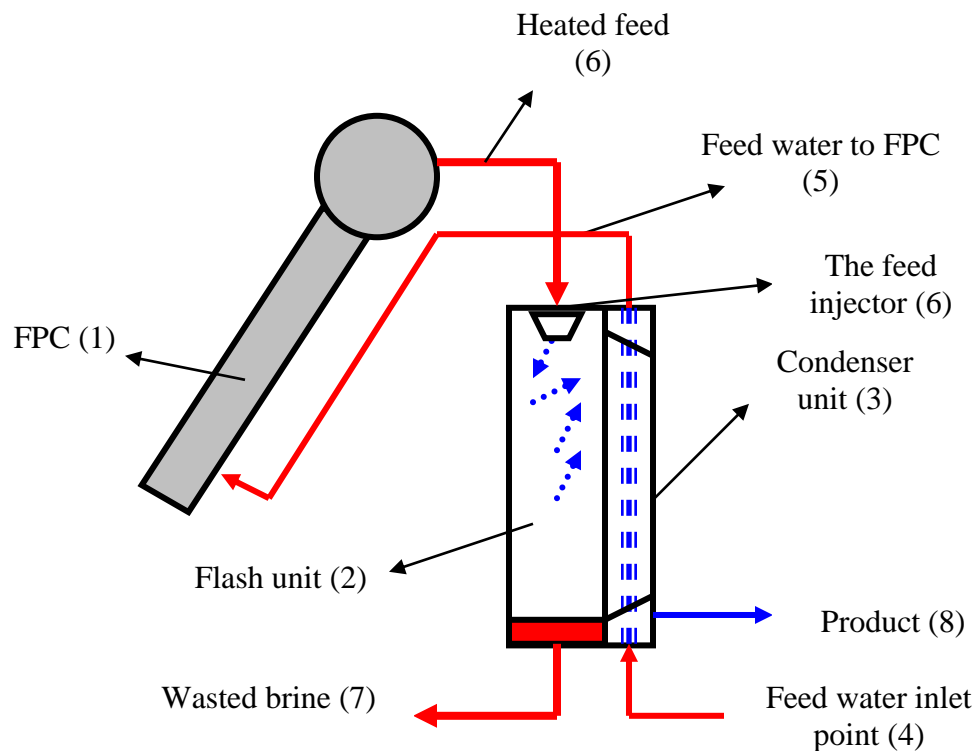


Figure (2.18) A schematic draw of the 1st configuration

21

For the second configuration, it involves a splitter and mixer units in the system to use the wasted brine again. The splitter unit is fixed at the outlet point of the brine from the flash unit, and the mixer unit is fixed at the inlet point of the condenser. Figure (2.19) represents a schematic diagram of the second configuration. It has advantage of using the wasted brine again in the process of heating. But increasing the energy of the inlet feeding water may cause an increasing in the energy that entering the collector and also will cause a decreasing in the effectiveness of the condenser unit. Increasing the inlet feed water temperature entering the collector may increase its efficiency. Also adding a splitter and mixer units to the system may increase the thermal losses to the ambient, will decrease the overall system efficiency and also will cause some problems in repair and control operations.
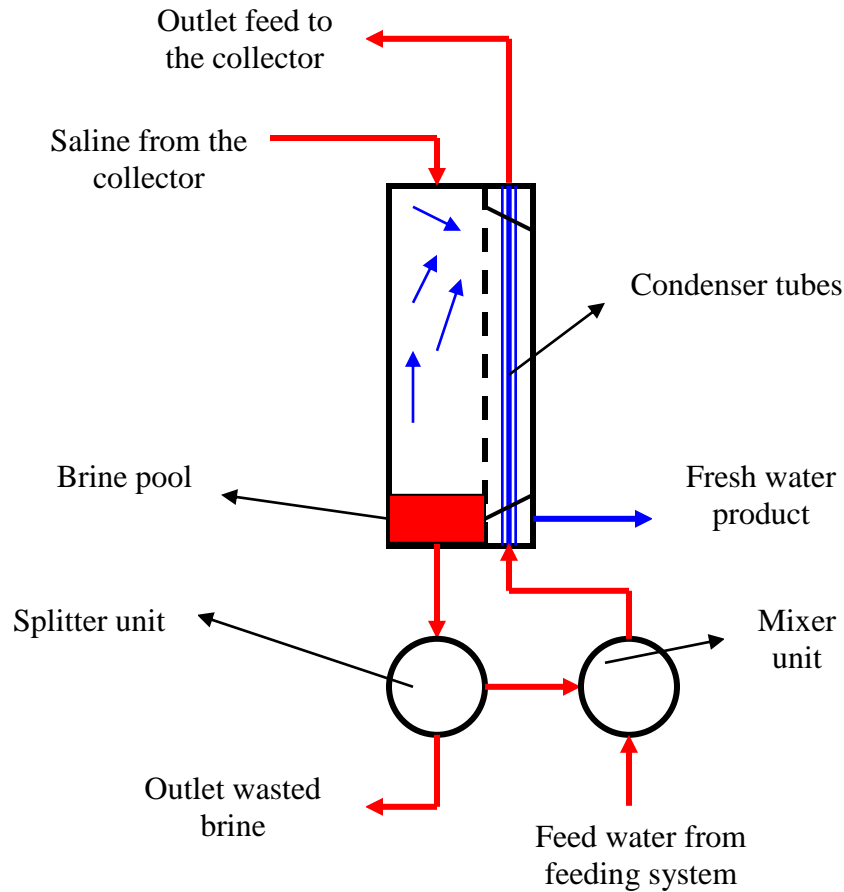
Figure (2.19) The schematic draw of 2nd configuration

The third configuration is shown in Fig. (2.20). The mixer unit is fixed at the outlet point of the condenser unit. The energy of the preheated brine through the condenser unit will gain energy again from the mixer unit before entering the solar collector without any effect on the condenser effectiveness.
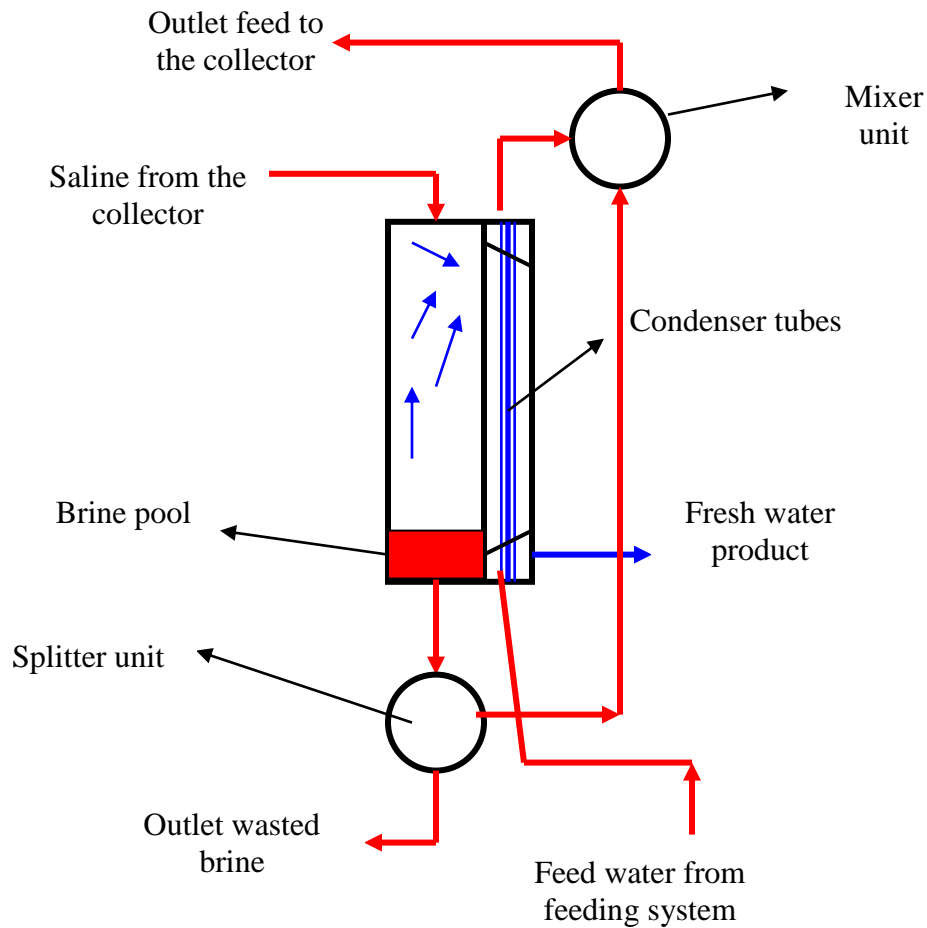
Figure (2.20) The schematic draw of 3rd configuration

## 2.4 PARAMETERS AFFECTING ON THE SYSTEM PRODUCTIVITY

There are many parameters (physical & environmental) affecting the system productivity and performance. Solar radiation, feed water flow rate, vacuum pressure, inlet feed water temperature and top brine temperature (TBT); all of these parameters are studied to show how it can be effect on the system productivity and performance.

### 2.4.1 The Effect of Solar Radiation

Solar flux is considered the prime mover in the operation of generating higher TBT [24]. Increasing in solar radiation may increase the heat gain to the feed water passing through the collector tubes, TBT, thermal losses and the system productivity. And that explains the reason of increasing the TBT in summer time against winter or midday results against

sun rise and sun set results. Also the useful energy collected in fact is depending on the thermal performance of the solar collector.

### 2.4.2 The Effect of Feed Water Flow Rate

Increasing feed water flow rate will increase the system productivity till a certain limit [24]. Because of using a thermal collector working as a brine heater; increasing the flow rate through the collector will decrease the time taken to transfer the useful energy from the absorber plate to the tubes (feed). So it is favorable to study this effect carefully just to synchronize between increasing or decreasing the TBT and the all system productivity.

### 2.4.3 The Effect of Vacuum Pressure

Increasing the value of negative pressure or increasing the pressure drop through the flashing chamber may increase the system productivity [24].

### 2.4.4 The Effect of TBT

The flashing efficiency operation occur in the flash chamber may increase caused by the increasing in TBT. Increasing the TBT with the feed flow rate will increase the inlet pressure to the stage and that also followed by increasing both of the pressure drop and system productivity [24].

### 2.4.5 The Effect of Inlet Feed Water Temperature

Preheating the inlet feed water flow rate before entering the condenser may increase the collector performance up to certain limit but will decrease the condensation surface area. This effect is not studied because it is an uncontrolled parameter.

### 2.4.6 The Effect of Collector Total Losses

Increasing in the total thermal losses (top losses, bottom losses, side losses and tubes losses) of the collector will decrease the collector efficiency and the TBT then the system productivity. This effect is studied in the next chapters.

### 2.5 THE AIM OF THIS WORK

In this chapter; a survey on the previous study on solar desalination technologies is made. The study shows that:
1.  It could be useful to simulate and design small units of solar desalination.

2. Small units of solar desalination techniques mean lower initial cost and ability of using it for small groups of people.
3. Flashing process, Multi effect process, humidification process and solar still technique; all of these technologies could be drive and operated by solar energy.
4. Lower TBT ranging between 50-80 $^{o}$C could drive a flashing process.

So the main objectives of this work are:

1- Egypt is a very high insolation country around the world. The sun shines hours almost equal to 3600hour/year. Also, Egypt has a water shortage problem. It is very important and valuable to utilize this huge energy in desalinating technology. Therefore, the first objective of this work is to examine a suitable configuration for producing the fresh water using the solar energy and MSF process?

2- Examining the performance of the selected configuration under different operating conditions is the second main objective.

3- Developing a simulating program to predict the productivity of the small size unit of MSF Process by using solar energy for different configurations is the third objective.

4- Evaluating the experimental and theoretical results is one of the main objectives of this study.

5- Studying the system productivity enhancement using surfactant additives.

# CHAPTER 3

# THE MATHEMATICAL MODEL

## 3.1 INTRODUCTION

In this chapter, numerical models of the system units are presented. Using this numerical model, the system performance is examined under different weather and operating conditions. A modular computer program is developed, and different configurations of the system are examined. The mathematical models for three different system configurations are studied in this chapter. The first configuration is once through desalination system containing single flash unit and flat plate solar collector works as a brine heater to supply a suitable top brine temperature. In the second configuration a known fixed quantity of outlet brine from the flashing chamber is mixed with the inlet feed water to the condenser unit. That's mean, mixing point at the inlet of the condenser. In the last configuration, the mixing point with the feed water is made at the outlet of the condenser unit before entering the solar water heater. The full developed equations are investigated and rearranged together for the three configurations and solved by matrix algebra technique.

## 3.2 SOLAR COLLECTOR MATHEMATICAL MODEL

Flat plate collectors are sophisticated as a greenhouse that traps the heat from the sun to rise the temperature of water up to about 70 ºC. Useful energy from the sun is transferred to the tubes that are mounted with the absorber plate. Solar collectors are widely used to provide hot water in hospitals, hotels, buildings, industrial applications and for thermal energy systems. The solar liquid heaters especially flat plate solar collector generally consists of a sheet of thermally conductive material called absorber plate to which are bonded the tubes carrying the heat transfer liquid, usually water. Solar radiation is transmitted through the transparent cover and is converted to heat on the absorber plate [26]. In this work, the solar collector (flat plate type) is coupled with a flashing unit to work as a boiler as a main source of heat. This thermal system presents a good real example about how to drive desalination units by using solar collectors such as flat plate collectors. The used collector is manufactured by Solar Energy Corporation Company at Cairo-Egypt. The measurement of the efficiency of solar devices is of prime importance for their application, the sizing of solar systems, and cost estimation [25]. So it's very important to calculate the thermal performance of the solar collector by evaluating and calculating all effective performance parameters such as, the overall heat loss, fin efficiency, efficiency factor, heat removal factor, solar collector thermal efficiency, and the collector effectiveness. All of these performance parameters are presented in this chapter.

### 3.2.1 The Overall Heat Loss Calculations

It is useful to develop the concept of an overall loss coefficient for solar collector to simplify the mechanism of losses through the collector [27]. Figure (3.1) represents the cross section in the solar water heater used as a boiler in the desalinating system. Solar flux is dropped on the glass cover, most of the rays is passed through the glass cover and is absorbed by the absorber plate and the energy is transferred to the tubes by conduction then convection to the liquid that passing through the tubes. Some of the dropped rays will reflected from the glass cover. By knowing the total losses through the collector; the real performance parameters will achieve because of most of these performance parameters like fin efficiency, efficiency factor and effectiveness considered function of the overall loss.
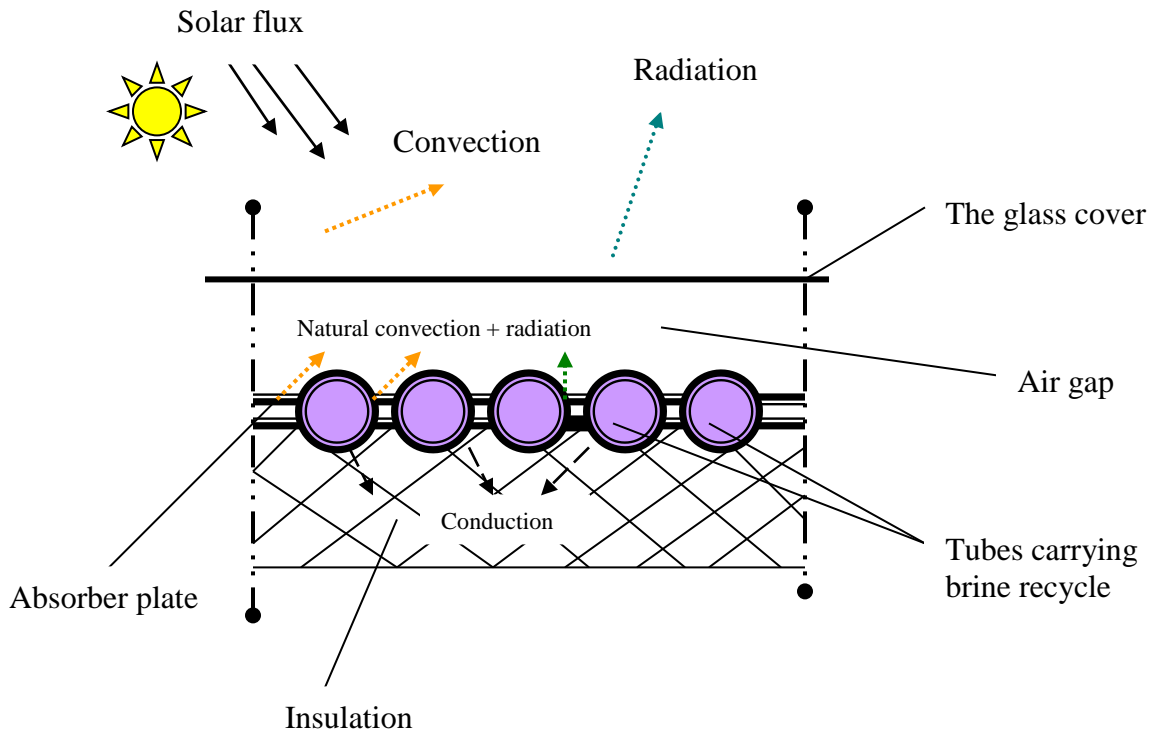


Figure (3.1) Collector heat loss mechanism

As it knew, solar flux is the sum of all heat losses and the useful energy transferred to the user. The main equation that described this relation is presented as following [31]:

$$I_S \times A_c = Q_{loss} + Q_u + Q_{stg} \qquad (3.1)$$

Where $I_S$ is the energy from the sun, $A_c$ is the collector effective area, $Q_{loss}$ is the heat loss from the collector and $Q_u$ is the useful energy transferred from the absorber plate to the flash chamber tubes and $Q_{stg}$ is the energy stored in the collector and could be vanished. The process of transferring the energy from the sun can be expressed in four steps. The 1st step is occurs while the flux reaches the glass cover, the 2nd when reaches

the absorber plate, The 3$^{rd}$ when the energy is transferred to the liquid that passes through the tubes and the final step that some portion of the energy is transferred to the insulation. The heat-loss mechanism from the absorber plate to the ambient is presented in Fig. (3.2).

Figure (3.2) shows that heat is lost from the top of the absorber plate by natural convection and by radiation to the interior surface of the glass cover plate. (Some of the radiation will actually pass through the glass cover, but this will be neglected in this analysis). This heat is conducted by the glass plate to its exterior surface, from which it is transferred to the outdoor atmosphere by convection and radiation, conducts this heat. The heat loss is expressed by Frederick [30] as;

$$Q_{loss} = A_c U_l F'(\overline{T}_f - T_{amb}) \tag{3.2}$$

The overall heat loss of the collector $U_l$ is the summation of three components; the top loss $U_t$, the bottom loss $U_b$, and the edge loss $U_e$ and the other variables are defined in the nomenclature.

$$U_l = U_t + U_b + U_e \tag{3.3}$$

Where, the bottom and edge losses are calculated respectively as following [46]:

$$U_b = k_b / l_b \tag{3.4}$$

$$U_e = (k_e / l_e) \times \frac{2(C_L + C_W)C_h}{C_L \times C_W} \tag{3.5}$$

The reciprocal of $U_t$ is the sum of the resistances to heat transfer from plate to ambient, which are represented by the simple parallel-series circuit of Fig. (3.2) [26]. The general equation of the resistance of the top heat-loss for the collector is,

$$R_t = \frac{1}{U_t \times A_c} = \frac{y}{K_{ins}} + \frac{1}{h_i + h_{ri}} + \frac{t}{K_g} + \frac{1}{h_o + h_{ro}} \tag{3.6}$$

And,

$$U_t \times A_c = 1 / R_t \tag{3.7}$$

All heat transfer coefficients are represented as following,

For natural convection from the glass cover to the air,

$$h_o = 5.7 + 3.8 \times V_w \tag{3.8}$$

Where,

$V_w$ is considered the wind speed in m/s and $h_o$ is the external heat transfer coefficient to the ambient.

For external radiation, the heat transfer coefficient can be calculated as following,

$$h_{ro} = \frac{\varepsilon_c \cdot \sigma \cdot (T_g^4 - T_{sky}^4)}{T_g - T_{sky}} \tag{3.9}$$

Where,

$T_{sky}$ is the approximate sky temperature and is given by Swinbank [27] as

$$T_{sky} = 0.0552(T_{amb}^{3/2}) \tag{3.10}$$

And $T_{amb}$ is the ambient temperature in degrees Kelvin (K).

To the ambient
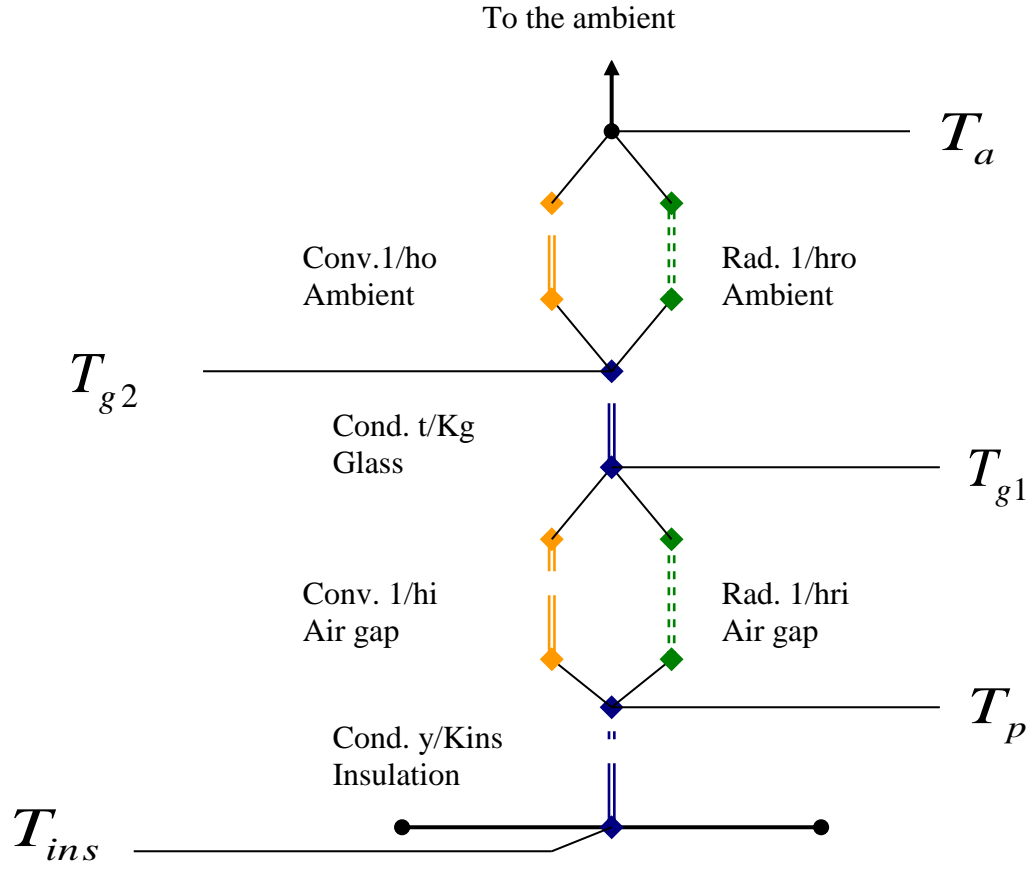


Figure (3.2) Equivalent circuit for the resistance to heat transfer
through the top of the collector

For the air gap distance between the glass cover and the absorber plate, it's considered a natural convection and radiation resistance as regarded later. For the inner heat transfer coefficient $h_i$ between the absorber plate and the glass cover it is represented as following,

$$R_{a_L} = Gr_L \cdot \text{Pr} = \frac{g \cos \beta \cdot \text{B}(T_p - T_{pm})L^3}{\nu \alpha} \tag{3.11}$$

Where, $\beta$ is the collector tilt angle and $T_{pm}$ is the mean temperature difference between the plate temperature and the glass cover temperature for the air gap that equal,

$$T_{mp} = \frac{T_p + T_g}{2} \tag{3.12}$$

All parameters like ($\alpha$, $\nu$, B, $K_f$ and Pr) can be evaluated at $T_{pm}$

And,

$$\overline{Nu_L} = \overline{h_i}L / K_f = 0.54 R_{a_L}^{1/4} \qquad (10^4 \leq R_{a_L} \leq 10^7) \tag{3.13}$$

For parallel plates the Nusselt number is the ratio of a pure conduction resistance to a convection resistance, so that a Nusselt number of unity represents pure conduction. In

more recent experimental study using air, Hollands et al. (1976) give the relationship between the Nusselt number and Rayleigh number for tilt angles ranges from 0 to 75° as [27]

$$Nu = 1 + 1.44 \left[ 1 - \frac{1708(\sin 1.8\beta)^{1.6}}{Ra \cos \beta} \right] \left[ 1 - \frac{1708}{Ra \cos \beta} \right] + \left[ \left( \frac{Ra \cos \beta}{5830} \right)^{1/3} - 1 \right] \qquad (3.14)$$

After substituting equation (3.12) in (3.11) and evaluating the results in equation (3.14), the heat transfer coefficient for the inner air gap between the glass cover and the absorber plate $h_i$ is found. The radiation part could be found by the following equations,

$$h_{ri}(T_p - T_g) = \frac{\sigma(T_p^4 - T_g^4)}{\dfrac{1}{\varepsilon_p} + \dfrac{1}{\varepsilon_g} - 1} \qquad (3.15)$$

Since,

$$h_{ri} = \frac{\varepsilon_p \varepsilon_g (T_p + T_g)(T_p^2 + T_g^2)}{\varepsilon_p \varepsilon_g - \varepsilon_p \varepsilon_g} \qquad (3.16)$$

To evaluate the heat transfer coefficients by convection through the tube, the following relation should be calculated. The useful energy that transferred to the fluid that passing through in the pipes in the water heater may be calculated by the following,

$$m^. = \rho A_p \overline{V} / n_p \qquad (3.17)$$

Where $n$ is the number of tubes, $D_p$ the pipe diameter, $A_p$ pipe cross section area and $\overline{V}$ is the average flow velocity m/s. Pipe cross section area is found by equation (3.18),

$$A_p = \frac{\Pi}{4} \times D_p^2 \qquad (3.18)$$

For turbulent or laminar flow passing through the pipe,

$$R_e = \frac{\rho \overline{V} D_p}{\mu} \qquad (3.19)$$

After estimating all variables and parameters, heat transfer coefficient for the internal flow through the pipe can be estimated by equation (3.20),

$$\overline{Nu} = \frac{\overline{h_f} D_p}{K_f} = 0.023 R_e^{0.8} \text{Pr}^{0.4} \qquad (3.20)$$

An empirical equation for the top losses $U_t$ that is useful for both hand and computer calculations was developed by Klein (1975) [27].

$$U_t = \left[ \frac{NG}{\dfrac{C}{T_{mp}} \left[ \dfrac{(T_{mp} - T_{amb})}{(NG + f)} \right]^e} + \frac{1}{h_w} \right]^{-1} + \frac{\sigma(T_{mp} + T_a)(T_{mp}^2 + T_{amb}^2)}{(\varepsilon_p + 0.00591 NG \times h_w)^{-1} + \dfrac{2NG + f - 1 + 0.133 \times \varepsilon_p}{\varepsilon_g} - NG}$$

$$(3.21)$$

Where, NG is the number of glass covers, $f = (1 + 0.089 h_w - 0.1166 h_w \varepsilon_p)(1 + 0.07866 NG)$, $C = 520 \times (1 - 0.000051 \beta^2)$ for

$0° < \beta < 70°$, $e = 0.43(1 - 100/T_{pm})$ where $\beta$ is the collector tilt angle in degree and $h_w$ is considered the wind heat transfer coefficient and equal to $h_o$ as presented above in equation (3.8).

### 3.2.2 Fin Efficiency, *F*

The fin efficiency is probably the single most important parameter in the design of liquid-type solar collectors. The absorber plate transfers its heat by conduction to the tubes, which are mechanically and thermally bonded to the absorber plate [26]. The fin efficiency equation is given as equation (3.22);

$$F = \frac{\tanh\left[\sqrt{\frac{U_t}{k\delta}\left(\frac{s_t - d}{2}\right)}\right]}{\sqrt{\frac{U_t}{k\delta}\left(\frac{s_t - d}{2}\right)}} \tag{3.22}$$

Where $U_t$ is the top loss, $s_t$ is the tube spacing, $d$ is the tube inner diameter, $k$ is the thermal conductivity and $\delta$ is the fin thickness. Also Fig. (3.3) shows the relation between the factors $\sqrt{\frac{U_t}{k\delta}\left(\frac{s_t - d}{2}\right)}$ and the fin efficiency parameter.
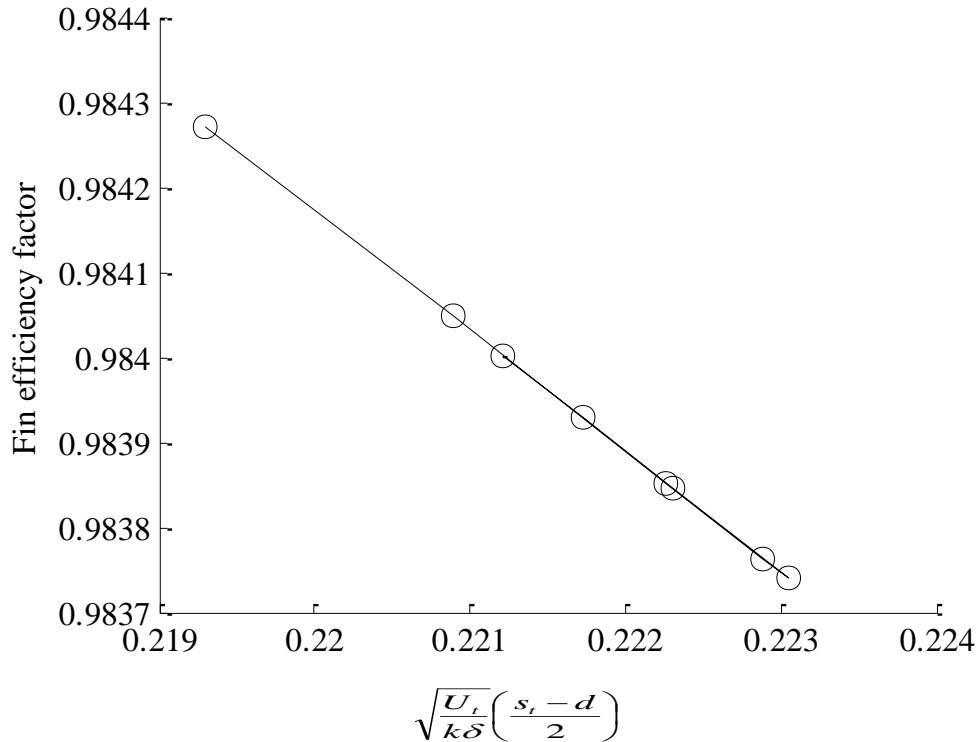


Figure (3.3) The fin efficiency curve of the flat plate collector

31

For any solar collector (FPC), fin efficiency is a measure of how well the radiator absorbed and converted into heat is conducted into base region of the fin. A survey of commercial collector, values of fin efficiency ranging from 0.92 to 0.95. Figure (3.4) shows a schematic diagram of the heat balance on a fin element.
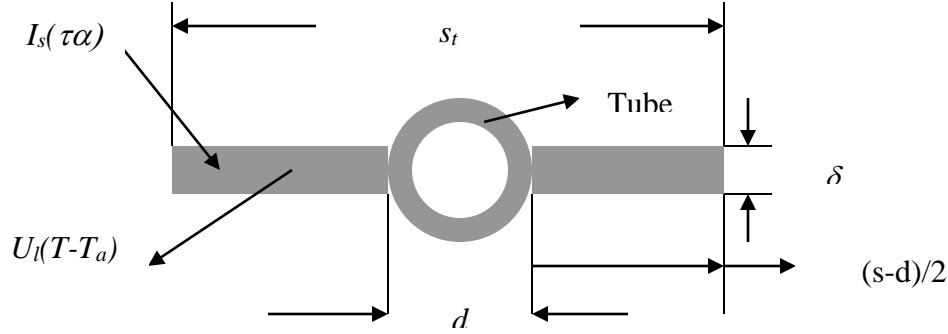


Figure (3.4) Schematic diagram of the heat balance on a fin element

### 3.2.3 Efficiency Factor, $F^{'}$

Because the temperature $T_p$ of the absorber plate varies both across and along the plate, the collector heat gain and efficiency equations are usually expressed in terms of inlet fluid temperature, which is relatively easily controlled and measured during testing and operation [26]. Efficiency factor $F^{'}$ allow using the average fluid temperature, so the efficiency factor is considered an important design parameter. Equation (3.23) represents the efficiency factor as following:

$$F^{'} = \frac{\dfrac{1}{U_t}}{s\left(\dfrac{1}{U_t[(s_t - d)F + d]} + \dfrac{1}{\dfrac{kb}{l}} + \dfrac{1}{h_f \pi d_i}\right)} \tag{3.23}$$

Where $b$ is the length of the bond and $l$ the thickness. The ratio $kb/l$ is called the bond conductance $C_b$. the resistance to heat flows between the tube wall and the fluid is $1/h_f \pi d_i$, where $h_f$ is the fluid convection coefficient and $d_i$ is the inside tube diameter.

### 3.2.4 Heat Removal Factor and Flow Factor, $F_R, F^{''}$

It is convenient to define a quantity that relates the actual useful energy gain of a collector to the useful gain if the whole collector surfaces were at the fluid inlet temperature [27]. The following expression presents the heat removal factor.

$$F_R = F^{'} \times \frac{GC_p}{U_t F^{'}}\left(1 - \exp-\left(\frac{U_t F^{'}}{GC_p}\right)\right) \tag{3.24}$$

Where $G=m/A_c$.

The flow factor parameter may be exists by dividing the heat removal factor and the efficiency factor.

$$F^{"} = \frac{F_R}{F^{'}}$$
(3.25)

Figure (3.5) shows the collector flow factor curve as a function of $\dot{m}C_p / A_cU_tF^{'}$. The quantity $F_R$ is equivalent to the effectiveness of a conventional heat exchanger, which is defined as the ratio of the actual heat transfer to the maximum possible heat transfer. The maximum possible useful energy gain in solar collector occurs when the whole collector is at inlet fluid temperature; heat losses to surroundings are then at a minimum. The collector heat removal factor times this maximum possible useful energy gain is equal to the actual useful energy gain $Q_u$ [27]:

$$Q_u = A_cF_R\left[I_S - U_t(T_{fi} - T_{amb})\right]$$
(3.26)
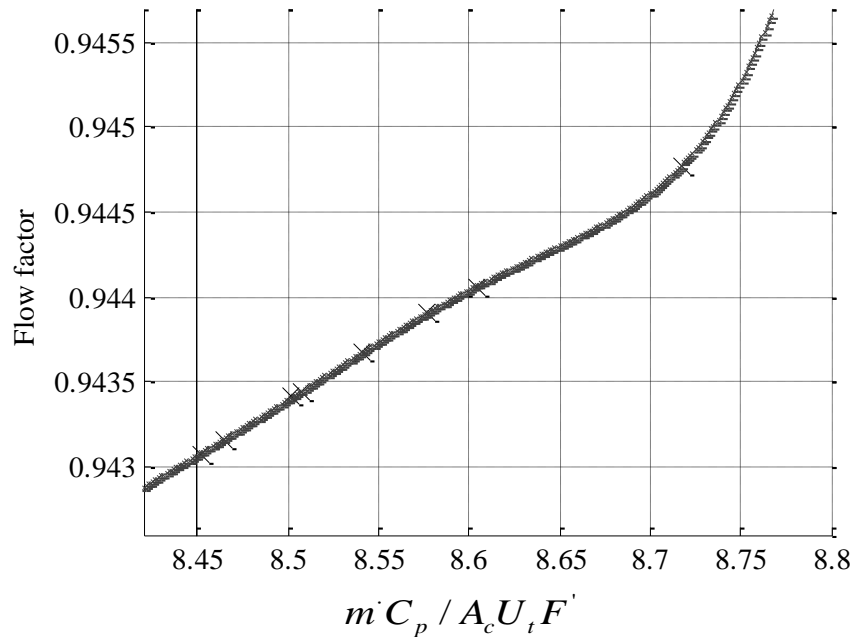


Figure (3.5) The flow factor curve of the flat plate collector

### 3.2.5 The Instantaneous Thermal Efficiency Equation of the Collector

One of the basic characteristics of the solar collector is its efficiency, which is usually determined from the results of field tests [31]. The heat gain or useful output of the collector is given as $F_R\left[I_S(\tau\alpha) - U_t(T_{fi} - T_{amb})\right]$. By dividing the output by the input, the thermal efficiency equation becomes,

$$\eta_{thc} = F_R(\tau\alpha) - F_RU_t\left(\frac{T_{fi} - T_{amb}}{I_S}\right)$$
(3.27)

33

For a given construction the collector efficiency depends on the operating regime parameters and the meteorological parameters. Since the overall number of variables is quite large and the field test conditions are always unsteady, it is difficult in practice to study the influence on the efficiency of each of these parameters, particularly the external influences [31]. Actually any increasing in the inlet flow temperature represents a decreasing in the thermal efficiency of the collector. Also the increase in collector efficiency at near ambient temperatures can easily be explained from the fact that, at temperature close to the reference temperature, the overall losses from the collector are minimal compared to when the temperature difference between the collector and ambient is very high [32]. Figure (3.6) shows the calculated efficiency curve for the flat plate collector.
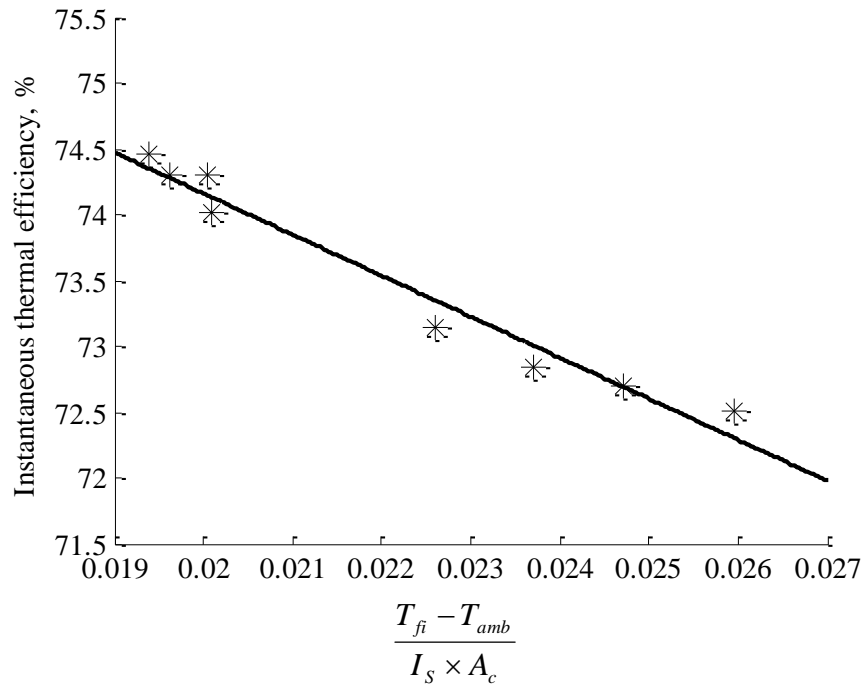


Figure (3.6) The instantaneous efficiency curve of the collector

### 3.2.6 The Collector Effectiveness, $\varepsilon_c$

Although the flat plate collector can be considered to be a special kind of heat exchanger, the concepts of heat exchanger theory are rarely used in solar engineering. Indeed, the heat removal factor being identified as the effectiveness of the collector does not seem consistent with heat exchanger theory [28]. In heat exchangers the temperature of each fluid changes as it passes through the exchanger, and hence the temperature of the dividing wall between the fluids also changes along the length of the exchanger. In heat exchanger design the efficiency of the heat transfer process is very important. Heat exchanger effectiveness $\varepsilon$ is defined as the ratio of the actual heat transferred to the

maximum possible heat transfer. In a flat plate collector the heat transfer occurs between the absorber plate and the cooling fluid. J. C. Francken expressed the effectiveness correlation as a function of efficiency factor.

$$\varepsilon_c = \frac{1 - \exp(-NTU_c(1 - F^{'}))}{1 - F^{'}\exp(-NTU_c(1 - F^{'}))} \tag{3.28}$$

Where $NTU_c$ is the number of transferring units of the collector heat exchanger and equal to $U_l A_c / m^{\cdot} C_p$.

It may be noted that the effectiveness, $E$ is defined by Edwards and Phillips is quite different from $\varepsilon_c$, as defined above in equation (3.29) [25].

$$E_c = 1 - \exp(-NTU_c(1 - F^{'})) \tag{3.29}$$

This means that $NTU_c(1 - F^{'})$ being given, $E$ does not explicitly depend on $F^{'}$, whereas $\varepsilon_c$ is very sensitive to the changes in $F^{'}$. For simplification, the term $NTU_c(1 - F^{'})$ may be considered as flow parameter $\phi_c$ of the collector.

$$\phi_c = NTU_c(1 - F^{'}) \tag{3.30}$$

For the effectiveness, it is varying versus the changing in flow parameter $\phi_c$. That's means large values of $\phi_c$ and a considerable temperature rise of the fluid in the flow direction [25]. The collector effectiveness may be expressed as a function of the collector tube effectiveness. The tube effectiveness equation presented by [29] as following;

$$\varepsilon_t = SNTU(1 - \exp(-1/SNTU)) \tag{3.31}$$

Where $SNTU$ is the solar number of transfer units, $m^{\cdot} C_p / F^* U_t A_t$ where $F^*$ is the collector parameter and is equal to;

$$F^* = \frac{W_e C_b h_f}{\pi d_i (C_b h_f + W_e U_t h_f) + W_e U_t C_b} \tag{3.32}$$

Where the effective tube spacing is;

$$W_e = (s - d_o)F + d_o \tag{3.33}$$

$SNTU$ presenting the ratio of the potential for the fluid to absorb energy to the loss potential for the solar collector. As the $SNTU$ increases, more energy is transferred to the fluid. However, the tube effectiveness is not a complete measure of the performance of the solar collector [29]. The relationship for the collector effectiveness as a function of $SNTU$ parameter is determined as following;

$$E_c = \psi(SNTU(1 - \exp(-1/SNTU))) \tag{3.34}$$

Where,

$$\psi = N_{tubes}F^* A_p / A_r \tag{3.35}$$

The collector effectiveness, as defined above describes only the heat transfer performance of the solar collector. The parameter $\psi$ is an overall design variable and is required to relate the tube effectiveness to the solar collector effectiveness. The parameter $\psi$ will have a value less than unity, whenever the heat transfer area for the working fluid is less than the absorber area [29]. So, for given values of $I_s$, $U_l$, $T_{Fi}$, and $T_{amb}$, the specific useful heat flux i.e. a maximum for maximum $F_R$. This means the lowest possible value of $\phi_c$ has to be used, i.e. the maximum specific flow rate. For known Julian day of the year, the

collector equations which are presented previously are calculated by a simulation program. Just environmental data and design parameters are fed to the program. After some iteration; the simulation program would estimate the collector performance parameters. Heat removal factor, efficiency factor, flow factor and fin efficiency; all of these performance parameters are presenting a good evaluation of the collector performance. Also there are some important physical parameters affecting the performance of solar collector like wind velocity, flow rate, temperature of the inlet fluid to the collector and indeed the solar intensity. A better performance of the considered collector not only depending on the reducing the heat loss from the collector but also depending on many terms that must be considered to insure a good collector design such as: the paint of the absorber plate, efficiency of the absorber plate to transfer the suitable heat, good insulation to prevent heat losses, and also transmittance of cover system.

## 3.3 FLASH UNIT MODEL

For a flash stage unit in Fig. (3.7), the thermodynamics analysis of this part is divided into two main sections, the first was about the flashing chamber and the other is the condenser/preheater. The mathematical model is based on the following assumptions:
1. The distillate product is salt free.
2. The flash chamber is in equilibrium with the brine leaving the stage.
3. The distillate vapor always condenses completely.

The energy balance for the flashing brine is expressed as follows [33],
$$B_o^{\cdot} h_o(T_{bo}, x_{bo}) = B_1^{\cdot} h_{b1}(T_{b1}, x_{b1}) + [(B_o^{\cdot} - B_1^{\cdot}) H_{V1}(T_{b1}, P(T_o))] \tag{3.36}$$
Where,
$$B_1^{\cdot} = W_{b1} + X_{b1} \tag{3.37}$$
Equations (3.38) and (3.39) below shows the overall mass balance for both flash and condenser units,
$$B_o^{\cdot} = D_1^{\cdot} + B_1^{\cdot} \tag{3.38}$$
$$F_i^{\cdot} = F_o^{\cdot} \tag{3.39}$$
And the flash unit enthalpy balance is;
$$B_o^{\cdot} h_o + F_i^{\cdot} h_{Fi} = B_1^{\cdot} h_{b1} + D_1^{\cdot} h_{D1} + F_o^{\cdot} h_{Fo} + Q_{loss} \tag{3.40}$$
While the overall heat transfer coefficient is represented by the following equation [14],
$$U_1 = f(\phi, T_{Fi}, T_{Fo}, T_{D1}, ID_1, OD_o, FF, R_F) \tag{3.41}$$
The amount of heat exchanges across the condenser heat transfer surface $Q_1$ is calculated by equation (3.42) [33],
$$Q_1 = m_{Fi,o}^{\cdot} c_p (T_{Fo} - T_{Fi}) = U_1 A_1 \times \Delta T_{lm1} \tag{3.42}$$
From equation (3.7),
$$\frac{U_1 \times A_1}{m_{Fi,o}^{\cdot} c_p} = \ln \frac{T_{D1} - T_{Fi}}{T_{D1} - T_{F0}} = -\ln \frac{T_{D1} - T_{F0}}{T_{D1} - T_{Fi}} \tag{3.43}$$
From equation (3.43), the following equation is obtained:
$$(1 - E) \times T_{Fi} + E \times T_{D1} - T_{Fo} = 0 \tag{3.44}$$

36

Where $E = 1 - e^{-NTU_1}$ and $NTU_1 = U_1 \times A_1 / \dot{m}_{Fi,o} c_p$

$$T_{d1} = T_{b1} - NEA - BPR \tag{3.45}$$

The non-equilibrium allowance *NEA* and *BPR* are calculated by the following equations [14];

Where,

$$NEA = A + B \times T_{b1} + C \times T_{b1}^2 + D \times T_{b1}^3 \tag{3.46}$$

Where *A*=2.556, *B*=-0.203E-1, *C*=-0.129E-1, and *D*=0.1123E-5

$$BPR = (B + C \times X) \times X \tag{3.47}$$

Where,

$$10^3 \times B = 6.71 + 6.43 \times 10^{-2} \times T_{b1} + 9.74 \times 10^{-5} \times T_{b1}^2$$

$$10^5 \times C = 2.38 + 9.59 \times 10^{-3} \times T_{b1} + 9.42 \times 10^{-5} \times T_{b1}^2$$
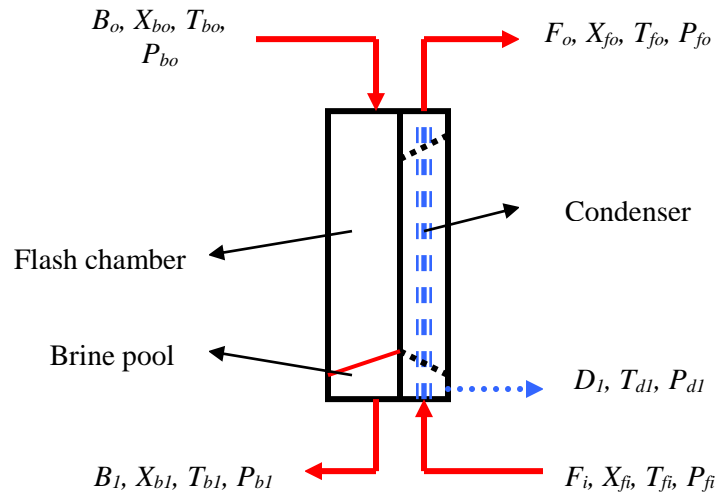


Figure (3.7) A flash stage unit

Using the measured values of solar intensity, wind velocity and ambient temperature as input data, the daily estimated productivity of the system can be calculated. The average values for climatic conditions such as ambient temperature, inlet seawater temperature, wind speed and solar intensity are taken during the day hours. Using these conditions, with initializing the unknown temperatures; the system units' heat transfer coefficients are calculated. With a reasonable specific tolerance, the mathematical model is solved by Gauss-Seidel iteration method.

## 3.4 MIXER AND SPLITTER MODEL

For the splitter unit mathematical equations, the output streams have the same properties as the input stream, only the mass flow rates are different. Equalities of temperature and pressure into and out of the unit like this,

$$T_{bi} = T_{bo1} = T_{bo2} \tag{3.48}$$

$$P_i = P_{o1} = P_{o2} \tag{3.49}$$

For the material balance [33],

$$B_i = B_{o1} + B_{o2} \tag{3.50}$$

Where B is the brine containing salt and water.

So,

$$B_{o2} = \alpha \times B_i \tag{3.51}$$

And,

$$B_{o1} = (1 - \alpha) \times B_i \tag{3.52}$$

Where $\alpha$ = splitter ratio.

Figure (3.8) represents a schematic draw of the splitter unit.
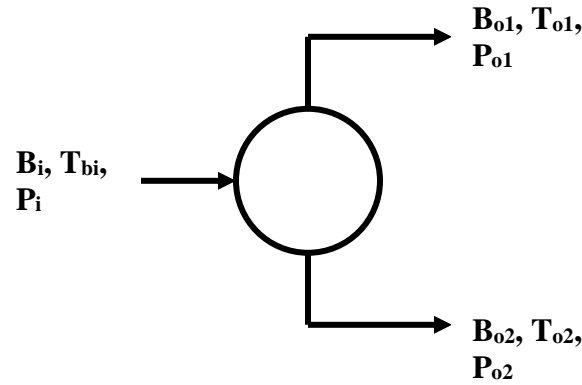


Figure (3.8) The schematic draw of the splitter
unit

The mixer unit can be thought of as the union of two pipes or a mixing tank with two inputs, and only one output streams as shown in Fig. (3.9). The energy balance for the mixer unit is,

$$B_{i1} \times h_{i1} + F_i \times h_{fi} = B_r \times h_r \tag{3.53}$$

And the mass balance is considered as,

$$B_{i1} + F_i = B_o \tag{3.54}$$

For the pressure equations, the pressure in and out of the mixer unit is assumed equal.
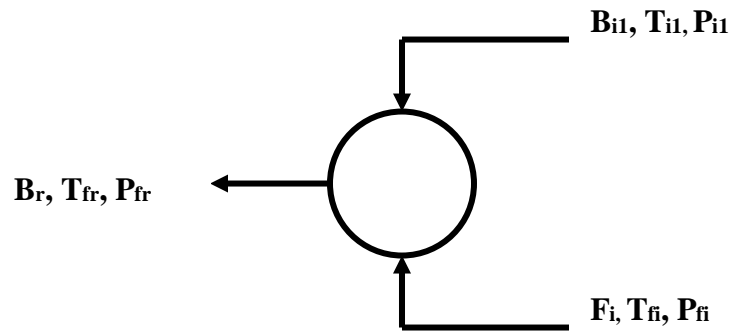
Figure (3.9) The schematic draw of the mixer unit

## 3.5 BUILDING THE SIMULATION PROGRAM

A mathematical model is developed to simulate the previous with its components and different configurations. The calculations are made for the different configurations to determine its performance under different operating conditions. The approximate equations for different configurations that presented previously in the above sections are normally developed to predict the simulation of the flashing process. Material and energy balance equations around the stage are combined and arranged to yield a set of independent simultaneous equations.

The model equations are simultaneously solved by matrix algebra to determine the main unknown parameters and variables (*TBT, $B_1$, $T_{Fo}$, $T_{d1}$,* and *DP*), see Fig. (3.10). Figure (3.10) shows the mathematical model for the first configuration arranged in a matrix form, and solved by the Mat-Lab program. For the second and the third configurations, the same technique is employed with some different equations (adding splitter and mixer equations). By using Mat-Lab program, the desired variable matrix will solve by dividing the coefficient matrix by constants matrix.
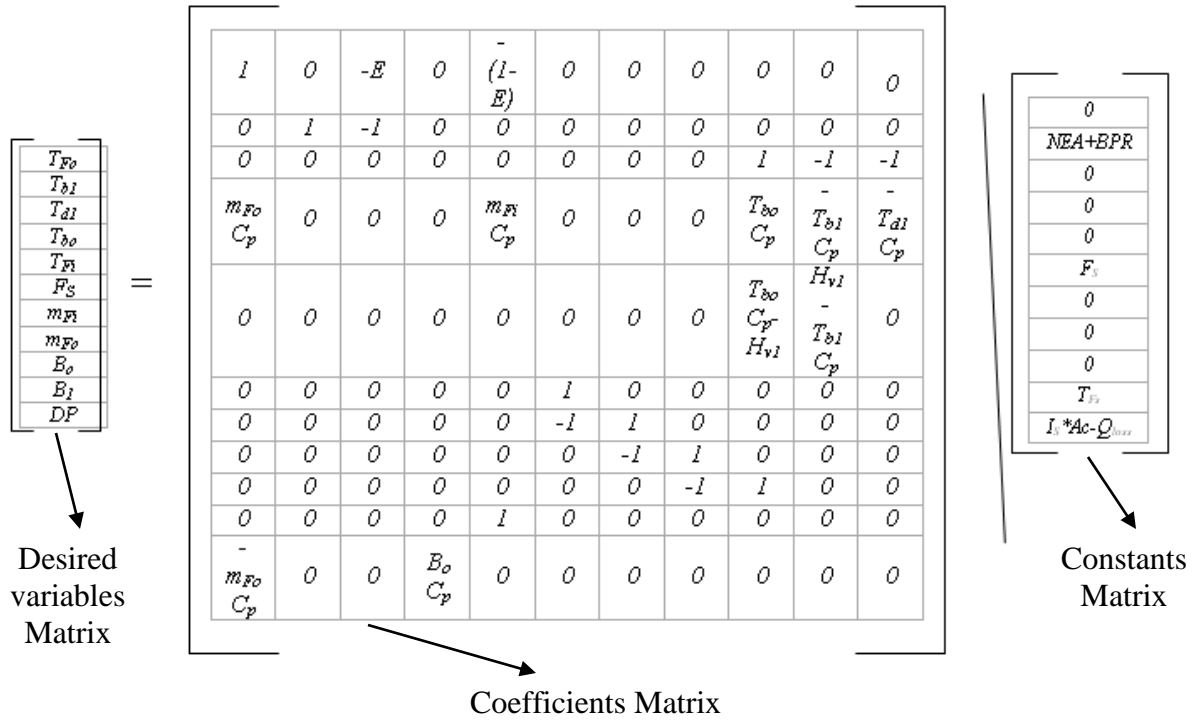
Figure (3.10) The schematic diagram of the different matrixes for 1$^{st}$ configuration: Desired variables matrix, coefficients matrix and constants matrix

Model variables data are divided into two parts:
1. Known or measured variables like $F_S$, $T_{Fi}$, $X_{Fi}$, $P_{Fi}$, $B_o$, $T_{amb}$, $T_g$, $T_{ins}$, $T_{sun}$, number of the day and so on.
2. Unknown or desired variables like $T_{Fo}$, $P_{Fo}$, $T_{bo}$, $P_{bo}$, $B_1$, $T_{d1}$, $DP$.

The hourly solar flux at a known day is predicted using the developed model presented in Chapter 4. The environmental conditions data are fed into the simulation program as a subroutine. Then design data (flash unit design parameters, collector design parameters) and physical properties of feed water ($\rho$, $\mu$, $\kappa$, $c_p$...) are estimated simultaneously with the main equations.

The desired variables are evaluated by solving the matrix form using Gauss elimination. By solving the matrix and evaluating the all desired variables, performance correlations (*PR for MSF, Exergy analysis, Thermal efficiencies, and Collector performance analysis*) are performed. The proposed program algorithm is presented in Fig. (3.11).

Input Data:
Read the design and operational parameters ($F_S$, $T_{Fi}$, $X_{Fi}$, $P_{Fi}$, $B_o$, $T_{amb}$, $T_g$, $T_{ins}$, $T_{sun}$, $F_{ci}$, $F_{co}$.
Design parameters (collector and flash chamber).

Read different weather conditions data:
$I_S$, $T_{amb}$, $V_w$, $T_{sun}$.

Recalculated $I_S$ from solar model.

Physical properties of feed water calculations and heat transfer coefficients correlations.

Iteration loop.

For i=1:N

Collector performance correlations.

Solving the desired variables matrix.

No

If Desired variables-assumed /Desired<0.001

Figure (3.11) Program flow chart

yes

Exergy analysis, Collector thermal efficiencies, flash unit performance parameters.

Results output.

41

A sample of the program results under summer and winter operating conditions is illustrated in Table (3-1).

Table (3-1) A sample of the program results under summer and winter operating conditions

| Items: | The average values estimated: | Units: |
|---|---|---|
| *Summer conditions: day(234) in August* | | |
| $I_s$ | 0.64 | $kWhr/m^2$ |
| $T_{amb}$ | 28.78 | $^oC$ |
| $V_w$ | 1.128 | $m/s$ |
| $T_g$ | 33.85 | $^oC$ |
| $T_{ins}$ | 30.83 | $^oC$ |
| $T_p$ | 88.02 | $^oC$ |
| $T_{mp}$ | 60.93 | $^oC$ |
| $T_{Fi}$ | 27.25 | $^oC$ |
| $T_{Fo}$ | 43.01 | $^oC$ |
| TBT | 60.18 | $^oC$ |
| $T_{b1}$ | 44.52 | $^oC$ |
| NEA | 1.671 | $^oC$ |
| BPR | 0.01 | $^oC$ |
| $F_i$ | 0.0185 | $kg/s$ |
| $B_1$ | 0.0179 | $kg/s$ |
| DP(total) | 14.5 | $kg/day$ |
| $X_f$ | 1 | $g/kg$ |
| $X_{b1}$ | 1.028 | $g/kg$ |
| *Winter conditions: day(16) in January* | | |
| $I_s$ | 0.323 | $kWhr/m^2$ |
| $T_{amb}$ | 18.62 | $^oC$ |
| $V_w$ | 1.33 | $m/s$ |
| $T_g$ | 28.37 | $^oC$ |
| $T_{ins}$ | 23.83 | $^oC$ |
| $T_p$ | 40.98 | $^oC$ |
| $T_{mp}$ | 34.67 | $^oC$ |
| $T_{Fi}$ | 18.5 | $^oC$ |
| $T_{Fo}$ | 25.39 | $^oC$ |
| TBT | 34.21 | $^oC$ |
| $T_{b1}$ | 27.33 | $^oC$ |
| NEA | 2.0875 | $^oC$ |
| BPR | 0.008 | $^oC$ |
| $F_i$ | 0.0185 | $kg/s$ |
| $B_1$ | 0.0182 | $kg/s$ |
| DP(total) | 5.08 | $kg/day$ |
| $X_f$ | 1 | $g/kg$ |
| $X_{b1}$ | 1.011 | $g/kg$ |

Similarly, a simulated program for more than one stage (two stages, three stages) is illustrated in Appendix-I. Also a simulated program for both configurations ($2^{nd}$ and $3^{rd}$) are illustrated in Appendix-I.

## 3.6 CONCLUSION

The mathematical model for the different configurations of flashing processes is investigated and presented in this chapter. Material and energy balance equations are combined and arranged in a matrix form. A computer program is developed to solve the system iteratively. The model has been translated into an algorithm to predict process variables such as temperatures of the flashing process. Also model analysis about an existing real flat plate solar collector is performed. The collector is manufactured by SOLAR ENERGY CORPORATION CAIRO-EGYPT. The collector is working in the Faculty of Petroleum & Mining Engineering at Suez Gulf area to support a suitable outlet fluid temperature providing a thermal flash evaporation unit. Estimating the performance of this collector is very important and useful to give a clear view about the collector performance.

# CHAPTER 4

# STATISTICAL EVALUATION OF SOME MODELS TO ESTIMATE INSTANTANEOUS TOTAL INSOLATION ON HORIZONTAL SURFACES WITHIN SUEZ GULF REGION

## 4.1 INTRODUCTION

Egypt is considered one of the high insolation countries of the world. The sunshine hours are estimated to be 3600 hours/year [15]. Therefore utilization of solar energy in Egypt as an alternative and renewable energy must be strongly taken into consideration in the future, especially, when new communities are established in the desert and remote areas [16]. To determine the feasibility of building solar energy system, it is necessary to know how much solar radiation would be available. At present there are many available models to predict the irradiation; however, these are constructed for specific regions. Hence suitable models for prediction of the irradiation in the different regions in Egypt should be selected. Solar radiation data are not easily available for many locations. Most of the solar energy applications require the estimation of the amount of insolation received on an inclined plane. Hence the quantity of diffuse radiation incident on a horizontal surface would be needed for this estimation [17]. It would not be enough for the scientists or engineers in this location to depend on the measured data only but it would be important to use a useful theoretical model which could estimate and predict the solar radiation. In the absence of measured data, theoretical models may be used to calculate the solar radiation. To estimate the theoretical solar radiation on the horizontal surfaces at Suez-Gulf region, seven models are chosen to evaluate the theoretical results. They are ASHREA [19], AWATER&BALL, DAVIS&HAY, HOYT, LACIS&HANSEN, BIRD and SIMPLE SPECTRAL2. All these models are used in the theoretical calculation of total irradiation (i.e,.. direct and diffuse) [18]. The main objective of this work is to evaluate statistically these seven models and compare its results with the local measured data. The data used in this comparison are measured by a pyranometer, which is calibrated to give an estimated error equals to $\pm 4\%$ at a location within the Suez Gulf region (latitude: 29º N; longitude: 33º E). The accuracy of these models is determined in terms of *MBE*, *RMSE* and *MPE* tests by statistically comparing the calculated and measured values. Based on the results of this comparison, a model is recommended for this region. And a new correlation is developed and suggested to be used in this region.

## 4.2 SOLAR ANGLES CALCULATIONS

The sun is the source of most energy on the earth and is a primary factor in determining the thermal environment of a locality. It is important for engineers to have a working knowledge of the earth's relationship to the sun. They should be able to make estimates of solar radiation intensity and know how to make simple solar radiation measurements [15]. For that, the intensity of solar radiation on the earth's surface depends on the path length

of the solar rays in the atmosphere, which in turn, depends on the angles of solar rays. The path length effect on the solar rays is due to the effects of the absorption and scattering of rays during their passage through the atmosphere as shown in Fig. (4.1).
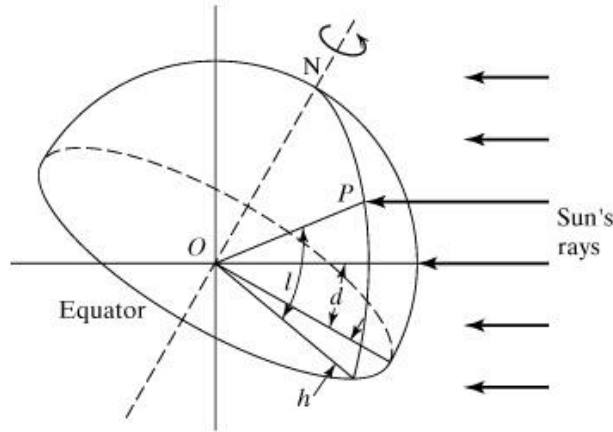


Figure (4.1) Latitude, hour angle, and sun's declination angle

The position of a point $P$ on the earth's surface with respect to the sun's rays is known at any instant if the latitude, $l$, and hour angle, $h$, for the point, and the sun's declination angle, $d$, are known. Figure (6.1) shows these fundamental angles. Point $P$ represents a location on the northern hemisphere. The latitude, $l$, is the angular distance of the point $P$ north (or south) of the equator. It is the angle between the line $\overline{OP}$ and the projection of $\overline{OP}$ on the equatorial plane. Point $O$ represents the center of the earth. The hour angle, $h$, is the angle measured in the earth's equatorial plane between the projection of $\overline{OP}$ and the projection of a line from the center of the sun to the center of the earth. At solar noon, the hour angle is zero. The hour angle expresses the time of day with respect to solar noon. One hour of time is represented by $360 \div 24 = 15$ degrees of hour angle. As part of the convention, the hour angle is negative before solar noon and positive after solar noon. The sun's declination angle, $d$, is the angular distance of a sun's rays north (or south) of the equator. It is the angle between a line extending from the center of the sun to the center of the earth and the projection of this line upon the earth's equatorial plane. The declination angle throughout the year can be well approximated by a sine function:

$$d = 23.45\sin\left[\frac{360}{365}(284+n)\right] \tag{4.1}$$

Where $n$ is the day of the year. The value of n for any day of the month $d$ can be determined easily with the aid of Table (4-1).

Table (4-1) Variation in *n* throughout the year for use in equation (4-1)

| Month | n for the Day of the Month, D | Month | n for the Day of the Month, D |
|---|---|---|---|
| January | D | July | 181 + D |
| February | 31 + D | August | 212 + D |
| March | 59 + D | September | 243 + D |
| April | 90 + D | October | 273 + D |
| May | 120 + D | November | 304 + D |
| June | 151 + D | December | 334 + D |

The hour angle **h** is calculated from the following expression:

$$h = 15(LST - 12) \tag{4.2}$$

Where LST = Local Solar Time [hr].

Besides the three basic angles (latitude, hour angle, and sun's declination), several other angles are useful in solar radiation calculations. Such angles include the sun's zenith angle $\theta_H$, altitude angle $\beta$, and azimuth angle $\phi$. For a particular surface orientation, the sun's incidence angle $\theta$, and surface-solar azimuth angle $\gamma$, may be defined. All of these additional angles may be expressed in terms of the three basic angles. Figure (4.2) schematically shows one apparent solar path and defines the sun's zenith, altitude, and azimuth angles. Point P represents the position of the observer, point O is the center of the earth, and $I_{DN}$ is a vector representing the sun's rays. The zenith angle $\theta_H$ is the angle between the sun's rays and local vertical, i.e. a line perpendicular to the horizontal plane at P. The altitude angle $\beta$ is the angle in a vertical plane between the sun's rays and the projection of the sun's rays on the horizontal plane. It follows that $\beta + \theta_H = \pi/2 = 90^o$. The azimuth angle $\phi$ is the angle in the horizontal plane measured from south to the horizontal projection of the sun's rays.
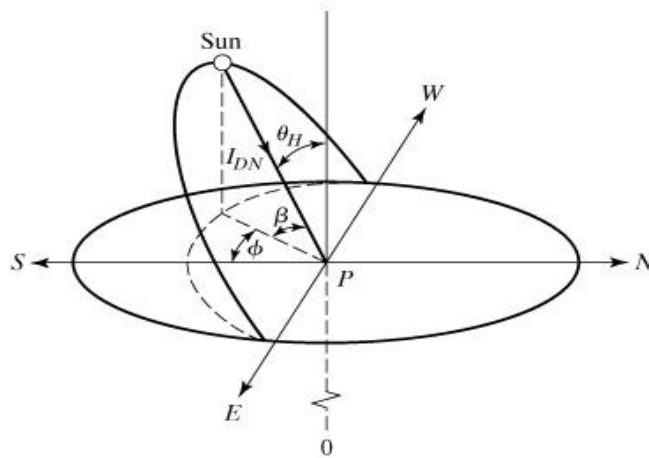


Figure (4.2) Definition of sun's zenith, altitude, and azimuth angles

The following equations are presented to calculate these angles:

$$\cos\theta_H = \cos l \cos h \cos d + \sin l \sin d \tag{4.3}$$

Since $\beta = 90 - \theta_H$, $\tag{4.4}$

$$\sin\beta = \cos l \cos h \cos d + \sin l \sin d \tag{4.5}$$

The relation gives the sun's azimuth, $\phi$:

$$\cos\phi = \frac{1}{\cos\beta}(\cos d \sin l \cos h - \sin d \cos l) \tag{4.6}$$

Equations 1 to 6 allow calculation of the sun's zenith, altitude and azimuth angles if the declination, hour angle, and latitude are known. In applying these equations, attention must be given to correct signs. A summary of the sign convention is:

**l**: north latitudes are positive, south latitudes are negative.

**d**: the declination is positive when the sun's rays are north of the equator, i.e. for the summer period in the northern hemisphere, March 22 to September 22 approximately, and negative when the sun's rays are south of the equator.

**h**: the hour angle is negative before solar noon and positive after solar noon.

**ϕ**: the sun's azimuth angle is negative east of south and positive west of south.

In calculations involving other than horizontal surfaces, it is convenient to express the sun's position relative to the surface in terms of the incidence angle, $\theta$. The sun's angle of incidence is the angle between the solar rays and the surface normal. (Notice: that for a horizontal surface, the surface normal is the local vertical and the incidence angle is equal to the zenith angle, $\theta_H$.)

The zenith angle is obtained from this relation:

$$\cos(z) = \sin(d)\sin(l) + \cos(d)\cos(l)\cos(h) \tag{4.7}$$

After estimating the solar angles of the location at Suez gulf region, which is spotted at (latitude: 29° N; longitude: 33° E) models could be estimated by defining zenith, declination and hour angles.

## 4.3 MODELS USED

The following models are considered in the present work:

1- The ASHREA model correlation (#1) calculates direct and diffuse radiation [19].

$$It1 = (G_{bn} \times \cos(z)) + G_d \tag{4.8}$$

Where $G_{bn}$ is the direct beam component, $G_d$ is the diffuse component, z is the zenith angle and $It1$ is the total or global radiation.

2- AWATER&BALL model (#2) [18].

$$It2 = I_o(\cos(z))(T_M - a_W) \times T_A /(1 - r_g r_s) \tag{4.9}$$

Where $I_o$ is the extraterrestrial direct normal solar irradiance and is equal to $I_o = I_{sc} \times (1 + 0.033 \times \cos(n/365 \times 189))$, where $I_{sc}$ is the constant solar flux and is equal to 1367 W/m$^2$[17], $n$ taken as the day in the year, $T_M$, $a_W$ and $T_A$ are transmission functions, $r_g$ and $r_s$ are the ground and sky albedos, respectively.

3- BIRD correlation (#3) [18].

$$It3 = (I_{d_B} + I_{as_B})/(I - r_g r_s)$$  (4.10)

$I_{d_B}$ is the direct solar irradiance; $I_{as_B}$ is solar irradiance from atmospheric scattering W/m$^2$.

4- DAVIS&HAY model (#4) [18].

$$It4 = I_{d_D} + I_{as_D} + I_{G_D}$$  (4.11)

$I_{G_D}$ is the solar irradiance on a horizontal surface from multiple reflections between the ground and sky in W/m$^2$. $I_{d_D}$ and $I_{as_D}$ are defined in the appendix-A for this model.

5- HOYT model (#5) [18].

$$It5 = I_{d_H} + I_{as_H} + I_{G_H}$$  (4.12)

Where $I_{d_H}$ is the direct solar irradiance in W/m$^2$, $I_{as_H}$ is solar irradiance from atmospheric scattering W/m$^2$ and $I_{G_H}$ is the solar irradiance on a horizontal surface from multiple reflections between the ground and sky in W/m$^2$. The values of $I_{d_H}$, $I_{as_H}$ and $I_{G_H}$ are defined in the appendix-A at HOYT correlations.

6- LACIS&HANSEN (#6) [18].

$$It6 = I_o(\cos(z))[(0.647 - r_s^{'} - a_0)/(1 - 0.0685 \times r_g) + 0.353 - a_W]$$  (4.13)

Where $r_s^{'}$, $a_o$ and $a_w$ transmission functions and $r_g$ is the ground albedo and almost equal to 0.2.

7- The seventh one is the SIMPLE SPECTRAL2 model (#7) [18].

$$I_{d\lambda} = H_{o\lambda} DT_{r\lambda} T_{a\lambda} T_{w\lambda} T_{o\lambda} T_{u\lambda}$$  (4.14)

$I_{d\lambda}$ is the direct irradiance on a surface normal to the direction of the sun at the ground level and is taken as a function of the transmission parameters [18].

All the above mentioned parameters are illustrated in appendix-A, and in the nomenclature. A computer program is developed for the above models to compute the total incidence on the horizontal surface hourly and instantaneously at different Julian days. The models are named numerically in the following sections and in all tables and figures.

## 4.4 STATISTICAL INDICATORS OF GOODNESS OF FIT

Three statistical tests; Mean Bias Error (*MBE*), Root Mean Square Error (*RMSE*) and Mean Relative Percentage Error (*MPE*) are used to evaluate the considered models. The mean bias error is defined by [22] as:

$$MBE = \sum_{j=1}^{N} \frac{Is_{j,calc} - Is_{j,meas}}{N}$$  (4.15)

Where $Is_{j,calc}$ and $Is_{j,meas}$ are the calculated and measured instantaneous values of solar radiation on the horizontal plates, respectively. $N$ is the numbers of considered day light hours. The lowest values of *MBE* are always the desired ones. So, the nearest values to the zero level are remarkable. The root mean square error is defined by [22] as:

$$RMSE = \left\{ \sum_{j=1}^{N} \frac{(Is_{j,calc} - Is_{j,meas})^2}{N} \right\}^{1/2} \qquad (4.16)$$

This test provides information on the short term performance of the correlations by allowing a term by term comparison of the actual deviation between the calculated and measured values. However, some large errors in the sum can produce a significant increase in *RMSE* [17]. The mean relative percentage error may be also applied for estimating the error as following [23]:

$$MPE = \left[ \sum_{j=1}^{N} \frac{(Is_{j,meas} - Is_{j,calc})}{Is_{j,meas}} \times 100 \right] / N \qquad (4.17)$$

For the past three indicators, the lowest error values (nearest to the zero level) are remarkable for all models.


## 4.5 DATA WERE COLLECTED AND EMPLOYED

The hourly mean total radiation values are estimated, using all models for one location in Suez Gulf region, especially, the area of Suez. The estimated data are compared graphically and statistically with the measured data reported by several authors for the same location through a time span from 1998 to 2005[11, 3, and 24]. A sample of these results is illustrated in Table (4-2). The measured data are taken by a high sensitive digital pyranometer; of course, there will be a normal uncertainty in these data. Most solar radiation models rely on measured data for their development or validation, and often the uncertainty or accuracy of that measured data are unknown [21]. The used pyranometer in this work is calibrated to give a scale of error less than about $\pm 4\%$. The all used points are illustrated in Appendix-H.

Table (4-2) Sample of the hourly average measured data recorded on different Julian days between 1998 and 2005 [11, 3 and 24]

| Year/day | Measured values obtained instantaneously in W/m² | | | | | | | |
|---|---|---|---|---|---|---|---|---|
| 1998/21 | 281 | 422 | 500 | 545 | 510 | 426 | 298 | 140 |
| 1999/265 | 468 | 599 | 730 | 790 | 710 | 660 | 563 | 488 |
| 2000/203 | 660 | 800 | 881 | 930 | 882 | 781 | 694 | 542 |
| 2001/234 | 600 | 750 | 833 | 885 | 811 | 705 | 580 | 480 |
| 2002/320 | 331 | 430 | 482 | 490 | 444 | 361 | 240 | 111 |
| 2003/274 | 544 | 662 | 721 | 735 | 691 | 543 | 463 | 384 |
| 2004/281 | 506 | 637 | 690 | 710 | 640 | 528 | 396 | 212 |
| 2005/160 | 500 | 622 | 712 | 741 | 706 | 623 | 544 | 467 |
| Time in hrs | 9 | 10 | 11 | 12 | 13 | 14 | 15 | 16 |

**4.6 RESULTS AND ANALYSIS**

Figs (4.3) to (4.10) show the deviation between the measured and estimated solar radiation values. A large deviation means that there is no matching between the estimated and these measured data. Fig. (4.3-a) shows the solar radiation for the considered models at the location on 21$^{st}$ of January, 1998. From this figure, it can be seen that measured data at this day are very close to models 4, 3 and 7. However, model 5 and 6 show large differences. Figs. (4.3-b,c,d) show the statistical indicators analysis *MBE*, *RMSE* and *MPE* respectively. The three statistical indicators are seen to give lowest values to models 4 and 3. Fig. (4.4-a) shows the data that are measured at a warm condition on the Julian day 265 in 1999.

These data show that model 4 curve matches extremely well. The results of models 3, 1 and 7 are apparent to become closer to the measured data on that day. Models 2, 5 and 6 are far matching with the measured data on the same day. The statistical data in Figs. (4.4-b,c,d) are seen to be very close to the zero level for models 4, 7 and 3 respectively. Fig. (4.5) shows the solar radiation data obtained on Julian day 203 in 2000. The measured data in Fig. (4.5-a) are very close to 2, 3 and 7, respectively. However, models 5 and 6 give poor results on the same day. Fig. (4.5-b) shows that the values of the *MBE* are very close to models 2, 3 and 7 respectively. Also the same conclusion can be derived from Figs. (4.5-c,d). Figs. (4.6-a,b,c,d) represent the solar radiation curves on Julian day 234 in 2001. The figures show that the measured data are very close to models 3, 2 and 7 respectively.

Models 5 and 6 are not match with the measured data on this day. Models 1 and 4 to some extent come next best. Figs. (4.7-a,b,c,d) show the results on Julian day 320 in year 2002 in which models 7 and 4 are considered little bit matching with the measured data. But the others are not to be applicable with the measured data on the same day. Models 3 and 2 come next best. Figs. (4.8-a,b,c,d) show the same comparison on Julian day 274 in year 2003. The results show that; models 3 and 2 are very close to the measured data. However, 5, 1, and 6 not be matched with the measured results.

Figs. (4.9-a,b,c,d) illustrate the comparison between the model results on Julian day 281 in year 2004. These results show that they are in agreement between model 3 and 4. Model 7 comes next best in the same Julian day. Figs. (4.10-a,b,c,d) show the results on Julian day 160 in year 2005. The measured results are very close to models 4 and 3 respectively. However, models 5 and 6 are not in match with the measured results. A similar analysis is performed for a large amount of measured data along the considered time span (1998-2005).
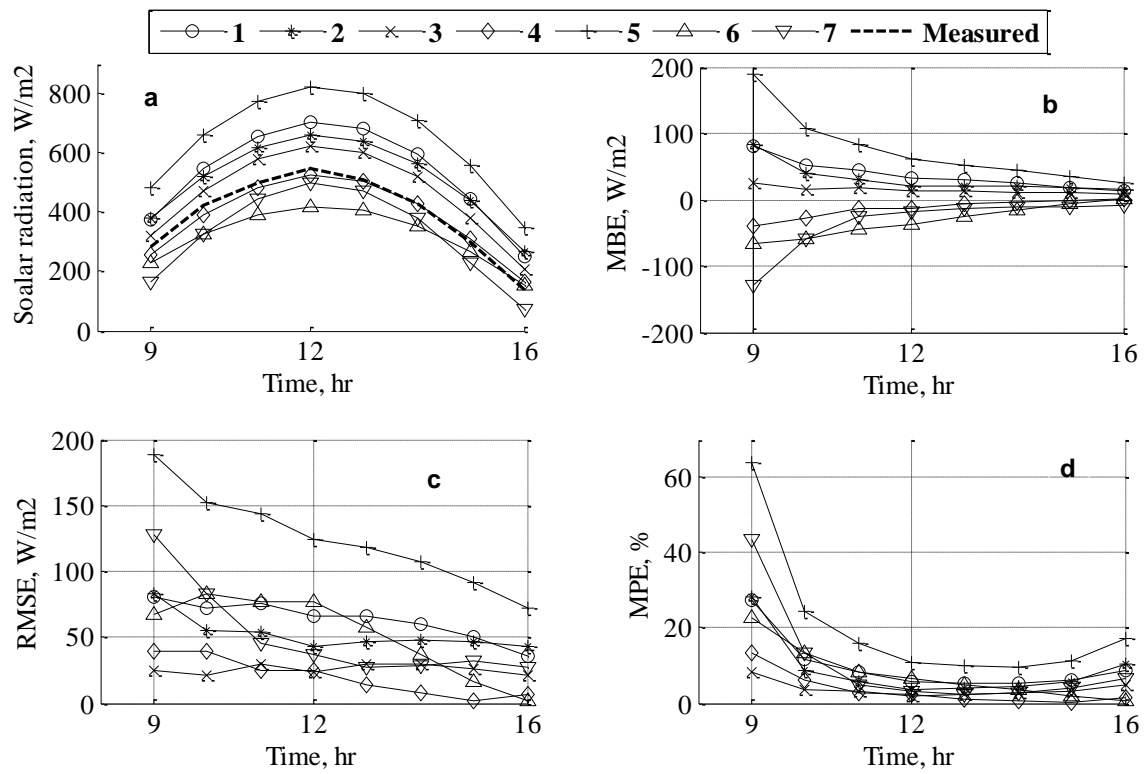
Figure (4.3) Solar radiation data measured on Julian day 21$^{st}$, 1998, compared with different models results and its statistical analysis
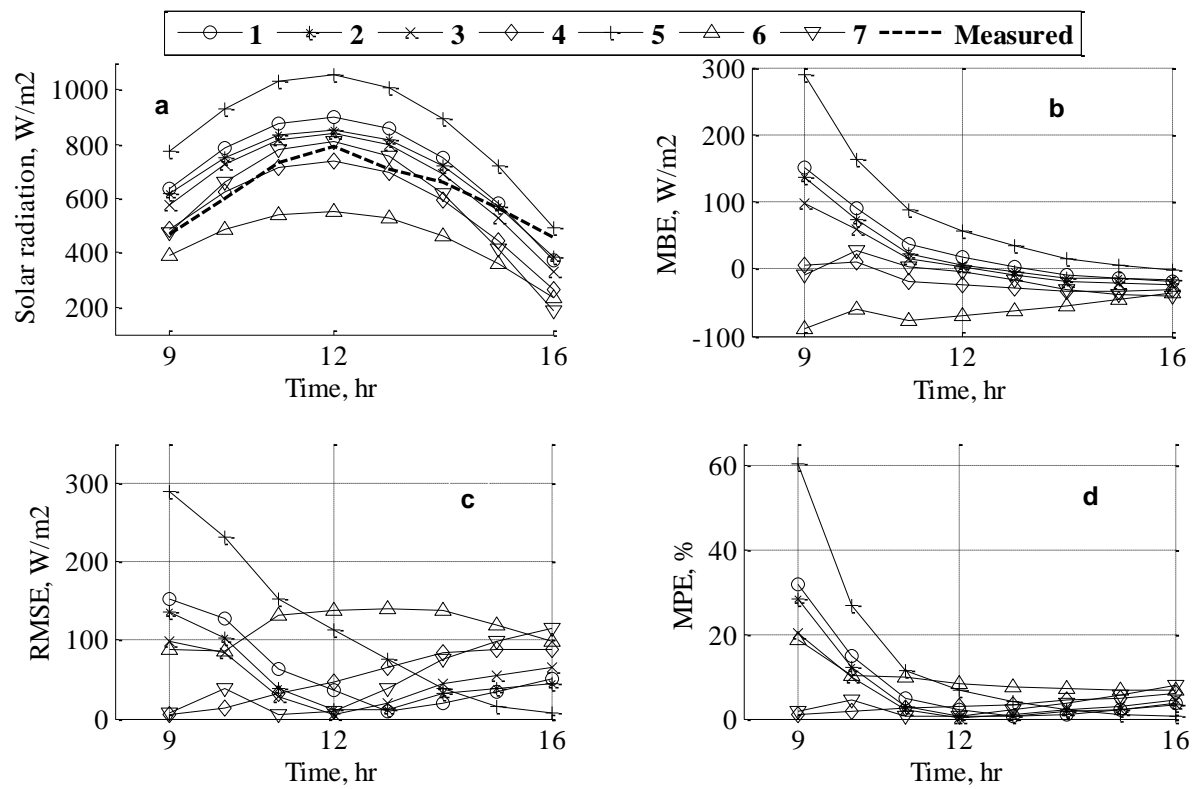
Figure (4.4) Solar radiation data measured on Julian day 265 in 1999
compared with different models results and its statistical analysis
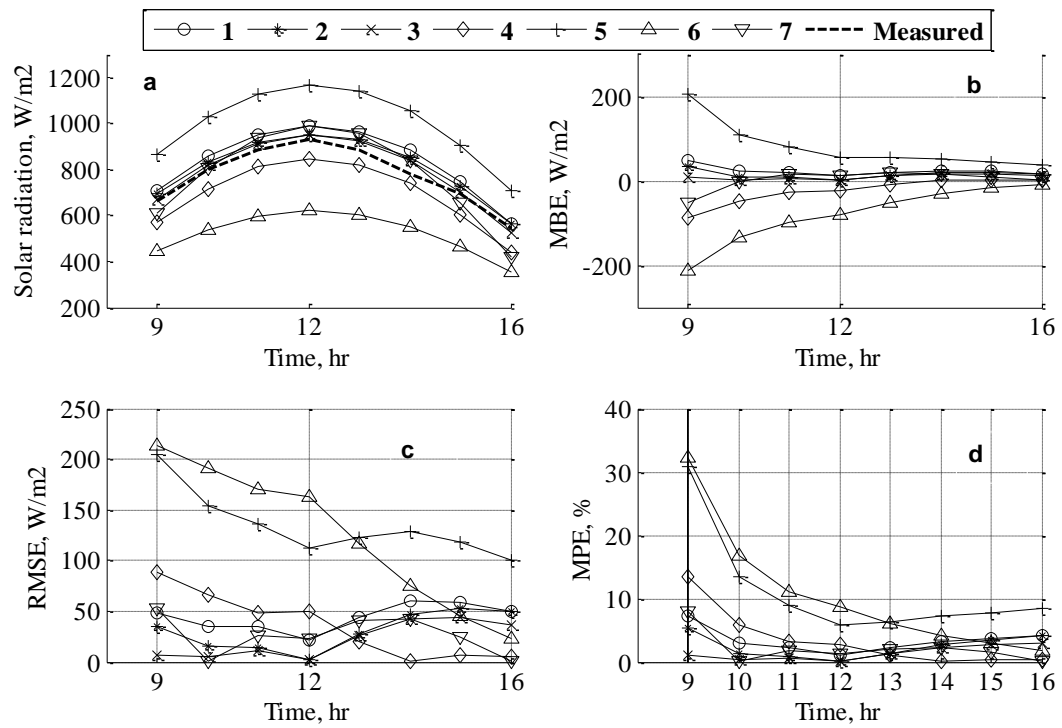
Figure (4.5) Solar radiation data measured on Julian day 203 in 2000
compared with different models results and its statistical analysis
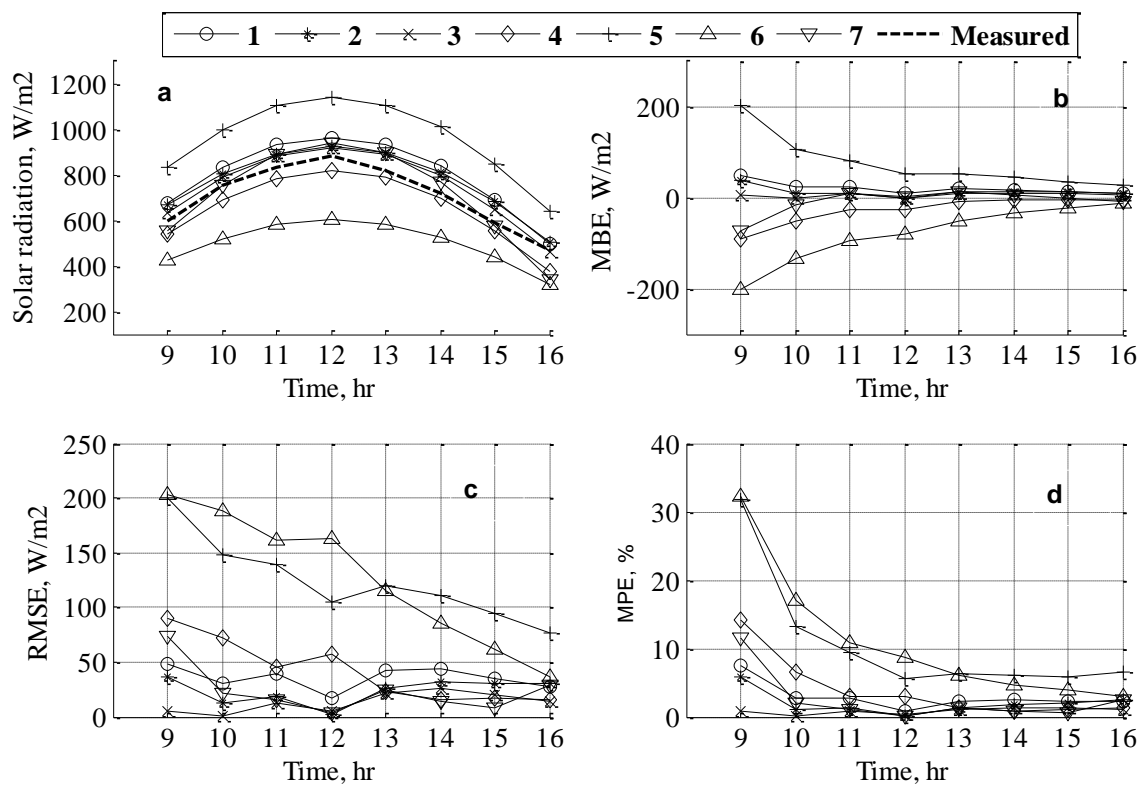
Figure (4.6) Solar radiation data measured on Julian day 234 in 2001
compared with different models results and its statistical analysis
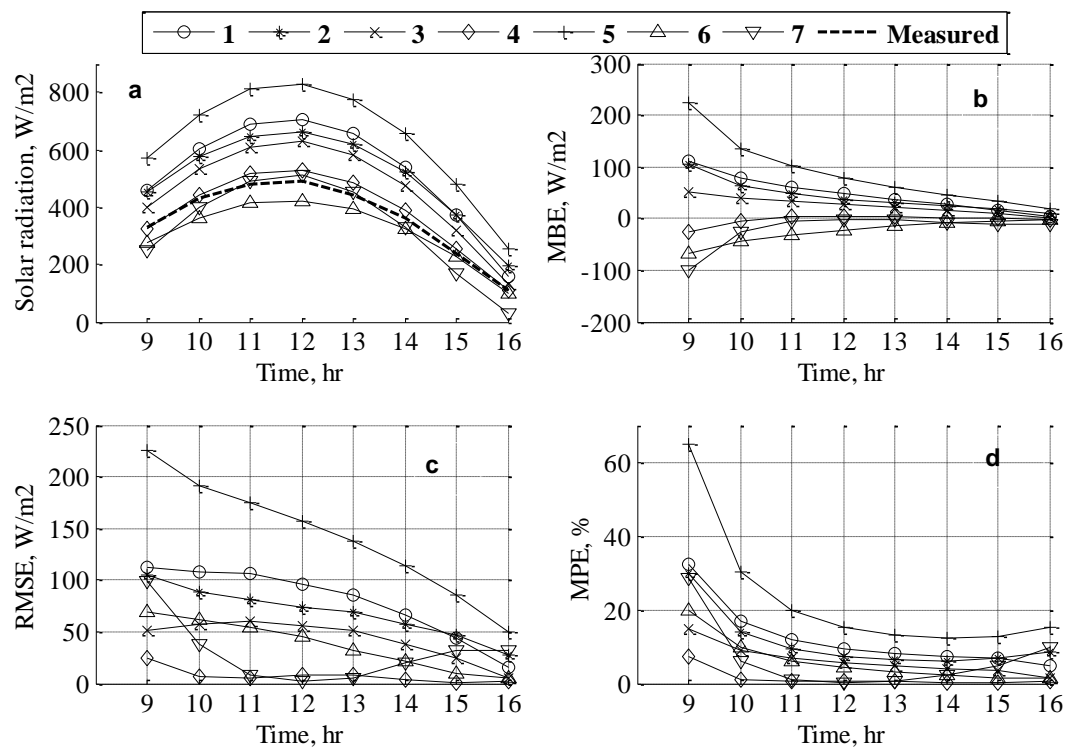
Figure (4.7) Solar radiation data measured on Julian day 320 in 2002
compared with different models results and its statistical analysis
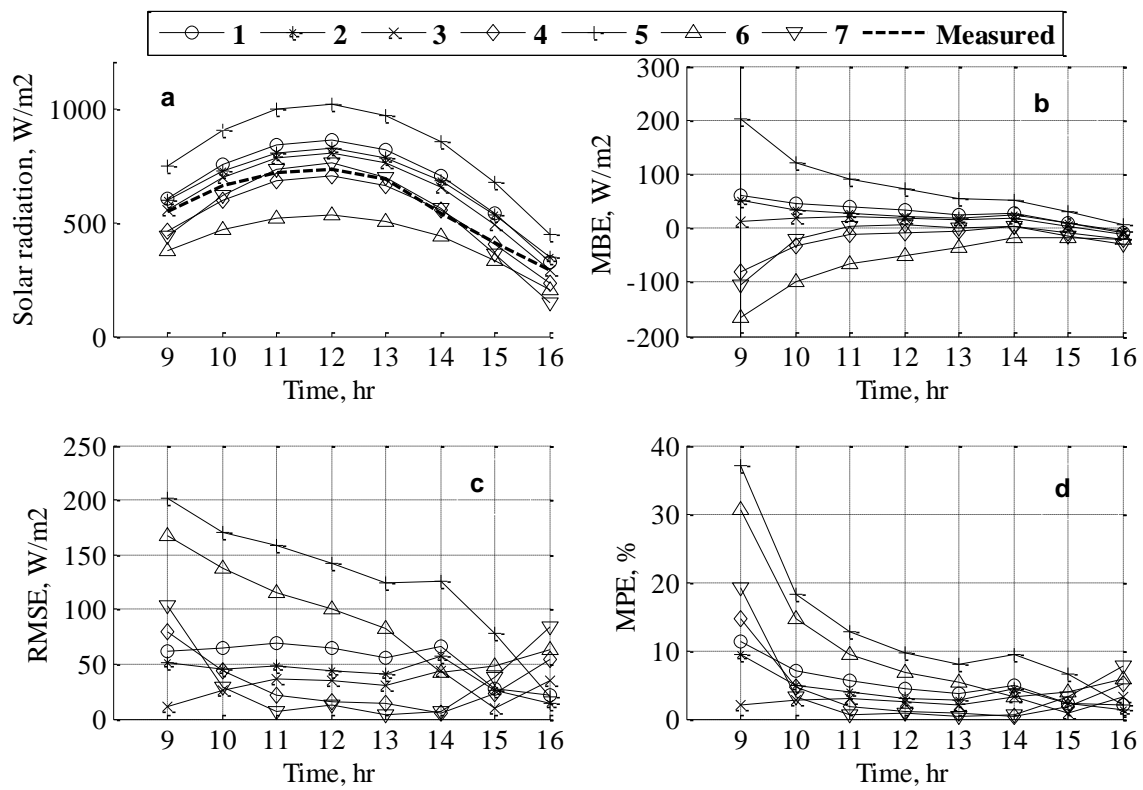
Figure (4.8) Solar radiation data measured on Julian day 274 in 2003
compared with different models results and its statistical analysis
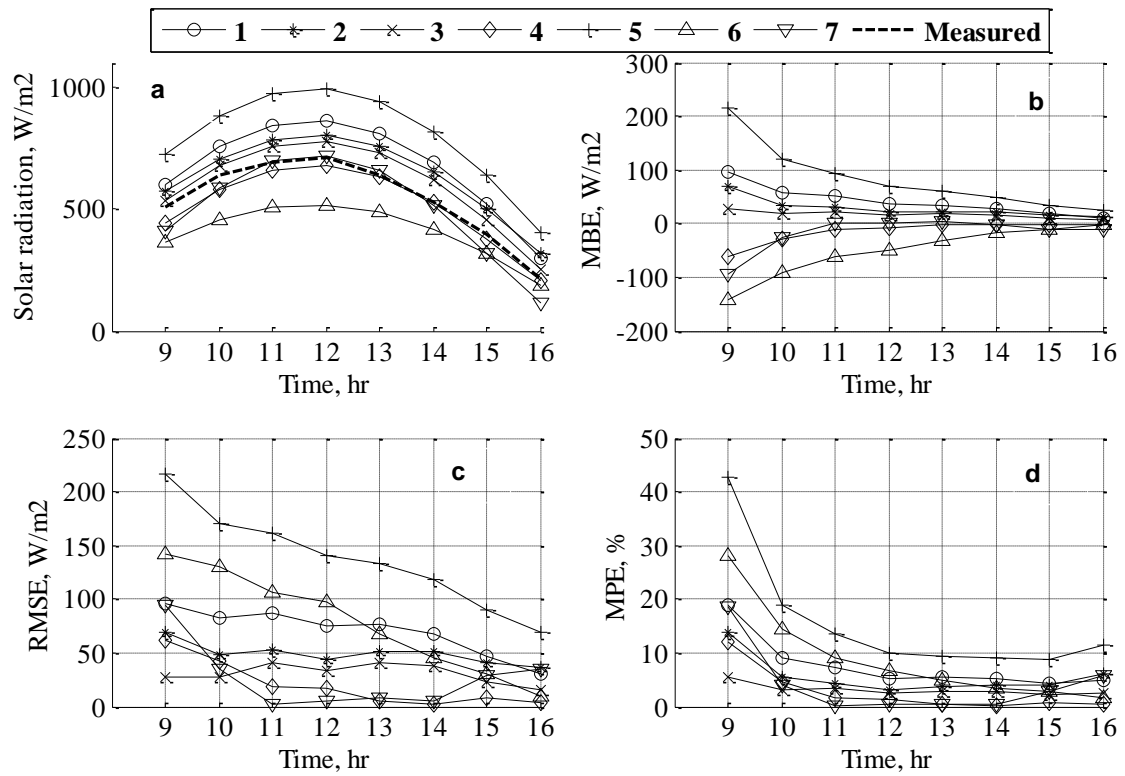
Figure (4.9) Solar radiation data measured on Julian day 281 in 2004
compared with different models results and its statistical analysis
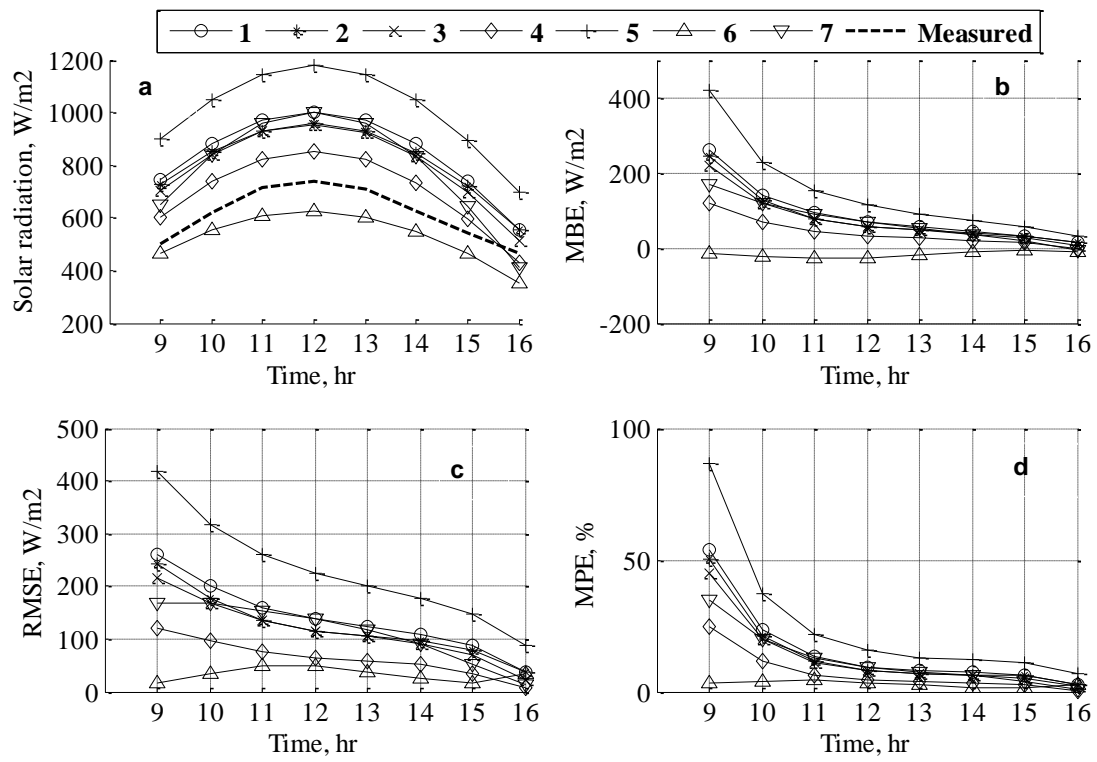
Figure (4.10) Solar radiation data measured on Julian day 160 in 2005
compared with different models results and its statistical analysis

For the *MBE*, Table (4-3) shows that model 4 provides lowest values in W/m$^2$ on Julian days 21/1998, 320/2002 and 160/2005. While model 3 provides the lowest values on Julian days 234/2001, 274/2003 and 281/2004. Models 5 and 6 give the highest values for all days. Model 2 gives the lowest value only on Julian day 203/2000. Model 7 gives only the lowest value on Julian day 265/1999.

For the *RMSE*, Table (4-4) shows that model 3 gives the lowest values in W/m$^2$ in 234/2001, 274/2003 and 281/2004 as 10.93, 17.41 and 15.42 W/m$^2$ respectively. Model 4 is repeated as the lowest value on 21/1998, 320/2002 and 160/2005 respectively. Models 2 and 7 are found the lowest only one time on 265/1999 and 203/2000 respectively. Models 5 and 6 are seen far to give the lowest values in W/m$^2$.

For *MPE %* in Table (4-5), on 21/1998, models 3 and 4 give the lowest values 3.49% and 3.57%, respectively. However, model 5 gives results which are deviated approximately by 20%. Models 6, 2 and 1 come next best as 7.7%, 8.2% and 9.8%, respectively. On the Julian day 265/1999, models 4 and 7 give the nearest values as 2.4% and 2.6%. While model 3 and 2 come next best since they vary by 4.3% and 5.5%, respectively. Model 5 gives a bad result (14.3%) on the same day. For the Julian day 203/2000, the average values estimated show that models 2, 1 and 3 give the lowest values as 0.36%, 0.92% and 1.02%, respectively. Models 7 and 4 come next best. Also models 5 and 6 give poor results. On Julian day 234/2001, models 3 and 2 give nearest values to the zero error level about 0.71%.

Models 7 and 1 come next best. Julian day 320/2002 represents models 4 and 6 as lowest results. Models 3 and 7 come next best. Models 3 and 2 give the lowest results as 1.5% and 2.2% on 274/2003, respectively. Model 6 gives a highest value which is estimated as 10.6%. On 281/2004, model 3 gives the lowest value as 1.3%. Models 2 and 4 comes next best on the same day as 3.6% and 4.1%, respectively. For Julian day 160/2005, model 4 yields the best results obtained as 4.2%. Models 6, 7 and 3 come next best as 5%, 8% and 9%, respectively. Model 5 gives an error percentage as 20.8%. From Tables 2, 3 and 4, globally, models 3 and 4 both are yield the best results. Models 2 and 1 come next as illustrated with the different types of three the error percentages. But model 2 is considered to be applicable only to extremely clear atmospheric conditions like model 1, with an atmospheric turbidity ranges between 0.1-0.5 ($\mu m$) wavelengths [18].

Although, this model is extremely simple but does not have a good method for treating the aerosol transmittance [18]. Models 3 and 7 give good results in the summer season, since they can estimate all the transmission parameters. Model 4 provides good agreement with the measured data, especially, in winter but also does not have a good method for treating the aerosol transmittance. Models 5 and 6 give unacceptable results since the errors would be very large. And when recalculating the transmittance and absorptance parameters at modified air mass values, this model will be relatively difficult to be used [18].

Table (4-3) The average *MBE* errors for the seven models on eight different Julian days for one location (W/m$^2$)

| Season | Win | Spr | Sum | Sum | Aut | Aut | Aut | Spr | Average |
|---|---|---|---|---|---|---|---|---|---|
| Model | 21/1998 | 265/1999 | 203/2000 | 234/2001 | 320/2002 | 274/2003 | 281/2004 | 160/2005 | |
| 1.ASHREA | 37.33 | 35.91 | 7.16 | 17.57 | 29.57 | 27.65 | 32.04 | 72.229 | 34.7 |
| 2.ATWATER&BALL | 31.54 | 26.63 | -0.874 | 10.21 | 41.5 | 12.25 | 19.12 | 62.889 | 25.7 |
| 3.BIRD | 13.09 | 16.41 | -6.84 | 2.86 | 25.26 | 1.25 | 7.37 | 57.409 | 16.3 |
| 4.DAVIES&HAY | -12.36 | -15.49 | -40.42 | -30.64 | -2.36 | -30.83 | -24.38 | 23.747 | 22 |
| 5.HOYT | 75.73 | 84.37 | 63.45 | 72.39 | 87.36 | 68.53 | 73.72 | 127.98 | 81.4 |
| 6.LACIS&HANSEN | -31.18 | -58.93 | -96.34 | -81.73 | -24.54 | -69.87 | -60.56 | -34.09 | 56.9 |
| 7.SPECTRAL2 | -34.68 | -10.23 | -14.34 | -11.62 | -20.57 | -29.77 | -26.52 | 52.189 | 25 |

Note: The shaded cells tend to the lowest values, Win: winter, Spr: spring, Sum: summer, Aut: autumn.

Table (4-4) The average *RMSE* errors for the seven models at eight different Julian days for one location (W/m$^2$)

| Season | Win | Spr | Sum | Sum | Aut | Aut | Aut | Spr | Average |
|---|---|---|---|---|---|---|---|---|---|
| Model | 21/1998 | 265/1999 | 203/2000 | 234/2001 | 320/2002 | 274/2003 | 281/2004 | 160/2005 | |
| 1.ASHREA | 63.62 | 60.23 | 12.74 | 30.01 | 49.12 | 51.66 | 55.04 | 112.42 | 58 |
| 2.ATWATER&BALL | 52.54 | 44.41 | 5.65 | 17.46 | 68.69 | 26.4 | 34.34 | 96.977 | 43.3 |
| 3.BIRD | 24.41 | 37.23 | 12.39 | 10.93 | 42.85 | 17.41 | 15.42 | 88.647 | 29 |
| 4.DAVIES&HAY | 19.48 | 36.54 | 64.38 | 47.89 | 7.47 | 47.64 | 34.92 | 40.03 | 37 |
| 5.HOYT | 122.71 | 126.27 | 102.68 | 118.5 | 142.02 | 111.5 | 122.12 | 202.5 | 130 |
| 6.LACIS&HANSEN | 52.83 | 106.65 | 156.37 | 132.77 | 37.51 | 111.31 | 93.46 | 60.293 | 93 |
| 7.SPECTRAL2 | 51.46 | 34.54 | 27.76 | 26.14 | 29.14 | 44.45 | 37.81 | 89.326 | 41 |

Note: The shaded cells tend to the lowest values, Win: winter, Spr: spring, Sum: summer, Aut: autumn.

Table (4-5) The average *MPE%* for the seven models at eight different Julian days for one location

| Season | Win | Spr | Sum | Sum | Aut | Aut | Aut | Spr | Average |
|---|---|---|---|---|---|---|---|---|---|
| Model | 21/1998 | 265/1999 | 203/2000 | 234/2001 | 320/2002 | 274/2003 | 281/2004 | 160/2005 | |
| 1.ASHREA | 9.83 | 7.03 | 0.92 | 2.47 | 7.52 | 4.61 | 5.68 | 11.744 | 6.8 |
| 2.ATWATER&BALL | 8.27 | 5.54 | 0.36 | 1.57 | 11.02 | 2.28 | 3.66 | 10.302 | 5.37 |
| 3.BIRD | 3.49 | 4.39 | 1.02 | 0.719 | 6.26 | 1.53 | 1.33 | 9.317 | 3.4 |
| 4.DAVIES&HAY | 3.57 | 2.43 | 5.17 | 4.24 | 1.44 | 5.16 | 4.16 | 4.215 | 3.7 |
| 5.HOYT | 20.91 | 14.34 | 8.04 | 10.03 | 22.95 | 10.687 | 13.11 | 20.828 | 15 |
| 6.LACIS&HANSEN | 7.72 | 9.25 | 12.09 | 11.12 | 6.1 | 11.12 | 10.07 | 5.365 | 9 |
| 7.SPECTRAL2 | 10.14 | 2.68 | 2.58 | 2.67 | 6.601 | 5.36 | 5.204 | 8.688 | 5.4 |

Note: The shaded cells tend to the lowest values, Win: winter, Spr: spring, Sum: summer, Aut: autumn.

Julian day's samples that are presented in the previous figures and tables just an example about the error values of the models at different seasons of the year. For example, Julian day 21/1998 shows the models error status as an example in winter seasons and so on for the all the chosen days. Table (4-6) shows the error analysis of *MPE%* for winter and summer seasons from 1998 to 2005. The table is illustrated just for most nearest models to zero error level (BIRD and DAVIES&HAY). Each season is compound from three months. The *MPE%* is estimated three times per month for each season. Table (4-6) shows that the lowest error values are remarkable for DAVIES&HAY model in winter seasons, and the same is existed for BIRD model during summer seasons. The average error values for each month helping to represent the total average error value for each season (Winter-Summer). For this reason the table shows that the average error values for each model are not exceeding about 2.68% for DAVIES&HAY model (winter) and 2.7% for BIRD model (summer).

Table (4-6) The *MPE%* for BIRD in summer and DAVIES&HAY in winter seasons from 1998 to 2005

| Season | Year | MPE% values for winter and summer: | | | | | | | | | Average: |
|---|---|---|---|---|---|---|---|---|---|---|---|
| | | December | | | January | | | February | | | |
| Winter for DAVIES& HAY | 1998 | 1.8761 | 1.5605 | 1.6548 | 1.717 | 3.4 | 4.1 | 2.7 | 2.6 | 4.4 | 2.6484 |
| | 1999 | 1.7861 | 1.6505 | 1.4558 | 1.613 | 3.344 | 4.102 | 2.127 | 1.96 | 3.4 | 2.5768 |
| | 2000 | 2.1 | 1.65 | 1.48 | 1.237 | 3.14 | 4.4 | 1.97 | 2.2206 | 4.41 | 2.5842 |
| | 2001 | 1.81 | 1.05 | 1.48 | 1.103 | 3.25 | 4.09 | 2.37 | 2.36 | 4.3 | 2.5905 |
| | 2002 | 1.62 | 1.209 | 1.358 | 1.862 | 3.31 | 3.91 | 2.66 | 2.97 | 2.994 | 2.6468 |
| | 2003 | 1.681 | 1.55 | 1.68 | 1.73 | 3.24 | 4.22 | 2.57 | 2.106 | 3.894 | 2.6124 |
| | 2004 | 1.71 | 1.605 | 1.58 | 1.67 | 3.41 | 4.91 | 2.507 | 2.76 | 4.293 | 2.5937 |
| | 2005 | 2.062 | 1.305 | 1.383 | 1.597 | 3.33 | 3.981 | 2.579 | 2.496 | 4.54 | 2.6876 |
| | | June | | | July | | | August | | | |
| Summer for BIRD | 1998 | 9.3 | 1.322 | 1.456 | 2.402 | 1.0206 | 3.1672 | 1.6317 | 0.72 | 2.816 | 2.6676 |
| | 1999 | 9.26 | 1.242 | 1.43 | 2.418 | 1.126 | 3.2 | 1.17 | 0.729 | 2.616 | 2.382 |
| | 2000 | 9.02 | 1.2 | 1.36 | 2.3102 | 1.006 | 3.2 | 1.7 | 0.662 | 2.8 | 2.512 |
| | 2001 | 10.001 | 1.2 | 1.4 | 2.12 | 1.01 | 3.12 | 1.1637 | 1.2 | 2.1 | 2.4237 |
| | 2002 | 9.42 | 1.32 | 1.536 | 2.42 | 1.26 | 3.162 | 1.31 | 0.742 | 2.651 | 2.4326 |
| | 2003 | 9.13 | 1.8 | 1.3 | 2.3 | 1.092 | 3.06 | 1.53 | 0.6 | 2.7 | 2.519 |
| | 2004 | 9.17 | 1.129 | 1.5 | 2.3 | 1.1 | 3.0962 | 1.737 | 0.81 | 2.501 | 2.7161 |
| | 2005 | 9.4 | 1.222 | 1.515 | 2.302 | 1.226 | 3.006 | 1.83 | 0.597 | 3.09 | 2.5859 |

## 4.7 A NEW CORRELATION

It is important to develop a simple, accurate and easy to use correlation for the considered location. Developing a new correlation has some advantages as the correlation being simple and valid along the different seasons of the year not only for winter or only for summer. For that a statistical linear regression technique is used to predict a new correlation for the estimation of the total insolation on horizontal surfaces. A new correlation S.C.S.G (Solar Correlation in Suez Gulf) is developed as follows;

$$It8 = (A \times I_o \cos(z)) - C_{season} \tag{4.18}$$

Where $It8$ is the total insolation on horizontal surfaces, *A* is the correlation non-varying constant and always equals to 0.709 for all seasons. $C_{season}$ is the correlation varying constant that changes according to the variation of the seasons. Table (4-7) shows the different values of the $C_{season}$.

Table (4-7) The S.C.S.G correlation constants *A* and $C_{season}$ for different seasons

| Seasons: | Dec, Jan, Feb: (winter) | Mar, Apr, May: (spring) | Jun, Jul, Aug: (summer) | Sep, Oct, Nov: (autumn) |
|---|---|---|---|---|
| A: | 0.709 | | | |
| C$_{season}$: | 90.36 | 84.13 | 60.031 | 88.178 |

Equation (4.18) is only deduced for the Suez-Gulf region (latitude: 29° N; longitude: 33° E). The new correlation is compared with the most accurate models; BIRD and DAVIES&HAY from the side of *MPE%*. And there is no need to compare between it and the other models. Figure (4.10) shows the *MPE%* for models S.C.S.G (*It8*), BIRD (*It3*) and DAVIES&HAY (*It4*) along different Julian days. The figure shows that on Julian day 21, S.C.S.G (*It8*) and DAVIES&HAY (*It4*) models presented a small deviation of error

compared with *It*3. *It*3 gives minimum *MPE%* for Julian days 203/2000, 234/2001, 274/2003, 281/2004 and 171/2005. Table (4-8) illustrates the *MPE%* for the proposed S.C.S.G model compared with (*It*3) and (*It*4) along different Julian days and seasons. *MPE%* for S.C.S.G model is found to be not exceeding about 4.9% error. However, *MPE%* for BIRD and DAVIES&HAY models is not exceeding about 6.25%, 5.17% respectively. Generally these three models (S.C.S.G, BIRD and DAVIES&HAY) yield the lowest values of *MPE%* error than the other examined models in this chapter.
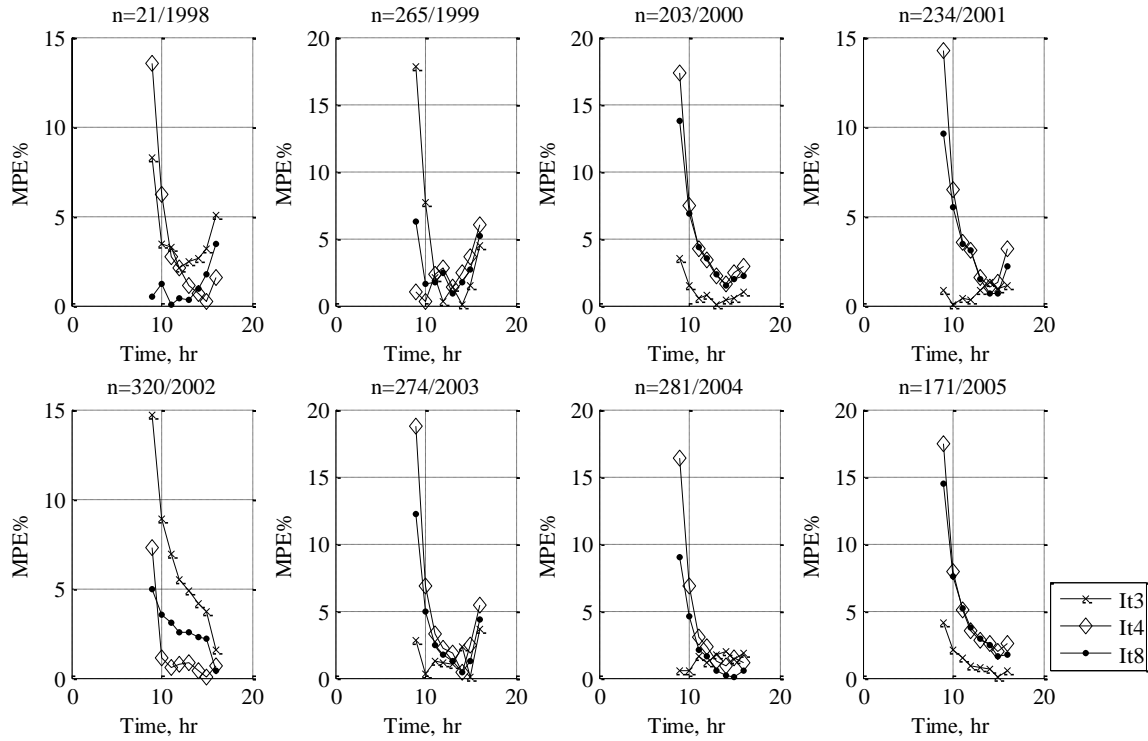


Figure (4.11) The *MPE%* for models: (*It*3), (*It*4) and (*It*8) along different Julian days

Table (4-8) The average *MPE%* for equation (4.18) compared with BIRD (*It3*) and DAVIES&HAY (*It4*) models along different Julian days

| Season | Win | Spr | Sum | Sum | Aut | Aut | Aut | Sum |
|---|---|---|---|---|---|---|---|---|
| Model | 21/1998 | 265/1999 | 203/2000 | 234/2001 | 320/2002 | 274/2003 | 281/2004 | 171/2005 |
| **BIRD (It3)** | 3.49 | 4.39 | 1.02 | 0.719 | 6.26 | 1.53 | 1.33 | 1.3 |
| **DAVIES&HAY (It4)** | 3.57 | 2.43 | 5.17 | 4.24 | 1.44 | 5.16 | 4.16 | 5.4 |
| **S.C.S.G (It8)** | 2.2428 | 2.7872 | 3.7166 | 2.3521 | 2.5486 | 3.8117 | 2.5848 | 4.9 |

Note: The shaded cells tend to the lowest values.

## 4.8 CONCLUSION

ASHREA, ATWATER&BALL, BIRD, DAVIES&HAY, HOYT, LACIS&HANSEN and SPECTRAL2, models are presented and used to estimate the instantaneous direct and diffuse insolation on horizontal surfaces at Suez-Gulf area. BIRD and DAVIES&HAY models are most accurate for this area. The lowest hourly *MBE*, *RMSE* and *MPE* are recorded to BIRD and DAVIES&HAY models while the highest deviations are found with HOYT and LACIS&HANSEN models. BIRD model gives superior results in summer; however, DAVIES&HAY gives the same superior results in the winter. ASHREA and SPECTRAL2 models would be the next best ones. HOYT and LACIS&HANSEN models give poor indications about this location compared with the measured data. Also a simple new correlation (S.C.S.G) is developed to predict the total insolation only in the Suez-Gulf region. The new suggested correlation gives an acceptable result compared with BIRD and DAVIES&HAY. S.C.S.G model gives minimum error results in winter seasons against summer. The developed correlation is simple and valid for all seasons at the mentioned location. Generally DAVIES&HAY, BIRD and S.C.S.G models would be recommended to be employed for the calculation of the total solar radiation (direct and diffuse) instantaneously at Suez-Gulf Area.

# CHAPTER 5

# EXERGY COMPARISON FOR DIFFERENT SYSTEM CONFIGURATIONS

## 5.1 INTRODUCTION

Second law of thermodynamics enables engineers to determine whether or not the desired conversion of energy is possible. The second law also enables to determine the maximum efficiency of the conversion process and system. As the energy conversion system is being designed, the engineers can apply the second law to determine the deviation of the actual system from an ideal one. First law of thermodynamics deals with the quantity of energy; the second law deals with the quality of energy. Exergy or availability is defined as the maximum available work can be produced from the system or the method by doing system analysis according to the conservation of mass, conservation of momentum and second law of thermodynamics [34]. This concept of exergy is embodied in the second law. Simply, the exergy method is a systematic approach to apply the first and second laws of thermodynamics [34]. Exergy analysis is an invaluable mean for finding the losses and real efficiency in a process due to the quality of the energy and always gives an indication about the process that this process can be improved or not or where is the part in this process have more losses from the other that affecting on the process production, efficiency, and so on. Slesarenko and Shtim utilized the exergy analysis to evaluate an MSF pilot plant [35]. Faleh A. AL-Sulaiman [35] introduced a simple scheme to quantify exergy losses for three major MSF desalination plants in Saudi Arabia. But, for small units that are deal with low range of top brine temperature especially that working by solar energy systems (solar water heaters) wasn't investigated before using exergy approach.

This chapter represents a simple exergetic analysis of the three different configurations of flashing process. Exergy analysis is performed for the three configurations that presented in the literature. The first configuration is simply designed as one chamber of flashing unit coupled with one collector. The first configuration is working as once through system. The second and the third configurations considered the same as the first one except adding splitter unit and mixer unit. For the second configuration, the splitter unit is put at outlet stream of the wasted feed from the flash chamber, and the mixer unit is put at the inlet point of the condenser unit. For the third configuration, the splitter unit is put as the same as the second configuration and the mixer unit is put at the outlet point of the condenser unit. The aim of this work is to find and quantify exergy losses, exergetic efficiency, and exergy-destruction terms associated with these three types of configurations as a function of top brine temperature (TBT) which is varying with solar intensity during the operating hours along the day light. The exergetic analyses in this work are used to recognize the best configuration from the exergy performance point of view. The analysis made for flash evaporation units under real operating conditions; also the analysis is made for the brine heater section that is represented in this work as a solar water heater (flat plate collector-FPC type). The developed equations for the three configurations are fed to a simulation program to perform the exergy analysis.

## 5.2 SYSTEM AND DIFFERENT CONFIGURATIONS DESCRIPTION

Figure (5.1) shows the first system configuration and it's components. The system consists of one unit of solar water heater represented as a flat plate solar collector type (FPC), flash unit manufactured vertically with its preheatre/condenser heat exchanger. This system has been divided exergetically into two sections, the 1st is the brine heater and the 2nd section is the flashing chamber with its entire heat exchanger.
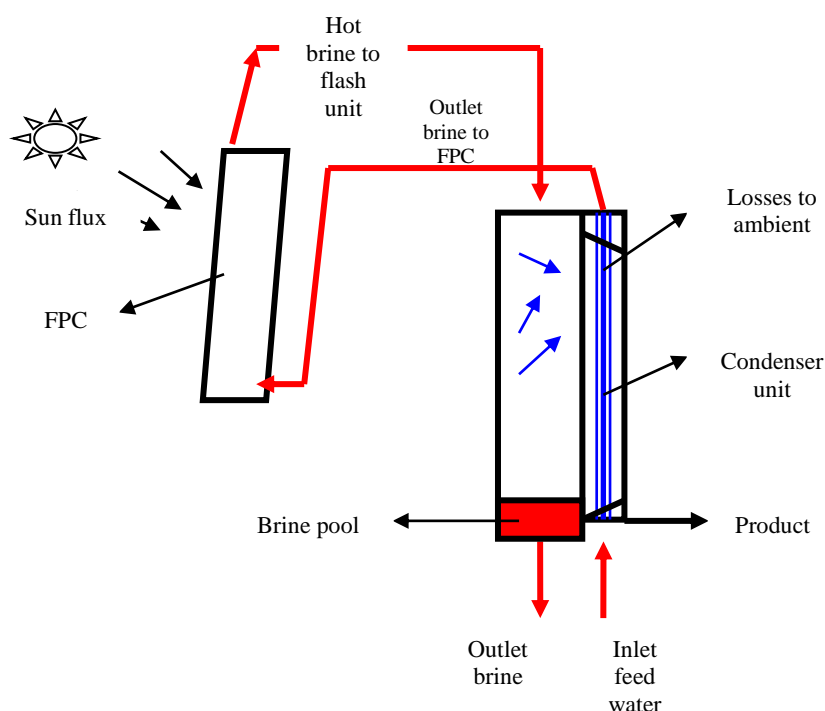


Figure (5.1) Schematic draw of 1st configuration

Feed water enters the condenser unit at a known feed temperature. The condenser unit is attached to the flashing chamber. The temperature of the inlet feed water will rise gradually till exiting from the condenser unit before entering the solar collector. The collector will rise the temperature of the inlet feed water to reach to the desiered top brine temperature (TBT). The desiered TBT is completely depending on solar intensity and the collector performance.

Feed will be ready to enter the flashing chamber and the vapor condensate across the condenser tubes where can transferring its latent heat to the feed water that passes through the condenser tubes. For the second configuration, involving a splitter and mixer units in the system to use the wasted brine. The splitter unit is fixed at the outlet point of the brine from the flash unit, and the mixer unit is fixed at the inlet point of the condenser. Figure (5.2) represents a schematic diagram of the second configuration. The mixer unit is fixed at the outlet point of the condenser unit for the third configuration as shown in Fig. (5.3).
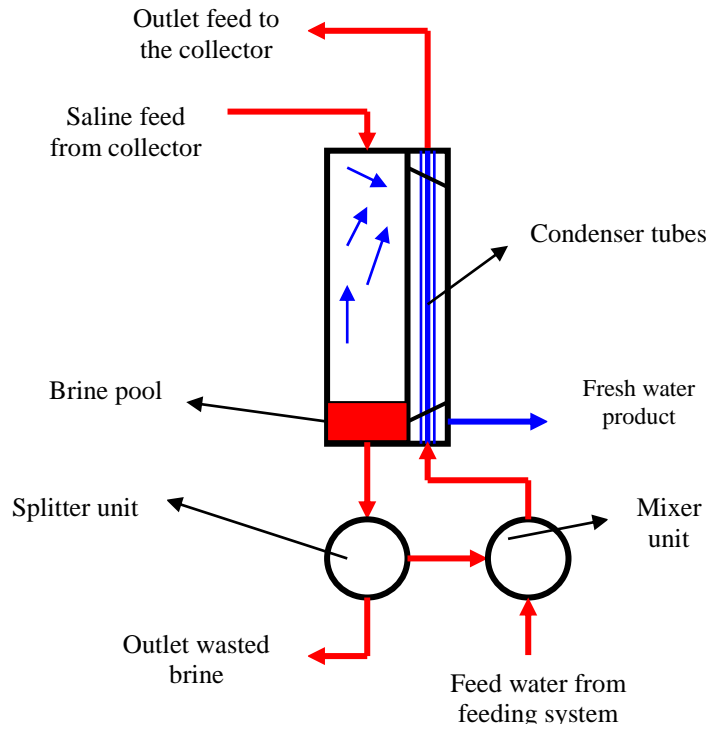
Figure (5.2) The schematic draw of 2nd configuration
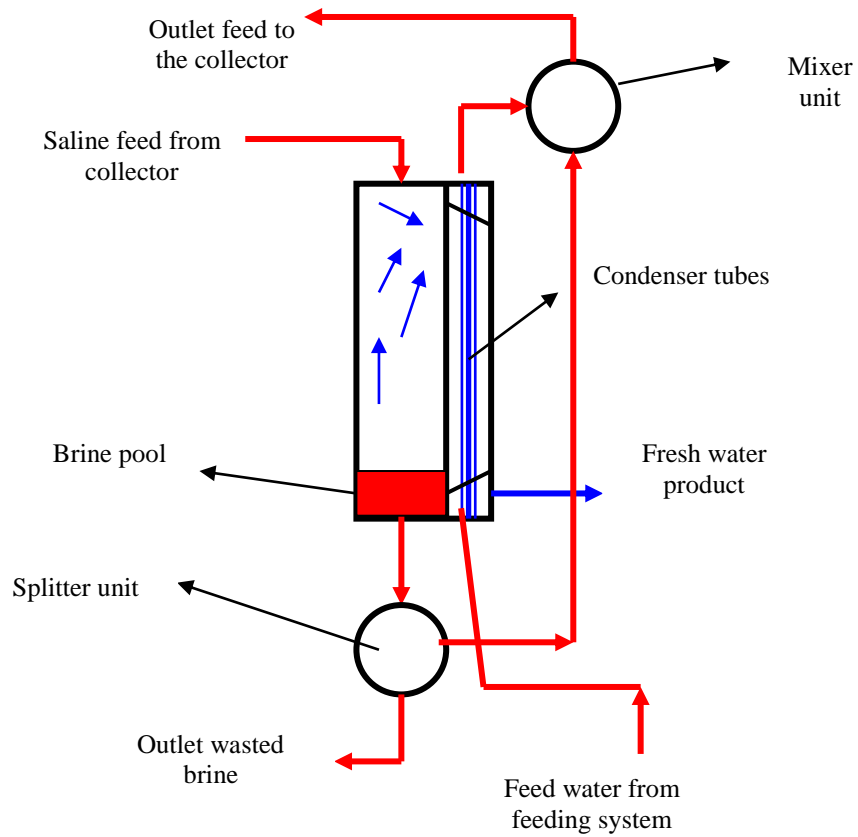


Figure (5.3) The schematic draw of 3rd configuration

66

## 5.3 THE EXERGETIC ANALYSIS

As regarded before, the available work is the maximum amount of work that could be produced by a device between any given two states. Unlike energy, which is conserved in any process according to the first law of thermodynamics, exergy is destroyed due to irreversibilities taking place in any process, which manifest itself in entropy creation or entropy increase. The availability equation for an open system in a uniform-state, uniform-flow process can be developed with the first and second law of thermodynamics. The general form of the availability is defined by equation (5.1) [34].

$$A_2 - A_1 = A_q + A_w + A_{f_i} - A_{f_e} - I \tag{5.1}$$

Where $A_2 - A_1 = 0$ is the nonflow availability change in steady state condition, $A_q = \sum_J (1 - \frac{T_0}{Tj})Q_j$ is the availability transfer due to the heat transfer between the control volume and its surroundings, $A_w = -W_{cv} + P_0(V_2 - V_1)$ is equal to the negative value of the work produced by the control volume but in most cases the control volume has a constant volume, therefore $A_w$ can be further simplified. And $I = T_0 \times Sgen$ is the availability destruction in the process. The flow availability expressed as $A_{f_{i,e}} = \sum_{i,e} m_{i,e} a_{f_{i,e}}$. So the general form in steady state condition would becomes [34]

$$A_q + A_w + A_{f_i} - A_{f_e} = I \tag{5.2}$$

### 5.3.1 Exergy Analysis for Solar Water Heater
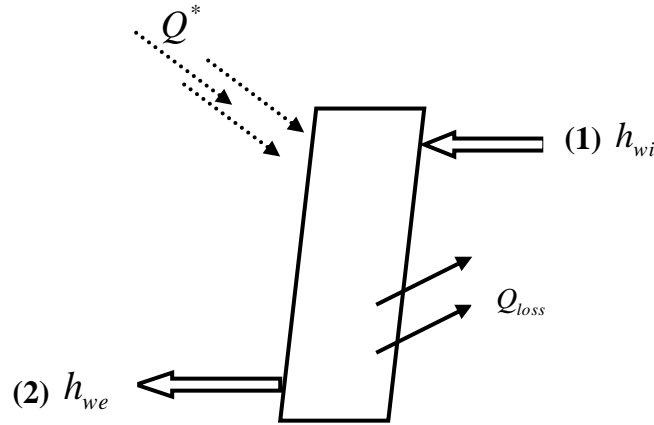


Figure (5.4) Schematic diagram of solar water heater (FPC)

Figure (5.4) shows the flow energy of one unit of solar water heater, in which the cold stream of water is at state No.1 (cold state) is moving towards the state No.2 with constant specific heat value and with equivalently in mass flow rate ($m_{wi} = m_{we}$) and $A_w = 0$. So the availability equation (5.2) becomes;

$$A_q + A_{f_i} - A_{f_e} = I \tag{5.3}$$

Where $A_q = Q^* (1 - \dfrac{T_0}{T^*})$ and $T^*$ is the apparent sun temperature as an exergy source.

Bejan (1988) has recommended $T^*$ =6000 K. this is used in this study [36].

By simplifying $A_{f_i}$ and $A_{f_e}$, equation (5.4) will be as follows;

$$A_{f_i} - A_{f_e} = m_{wi,e}^{\cdot}((h_i - h_e) - T_0(s_i - s_e))$$ (5.4)

And $h_e - h_i = m_{wi,e}^{\cdot} c_{pm}(T_e - T_i)$,

And the rate of entropy change of the fluid between outlet and inlet with neglecting the pressure drop is introduced in equation (5.5)

$$s_e - s_i = m_{wi,e}^{\cdot} c_{pm} \ln \dfrac{T_e}{T_i}.$$ (5.5)

Thus the entropy generation production equation after simplification and substitution in (5.3) by (5.4) and (5.5) becomes

$$Sgen_{col} = \dfrac{1}{T_0}(Q^*(1 - \dfrac{T_0}{T^*}) - m_{wi,e}^{\cdot} c_{pm}(T_{we} - T_{wi} - T_0 \ln \dfrac{T_{we}}{T_{wi}}))$$ (5.6)

### 5.3.2 Exergy Analysis for Flash Unit

For the second part of the system (flash unit), Fig. (5.5), which consist of the flash chamber and the condenser, the availability analysis is estimated as follows.



Brine in.
$B_i \times a_{fbi}$

Feed out.
$F_{cwe} \times a_{fcwe}$

Product.
$D_e \times a_{fde}$

Brine out.
$B_e \times a_{fbe}$

Feed in.
$F_{cwi} \times a_{fcwi}$
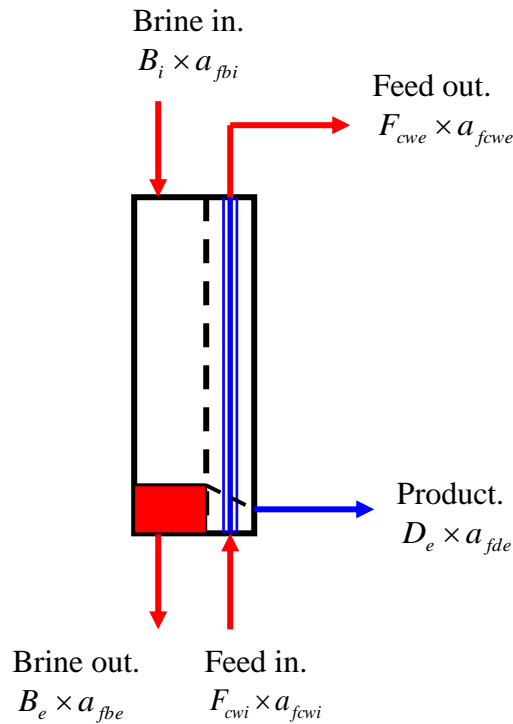
Figure (5.5) Schematic diagram of the availability
streams inlet and outlet in flash chamber

First the availability equation for the flashing chamber exists by the overall availability equation in its general form as shown by equation (5.2). For steady state

condition and with neglecting the losses to the ambient, the internal irreversibility $I$ in equation (5.2) should be used and reformed as,

$$I = \sum_i A_{fi} - \sum_e A_{fe}.$$

So the internal irreversibility for one chamber should becomes,

$$I_{fch} = I_{fu} + I_{cw} \tag{5.7}$$

Where $I_{fch}$ the internal irreversibility of the flash chamber and $I_{fu}$ is for the flash unit and $I_{cw}$ is for the condenser cooling water through the flash chamber.

For flashing part,

$$I_{fu} = A_{fbi} - A_{fbe} - A_{fde} \tag{5.8}$$

And for cooling water streams passing through the condenser,

$$I_{cw} = A_{fcwi} - A_{fcwe} \tag{5.9}$$

Equations (5.8) and (5.9) are applicable for units with adiabatic walls. For each stream the flow availability is calculated by the equation (5.10) multiplying by the mass flow rate of the stream.

$$A_{fi,e} = \dot{m}_{i,e} \times a_{fi,e} \tag{5.10}$$

Where $a_{fi,e} = (h_{i,e} - h_o) - T_o(s_{i,e} - s_o)$ \hfill (5.11)

So, after evaluating the equations, equation (5.12) represents the final state for the flashing part.

$$I_{fu} = B_i (C_{pbi}(T_{bi} - T_o) - T_o(C_{pbi}\ln(T_{bi}/T_o) - V_w(P_{bi} - P_o)/T_o)) -$$
$$B_e(C_{pbe}(T_{be} - T_o) - T_o(C_{pbe}\ln(T_{be}/T_o) - V_w(P_{be} - P_o)/T_o)) - \tag{5.12}$$
$$D_e(C_{pde}(T_{de} - T_o) - T_o(C_{pde}\ln(T_{de}/T_o) - V_w(P_{de} - P_o)/T_o))$$

For cooling water stream in the condenser, the internal irreversibility may be expressed as;

$$I_{cw} = F_{cw}(C_{pl}(T_{cwi} - T_{cwe}) - T_o(C_{pl}\ln(T_{cwi}/T_{cwe}) - V_w(P_{cwi} - P_{cwe})/T_o)) \tag{5.13}$$

The total exergy destruction in the flashing part is found by adding equations (5.12) and (5.13). So, the total entropy generation for the flashing part (flash chamber and condenser) becomes,

$$Sgen_{fch} = \frac{1}{T_o} \times I_{fch} \tag{5.14}$$

For the mixer and the splitter units shown in Fig. (5.6); and the irreversibility equations takes the form of;

$$I_{mix} = B_{mi1} \times a_{f,bmi1} + F_{mi2} \times a_{f,Fmi2} - R \times a_{fme} \tag{5.15}$$

$$I_{spl} = B_{spi} \times a_{f,spi} - B_{sp,e1} \times a_{f,spe1} - B_{sp,e2} \times a_{f,spe2} \tag{5.16}$$
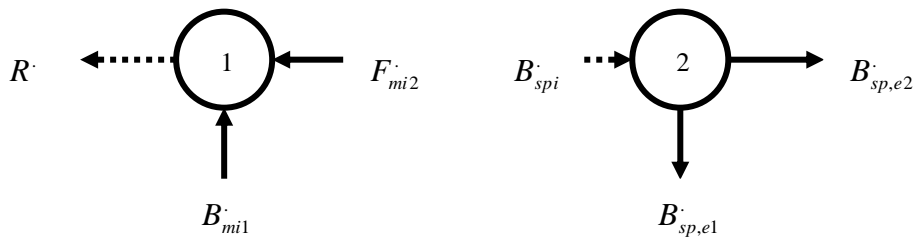


Figure (5.6) Schematic draw of mixer and
splitter units: 1. Mixer, 2. Splitter

### 5.3.3 The Exergetic Efficiency of the System

Exergy efficiency can be measured as a relationship between ingoing and outgoing exergy flows or the ratio of net exergy output to the actual exergy input for any given system when achieving the required task [37].

$$\eta_{ex} = \frac{\sum E_{xout}}{\sum E_{xin}}$$
(5.17)

Therefore, the exergy efficiency for solar water heater becomes;

$$\eta_{ex_{col}} = \frac{\dot{m}_{we} c_{pl} (T_{we} - T_{wi} - T_0 \ln \frac{T_{we}}{T_{wi}})}{Q^* (1 - \frac{T_0}{T^*})}$$
(5.17-a)

And for the flashing unit, the exergy efficiency becomes

$$\eta_{ex_{fch}} = \frac{B_e a_{fbe} + F_{cwe} a_{fcwe} + D_e a_{fde}}{(B_i a_{fbi} + F_{cwi} a_{fcwi})}$$
(5.17-b)

The overall exergy efficiency for the system configurations becomes;

$$\eta_{overall} = \frac{\dot{D}_e a_{fde}}{F_{cwi} a_{fcwi} + Q^* (1 - \frac{T_0}{T^*})}$$
(5.18)

### 5.3.4 Exergy Destruction Analysis

Exergy destruction term is a very useful tool to compare between different configurations of the process units. The dimensionless exergy destruction term $E_d$ for the solar water heater is defined by [37] as;

$$E_{d_{col}} = \frac{1}{\eta_{excol}} - 1$$
(5.19)

So for the brine heater section, the exergy destruction term becomes,

$$E_{dcol} = \frac{Q^* (1 - \frac{T_0}{T^*})}{\dot{m}_{we} c_{pm} (T_{we} - T_{wi} - T_0 \ln \frac{T_{we}}{T_{wi}})} - 1$$
(5.20)

The exergy destruction term for flashing units also defined by Faleh A. and Basil Ismail [35] as,

$$E_{d_{fch}} = \frac{exergy loss}{\dot{D}_t} = \frac{I_{fch}}{\dot{D}_t}$$
(5.21)

But the total exergy destruction for the system simply refers to the loss of exergy in a process component is obtained as;

$$\dot{E}_{Xd} = \sum_{in} \dot{E}_X - \sum_{out} \dot{E}_X$$
(5.22)

## 5.4 RESULTS

The results obtained for the system and its configurations at a known day of the year, are established in Table (5-1). All processes are assumed to be in steady state condition, all units assumed to be adiabatic walls and have the same shape design. Ambient conditions are the same and fixed for each configuration; see Table (5-1). The results are established and obtained in the summer period just to quantify good aspects for both sun and ambient conditions and also to manipulate higher values of top brine temperature more than winter conditions. It is very important to estimate the number of minimum entropy generation number for an existing solar collector has a known heat transfer area. The minimum entropy generation number is the parameter that takes care of this optimal design and operation, if it is a minimum [39]. The minimum number of entropy generation for the solar collector can be estimated as presented in equation (5.24).

$$Ns = \frac{\overset{.}{S}_{gen} T_o}{Q^* A_c (\tau\alpha)} \tag{5.23}$$

Figure (5.7) shows the entropy generation number for the collector under summer operation while operating with each configuration (1st, $2^{nd}$ and $3^{rd}$ configuration). Actually all experimental data like ambient temperature and solar radiation that corresponds to the collector operation are evaluated so the $N_s$ may be achieved. The identification of the dimensionless relation $N_s$ is useful for characterizing the performance of existing solar equipments. This procedure gives an important guide for decision making in solar engineering design [39]. From Fig. (5.7), the first configuration represents the minimum number of entropy generation for the collector. The third configuration comes next best, and the second configuration represents the highest value of $N_s$. Higher outlet water temperature from the collector considered effective in the operation of producing fresh water. A second-law analysis of the collector can provide the answer for achieving maximum convertible energy output; this is a quantity of major importance, whether a thermodynamics conversion into shaft work is involved or not [38]. Figure (5.8) describes the exergetic efficiency of the thermal flat plate collector during the operation on a day in summer season against the exergy destruction parameter. The figure shows that by increasing the exergy destruction term the collector exergy efficiency will decrease. In Fig. (5.10); the results of the exergetic efficiency are calculated based on equation (5.17-a). It can be noted here that the exergetic efficiency curves depends significantly on the solar insolation intensity at known Julian day of the year. For the first configuration, the overall exergy efficiency found to be 0.157% and the maximum allowable top brine temperature found to be 66 °C. The Exergetic efficiency of the solar collector is found to be ranged as 13-17.4% and found to be range as 22-25% in the flashing unit. For the first configuration the exergy destruction term ranged as 0.4-0.6 kJ/s; and that considered high for this configuration and depending on the increasing or decreasing in top brine temperature that also depending on the instant solar radiation. For the second configuration the results are depending on the splitter ratio taken and operated. Table (5-1) represents the data obtained at splitter ratio equal to 0.25. Increasing the value of the splitter ratio means increasing the rate of flow and that's mean decreasing in top brine temperature and decreasing of all the dependant parameters that depending on the change of top brine temperature. Top brine temperature ranged from 49-61 °C, the overall exergy efficiency is ranged from 0.08-0.16%, and the total exergy destruction is about 0.4-0.64 kJ/s, the exergy destruction term for the solar

collector brine heater obtained as 0.57kJ/s, and the exergy efficiency of the collector calculated to become 12.5-16.5%. For the third configuration, the results considered little bit the same as the presented in the first. Also all data for the third type are established in Table (5-1). The overall exergy efficiency of the system is ranged between 0.09-0.163%, and the collector exergy efficiency is found to be not exceeding about 16.6%. The exergy destruction term for both flash unit and solar collector is about 0.57 kJ/s. The maximum allowable top brine temperature obtained for this configuration is found to be about 61.4 °C. Figure (5.9) shows the comparisons between all configurations based on TBT. The first configuration recorded the highest TBT value obtained as 66 °C recorded as 61 °C and 61.4 °C for the 2nd and the 3rd configurations respectively. Overall exergy efficiency for the three configurations is illustrated in Fig. (5.10).

The third and second configurations both are show the highest values of the overall exergy efficiency. However, they represent the highest values of exergy destruction term than the first. Figure (5.11) shows the variation of the exergy destruction term for the three configurations. From Fig. (5.11), it should be noted that the first configuration represents the lowest values of the exergy destruction components and that is considerably favorable and effective. Actually studying the effect of top brine temperature on the exergy destruction term for the three types represented in Fig. (5.12). The effect of top brine temperature on the other parameters suggests that top brine temperature is directly proportional to exergy losses and exergy destruction for the overall system. The exergy destruction term appears to be effectual in design optimization of flash evaporative systems and is a viable parameter for systems comparison [35]. Figure (5.13) represents the hourly variations of the productivity for the different configurations. Configuration No.1 gives the highest productivity equal to 16.75kg/day. However configuration No.2 gives 16.56kg/day. Configuration No.3 comes next best after No.1 by total productivity equal to 16.71kg/day.
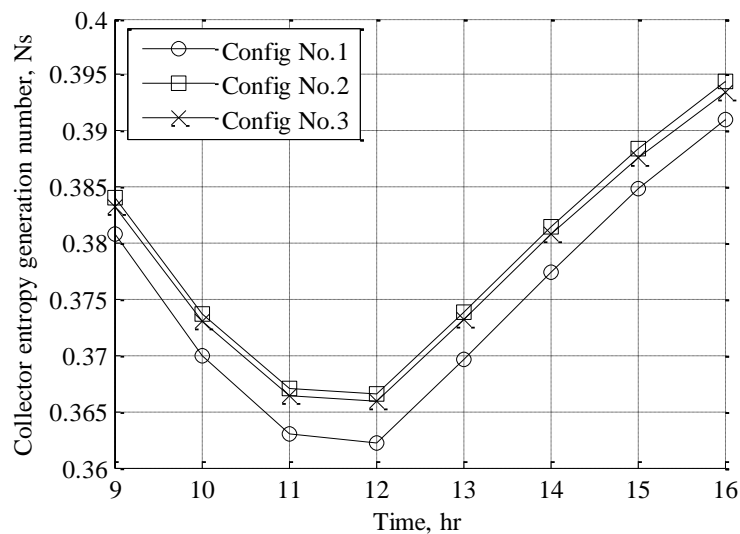


Figure (5.7) The entropy generation number for the solar collector
operated for the three configurations in summer operation
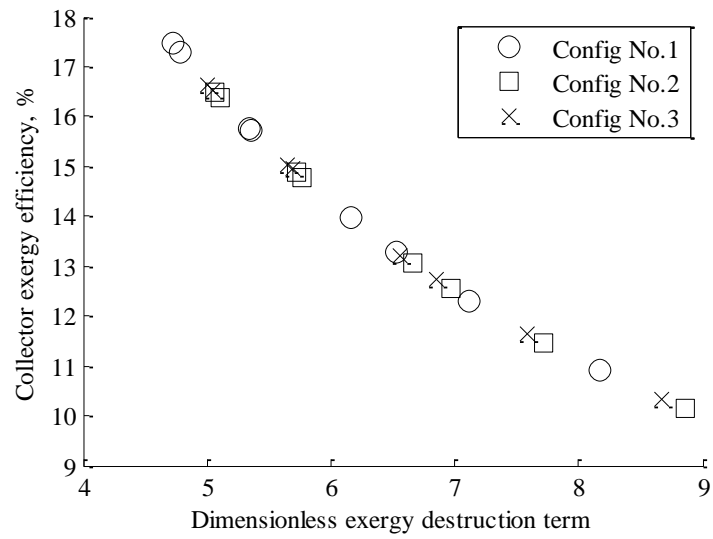
Figure (5.8) The relation between collector exergetic efficiency
and the dimensionless exergy destruction term
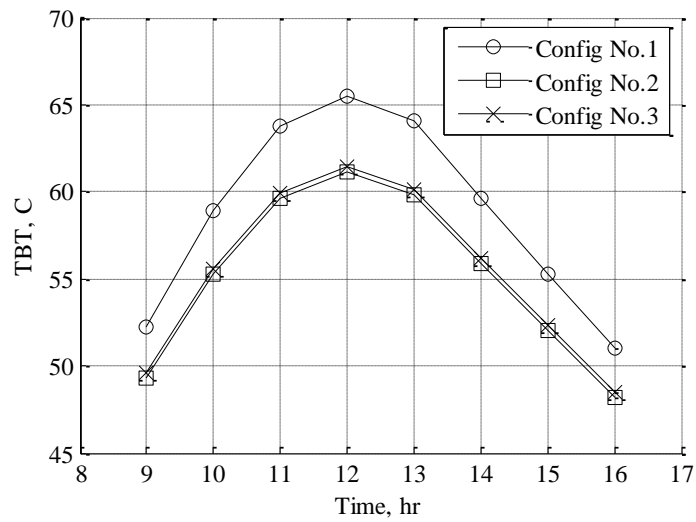


Figure (5.9) The comparison between all configurations
based on TBT
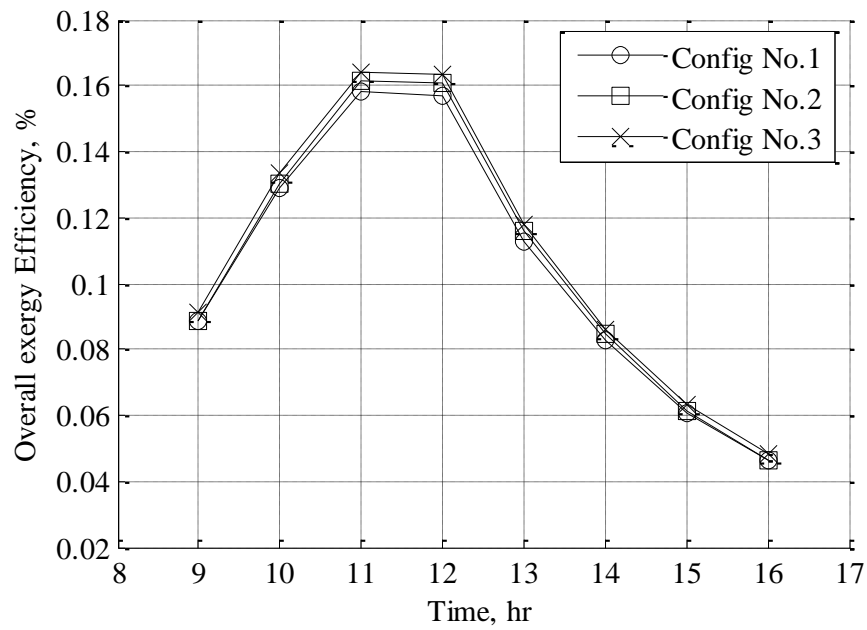
Figure (5.10) The comparison between the three system
configurations based on the hourly variation in the overall exergy
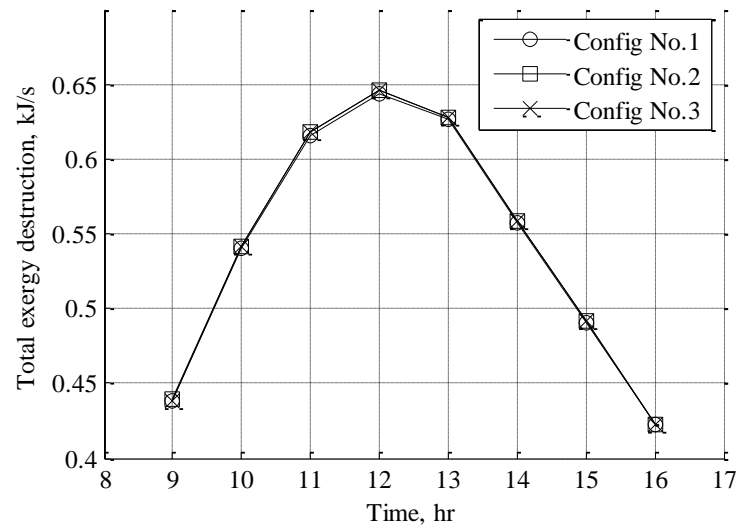


Figure (5.11) The hourly variation of exergy destruction term
for the three configurations
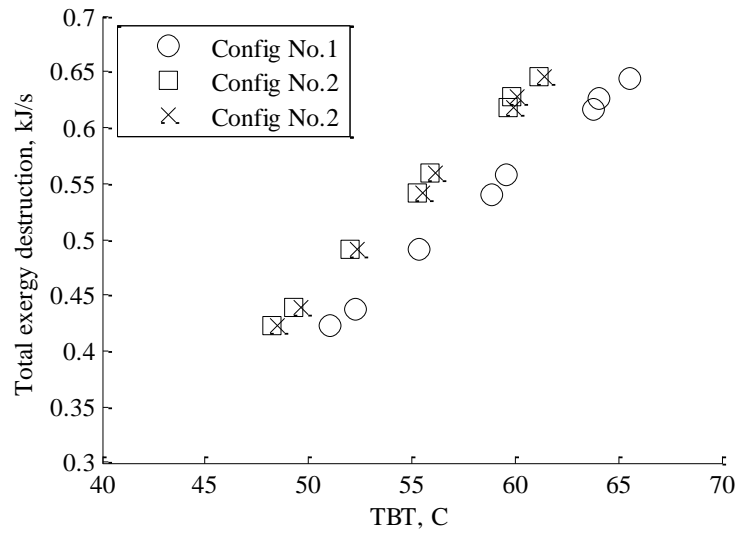
Figure (5.12) The relation between TBT and exergy destruction term



Total DP:
Config No.1=16.75kg/day.
Config No.2=16.56kg/day.
Config No.3=16.71kg/day.
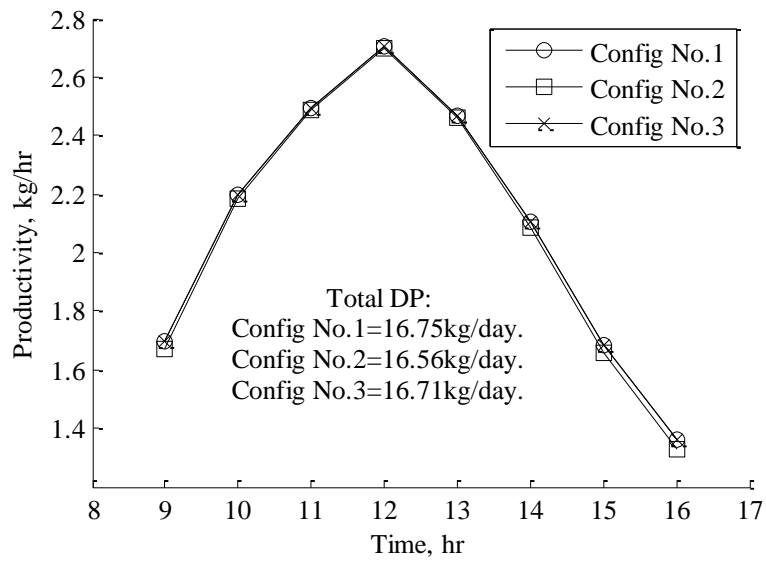
Figure (5.13) The hourly variations of the productivity of the different configurations

Table (5-1) The average values estimated on Julian day 195 in year 2005 for different types at the noon

| Weather and operating conditions: | | | | | |
|---|---|---|---|---|---|
| **Solar radiation:** | 741 W/m$^2$ | | | | |
| **Ambient temperature:** | 35 ºC | | | | |
| **Inlet feed water temperature:** | 28 ºC | | | | |
| **Wind velocity:** | 0.6 m/s | | | | |
| **Feed flow rate:** | 0.0185 kg/s | | | | |
| **Results:** | | | | | |
| **Configuration #** | **Terms:** | **Flash unit:** | **FPC:** | **SPL:** | **MIX:** |
| Configuration #1: | $\dot{E}_{Xd}\ kW$ | *0.03-0.08* | *0.4-0.56* | *Not exist* | *Not exist* |
| | $\eta_{ex}\ \%$ | *22-25* | *13-17.4* | *Not exist* | *Not exist* |
| | **Overall:** | | | | |
| | $\dot{E}_{Xd}\ kJ/s$ | *0.4-0.6* | | | |
| | $\eta_{ex}\ \%$ | *0.08-0.157* | | | |
| Configuration #2: | $\dot{E}_{Xd}\ kW$ | *0.027-0.06* | *0.4-0.57* | *0.033* | *0.01* |
| | $\eta_{ex}\ \%$ | *29-31* | *12.5-16.5* | *25* | *11* |
| | **Overall:** | | | | |
| | $\dot{E}_{Xd}\ kJ/s$ | *0.44-0.64* | | | |
| | $\eta_{ex}\ \%$ | *0.08-0.16* | | | |
| Configuration #3: | $\dot{E}_{Xd}\ kW$ | *0.03-0.07* | *0.4-0.57* | *0.033* | *0.00005* |
| | $\eta_{ex}\ \%$ | *22-24* | *12.7-16.6* | *25* | *99.8* |
| | **Overall:** | | | | |
| | $\dot{E}_{Xd}\ kJ/s$ | *0.43-0.64* | | | |
| | $\eta_{ex}\ \%$ | *0.09-0.163* | | | |

Note: Flat plate collector (FPC), Splitter unit (SPL), Mixer unit (MIX).

## 5.5 CONCLUSIONS

An exergy analysis of one stage of flash evaporation desalination unit operated and examined at Faculty of Petroleum & Mining Engineering at Suez-Egypt is presented and investigated. The exergy analysis is made for low range of top brine temperature to drive one stage of flash unit with its different configurations. The three configurations are compared by evaluating the results obtained from summer season. In the summer conditions the results show that the exergetic efficiency of one stage without mixing is about 0.08-0.157% and for the second configuration with mixing is 0.08-0.16% and for the third was 0.09-0.163% at noon. The exergy destruction value for the three configurations represents a good indication to compare between these configurations. Exergetic efficiency and exergy destruction are found to be directly proportional to the top brine temperature. $N_s$ of the solar collector for the 1$^{st}$ configuration considered low more than the 3$^{rd}$ and the 2$^{nd}$ respectively. Adding a splitter and mixer units may increase the flow rate through the collector and that will result lower top brine temperature followed by low system productivity. Finally,

configuration 1 is representing higher results of TBT and DP; and lower in exergy destruction. The total DP is equal to 16.75, 16.56 and 16.71kg/day for configurations 1, 2 and 3 respectively. Configuration 2 gives the same results of exergy destruction as configuration 3. Configuration 3 comes next best after configuration 1. Higher results may achieve in summer conditions due to higher solar intensity.

# CHAPTER 6

# EXPERIMENTAL SETUP

## 6.1 INTRODUCTION

In this chapter the test rig is constructed and fully designed based on the theoretical results that obtained in the previous chapters (chapter 2, 3 and 5). Configuration 1 is chosen to be designed and operated. The system experimentally designed and operated to examine the performance of each component under wide range of out door conditions. Also; the system is examined to study the main parameters affecting on the system productivity.

By recognizing the real system performance; some proposed methods are investigated to enhance the system productivity. The obtained experimental results are used to evaluate the obtained theoretical results under different operating conditions. Simply; the system contains a flat plate solar collector and a small size flash evaporation chamber with its entire condenser. For each part of the system; technical description is presented in this chapter. Also measurement devices are introduced.

## 6.2 SYSTEM DESCRIPTION

The system is presented in Fig. (6.1) containing: solar water heater (FPC) (1) and flash evaporation unit (2) designed vertically and attached to the condenser/preheater unit (3). Feed water enters the condenser inlet point (4) at a feed temperature then passing through the condenser tubes till out going from the outlet point (5) with a higher temperature value caused by the heat transferred from the vapor that condensate across the outside surface of the condenser tubes.

Then feed water enters the solar collector with its higher temperature to raise it to the top brine temperature (TBT) before entering the flash chamber. Then hot feed enters the flash chamber by passing through the feed injector (6). The feed injector is adjusted to operate with a feed range equal to 0.023kg/s to 0.0133kg/s. The wasted brine then exits after releasing its vapor (7) those condensates on the condenser tubes (8) to produce fresh water.
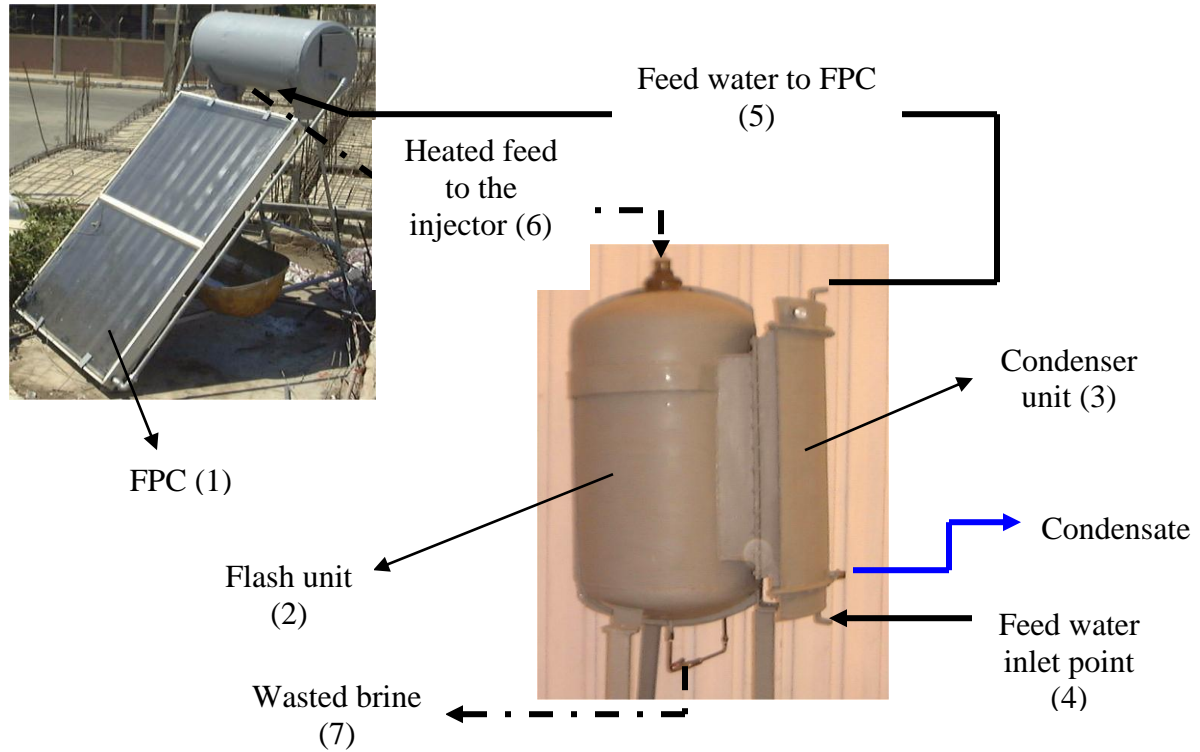
Figure (6.1) A photograph of the test rig

### 6.2.1 Technical Description of the Feed Heater (FPC)

The brine heater in this work is a flat plate solar collector. The collector is manufactured by Solar Energy Corporation Foundation at Egypt-Cairo. The collector technical data are listed in Table (6-1).

Table (6-1) The manufactured characteristics of the collector

| | |
|---|---|
| **Absorber material:** | Aluminum plate thickness=0.5mm |
| **Collector area:** | $A_c$=2.39m$^2$ |
| **Absorber area:** | $A_p$=2.1m$^2$ |
| **Effective area:** | $A_e$=88% of the collector area |
| **Coating absorptance:** | 92% |
| **Coating emittance:** | 15% |
| **Glass cover transmittance:** | 91% |
| **Insulation thickness:** | 0.037m |
| **Absorber thickness:** | Aluminum steel=0.0005m |
| **Glass cover thickness:** | 0.003m |
| **Collector weight:** | 58.5 kg |
| **Tube risers mean diameter:** | 0.016m |
| **Tube headers mean diameters:** | 0.028m |
| **Tube spacing across the collector:** | $S_t$=0.163m |
| **The plate to glass cover spacing:** | 0.07m |
| **Number of glass cover:** | 1 |

The collector is operated at a slope angle 45º. The collector aspects degree is 180º south. The connections tubes between the collector and the flashing unit are made of plastic material and insulated by a reflectance material. The tubes are made of plastic to reduce thermal losses to the ambient. The diameter of the plastic tubes is ¾ inch. The position of the collector is 3 m above the flashing unit. Figure (6.2) shows the photograph of the collector at its real location in Suez-Egypt. Figure (6.3) shows the positions of entering and exiting feed water streams to and from the collector.
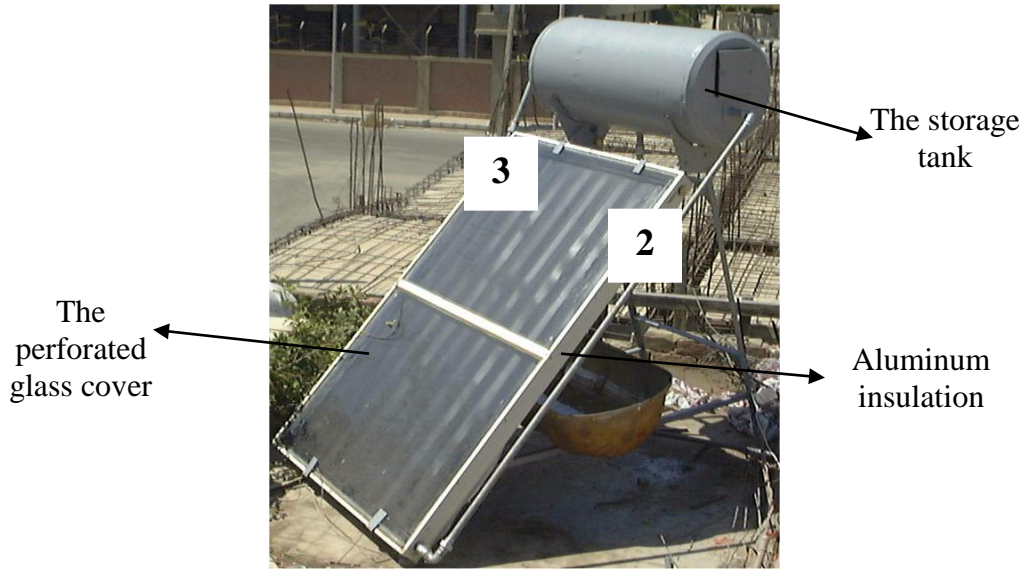


Figure (6.2) The flat plate solar collector as a brine heater at its operating location
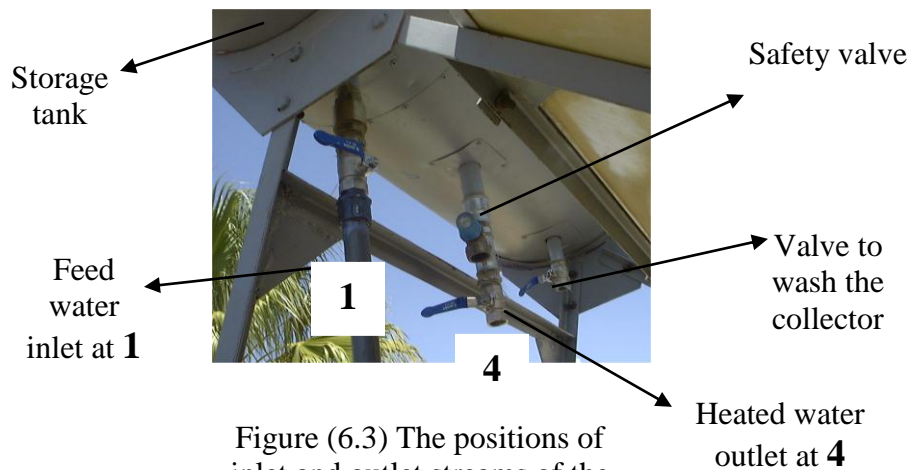


Figure (6.3) The positions of inlet and outlet streams of the collector

The absorber plate in Fig.(6.4) is manufactured from a very thin sheet of aluminum material and performed with the copper tube that passes through the collector. This sheet is paint with a very high absorbance material with 92% absorbitivity. Inside the collector the tubes are welded and designed to let a suitable spacing between each of them equal to 16.3cm. For the outer tube connections; there are 4 positions, the 1st is entering feed water to the storage tank to gain some heat at **1** then at the 2nd water leaves the storage tank at **2** then entering the collector at the lower side of it. After heat transfer operation, heated water rise through the collector up to the upper side at **3** and then entering the storage tank again, the exit as a suitable top brine temperature (TBT) at position **4**. The outside cover made from aluminum material to prevent corrosion. The glass cover is made from a very special material and thermally treated and has a 3mm thickness.
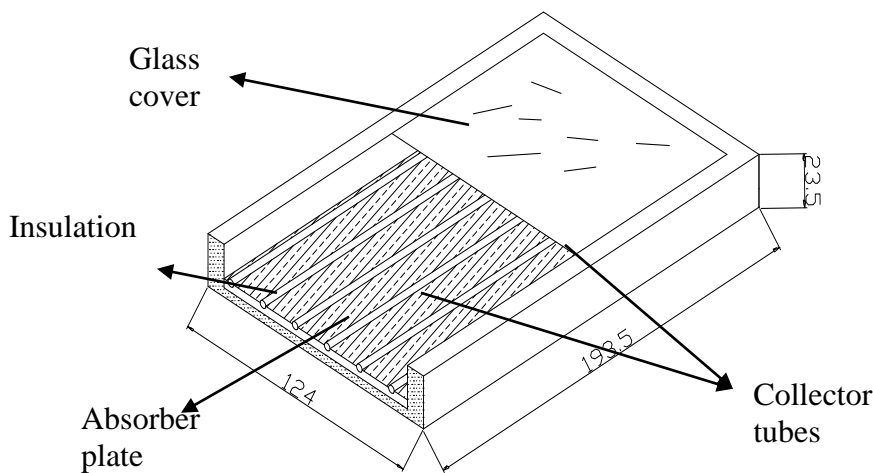
Figure (6.4) Schematic diagram of the isometric view of the collector

### 6.2.2 Technical Description of the Flash Chamber

The flash chamber is designed and manufactured from a cylindrical chamber coated with epoxy steel to prevent outside environmental corrosion effects and to reduce the thermal losses to the ambient. The height of the flash chamber is 1m, width diameter is 0.5m. The brine depth is controlled to be not exceeding about 0.2m in the flash chamber and should be kept as low as possible to avoid high non-equilibrium losses, brine entrainment, and stage flooding. The hot feed water enters the flash chamber through the feed water injector at a pressure equal to 2.5bar at maximum flow rate, and 1.5bar when operating at minimum flow rate. The injector is designed to control the feed water to the system by a three opening positions control valve. Figure (6.5) shows the flash unit attached to the condenser unit. Figure (6.6) shows a photograph of the flash chamber without attaching to the condenser unit.

81
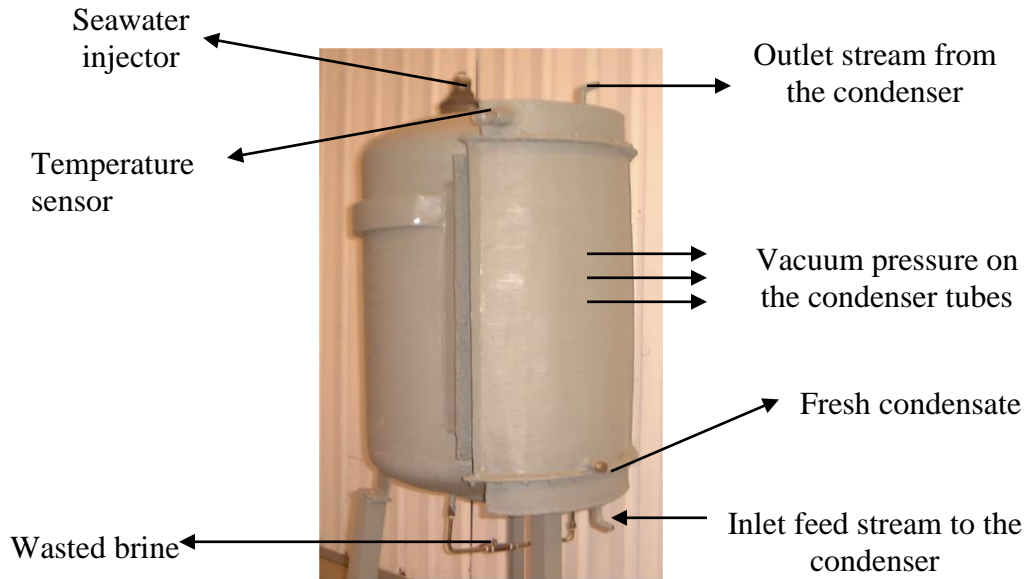
Figure (6.5) The photograph of the flash chamber
attached to the condenser unit
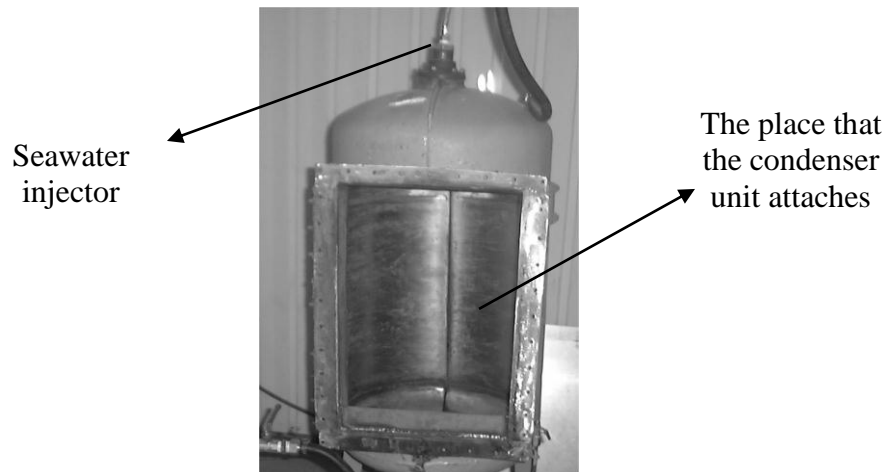


Figure (6.6) The flash chamber
without its condenser

The injector is designed to hold from one nozzle up to nine. The nozzles are attached to the flash chamber by a flange with a gland to prevent leakage. The feed water injector is presented at Fig. (6.7) that the injector attached by its nozzles.

Figure (6.8) shows the injector while attaching in the flash chamber. The height of the injector is about 26.8cm. Table (6-2) illustrates the technical specifications of the flash unit.

Flange

Hot brine inlet

Tube of flow
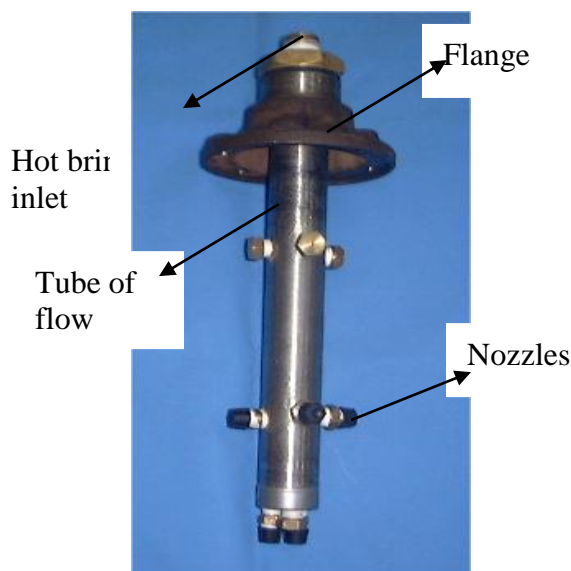
Nozzles

Figure (6.7) The injector
with its nozzles



Figure (6.8) The photograph of the
injector inside the flash chamber

Table (6-2) The technical description of the flash unit

| Item: | Description: |
|---|---|
| 1. Height: | 1m |
| 2. Width: | 0.6m |
| 3. Body thickness: | 0.003m |
| 4. Cover material: | Stainless steel |
| 5. Brine level (min-max): | 0.1-0.2m |
| 6. Welding material: | Copper |
| 7. Capacity (summer-winter): | 16.5-3.5 kg/day/total area(2.39m$^2$) |
| 8. TBT (summer-winter): | 70-42 °C |
| 9. Performance ratio (summer-winter): | 0.95-0.78 |
| 10. Average feed flow rate: | 0.0185 kg/s |

## 6.2.3 Technical Description of the Condenser Unit

The main parts of condenser unit are tubes, upper and lower headers and the outside cover. The tubes across the condenser unit are made from copper with thermal conductivity 387 W/m.K. The tube length is 0.65m and the inner diameter is 0.008m and the outer diameter is 0.0098m. The number of tubes is 69 tubes and performs a total length equal to 45m and total condenser area equal to 1.388 m$^2$. Every tube bank contains 5 tubes staggered distribution. The tubes are welded at their ends by an epoxy steel welding material in a flange made of steel copper to prevent leakages. To fix the condenser to the flash unit without any leakages; a rubber frame is welded to the condenser. Table (6-3) shows the technical descriptions of the condenser unit. Figure (6.9) shows the condenser different views with its inside tubes without covering or

headers. Figure (6.10) shows the distribution of the tubes at the upper side of the condenser. Both the upper and lower headers have the same dimensions which concluded in height that equal to 15cm. Figure (6.11) shows a diagram of the tube banks attached to the condenser from the top view. Figures (6.12) show the photographs of different views of the upper and lower headers of the condenser unit.

Table (6-3) The technical description of the condenser unit

| Item: | Description: |
|---|---|
| 1. Total surface area: | $1.3808m^2$ |
| 2. # of tubes: | 69 |
| 3. Tubes distribution: | Staggered connection |
| 4. Tube outer diameter: | 0.0098m |
| 5. Tube inner diameter: | 0.008m |
| 6. Tubes material: | Copper |
| 7. Tubes thermal conductivity: | 385 W/m.K |
| 8. Cover material: | Stainless steel |
| 9. Welding material: | Copper with Epoxy steel |
| 10. Average flow rate: | 0.0185 kg/s |



Copper flange to fix the upper header

Steel frame covered by rubber

Tubes welded to the copper flange by epoxy steel welding

Tubes across the condenser
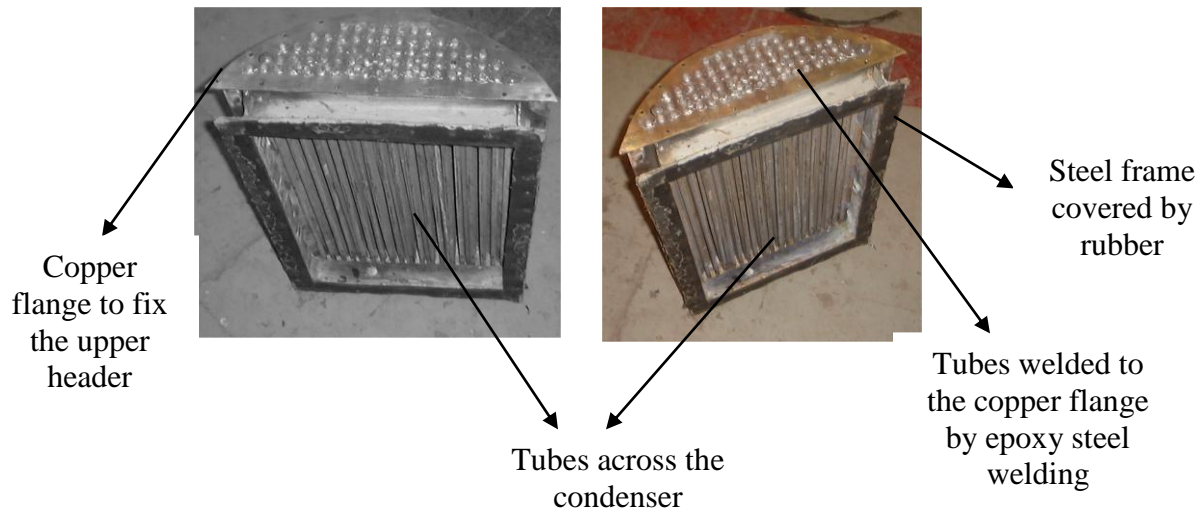
Figure (6.9) The different views of the condenser unit with its tubes



Figure (6.10) The distribution of the tubes at the upper side from the condenser
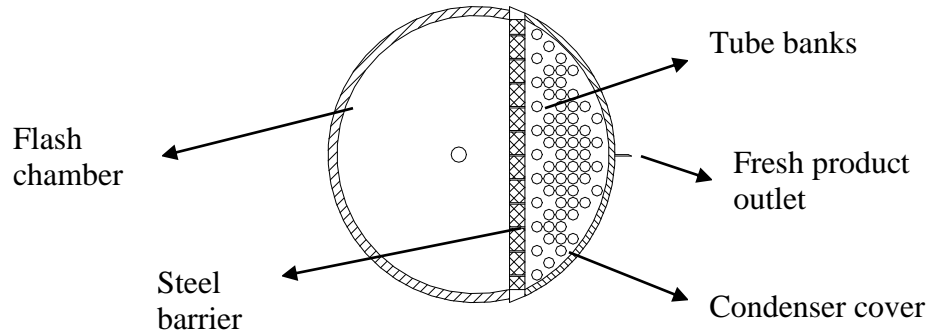
Figure (6.11) The top view of the
distribution of the tubes across the
condenser unit



Fluid in
or out

Figure (6.12) The photograph of different
views of the upper and lower covers of the
headers of the condenser

## 6.3 THE EXPERIMENTAL DATA MEASUREMENTS

### 6.3.1 Temperature

Temperatures are measured by a digital volt meter through signals provided by number of thermocouples. The device relative error is less than $\pm 1\%$. Figures (6.13) and (6.14) show the inlet feed water temperature sensors. The device error percentage is about $\pm 5\%$ ℃. The ambient temperature is measured by a common glass-tube-mercury temperature meter. Figure (6.16) shows the temperature sensor for measuring the temperature of the preheated feed water before entering the solar collector.

Figure (6.13) The digital temperature
sensor
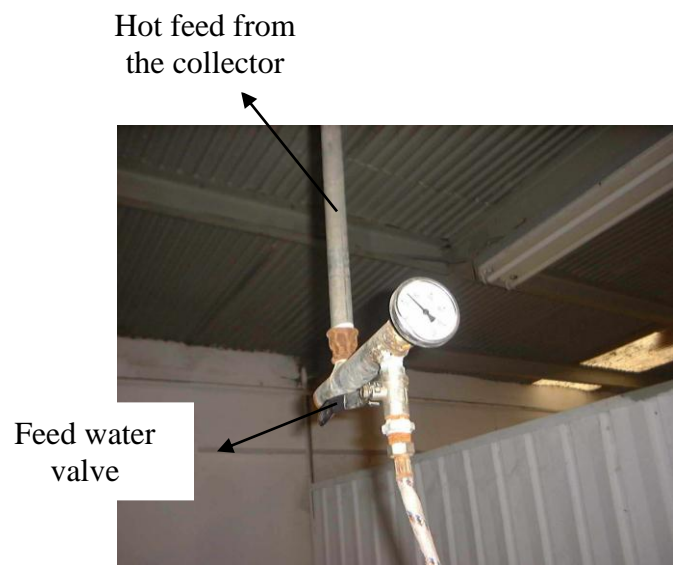


Figure (6.14) The inlet feed water
thermocouple
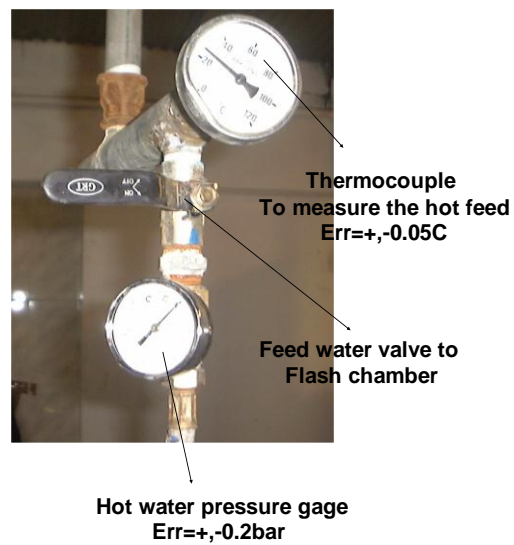


Figure (6.15) The temperature and pressure
sensors that are fixed on the feed water tube

Figure (6.16) The position of the temperature sensor that
measure the preheated feed temperature

## 6.3.2 Measurement of Weather Conditions

Global irradiation is measured by silicon pyranometer with integrator SOLAR 188 as shown in Fig. (6.17). Solar radiation pyranometer laid on the collector surface with slope angle equal to 45°. The error of the device is about $\pm 3\%$. An anemometer in Fig. (7.17) is used to measure the wind speed in m/s and measures the ambient temperature. The sensor emits an output signal proportional to the irradiance, which is carried by a two-core cable to the integrator. The sensor is a silicon pyranometer comprising a silicon solar cell with optically corrected special range. Measurement takes place according to the law of radiation on flat surface. The signal is converted into a digital via a potential integrator circuit design. The irradiance output is displayed on a four-digital liquid crystal display. For radiant exposure reading further integration of the irradiance signal is carried out. This signal is fed to a storage memory bank for display when is requested.
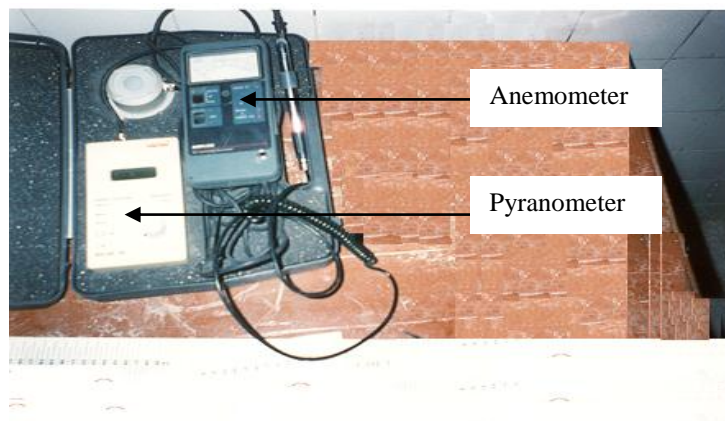


Figure (6.17) Photograph of pyranometer and anemometer

### 6.3.3 The Pressure Sensors

The inlet feed water and vacuum pressures are measured by pressure sensors. The pressure sensor for the inlet feed water is put directly after the brine injector valve. The vacuum pressure sensor is put at distillate outlet valve. Figure (6.18) shows a photograph of the pressure sensors for the inlet feed water pressure and the vacuum pressure of the flashing stage.

Feed water valve

Inlet feed pressure gage

Feed water to flash chamber

Vacuum pressure gage

Two ways valve
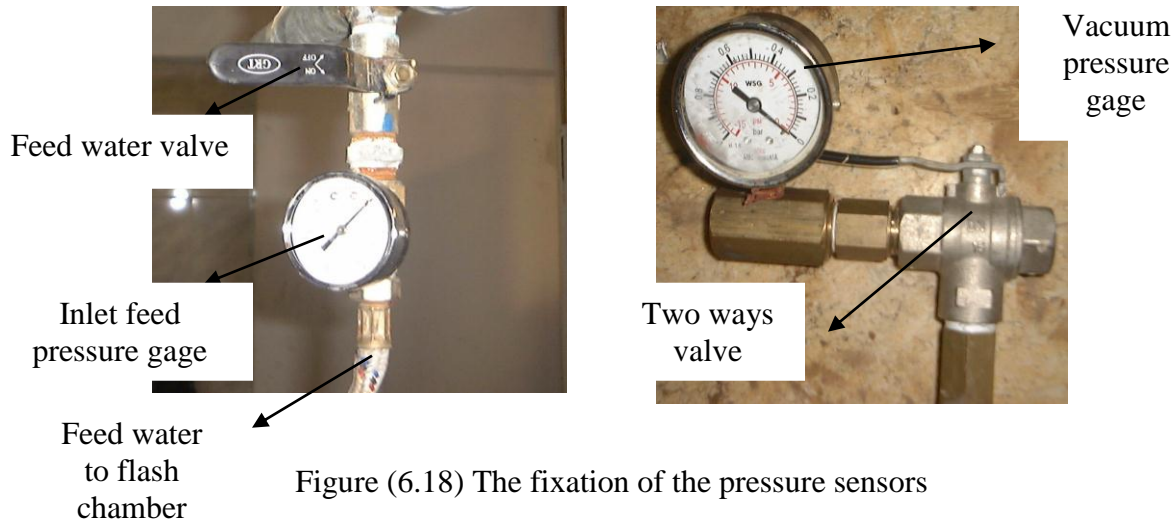
Figure (6.18) The fixation of the pressure sensors

### 6.3.4 Measurements of Different Flow Rates

Feed water flow rate is controlled by exceeding or decreasing the numbers of nozzles fixed on the injector. The flow rate of one nozzle equal to 10lit/hr and the operating pressure is equal to 5 bar. The flow rate across the system considered constant and in the whole system is operating under the steady state conditions.

By collecting the condensate and outlet wasted brine in two calibrated tanks at a certain time, the flow rate of both the condensate and brine can be measured. The brine level in the flash chamber is controlled by a fixed plastic tube outside the chamber. The level is controlled at a range about 0.1-0.2 m height (brine pool). Figure (6.19) shows the position of the tube that measured the brine level in the flash chamber side.

Figure (6.19) The position of the level indicator tube

## 6.4 THE EXPERIMENTAL PROCEDURE

The considered system is experimentally examined under real environment and operating conditions. The obtained experimental results are evaluated and examined by comparing the theoretical results. These data results are obtained by loading the developed mathematical model using the same operating conditions. Also, the developed mathematical model and its program give the capability to examine the system performance under a wide range of operating conditions. The procedure of the running device explains the operation of the test rig. Figure (6.20) shows the system flow chart that presents the map of operation of this system at its location. The procedure of running the system considered like this:

1- Feed water is pumped with its initial temperature at point 1. All chamber's valves are completely closed for the evacuation operation.
2- Valve 12 will be opened and the chamber is evacuated till the pressure gage reaches –ve0.2bar then the valve is closed.
3- After evacuating the chamber, the valves 6, 7 and 10 are opened while Valve 11 is still closed.
4- Then by opening the valve 2; feed water enters the condenser/preheater unit at point 3.
5- Feed water leaves the condenser at 4 with its higher temperature that gained from the preheater. The thermometer at 5 will read the new temperature of the feed water.
6- Feed water enters the flat plate solar collector (FPC) at 6.
7- After entering the collector at 6; the heated feed will gain the thermal useful heat from the collector and will exit again at point 7.

8- The heated feed leaves at point 8 and enter the thermometer point at 9 with its higher temperature that called top brine temperature (TBT).
9- Valve 10 will then completely open to release the heated feed through the feed injector at point 10.
10- The hot feed will flash and the vapor will go ahead towards the condenser tubes to complete the condensation process.
11- The brine water will accumulate in the brine pool.
12- Valve 11 is still closed till the level in the flash chamber at point 13 reaches to a suitable level adjusted at 0.2m height in the brine pool.
13- Solar intensity, ambient temperature, collector glass cover temperature, wind speed and inlet flow temperature are recorded at every hour during the operation.



Figure (6.20) The flow chart of the system operation

Table (6-4) shows some of experimental data measured on 15/8/2004 (summer season). The table shows that the total system productivity was about 6.9kg/day/m$^2$. The maximum obtainable TBT was about 67 $^o$C. The average wind speed was about 0.5 m/s. The total solar radiation measured for eight hours at that day was about 5.120 kWhr/m$^2$. The ambient temperature was ranged between 31 to 37 $^o$C. The average inlet fluid temperature was 28.75 $^o$C. The average operated feed flow rate was about 0.0183kg/s.

Table (6-4) Some of the experimental results obtained on 15/8/2004

| Tfs | Tco | TBT | Tb1 | Is | Tamb | Tg | Tins | Vw | Hr | product |
|---|---|---|---|---|---|---|---|---|---|---|
| *N=227* | *15/8/2004* | *FEED=0.0183kg/s* | | | | | | | | |
| 28 | 36 | 59 | 42 | 560 | 29 | 33 | 31 | 1.5 | 9 | |
| 28 | 38 | 61 | 43 | 652 | 30 | 36 | 32 | 0 | 10 | |
| 29 | 40 | 64 | 45 | 704 | 32 | 37 | 34 | 0.1 | 11 | |
| 30 | 42 | 67 | 46 | 773 | 35 | 38 | 36 | 0 | 12 | |
| 30 | 41 | 67 | 45 | 710 | 36 | 38 | 37 | 1.1 | 13 | |
| 29 | 39 | 66 | 44 | 654 | 35 | 37 | 36 | 0.2 | 14 | |
| 28 | 39 | 65 | 43 | 575 | 34 | 37 | 35 | 0.8 | 15 | |
| 28 | 38 | 63 | 42 | 492 | 34 | 36 | 35 | 0.9 | 16 | |
| **28.75** | **39.125** | **64** | **43.75** | **5120** | **33.125** | **36.5** | **34.5** | **0.575** | **8** | **16.5kg** |

Tfs: Inlet feed temperature, Tco: Condenser outlet feed temperature, TBT: Top brine temperature, Tb1: Wasted brine temperature, Is: Solar radiation, Tg: Collector glass cover temperature, Tins: Collector insulation temperature, Vw: wind speed, N: Day #.

Table (6-5) shows some of experimental data measured on 1/1/2005 (winter time). The table shows that the total system productivity was about $2.5kg/day/2.39m^2$. The maximum obtainable TBT was about 42 $^oC$. The average wind speed was about 2 m/s. The total solar radiation measured at that day was about 3.470 $kWhr/m^2$. The average inlet fluid temperature was 18.75 $^oC$. The average operated feed flow rate was about 0.0183kg/s.

Table (6-5) Some of the experimental results obtained on 1/1/2005

| Tfs | Tco | TBT | Tb1 | Is | Tamb | Tg | Tins | Vw | Hr | product |
|---|---|---|---|---|---|---|---|---|---|---|
| *N=25* | *1-1-2005* | *FEED=0.0183 kg/s* | | | | | | | | |
| 15 | 22 | 38 | 25 | 380 | 17 | 22 | 20 | 2.1 | 9 | |
| 16 | 25 | 39 | 27 | 455 | 18 | 23 | 20 | 1.2 | 10 | |
| 18 | 26 | 40 | 29 | 535 | 20 | 25 | 21 | 1.2 | 11 | |
| 19 | 27 | 42 | 31 | 562 | 22 | 25 | 23 | 2.3 | 12 | |
| 21 | 26 | 41 | 31 | 488 | 22 | 23 | 23 | 2.1 | 13 | |
| 21 | 26 | 41 | 30 | 436 | 21 | 23 | 22 | 3.1 | 14 | |
| 20 | 25 | 40 | 30 | 342 | 20 | 22 | 21 | 2.8 | 15 | |
| 19 | 24 | 39 | 29 | 271 | 19 | 21 | 20 | 3.2 | 16 | |
| **18.625** | **25.125** | **40** | **29** | **3469** | **19.875** | **23** | **21.25** | **2.25** | **8** | **2.5kg** |

Tfs: Inlet feed temperature, Tco: Condenser outlet feed temperature, TBT: Top brine temperature, Tb1: Wasted brine temperature, Is: Solar radiation, Tg: Collector glass cover temperature, Tins: Collector insulation temperature, Vw: wind speed, N: Day #.

Some of the measured data and parameters and the solar radiation are illustrated in the Appendixes (G) and (H) respectively.

## 6.5 CONCLUSION

System and its components are designed and shown in this chapter. All components are graphically and photographically illustrated. Experimentally; the maximum allowable productivity of the system is recorded as 6.9 kg/day/1m$^2$. The operating hours totally ranged about 8 hours. All measurements devices are shown and explained. The recorded data are taken under a wide range of weather and different operating conditions. All system components (condenser unit, flash chamber and the feed water injector) are designed and constructed in the location of operation at Suez-Egypt. For the collector; it is constructed by SOLAR ENERGY CORPORATION (S.A.E) at Cairo-Egypt.

# CHAPTER 7

# RESULTS AND DISCUSSIONS

## 7.1 INTRODUCTION

In this chapter the system performance is examined experimentally. The validity and accuracy of the experimental results are evaluated by comparing with theoretical analysis. The system performance is examined along one year of operation. However, two results samples are presented in this chapter, one for summer season and the other for winter. Also, productivity under a wide range of operating conditions is examined and illustrated. Summer measured data give higher results than winter. The average accumulative productivity of the system in November, December and January raged between 1.04 to 1.45 kg/day/m$^2$. The average summer productivity ranged between 5.44 to 7 kg/day/m$^2$ in July and August and 4.2 to 5 kg/day/m$^2$ in June.

## 7.2 THE RESULTS OF THE EXPERIMENTAL WORK

The experimental data are obtained under summer and winter conditions. The higher results are obtained in June, July and August respectively. Environmental data such as inlet feed water temperature; solar intensity and wind speed are considered uncontrolled data. So to compare between different results that are depending on these parameters that will take to obtain the results in a few days intervals. Comparing between the summer and winter data are important to show the difference and the effect of the various operating conditions on the system productivity. For illustration, the detailed results for just two samples days (one during the summer season and the other during the winter season) are presented in the following sections. The number of operating hours is eight for each day. The operating hours are not being changed (eight hours for summer and winter) just for comparison purposes. Figure (7.1) shows the variations of solar intensity along one day of operation in summer and winter seasons. These curves exhibits a sinusoidal shape predicted by Bird's model. Summer curves are shifted upper due to higher solar radiation values. Also the figure shows that there is a good agreement between the theoretical model and the measured data for both seasons and the maximum deviations is about 2%. Figure (7.2) shows experimentally the characteristic efficiency and operating temperatures curves of the collector (brine heater). Efficiency curve is based on gross collector area and is determined using the outdoor conditions. The thermal efficiency is a function of the outdoor temperature, the level of solar radiation, and the temperature of the fluid at the inlet. So the instantaneous efficiency is obtained by dividing the energy obtained from the collector over the proper time period by the integrated value of incident solar energy over the period. The thermal efficiency of the collector is presented as follows [26];

$$\eta_c = F_R(\tau\alpha) - F_R U_l\left(\frac{T_{icol} - T_{amb}}{I_S}\right) \qquad (7.1)$$

So; Fig. (7.2) gives a clear aspect about the collector ranking to any other collectors due to the efficiency factor, heat removal factor and thermal efficiency values. It should be noted that the mean plate temperature $T_{mp}$ can be approximately related to the average fluid temperature and that is clearly seen in Fig. (7.2). Figs. (7.3) to (7.6) show the experimental and theoretical results of the system operation during same chosen days in winter and in summer. Also the figures show the validity of the experimental work in comparison with the theoretical results.
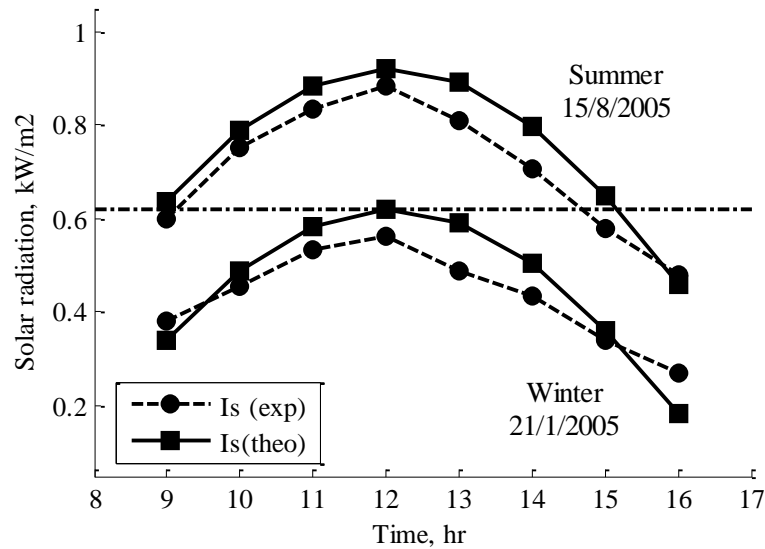


Figure (7.1) The hourly variation of solar radiation during a
sample day for both winter and summer seasons
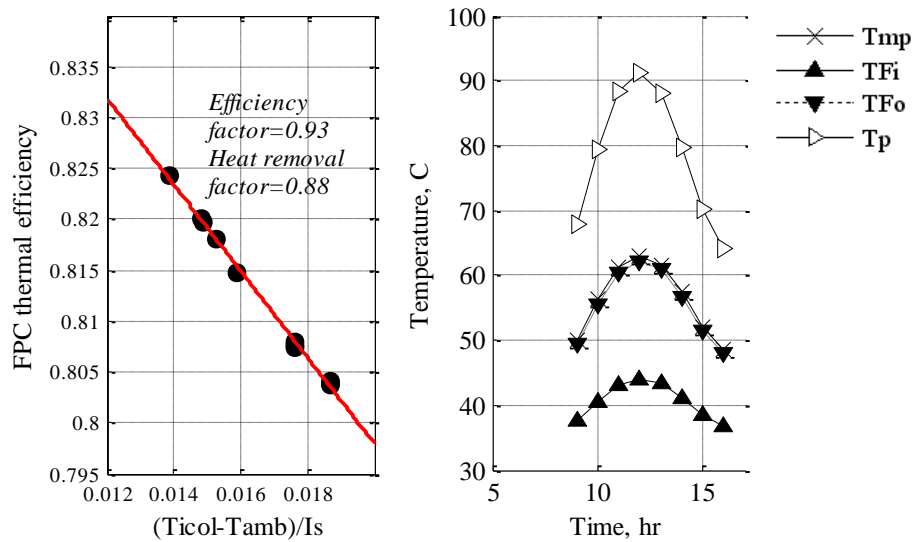


Figure (7.2) The experimental characteristic efficiency and
operating temperatures curves of the collector (saline water heater)

Figure (7.3) shows the variation of hourly temperatures for the test rig carried out on summer and winter seasons. All the temperatures showed similar trends of increasing with the increases of solar radiation during the day. For summer conditions; it was found that the water temperature $T_{bo}$ was the highest. The highest temperatures occurred between the hours of 10am-15pm. Theoretical and experimental results for the temperatures distributions are in a good agreement as shown in Fig. (7.3).
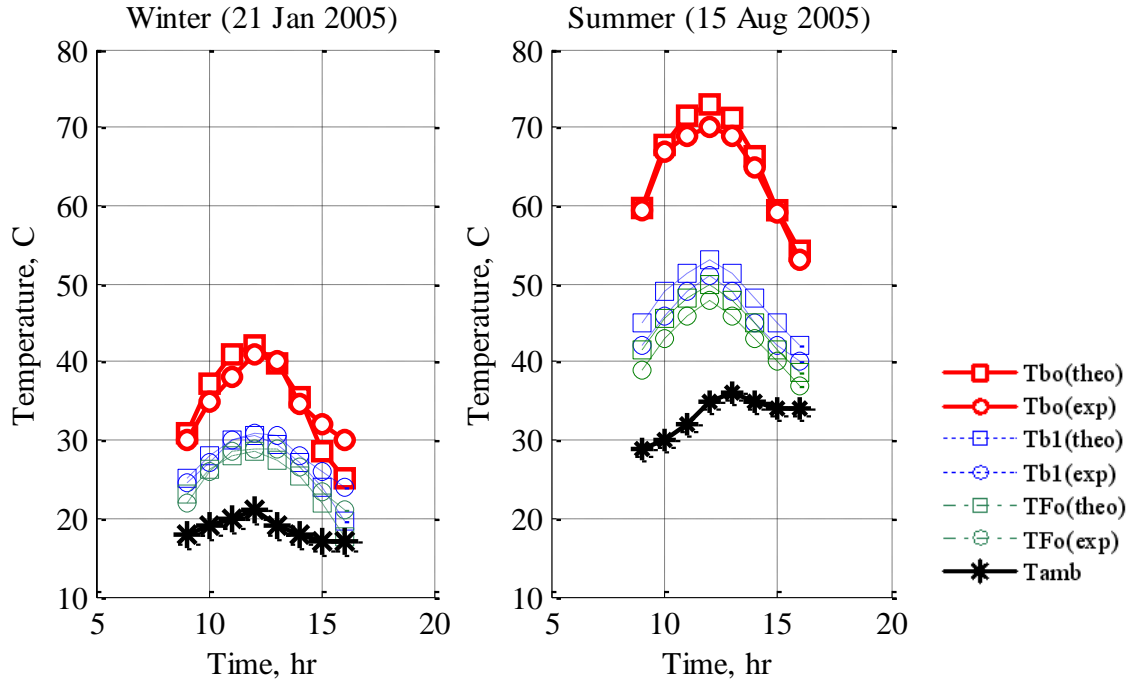


Figure (7.3) The temperature distribution of the test rig along a
sample day in winter and summer seasons

The performance of desalination system is a measure of its efficiency for producing water [47]. So; the system performance ratio can be estimated as follows [24]:

$$PR = \frac{D_t \times Hv1}{I_S \times A_c}$$

(7.2)

Where $I_S$ is the solar intensity in $W/m^2$ and $A_c$ is the collector heat transfer area in $m^2$, $Hv1$ is the latent heat of vaporization, $D_t$ is the rate of total productivity. The stage temperature drop, $T_{stage}$ °C is equal to the difference between TBT and the wasted blow down brine temperature $T_{b1}$, and is known as the flashing range. Figs. (7.4) and (7.5) shows the hourly variations in the system performance ratio (PR) and the flashing range $T_{stage}$ °C for summer and winter seasons respectively. Summer aspects show that the PR is almost ranged between 0.87-0.95 and $T_{stage}$ is ranged between 12-22 °C. For winter; PR is not exceeding about 0.7 to 0.8, and $T_{stage}$ is ranged from 10 to 12 °C. The PR is almost less than unity and the flashing range is high (equal to the flashing range in actual MSF

plants) due to operating single unit. The flashing range in summer is higher than winter due to increasing of solar radiation and TBT. Figure (7.6) shows the system hourly productivity for both season's winter and summer. The accumulative productivity on the summer time is about 7 kg/day/m². The total distillate productivity DP in winter is not exceeding about 1.04 kg/day/m² on 21$^{st}$ of January.

The figure shows that the comparison between the theoretical and measured results is acceptable with an error ranged about 6%-9% during summer and winter respectively. The lower productivity in winter is caused by the lower solar radiation against summer value. In the real outdoor operation, a delay time was noticed between the start of the run and the start of fresh water production. It is also noticed that most of the energy received in early hours is used as sensible heat to warm up the fluid mass of the system.
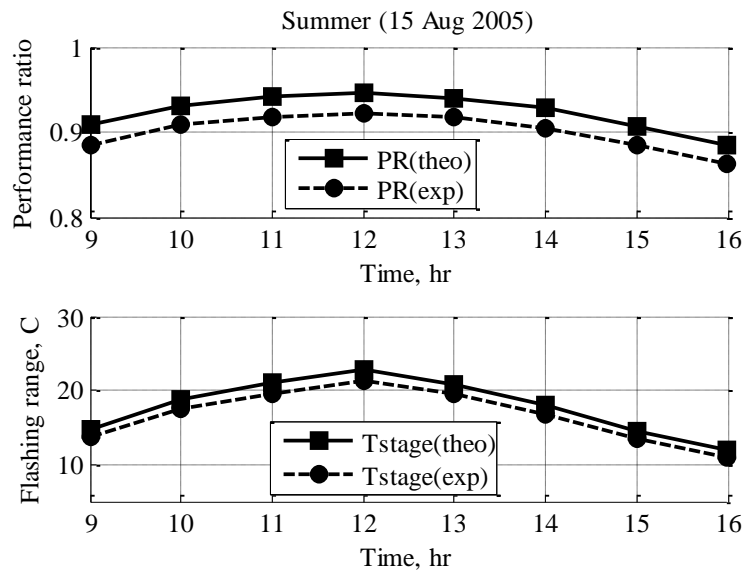


Figure (7.4) The system performance ratio and the system flashing range during the 15$^{th}$ of August 2005

Winter (21 Jan 2005)
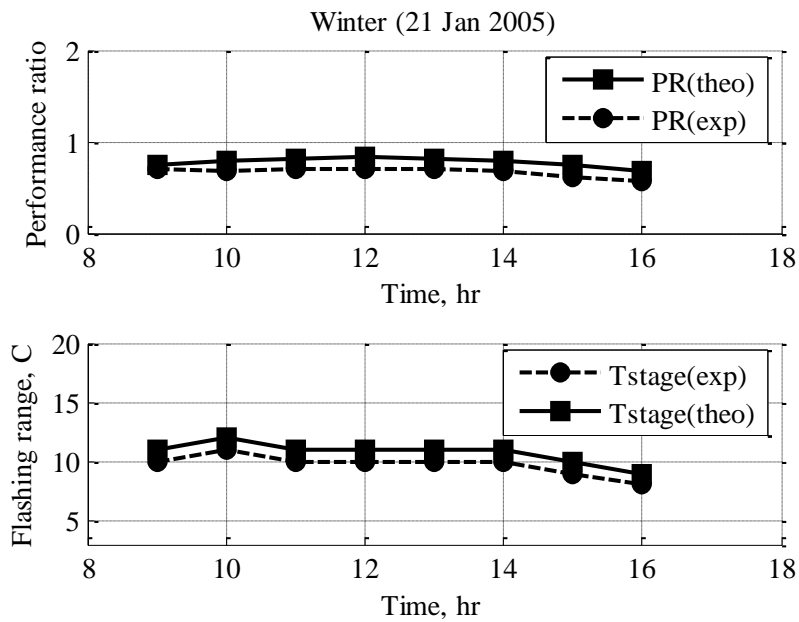


Figure (7.5) The system unit performance ratio and the system flashing range during the 21$^{st}$ of January 2005
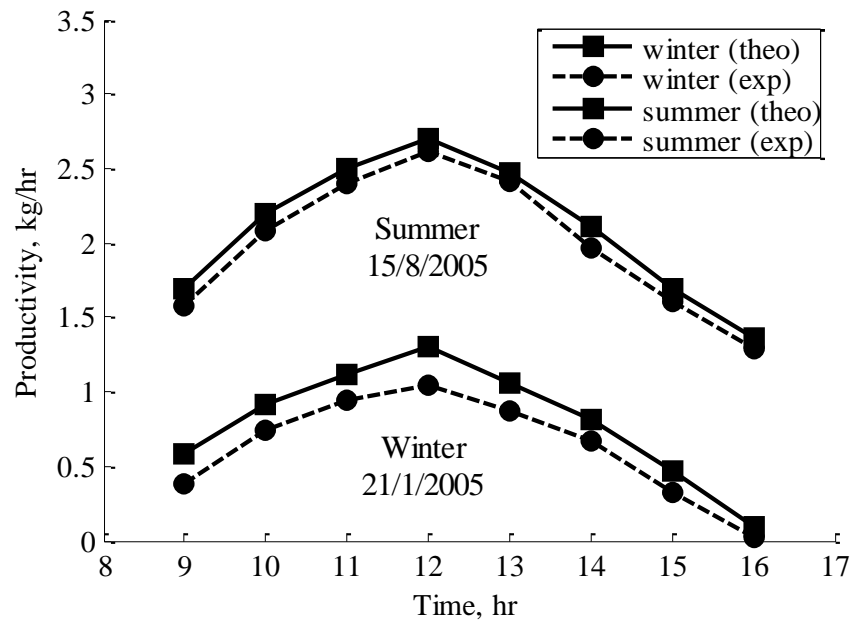


Figure (7.6) The hourly productivity of the test rig in winter and summer seasons

Following the same sequence for the days of one year long, the chosen measured data and results are tabulated in Table (7-1) below. Also Fig (7.7) shows the average variations of all system operating temperatures along one year of operation.

Table (7-1) The average values obtained for the system operation along one year

| Month | $T_{Fi}$ ºC | $T_{Fo}$ ºC | TBT ºC | $T_{b1}$ ºC | $I_S$ Whr/m² | $T_{amb}$ ºC | $T_g$ ºC | $T_{ins}$ ºC | $V_w$ m/s | Product kg/day |
|---|---|---|---|---|---|---|---|---|---|---|
| 1/2005 | 18 | 25.125 | 40 | 26 | 3144 | 20 | 24 | 22 | 2.25 | 2.5 |
| 2/2005 | 19 | 25.357 | 44.25 | 28 | 3469 | 23 | 30 | 26 | 1.3 | 4.5 |
| 3/2005 | 20.25 | 28.125 | 48 | 34.5 | 4049 | 24 | 30.5 | 27 | 4.2 | 6.5 |
| 4/2005 | 22.6 | 32 | 49 | 35.5 | 4462 | 25 | 31 | 28.25 | 3.7 | 8 |
| 5/2005 | 24 | 34 | 52 | 36.5 | 4495 | 27.5 | 30 | 30 | 1.05 | 8.5 |
| 6/2005 | 27.25 | 36.125 | 53 | 40 | 4750 | 29 | 34 | 30.25 | 2.5 | 11 |
| 7/2005 | 27.6 | 38 | 60 | 44 | 4867 | 31 | 35 | 32.357 | 1.5 | 14 |
| 8/2005 | 28.75 | 39 | 67 | 43.75 | 5120 | 33 | 36.5 | 34.5 | 0.8 | 16.5 |
| 9/2004 | 26.75 | 36.5 | 52 | 42 | 4601 | 29 | 36.5 | 30.75 | 3.25 | 12 |
| 10/2004 | 26.5 | 35.25 | 49 | 37 | 3858 | 28 | 35.6 | 31 | 3.7 | 9 |
| 11/2004 | 20.375 | 34 | 44 | 35 | 2888 | 23 | 32 | 30 | 3.8 | 5 |
| 12/2004 | 17.125 | 32 | 42 | 34.5 | 2791 | 19 | 28.5 | 23.5 | 1.625 | 3.5 |
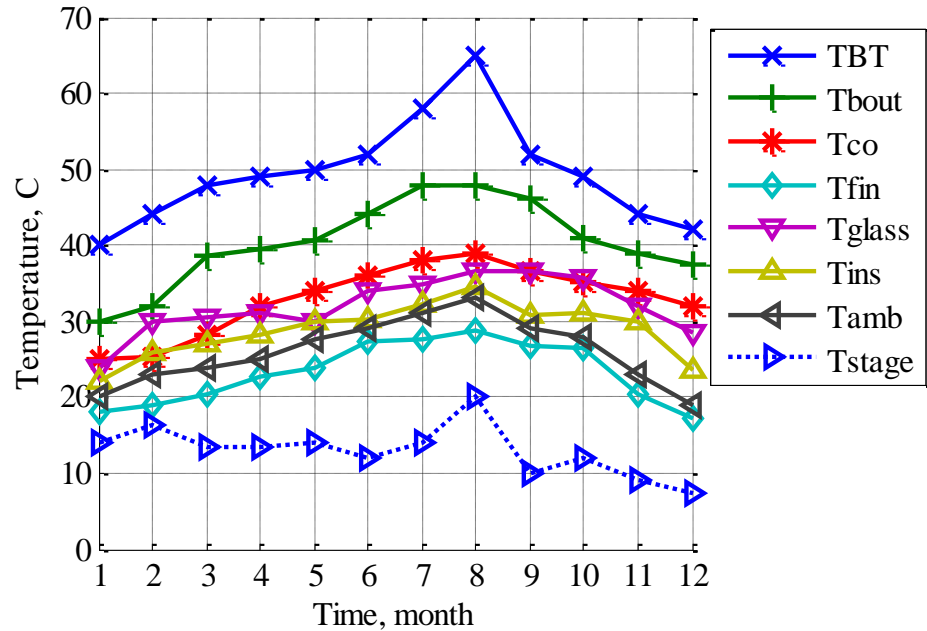


Figure (7.7) The variation of all system temperatures during one year operation

## 7.3 OPERATING CONDITIONS EFFECT ON THE SYSTEM PERFORMANCE

Sensitivity of the system as a function of different operating conditions is analyzed in this section. Solar radiation, feed flow rate, vacuum pressure and also top brine temperature; the effect of these parameters on the system productivity are illustrated in this section. Analysis is performed under a constant solar flux obtained on one day in summer season.

### 7.3.1 Solar Radiation Effect

By increasing the energy input to the system, the operating temperatures will increase. Then the vaporization rate is increase, and hence the productivity increases. And that is quite obvious between summer and winter results. Figure (7.8) shows the effect of solar radiation on the productivity. The figure shows that the system TBT and DP are proportional to the solar radiation, which depends on climatic condition of each day in summer and winter.
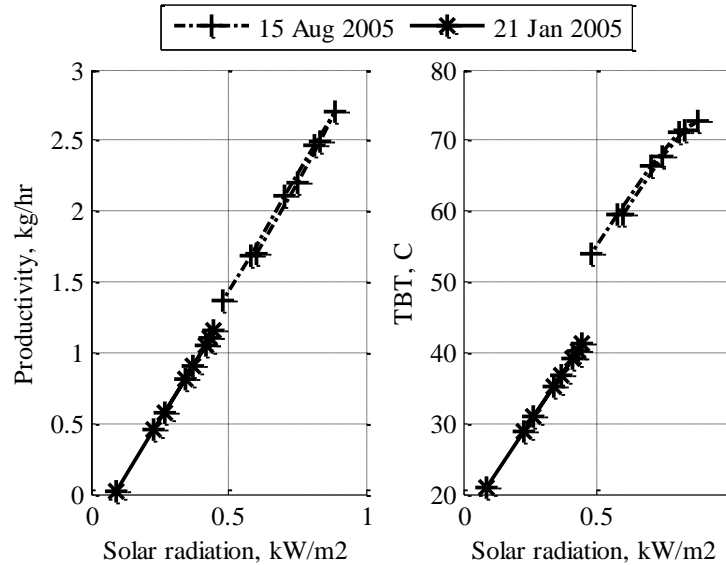


Figure (7.8) The effect of solar radiation on the system
productivity and TBT during summer and winter conditions

### 7.3.2 Feed Water Flow Rate Effect

Figure (7.9) presents experimentally the effect of increasing the feed water flow rate on the system productivity (DP) and on the all system operating temperatures (TBT, wasted brine temperature $T_{b1}$, outlet feed temperature from the condenser $T_{Fo}$). At lower values of feed water flow rates (ranged between 0.0045 and 0.0183 kg/s) the operating temperatures (*TBT*, $T_{b1}$ and $T_{Fo}$) are found to be considerably high. And that for decreasing the time needed to the flow rate through the collector to capture larger

amounts of transferring energy from the absorber plate. But at the same time, lowering feed water flow rate means lowering the overall system DP. So by increasing of the feed flow rate gradually, the system productivity will increase while the operating temperature will gradually decrease. The system productivity will increase against the increasing of feed water till the feed reaches a certain value (0.0183 kg/s) then by increasing the flow rate the productivity will decrease because of the decreasing in TBT of the system.

Figure (7.10) shows the experimental the effect of TBT on the system productivity for both season's winter and summer. The figure aspects are considered the same as the effect of solar radiation on the TBT and DP. Increasing the TBT by the solar collector will increase the system DP.
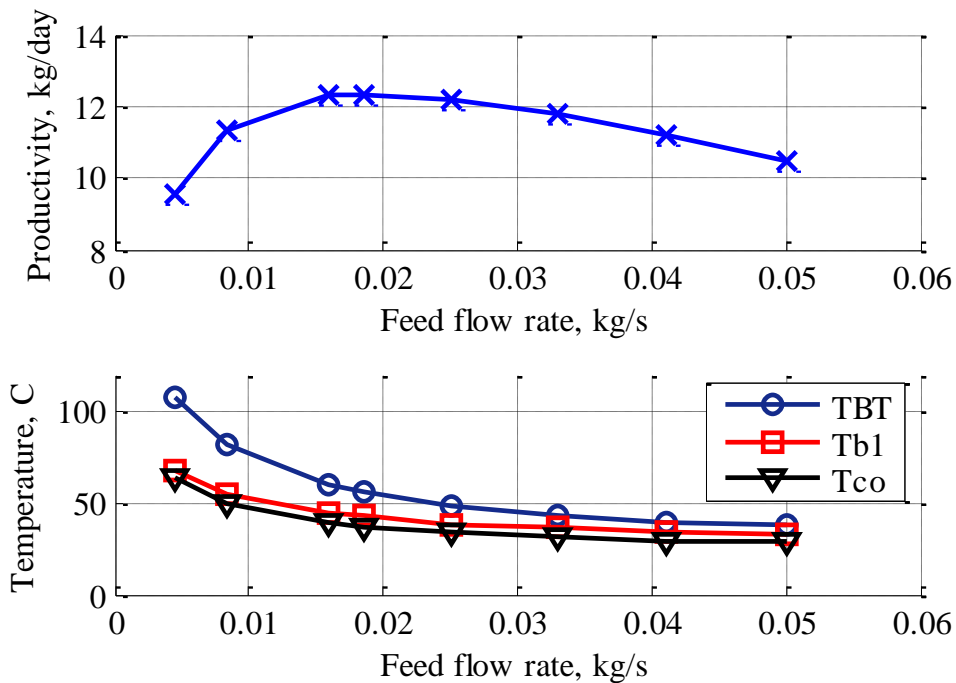


Figure (7.9) The effect of increasing the flow rate on the system total productivity kg/day, and on TBT, wasted brine and preheated feed temperatures
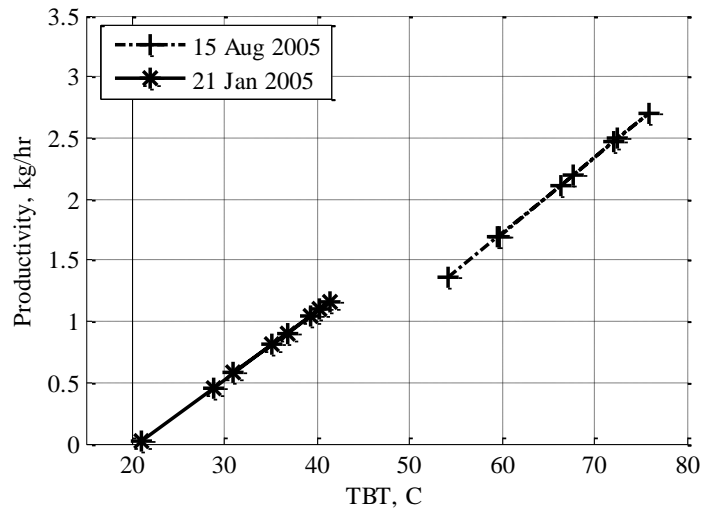
Figure (7.10) The effect of TBT on the hourly DP kg/hr, for both
season's summer and winter

### 7.3.3 Vacuum Pressure Effect

Figure (7.11) shows the variations of the system productivity with varying feed flow rate
at different pressures. By increasing the feed flow rate, the productivity increases. Figure
(7.11) shows that increasing of the vacuum pressure $P_v$ increases the *DP* of the system.
So; by increasing the pressure difference across the stage ($\Delta P_{stage}=P_{in}-P_{op}$) the productivity

increases. Where $P_{op}$ is the operational pressure that adjusted by the user and equal to $P_{atm}$
or $P_v$. To study this effect clearly; data were obtained from the system under almost the
same solar intensity and operating conditions. Table (7-2) illustrates the values of the
percentage of increasing the *DP* under the changing of the stage pressure.

Table (7-2) The average percentage increasing values of the *DP* due the variation in stage
pressure

| Operating pressure $P_{op}$, bar | Feed, kg/s | $P_{in}$, bar | $\Delta P_{stage}$ | DP, kg/day | Percentage of increase % |
|---|---|---|---|---|---|
| **Without vacuum** | 0.0133 | 1.5 | 0.5 | 9 | 8% |
| | 0.018 | 2 | 1 | 9.25 | |
| | 0.02 | 2.5 | 1.5 | 10 | |
| **$P_v$=-0.1** | 0.0133 | 1.5 | 1.6 | 9.25 | 10% |
| | 0.018 | 2 | 2.1 | 9.5 | |
| | 0.02 | 2.5 | 2.6 | 10.25 | |
| **$P_v$=-0.2** | 0.0133 | 1.5 | 1.7 | 9.75 | 12% |
| | 0.018 | 2 | 2.2 | 9.8 | |
| | 0.02 | 2.5 | 2.7 | 11 | |

At vacuum pressure equal to the atmospheric pressure, and $\Delta P_{stage}$ equal to 0.5 bar, the *DP* is collected as 9 kg/day. At $\Delta P_{stage}$ equal to 1 bar the *DP* is found to become 9.25 kg/day.

Also the *DP* is found to reach 10 kg/day at $\Delta P_{stage}$ equal to 1.5 bar. The average percentage of increasing in *DP* without vacuum is found to be not exceeding about 8%. At $P_v$= -0.1 bar, the percentage of increasing in the *DP* is about 10%, while it reaches 12% at $P_v$= -0.2 bar.
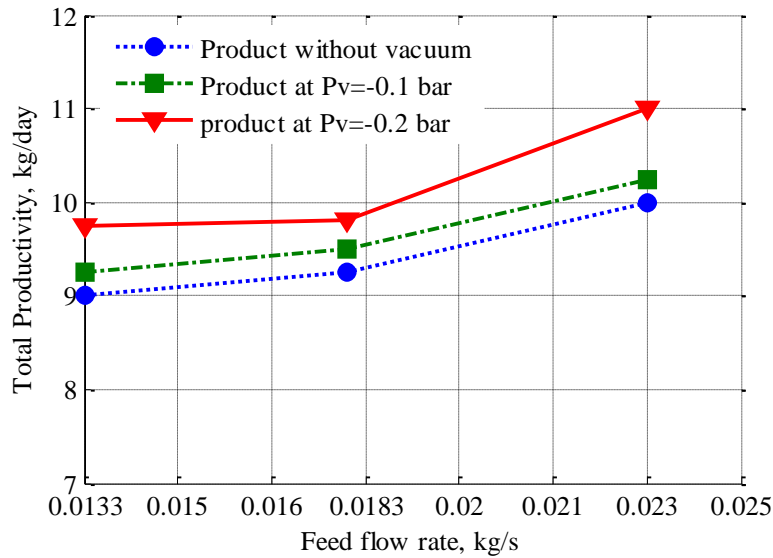


Figure (7.11) The effect of operating feed and vacuum pressure on the system total productivity kg/day

## 7.3.4 Feed Water Salinity Effect (X$_f$)

The effect of feed water salinity is investigated. Figure (7.12) shows the effect of feed water salinity concentrations on the system *DP*. The results verify that the change of the system productivity with the feed water salinity is very small. The figure shows that by increasing the salt concentration for the feed water flow rate the system total productivity (kg/day) decreases.
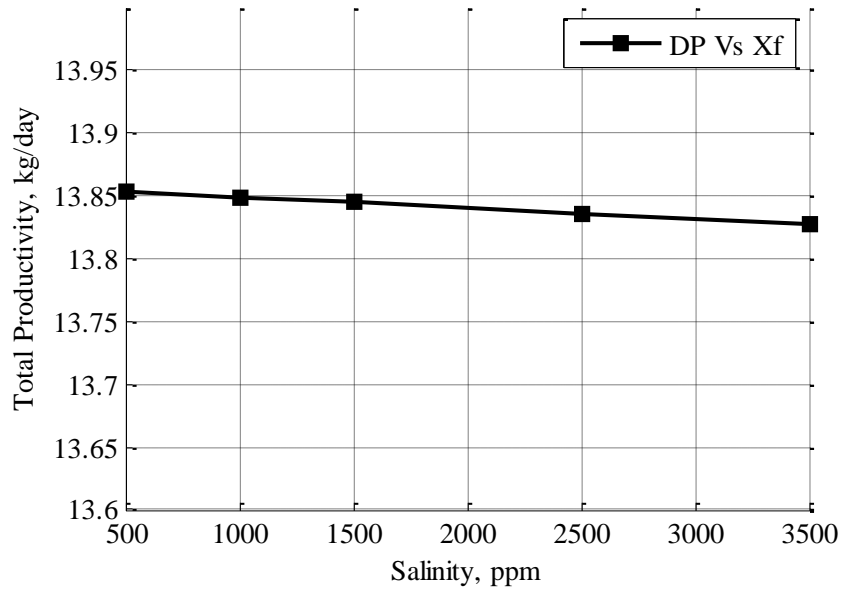
Figure (7.12) The effect of inlet feed water salinity on the system
daily productivity


## 7.4 DESIGN PARAMETERS EFFECT

Process simulation has become an accepted tool for performing the performance, design and optimization calculations of thermal processes [33]. The effect of different design parameters on the system productivity can be examined easily. In this section, the effect of the solar collector area and the number of flashing stages are theoretically examined and illustrated.


### 7.4.1 Collector Area Effect

As regarded before; collector is the prime mover of the system productivity. Increasing the collector surface area means increasing the heated surface area. Due to this increasing; the TBT will increase till reaches to the desire degree. The mathematical model studied the changing in system productivity, performance, TBT, and exergy efficiency according to different values of collector surface area.

Figure (7.13) shows the effect of the increasing in collector surface area on the system productivity, TBT, exergy efficiency and unit performance ratio of one stage. Also Table (7-3) represents the percentage of increasing in the system performance parameters. The investigated data are obtained at constant operating conditions.
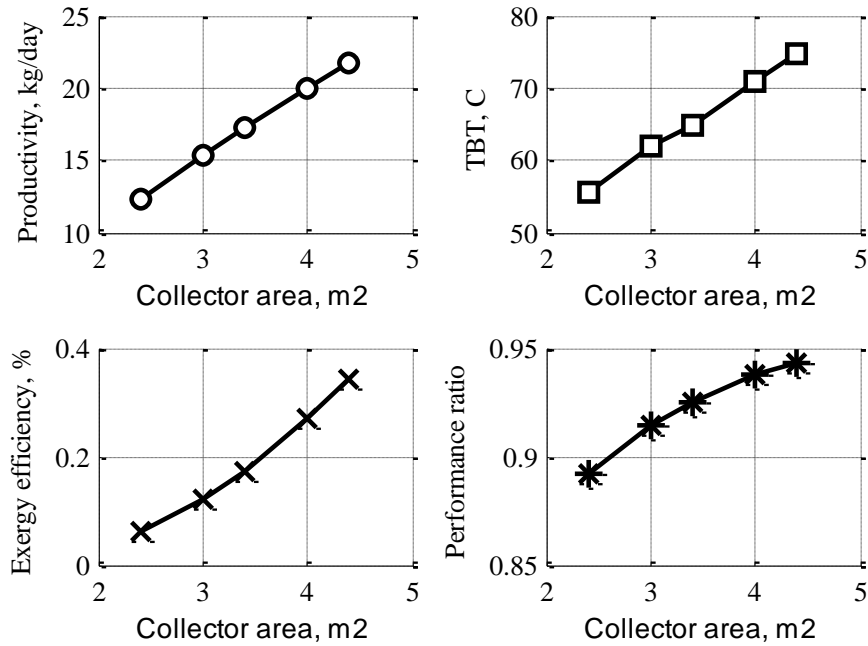
Figure (7.13) The effect of increasing in the collector surface area on the
system productivity, TBT, exergy efficiency and unit performance ratio

Table (7-3) The percentage of increasing in system productivity due to the increasing in
collector surface area

| Collector area, m² | Productivity, kg/day | TBT, ºC | Exergy efficiency, % | Performance ratio | Percentage of increasing, % |
|---|---|---|---|---|---|
| 2.4* | 12.5 | 57 | 0.085 | 0.89 | -- |
| 3 | 15.35 | 61 | 0.1226 | 0.91 | 20% |
| 3.4 | 17.3 | 65 | 0.1742 | 0.92 | 29% |
| 4 | 20 | 71 | 0.268 | 0.93 | 40% |
| 4.4 | 21.75 | 75 | 0.3423 | 0.94 | 42% |

Note: *: The actual surface area of the collector.

The percentage of increasing in system productivity is found to be 20% at collector area
equal to 3m², and 42% at 4.4 m². The performance ratio is ranged between 0.89 at
collector area equal to 2.4 m² up to 0.94 at area equal to 4.4 m². TBT increased from 57
ºC to 75 ºC. Also exergy efficiency increased gradually from 0.085% to become 0.34%.
So, the increasing of collector surface area causes an increasing in all performance
parameters.

## 7.4.2 Number of Stages Effect

Results obtained from this effect show that increasing the number of stages will increase the system productivity. Connecting one small unit powered by one solar collector gives 12.5 kg/day per total area of the collector (2.39m²), while connecting two stages with the same collector area (2.39m²) gives 22.5 kg/day. Operating three stages with the same collector area (2.39m²) gives 31.5 kg/day.

The average TBT increased from 57 °C in one stage up to 66 °C in two stages till reaches 71 °C in three stages. The unit performance ratio increased from 0.9 in one stage to 1.70 in two stages finally up to 2.60. Figure (7.14) shows the effect of increasing the number of stages on the system performance parameters. Also Table (7-4) gives clear aspects about the performance parameters values obtained from one, two and three stages.

For two stages, the percentage of increasing (P.O.I) in the *DP* reaches about 44% and the *PR* is increased from 0.89 to 1.7. While operating three stages, the P.O.I of the *DP* is found to reach 61%. And the *PR* is increased to become 2.6. The exergy efficiency is increased from 0.085% for one stage to become 0.33% and 0.72% for two and three stages respectively.
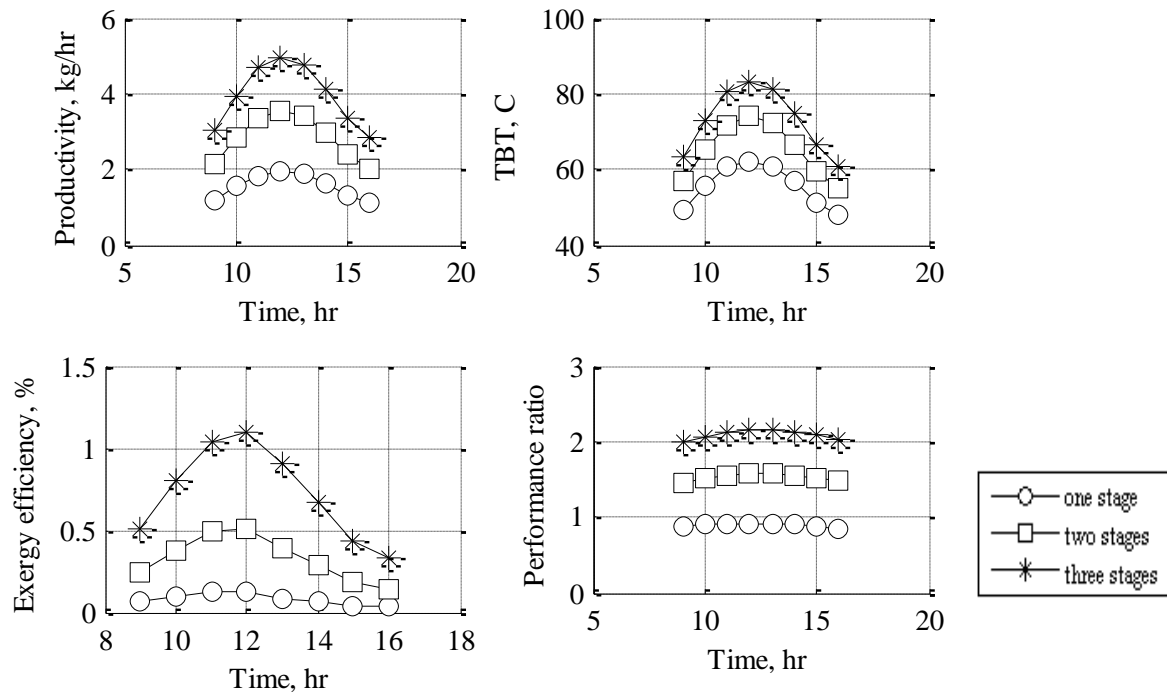
Figure (7.14) The effect of increasing number of flash unit stages on the system productivity, TBT, exergy efficiency and unit performance ratio

105

Table (7-4) The values obtained due to the increasing of number of stages

| Stage number: | Productivity, kg/day | TBT, ºC | Exergy efficiency, % | Performance ratio |
|---|---|---|---|---|
| 1 stage | 12.5 | 57 | 0.085 | 0.9 |
| 2 stages | 22.5 | 66 | 0.33 | 1.7 |
| 3 stages | 31.5 | 71 | 0.72 | 2.6 |

Note: Values for the three stages are obtained at the same surface area of the solar collector.

## 7.5 THE ERROR ANALYSIS OF THE EXPERIMENTAL WORK

The measured experimental data includes some errors due to the uncertainty of the measuring process and the limited precision of the experimental instruments. For the examination of the validity of the experimental work; fractional error ($Fr$) equation is used defined as following:

$$\% Fr = \frac{Calculated - Measured}{Calculated} \times 100.$$ Presented as a sample of measured error in June;

the average $Fr$ percentage for the measuring of the solar radiation was about 1%-2%. For the TBT; the percentage was not exceeding about 6%-7%. Also for the wasted brine and outlet feed water temperatures; the percentage was about 9% and 8% respectively. The percentage for the system performance ratio $PR$ is about 4% and 7% for the system productivity $DP$. Table (7-5) shows the average values of $Fr$ percentage for different operating and performance parameters in June. Figure (7.15) shows the fractional error percentage between the measured and calculated data of the $DP$. The maximum error percentage isn't exceeding about 7% in June. And the minimum error percentage is recorded in January as 4%.

Table (7-5) The $FR$ error percentage of the measured data

| Parameter: | $Fr$ Percentage%: |
|---|---|
| $I_S$ | 1%-2% |
| $TBT$ | 6%-7% |
| $T_{b1}$ | 9% |
| $T_{icol}$ | 8% |
| $DP$ | 7% |
| $PR$ | 4% |
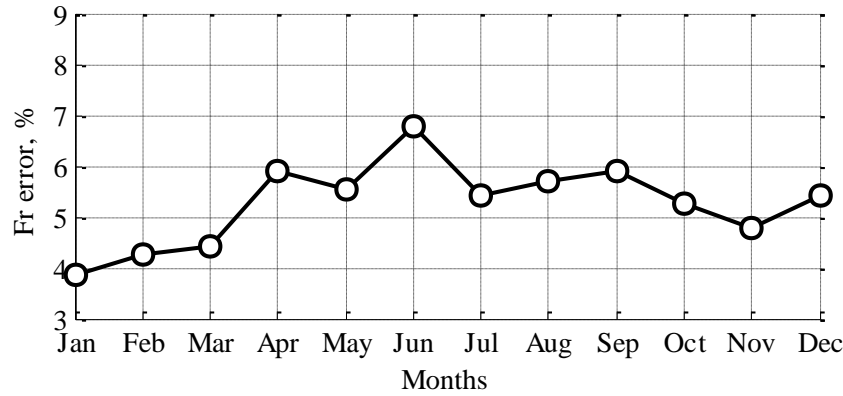
Figure (7.15) The deviation of the *Fr* error between the calculated
and measured *DP*

## 7.6 CONCLUSION

To summarize and conclude the results and the discussions in this article, the following points could be withdrawn:

1. Increasing in solar intensity will increase the system productivity.
2. The unit performance ratio considered low ranged about 0.7 to 0.8 in winter and 0.8 to 0.95 in summer.
3. The stage 1$^{st}$ low efficiency considered high in summer and low in winter and globally ranged from 78 to 90% at the optimum operating hours.
4. The system daily productivity in summer is about 10 to 16.5 kg/day per total area of the collector (2.39m$^2$). And for winter it is found to be about 2.5 to 3.5 kg/day per total area of the collector (2.39m$^2$).
5. The results of the proposed mathematical model are in good agreement with those of the experimental model of the system.
6. Increasing the vacuum pressure will increase the system productivity. The percentage of increasing of the system productivity is varying between 8% at $P_v=P_{atm}$ to 12% at $P_v=0.2$ bar.
7. The *Fr* percentage error of the system productivity along one year of operation is not exceeding about 7% as a sample day in June.
8. The collector efficiency factor is about 0.93 and the heat removal factor is about 0.88. Increasing the collector surface area from 2.4m$^2$ to 4.4m$^2$ may increase the total productivity by 42%.
9. Increasing the number of stages will increase the condenser surface area and so the system productivity. Increasing the number of stages up to two stages was found to exceed the productivity as 44.5%. While increasing the number of stages up to three may cause an increasing equal to 60% of the system productivity. The total productivity for one stage operated by one collector was 12.5 kg/day and 22.5 kg/day for two stages and 31.5 kg/day for the three stages.

10. The effect of increasing the number of stages for one collector considered valuable more than the changing in the system configurations.
11. Finally, the system gives higher productivity in summer due to higher TBT, i.e., higher solar intensity. Reasonable rate of feeding water is ranged about 0.0183 kg/s. The feed water salinity is controlled to be 1000ppm. System productivity considered good compared with the solar collector area and operation of single flash unit.

# CHAPTER 8

# ENHANCEMENT OF SOLAR WATER DISTILLATION PROCESS BY SURFACTANT ADDITIVES

## 8.1 INTRODUCTION

Surfactants are specialized additives, are being used in many areas such as mineral processing, paper making, paint making, etc…, formulated to improve the emulsifying, spreading, sticking and absorbing properties of liquids [40]. Generally; surfactants are used to change the surface properties of water. Many effects of surfactants are known – they reduce surface tension, skin friction in tubes and enhance boiling heat transfer. Most of them can be explained by the basic structure of the surfactant molecules [42]. Ionic surfactant consists of one hydrophilic and another hydrophobic end and when it is introduced into water may form micelles depending on the concentration spherical, disc or rod shaped conglomerations of molecules are formed. They also form hydrogen bonds with water and with each other, thus changing the properties of water. Also Surfactants are effective at extremely low concentrations - in the range of 100ppm or so - and hence find application in almost all industrial processes in addition to their use in cleaning and detergent products. Boiling heat transfer is a very effective and efficient mode of heat transfer, and it is encountered in numerous engineering applications. Also heat/mass transfer enhancement additives are routinely used in absorption chillers primarily to increase the rate of the transfer process occurring in the absorber. The enhancement additives also increase the condensation rates [50].

Though enhancement additives have been in use in commercial absorption chillers since the 1950's there has been no complete understanding of the enhancement mechanism. Boiling with surfactant additives is generally an exceedingly complex process, and it is influenced by a larger number of variables than the phase- change process of pure water [44]. A few numbers of studies have been made in the past to relate the nucleate boiling heat transfer coefficient to the surface tension of a boiling liquid. Many researchers examined the behavior of the surfactant additives on pool boiling heat transfer. Ying, et al [45] examined such effect on pool boiling. The experiments were carried out for relatively wide ranges of surfactant concentration and heat flux. It is claimed that the obtained results verify that a small amount of surfactant additive makes the nucleate boiling heat transfer coefficient of water considerably high. It was also found that there was an optimum additive concentration for high heat flux. Hetsroni, et al [43] examined the same effect with different values of surfactant concentration. The experimental results showed that the addition of small amount of environmentally acceptable alkyl glycosides makes the boiling behavior quite different from that of pure water. Todor Stoyanov [42] studied the effect of surfactant on heat transfer and bubble formation in sub cooled pool boiling. Toshiaki Inoue, et al [51] measured surface tension of ethanol/water mixtures over the whole ethanol fraction range and the effect of the surface-active agent on surface tension is also measured in the mixtures, in order to gain basic data related to enhancement of the heat transfer coefficient in water and the mixtures. The experiment

was carried out in the whole range of the ethanol fraction and in a surfactant concentration of 0–5000ppm. It is found that depression of the surface tension by the surfactant remarkably enhances the heat transfer coefficients in the nucleate pool boiling. S. Kulankara, et al [50] measured the surface tension of aqueous lithium bromide with and without various surfactant additives, using a drop weight method. Measurements were also made on water, with and without an additive. The results provide new information that clarifies several confusing aspects of the literature data. The major result is the realization that the surface tension of aqueous lithium bromide is strongly affected by the presence of surfactant vapor around the liquid interface. One important field of the application of boiling and evaporation is in desalination of seawater, which is becoming essential in some arid regions [44]. It was shown by Sephton [48] in 1974 that addition of small amounts of surfactants to seawater can substantially enhance the boiling process, and reduce the price of the desalinated water to an acceptable level. At that time, the research was discontinued because the environmental impact of surfactants was not known. Since the concentrations are usually low, addition of the surfactant to water causes no significant change in the saturation temperature and the majority of other physical properties, except for the surface tension and, in some cases, the viscosity. Sayed Siavash, et al [52] examined the fouling restricts membrane performance. In that work reverse osmosis membranes were fouled with water. Chemical cleaning of the RO membranes using acid, alkaline, surfactant and detergent solutions was discussed. Cleaning efficiency depends on the type of the cleaning agent and its concentration. It was shown that the efficiency increases with increasing the concentration of the cleaning agent.

Desalination by means of renewable energy sources is a suitable solution for providing fresh water to a number of regions so far apart as the Mediterranean basin, Africa and world-wide remote areas [49]. This solution becomes more competitive, especially for remote and rural areas where small quantities of water for human consumption are needed. For some time, a single-effect basin-type solar still has been the cheapest way to produce drinkable water using solar resources. Due mainly to the rejection of the latent heat condensation, small daily production less than 4–5 kg/m$^2$, with specific energy consumption around 7000 kJ/kg was obtained [49]. Badran et al [46] presented a flat plate solar collector coupled with solar still unit. The experimental investigation was made to study the effect of coupling a flat plate solar collector on the productivity of solar stills. It was found that coupling of a solar collector with a still has increased the productivity by 36%. The still area was about 1m$^2$ filled with brackish water supplied to it from a collector. The flat plate collector area was found to be about 1.08m$^2$. The system total productivity was found to give 3.51 kg/day and found to be 36% more than that when the still was operated alone (2.24 kg/day). Also Soliman [3] examined a humidification dehumidification desalination system powered by solar concentrator collector (area=2.5m$^2$) with total unit productivity equal to 8 kg/day. Nafey, et al [24] presented a small size flash evaporation unit that operates by the solar energy for producing a small amount of potable water. The system is mainly consists of a flat plate solar collector (FPC) and a flash evaporation unit. The system is operated and investigated under real environmental conditions during winter and summer seasons. The total productivity of the system in winter ranged between 1.04 to 1.46 kg/day/m$^2$, while

the summer productivity ranged between 4.18 to 7 kg/day/m$^2$. From the literature [9-12]; it should be noted that solar desalination technologies have a limited productivity compared with other technologies. So, surfactant additives may be used to enhance the distillation process productivity by increasing the bubbles formations (releasing more vapors). The main objective of the current article is to examine the performance of the solar distillation system proposed by Nafey et al [24] with different surfactant dosages. This study is performed at five concentration values of environmentally acceptable anionic (*SLS*) surfactant [4] in order to find out their effects on the top brine temperature (TBT) and the daily productivity (DP) of the considered system. For that aim, natural solar energy over the collector (original system) is replaced by a solar simulator system (new system) to examine the effect of surfactant concentration under a constant power input to the system.

## 8.2 SYSTEM DESCRIPTION AND EXPERIMENTAL WORK PROCEDURE

Fig. (8.1) shows a schematic diagram of the system components. Simply the original system containing: solar water heater (FPC) (1) and flash evaporation unit (2) designed vertically and attached to the condenser/preheater unit (3). Feed water enters the condenser inlet point (4) at a known temperature then passing through the condenser tubes till its discharge from the outlet point (5) with a higher temperature value which caused by the heat transferred from the vapor that condensate across the outside surface of the condenser tubes. Then feed water enters the solar collector (with its higher temperature) to raise it to the top brine temperature (TBT) before entering the flash chamber. Then hot feed water enters the flash chamber by passing through a feed injector (6). The wasted brine then exits after releasing its vapor (7). Vapor condensates on the condenser tubes (8) to produce fresh water. For the operation of the solar simulator; an A.C. electric heater (9) is used as a heat source to replace the solar flux in actual solar collectors.

A variac transformer (10) is used to control the heating power input in the range of 0-2000 watts, through controlling the voltage on the heater. A voltmeter and ammeter are used to measure the power input. The heater maximum load is about 2000 watts, and its net surface area is about 140 cm$^2$. By switching the volt variation arm of the variac transformer to the desired watt (simulating the solar flux); the electric heater output load will become under control. The collector is full covered (11) and insulated just to quantify only the effect of electrical heater without the sun flux effect. So the collector is replaced to work as a storage system (tank) heated by electricity instead of the sun. Fig. (8.2) shows a photograph of the variac transformer connected with the voltmeter and the ammeter.

Figure (8.1) A schematic draw of the system components

The surfactant is introduced at different dosages of concentrations into the inlet feed water tube (4). The experiments are run along eight hours for one concentration. Yang and Tzan [45] demonstrates that the effect of additives, on boiling heat transfer, decreases when the concentration of the solution was higher than 700ppm. Therefore, surfactant dosages equal to 50, 100, 200, 300, 400 and 500ppm are used for this system. Actually, the results of the present work show that there is no significant increasing in the system productivity with additives concentrations more than 300ppm.

The original system (natural solar energy) is found to give a higher productivity when it is operated under the summer conditions than winter conditions. Therefore, the summer solar flux values are simulated and adjusted by the variac transformer to give the same equivalent power input to the electric heater. Eight different values of heating power input are adjusted for eight hours along the day. The eight values for eight hours of operation are illustrated in Table 1 in watt, and are equivalent to eight values of solar flux $W/m^2$ respectively.

Figure (8.2) A photograph of the variac transformer with its components (voltmeter and ammeter)

## 8.3 MEASUREMENTS OF THE EXPERIMENTAL DATA

### 8.3.1 Temperature

Different temperatures of the system (see Fig. (8.1)) are measured by a digital volt meter through signals provided by number of thermocouples. The device relative error is less than $\pm 1\%$. The ambient temperature is measured by a common glass-tube-mercury temperature meter.

### 8.3.2 Condensate and wasted brine flow rates

By collecting the condensate and outlet wasted brine in two calibrated tanks at a certain time, the flow rate of both the condensate and brine are measured.

### 8.3.3 Electric power input

In the original system, solar radiation is measured by a solar radiation pyranometer laid on the collector surface with slope angle equal to 45°. But for the solar simulator, the input power to the electric heater is measured by both digital voltmeter and ammeter. The voltmeter range is from 0-500 V with an error percentage equal to $\pm 1$ digit and frequency equal to 50-60 Hz. The ammeter range is about 0-15 A with an error percentage equal to $\pm 0.1$ A. The estimation of the electric power input is presented as follows;

$$Epower = I_s \times A_c \qquad (8.1)$$

Where $A_c$ is the collector effective heat transfer area of the absorber plate and equal to $2.1\text{m}^2$, and $I_s$ is the solar radiation from the sun.
Also;

$$Epower = V \times I \times PF_H \qquad (8.2)$$

Where;

$PF_H$ is the electric heater power factor, nearly equal to one ($PF_H \approx 1$), $I$ is the electric current and $V$ is the voltage input power. From equations (8.1) and (8.2) the equivalent power input to the electric heater is given as;

$$Epower = V \times I \times 1 = I_s \times 2.1 \tag{8.3}$$

By knowing the power input from the sun (previously recorded day by the original system) the variac transformer can be adjusted by multiplying the volt reading by current reading from the voltmeter and ammeter respectively. Equation (8.3) is presented in Figure (8.3).

## 8.4 RESULTS AND COMMENTS

For the original system (without surfactant); the system is operated and investigated along one year (2005), and the system summer productivity was higher than winter [24]. The maximum allowable system productivity was ranged between 1.04 to 1.46 kg/day/m$^2$ in winter and about 4.18 to 7 kg/day/m$^2$ in summer. So the system productivity under summer operating conditions (solar radiation) is higher than winter productivity by 80%. Therefore; summer operating conditions and environmental data (solar radiation) are simulated and adjusted for the variac transformer to quantify higher system DP. The experiments are performed based on these following assumptions:

1. The fluid feed flow rate is constant and equal to 0.0183 kg/s.
2. Thermal losses to the ambient are neglected.
3. The energy stored in the collector is neglected.
4. The collector glass cover is full covered and insulated to quantify only the effect of the electric heater on the process.
5. The system goes under steady state condition.
6. The experiments were carried out under atmospheric pressure.

Table (8-1) shows that at C=0ppm the maximum obtained TBT is 70 °C with total daily productivity equal to 14.21kg/day. However, at C=50ppm, the results show that there is a little bit increasing in the DP and TBT. The TBT is measured 70.5 °C and the increasing percentage of the DP is 0.7%. The total DP is found to be not exceeding about 14.32 kg/day. At C=100ppm, the DP is increased by 2.5% while the TBT is reached to 71 °C. The total system productivity is increased to 14.57kg/day.

At C=200ppm, the system produces an amount of distillate water reaches to 14.9kg/day with increasing percentage equal to 4.6%. At 300ppm; the DP is increased by 7% with accumulative productivity equal to 15.3kg/day. At surfactant concentration ranged from 300ppm to 400ppm, the system productivity has not been changed. From Table (8-1) it may be noted that by increasing the surfactant additives concentration the TBT, and DP would increase.

Table (8-1) The results obtained for the system at different values of surfactant additives

| Oeratin g conditio ns | Time | 9 | 10 | 11 | 12 | 13 | 14 | 15 | 16 | Hr |
|---|---|---|---|---|---|---|---|---|---|---|
| | Is | 560 | 652 | 704 | 773 | 710 | 654 | 575 | 492 | W/m² |
| | Epower | 1176 | 1370 | 1478 | 1623 | 1490 | 1373 | 1207 | 1033 | watts |
| C=0 ppm | TBT | 54 | 57 | 63 | 70 | 68 | 63 | 53 | 50 | ºC |
| | DP | 1.5 | 1.61 | 2 | 2.3 | 2.28 | 2 | 1.31 | 1.21 | kg/hr |
| C=50 ppm | The average values of TBT and DP at concentration=50ppm are 60.25 ºC and 1.79 kg/hr respectively | | | | | | | | | |
| | TBT | 54 | 57 | 63.5 | 70.5 | 68.5 | 64 | 53.5 | 51 | ºC |
| | DP | 1.5 | 1.61 | 2.01 | 2.31 | 2.29 | 2.06 | 1.32 | 1.22 | kg/hr |
| C=100 ppm | The average values of TBT and DP at concentration=100ppm are 60.65 ºC and 1.82 kg/hr respectively | | | | | | | | | |
| | TBT | 54.5 | 57.75 | 64 | 71 | 68.7 | 64.5 | 53.5 | 51.25 | ºC |
| | DP | 1.52 | 1.64 | 2.06 | 2.39 | 2.298 | 2.07 | 1.328 | 1.27 | kg/hr |
| C=200 ppm | The average values of TBT and DP at concentration=200ppm are 61.09 ºC and 1.86 kg/hr respectively | | | | | | | | | |
| | TBT | 54.5 | 58 | 65 | 71.5 | 69 | 64.75 | 54 | 52 | ºC |
| | DP | 1.57 | 1.7 | 2.07 | 2.4 | 2.3 | 2.08 | 1.5 | 1.28 | kg/hr |
| C=300, 400 ppm | The average values of TBT and DP at concentration=300, 400ppm are 61.65 ºC and 1.91 kg/hr respectively | | | | | | | | | |
| | TBT | 55 | 58.5 | 66 | 72 | 69.25 | 65 | 55 | 52.5 | ºC |
| | DP | 1.58 | 1.85 | 2.15 | 2.44 | 2.32 | 2.09 | 1.57 | 1.29 | kg/hr |
| C=500 ppm | The average values of TBT and DP at concentration=500ppm are 59.87 ºC and 1.79 kg/hr respectively | | | | | | | | | |
| | TBT | 54 | 57 | 63 | 69 | 67.5 | 64 | 53 | 51.5 | ºC |
| | DP | 1.51 | 1.618 | 2.013 | 2.32 | 2.3 | 2.06 | 1.325 | 1.23 | kg/hr |

Fig. (8.3) shows the variations in electric power input (Epower) based on the variations in solar flux under summer conditions. The equivalent electric power input (watt) is found to be equal to $I_s \times A_c$. Where $A_c$ is the collector effective heat transfer area and equal to 2.1m². Fig. (8.4) shows the hourly variations of DP under different surfactant concentration at the same operating conditions. The figure shows that by increasing the surfactant concentration the DP increases. The DP increased till 300ppm of additives concentrations. The increase of DP may be explained by the decrease in the surface tension relative to water surface. Increasing the additive concentration up to 400ppm gives nearly the same results as 300ppm. However, increasing the additive concentration up to 500ppm leads to decreasing the DP and TBT. This is happened due to the formation of some foam. Adding surfactant up to 500ppm decreases the DP by 6% (from 15.3kg/day to 14.38kg/day). Fig. (8.5-a) shows the variation of DP with the variation of surfactant concentrations. The figure shows that the DP has no significant change at additives from 300 to 400ppm and the system DP nearly constant at this case. However the DP is decreased at surfactant additives equal to 400-500ppm as regarded before. Fig. (8.5-b) shows the changing of DP against the changing in additives at different values of input power. The figure represents the effect of increasing the input power and surfactant concentration on the DP. By increasing the input heat flux; the DP is increased. This may because by increasing the heat fluxes, the dynamic and kinematic viscosity decrease gradually allowing more vapor to produce more distillate. But by increasing the surfactant concentrations the viscosity will increase. Also, viscosity is decreasing with the increasing the TBT. Fig. (8.6) shows the hourly variations of TBT at different surfactant concentrations. The figure shows that by increasing the surfactant concentration the TBT is increased. Fig. (8.7) represents the effect of the equivalent power on the DP with the variation in surfactant concentration. The figure shows that the

DP increases with increasing the equivalent power. At constant equivalent power the DP increases with increasing the surfactant concentrations until C=400ppm, then the DP decreases. This is due to; by increasing the surfactant concentrations the viscosity will increase and also the surface tension and that will retard interfacial evaporation of the solution. Thus, the effect of surfactants in the solution on interfacial evaporation has two effects: as the concentration of surfactant is lower than the optimal value (300ppm) and the interfacial superheat is not extremely high, the application of surfactant additives promotes the interfacial evaporation; otherwise, retards the interfacial evaporation. Fig. (8.8) shows the same behavior of the effect of equivalent power input on the TBT. Thus, it is evident that the influence of the surfactant on the TBT curve behavior has an optimum, depending on the concentration. So; for adding surfactant materials; it is not allowed to be exceeded over the range of 300-400ppm.
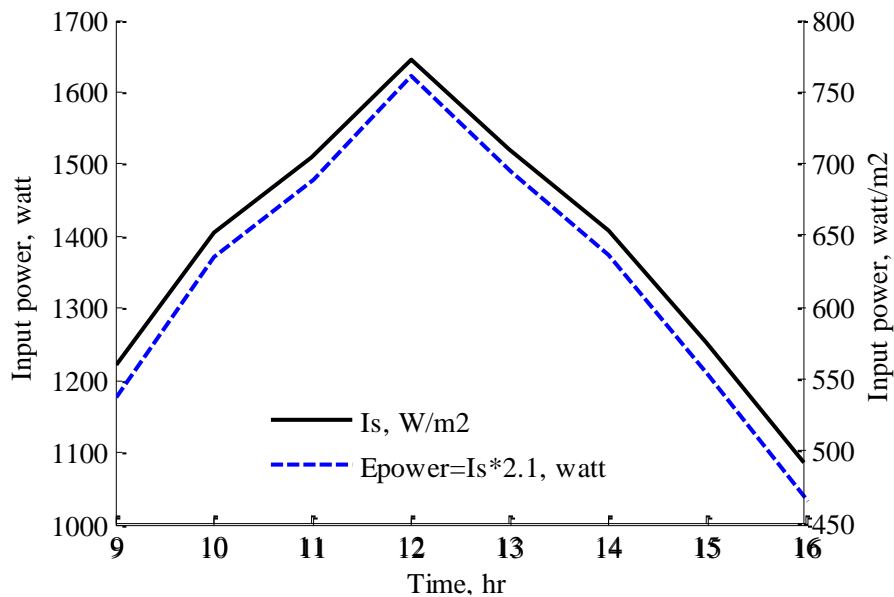


Figure (8.3) Variation of the equivalent electric heater power input
based on the solar flux input
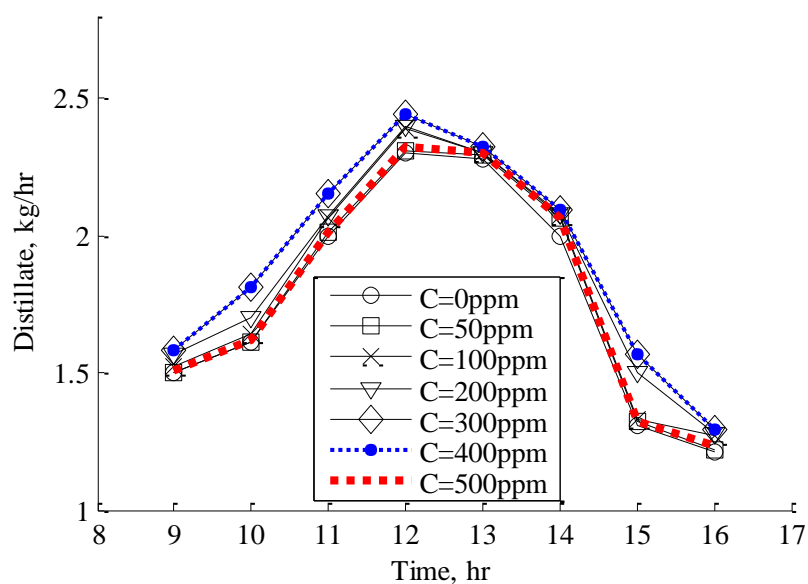
Figure (8.4) The variation in the distillate product according
to the variation in surfactant concentration
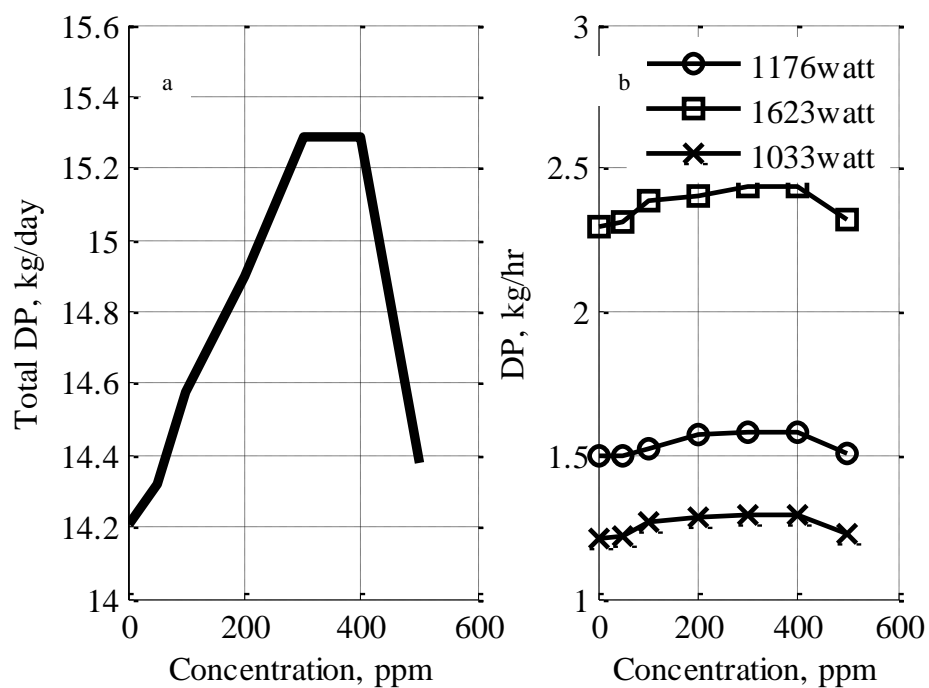


Figure (8.5) The relation between distillate productivity and the
concentration: a. The total DP Vs concentration, b. The DP/hr Vs
concentration at different values of input power
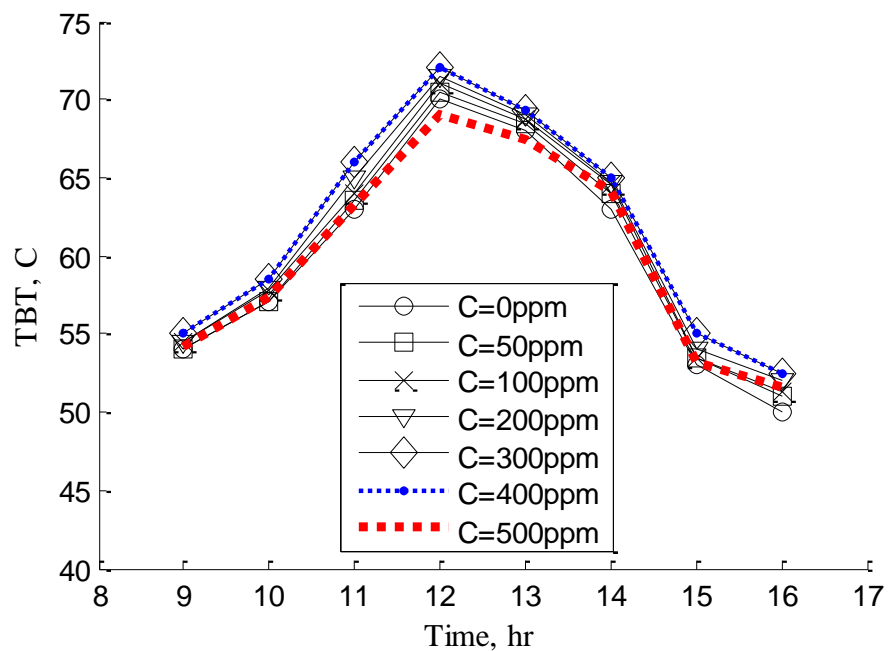
Figure (8.6) The variation of the TBT according to the variation in surfactant concentration
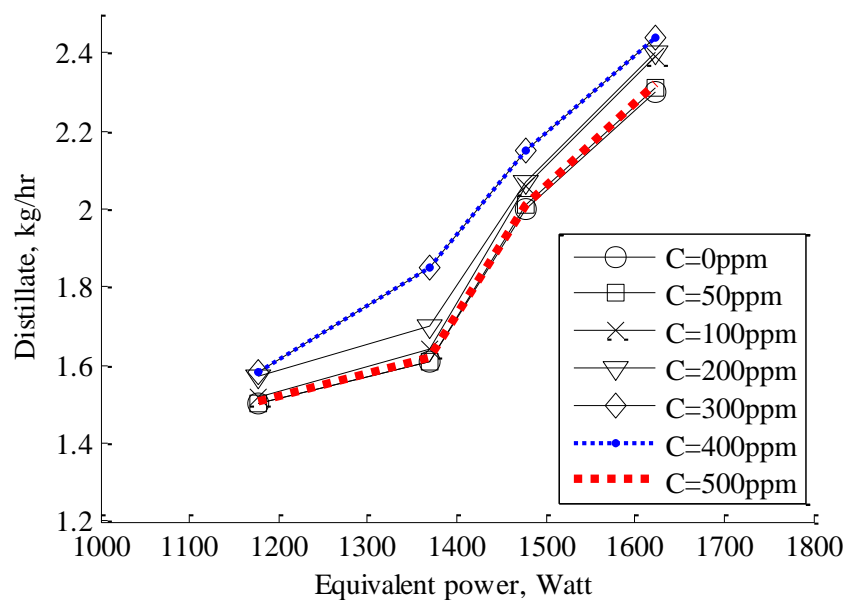


Figure (8.7) The effect of increasing the equivalent power on the DP at different concentrations
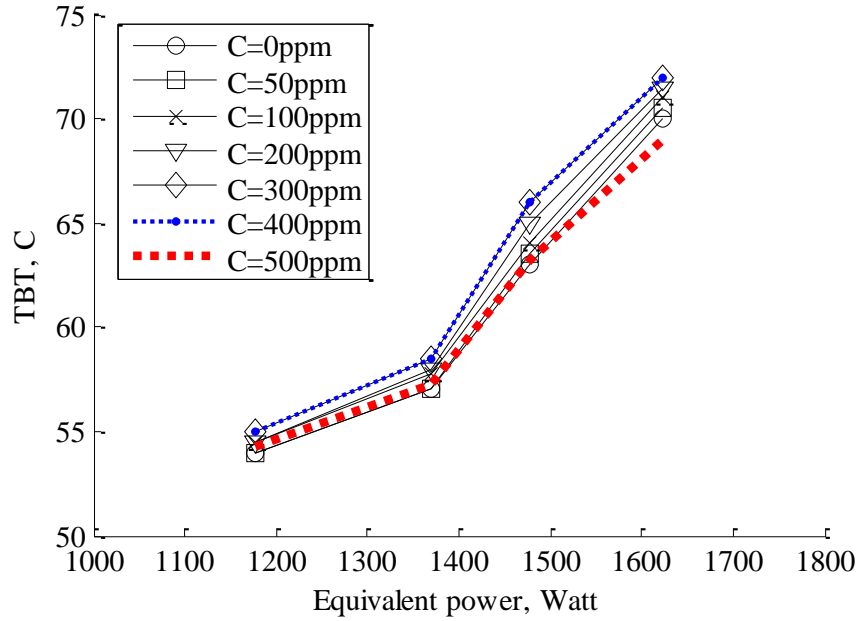
Figure (8.8) The effect of increasing the equivalent power on the
TBT at different concentrations

The coefficient of performance of the system (C.O.P) which can also be defined as the energy recovery or the performance ratio, it is the measure of energy efficiency of the thermal consumption of the system. The C.O.P can be determined from the following relation:

$$C.O.P = \frac{DP \times H_v}{Epower} \tag{8.4}$$

Where $H_v$ is the latent heat of condensation and DP is the distillate product of the system and *Epower* is the electric power input to the electric heater (data from table 8-1). Fig. (8.9) shows the hourly variations of the system C.O.P at different dosages of the surfactant material. The figure shows that the C.O.P increases gradually with the concentration increase. However, it decreases with additives concentration 500ppm.

A sample of the obtained distillate water is analyzed to examine if there are some organic or toxic particles in the distillate or not. Table (8-2) illustrates the water ingredients before and after adding the surfactant material. For these two cases; the total dissolved salts (T.D.S) of water is not exceeding about 113-115*mg/l*. Also the analysis show that the organic or toxic particles are not appear in the distillate even after using surfactant concentration equal to 400-500ppm. May that because the high efficiency of the condensation operation.

119
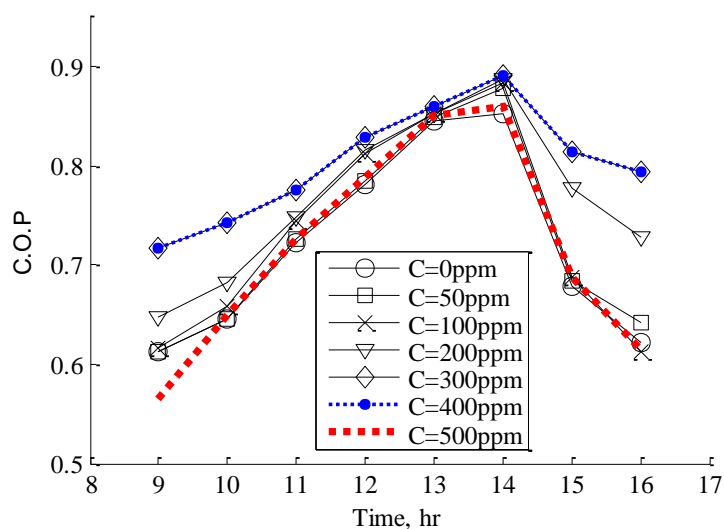
Figure (8.9) The hourly variation of the C.O.P versus time

Table (8-2) The water samples ingredients before and after adding surfactant material

| Item: | Sample of tap water: | Sample of distillate water without surfactant: | Sample of distillate water with surfactant: | Units |
|---|---|---|---|---|
| T.D.S | 350 | 115 | 113 | *mg/l* |
| pH | 8.1 | 8.48 | 8.48 | |
| Phosphate | 0.2 | 0.05 | 0.05 | *µg/l* |
| Nitrite | 0.3 | 0.26 | 0.26 | *µg/l* |
| Ammonia | 2 | 3.68 | 3.68 | *µg/l* |
| Calcium | 60 | 26 | 25 | *µg/l* |
| Magnesium | 19 | 3.8 | 3.3 | *µg/l* |
| Sodium | 35 | 11 | 10 | *µg/l* |
| Potassium | 3 | 2.2 | 2 | *µg/l* |
| Bicarbonates | 115 | 60 | 60 | *µg/l* |
| Sulphates | 31 | 10 | 10 | *µg/l* |
| Silica | 10 | 7 | 6 | *µg/l* |
| Conductivity | -- | 239 | 239 | *µ/s* |
| Fluorides | -- | 0.1 | 0.1 | *µg/l* |
| Nitrate | -- | 0.98 | 0.98 | *µg/l* |
| Organic | -- | -- | -- | **--** |

## 8.5 CONCLUSION

A solar distillation system compound from a flat plate solar collector and flash a evaporation unit was explained. This original system was operated under out door conditions (solar energy). The original system productivity was limited (10 to 16.5 kg/day in summer and about 2.5 to 3.5 kg/day during the winter). To examine the effect of the system concentration at a constant input power an electrical heater with variant transformer is used as a sun simulator. An environmentally acceptable anionic surfactant is used to study its effect on the system DP and TBT. The results verify again that a small amount of surfactant material makes the TBT and DP considerably higher. 50, 100, 200 and 300ppm of surfactant concentrations are studied. The DP is increased as 0.7%, 2.5%, 4.7% and 7% at additive concentration equal to 50, 100, 200 and 300ppm respectively. The effect of power input on the system productivity at different values of surfactant concentration is also studied. The system C.O.P is affected by the increasing of surfactant additives hence the TBT. Increasing the surfactant concentration more than 300ppm is not affecting the system DP and TBT. Using surfactant concentration more than 400ppm decreases the DP by 6%. Thus, the effect of *SLS* surfactants in aqueous solution on evaporation operation is dual: as the concentration of *SLS* surfactant additives is lower than a certain value (400ppm) and the heat flux is not extremely high, the application of *SLS* surfactant promotes the interfacial evaporation; otherwise, retards the interfacial evaporation. A sample of distillate water is analyzed and showed that there is no appearing of organic or toxic particles in the distillate water. The mechanism of interfacial evaporation in heating and condensation process with the application of surfactants has still not been clarified. Results verify that there is an important possibility to enhance the water distillation process by surfactant additives.

# CHAPTER 9

# CONCLUSIONS AND FUTURE WORK

## 9.1 CONCLUSIONS

To summarize and conclude the results and the discussions in this thesis, the following points could be withdrawn:

1. A survey about different techniques of solar desalination processes is presented and evaluated.
2. A mathematical model was developed for the system components (collector, flash unit, condenser unit) and for different configurations to predict the system productivity under different and wide range of operating conditions. Material and energy balance equations are combined and arranged in a matrix form. A computer program is developed to solve the system iteratively.
3. It is very important to estimate the solar radiation for any solar thermal system. Therefore, ASHREA, ATWATER&BALL, BIRD, DAVIES&HAY, HOYT, LACIS&HANSEN and SPECTRAL2, models are presented and used to estimate the instantaneous direct and diffuse insolation on horizontal surfaces at Suez-Gulf area. BIRD and DAVIES&HAY models are most reasonable for this area. The lowest hourly mean bias error (*MBE*), root mean square error (*RMSE*) and mean percentage error (*MPE*) are recorded to BIRD and DAVIES&HAY models while the highest deviations are found with HOYT and LACIS&HANSEN models. BIRD model gives superior results in summer; however, DAVIES&HAY gives the superior results in the winter. Also a simple new correlation (S.C.S.G) is developed to predict the total insolation in the Suez-Gulf region. The new suggested correlation gives an acceptable result compared with BIRD and DAVIES&HAY. The developed correlation is simple and valid for all seasons at the mentioned location. Generally DAVIES&HAY, BIRD and S.C.S.G models would be recommended to be employed for the calculation of the total solar radiation (direct and diffuse) instantaneously at Suez-Gulf Area.
4. Exergy analysis is performed for a low range of top brine temperature of the system and different configurations. Three different configurations are compared by evaluating the results obtained under summer conditions. The results show that the exergetic efficiency of the 1$^{st}$ configuration without mixing is about 0.08-0.157% and for the 2$^{nd}$ configuration with mixing is 0.08-0.16% and for the 3$^{rd}$ was 0.09-0.163%. Exergetic efficiency and exergy destruction are found to be directly proportional to the top brine temperature. Configuration 1 represents higher results of TBT; and lower in exergy destruction. The total DP is equal to 16.75, 16.56 and 16.71kg/day for configurations 1, 2 and 3 respectively. Configuration 2 represents the same results of exergy destruction component as configuration 3. The 1$^{st}$ configuration is chosen to be designed and constructed based on the exergetic comparison with 2$^{nd}$ and 3$^{rd}$ configurations.
5. Experimental rig for the 1$^{st}$ configuration (without mixing) is designed and investigated under a wide range of operating conditions. Results verify that the unit performance ratio is low because it ranged about 0.7 to 0.8 in winter and

0.8 to 0.95 in summer. The average accumulative productivity of the system in November, December and January raged between 1.04 to 1.45 kg/day/m$^2$. The average summer productivity ranged between 5.44 to 7 kg/day/m$^2$ in July and August and 4.2 to 5 kg/day/m$^2$ in June. The fractional (*Fr*) percentage error of the system performance ratio is not exceeding about 7% of the total productivity DP. The system produces higher productivity at higher TBT, i.e., higher solar intensity. Reasonable rate of feeding water is ranged about 0.0183 kg/s.

6. Increasing the collector surface area from 2.4 m$^2$ to 4.4 m$^2$ may increase the total productivity by 42%.

7. Increasing the number of stages will increase the condenser surface area and so the system productivity. Increasing the number of stages up to two stages was found to exceed the productivity by 44.5%. While increasing the number of stages up to three may cause an increasing equal to 60% of the system productivity.

8. The literatures are noted that adding surfactant material would increase heat transfer coefficient. To perform this experiment on the system; an electrical heater with variant transformer is used as a sun simulator. An environmentally acceptable anionic surfactant is used to study its effect on the system DP and TBT. The results illustrates that a small amount of surfactant material makes the TBT and DP considerably higher. The effect of 50, 100, 200 and 300ppm of surfactant concentrations are studied. The DP is increased as 0.7%, 2.5%, 4.7% and 7% at additive concentration equal to 50, 100, 200 and 300ppm respectively. The effect of power input on the system productivity at different values of surfactant concentration is also studied. The system C.O.P is affected by the increasing of surfactant additives hence the TBT. Increasing the surfactant concentration more than 300ppm is not affecting the system DP and TBT. Using surfactant concentration more than 400ppm decreases the DP by 6%. Thus, the effect of *SLS* surfactants in aqueous solution on evaporation operation is dual: as the concentration of *SLS* surfactant additives is lower than a certain value (400ppm) and the heat flux is not extremely high, the application of *SLS* surfactant promotes the interfacial evaporation; otherwise, retards the interfacial evaporation. A sample of distillate water is analyzed and showed that there is no appearing of organic or toxic particles in the distillate water.


## 9.2 FUTURE WORK

For the future work, studying the behavior of the system performance with deferent types of surfactant dosages is in concern. Also and based on all experimental data recorded form sun, collector and flashing unit; neural network technique could be useful to simulate the system comparing with theoretical and experimental data. Also redesigning the test rig in lighter and cheaper materials making it competitive in small scale desalinating market is in concern. Studying the capability and effect of combining between deferent types of solar collectors (concentrating, evacuated) and flashing system.

# REFERENCES

[1] Ali M. El-Nashar, "The economic feasibility of small solar MED seawater desalination plants for remote arid areas", Desalination 134 (2001) 173–186.

[2] Essam E. Khalil, "Water strategies and technological development in Egyptian coastal areas", Desalination 165 (2004) 23–30.

[3] A. Soliman, " Study of Water Desalination by Solar Energy Using Humidification-Dehumidification Processes", Mech. Eng. Dep., Fac of Petroleum & Mining Eng, Suez Canal Univ., M. Sc. Thesis, Egypt, 2002.

[4] Voros N. G, Kiranoudis C. T, Maroulis Z. B, " Solar energy exploitation for reverse osmosis desalination plants", Desalination 115 (1998) 83–101.

[5] Lourdes Garcia Rodriguez, Carlos Gomez Camacho, " Conditions for economical benefits of the use of solar energy in multi-stage flash desalination", Desalination 125 (1999) 133–138.

[6] H. G. Pham, T. M. Liu, L. P. Leibowitz "Advanced Solar Thermal Technology: Potential for water desalination", Chapter 55.

[7] Hisham T. El-Dessouky, Hisham M. Ettouney, Yousef Al-Romi "Multi-stage flash desalination: present and future outlook", Desalination, vol. 73, 173-190 (1999).

[8] N.G. Voros, C.T. Kiranoudis, Z.B. Maroulis, "Solar energy exploitation for reverse osmosis desalination planmts", Desalination 115 (1998) 83-101.

[9] Lourdes Garcia-Rodriguez, Carlos Gomez-Camacho, "Preliminary design and cost analysis of a solar distillation system", Desalination 126 (1999) 109–114.

[10] Nafey SA, Abdelkader M, Abdelmotalip A, Mabrouk AA, "Enhancement of solar still productivity using floating perforated black plate", Energy Conversion & Management, vol. 43, 937-946, 2002.

[11] WEIR WESTGARTH LTD, MINISTRY OF ELECTRICITY AND WATER OMAN.

[12] Kriesi R, "Design and operation experience with solar powered multistage desalination plants", Desalination 39 (1981) 109–116.

[13] Anil K. Rajvanshi, "A scheme for large scale desalination of sea water by solar energy", Solar Energy 24 (1980) 551–560.

[14] Ziad M, Badawi W. Tleimat, "TEST RESULTS FROM A SOLAR BOILER FOR SALINE WATER DISTILLATION", Desalination, vol. 39, 63-70, 1981.

[15] Said M. A. Ibrahim, "Predicted and measured global solar radiation in Egypt", solar energy 35, 185-188, (1985).

[16] M. A. Mosalam Shaltout and A. H. Hassen, "Solar energy distribution over Egypt using cloudiness from meteosat photos", solar energy 45, 345-351, (1990).

[17] C. C. Y. Ma and M. Iqbal, "Statistical comparison of solar radiation correlations. Monthly average global and diffuse radiation on horizontal surfaces", solar energy 33, 143-148, (1984).

[18] Richard E. Bird and Roland L. Hulstrom, A SIMPLIFIED CLEAR SKY MODEL FOR DIRECT AND DIFFUSE INSOLATION ON HORIZONTAL SURFACES, solar energy research institute, Golden, Colorado USA (1981).

[19] Moustafa M. Elsayed, Ibrahim S. Taha, Jaffar A. Sabbagh, "Design of solar thermal systems", Scientific publishing center King Abdulaziz University, Jeddah, 57-61.

[20] R. E. Bird, C. Riordan, "Simple solar spectral model for direct and diffuse irradiance on horizontal and tilted planes at the earth's surface for cloudless atmospheres", www.rredc.nrel.gov

[21] Daryl R. Myers, "Solar radiation modeling and measurements for renewable energy applications: data and model quality", National Renewable Energy Laboratory, Golden CO.

[22] V. Badescu, "Comment on the statistical indicators used to evaluate the accuracy of solar radiation computing models", solar energy 40, 479-480, (1988).

[23] K. K. Gopinathan, Solar sky radiation estimation techniques, solar energy 49, 9-11, (1992).

[24] Nafey A. S, Sharaf M. A, Mohamad M. A, "Theoretical and experimental study of a small unit for water desalination using solar energy and flashing process", Proceedings of the Tenth International Water Technology Conference, 23-25th March 2006, Alexandria, Egypt.

[25] N. Nijegorodov, P. K. Jain and K. R. S. Devan, A Graphical Method of Measuring The Performance Characteristics of Solar Collectors, Renewable Energy 7, 23-31, (1996).

[26] Ted J. Jansen, Solar Engineering Technology, Englewood Cliffs, New Jersey, U.S.A. (1985).

[27] J.A. Duffie and W. A. Beckman, Solar Engineering of Thermal Processes, 2nd edition. John Wiley, New York, U.S.A. (1991).

[28] J. C. Francken, On the Effectiveness of a Flat Plate Collector, solar energy 33, 363-366, (1984).

[29] Gregory J. Kowalski, Arthur R. Foster, Heat Exchanger Theory Applied to the Design of Water – and Air- Heating Flat-Plate Solar Collectors, Journal of solar energy engineering, v 110, 1988 .

[30] Frederick F. Simon, Flat Plate Solar Collector Performance Evaluation With a Solar Simulator as a Basis For Collector Selection and Performance Prediction, solar energy 18, 451-466, (1976).

[31] Yu. N. Malevskii, Yu. L. Myshko, S. I. Simrnov and B. V. Tarnizhevskii, Method For Determining Solar Collector Thermal Characteristics Under Laboratory Conditions, Geliotekhnika, vol. 16, No. 4, pp. 50-54, 1980.

[32] S. A. M. Said, S. M. Zubair, On Second-Law Efficiency of Solar Collectors, Transactions of the ASME, vol. 115, February 1993.

[33] Nafey A. S, "Design and simulation of seawater-Thermal desalination plants", Leeds University, ph. D. Thesis, 1988.

[34] WLi Kam, *"Applied Thermodynamics-Availability Method and Energy conversion''* Chaps 1,2,3. University of North Dakota State, 1995.

[35] A Faleh, Al-Sulaiman, Basil Ismail, Desalination, 103 (1995) 267.

[36] Adrian Bejan "*Entropy Generation Minimization*" Chapter 9 p 251. Duke University.

[37] S.A.M. Said, S.M. Zubair "*On the second law efficiency of solar collectors*''
Mechanical engineering department, King Fahd University of Petroleum and Minerals,
Dhahran 31261, Saudi Aribia.

[38] G. Manfrida, "*The choice of an optimal working point for solar collectors*", solar
energy, 34, 513-515, 1985.

[39] E. Torres-Reyes, J.G. Cervantes-de Gortari, B. A. Ibarra-Salazar, M. Picon-Nunez,
"*A design method of flat-plate solar collectors based on minimum entropy
generation*", Exergy an international journal, 46-52, 2001.

[40] Miller P, Westra P, How Surfactants Work, Colorado State University, Cooperative
Extension, 11/98, www.colostate.edu/Depts/CoopExt.

[41] Uniqema: Imperial Chemical Industries PLC, Atlox Polymeric Surfactants:
Stabilizers for Concentrated Emulsions (EW), www.uniqema.com Printed in USA on
recycled paper.

[42] Todor Stoyanov, The Effect of surfactant solutions on heat transfer and bubble
formation in subcooled pool boiling, Mech Sofia 1000, ACS P.O. Box 873, Bulgaria.

[43] G. Hetsroni, J.L. Zakin, Z. Lin, A. Mosyak, E.A. Pancallo and R. Rozenblit, The
effect of surfactants on bubble growth, wall thermal patterns and heat transfer in pool
boiling, Int. J Heat and Mass Transfer. 44, 485-497, 2001.

[44] G. Hetsroni, M. Gurevich, A. Mosyak, E. Pogrebnyak, R. Rozenblit, Z. Segal, The
effect of surfactants on boiling heat transfer, Proceedings of The ASME – ZSIS
International Thermal Science Seminar II Bled, Slovenia, June 13 – 16, 2004.

[45] Y.L. Tzan, Y.M. Yang, Experimental study of surfactant effects on pool boiling heat
transfer, Journal of Heat Transfer 112 (1990) 207-212.

[46] O.O. Badran, H.A. Al-Tahaineh, The effect of coupling a flat plate collector on the
solar still productivity, Desalination, 183 (2005) 137-142.

[47] Salah Al-Hengari, Mohamed El-Bousiffi, Walid El-Mudir, "Performance analysis of
a MSF desalination unit", Desalination, vol. 128, 73-85, 2005.

[48] H. Sephton, US Patent No. 3846254, 1974.

[49] António Joyce, David Loureiro, Carlos Rodrigues, Susana Castro, " Small reverse ososis units using PV systems for water purification in rural places", Desalination, 137 (2001) 39-44.

[50] S. Kulankara, K.E. Herold, Surface tension of aqueous lithium bromide with heat/mass transfer enhancement additives: the effect of additive vapor transport, International Journal of Refrigeration 25 (2002) 383–389.

[51] Toshiaki Inoue, Yoshio Teruya, Masanori Monde, Enhancement of pool boiling heat transfer in water and ethanol/water mixtures with surface-active agent, International Journal of Heat and Mass Transfer 47 (2004) 5555–5563.

[52] Sayed Siavash Madaenl, Toraj Mohamamdi, Mansour Kazemi Moghadam, Chemical cleaning of reverse osmosis membranes, Desalination 134 (2001) 77-82.

# APPENDIX (A)

## Calculations of solar flux models based on the calculation of solar angles

### A.1. Solar angles correlations:

The declination angle throughout the year is defined as following:

$$d = 23.45 \sin\left[\frac{360}{365}(284 + n)\right]$$

(A.1)

Where $n$ is the day of the year. The value of $n$ for any day of the month $d$ can be determined easily with the aid of Table (A-1).

Table (A-1) Variation in $n$ throughout the year for use in equation (A.1)

| Month | n for the Day of the Month, D | Month | n for the Day of the Month, D |
|---|---|---|---|
| January | D | July | 181 + D |
| February | 31 + D | August | 212 + D |
| March | 59 + D | September | 243 + D |
| April | 90 + D | October | 273 + D |
| May | 120 + D | November | 304 + D |
| June | 151 + D | December | 334 + D |

The hour angle $h$ is calculated from the following expression:

$$h = 15(LST - 12)$$

(A.2)

Where LST = Local Solar Time [hr].
The following equations are presented to calculate these angles:

$$\cos\theta_H = \cos l \cos h \cos d + \sin l \sin d$$

(A.3)

Since $\beta = 90 - \theta_H$,

(A.4)

$$\sin\beta = \cos l \cos h \cos d + \sin l \sin d$$

(A.5)

The relation gives the sun's azimuth, $\phi$:

$$\cos\phi = \frac{1}{\cos\beta}(\cos d \sin l \cos h - \sin d \cos l)$$

(A.6)

A summary of the sign convention is:

  **l**: north latitudes are positive, south latitudes are negative
  **d**: the declination is positive when the sun's rays are north of the equator, i.e. for the summer period in the northern hemisphere, March 22 to September 22 approximately, and negative when the sun's rays are south of the equator.
  **h**: the hour angle is negative before solar noon and positive after solar noon.
  **$\phi$**: the sun's azimuth angle is negative east of south and positive west of south.

## A.2. The solar models for the estimation of the total insolation on horizontal surfaces:

### A.2.1. ASHREA correlations:

$$It1 = (G_{bn} \times \cos(z)) + G_d \tag{A.7}$$

$$G_{bn} = A\exp(-B/\cos(z)) \tag{A.8}$$

$$G_d = C \times G_{bn} \tag{A.9}$$

And,

$A$ is the apparent solar irradiance at air mass zero, $B$ is the atmosphere extinction coefficient, and $C$ is the diffuse radiation factor.

Table (A-2) Coefficients for average clear day solar radiation calculations

| | A | | B | C | Declination, deg | Equation of Time, hr |
|---|---|---|---|---|---|---|
| | $\dfrac{Btu}{hr \cdot ft^2}$ | $\dfrac{W}{m^2}$ | Dimensionless Ratios | | | |
| January | 390 | 1230 | 0.142 | 0.058 | −20.0 | −0.19 |
| February | 385 | 1215 | 0.144 | 0.060 | −10.8 | −0.23 |
| March | 376 | 1186 | 0.156 | 0.071 | 0.0 | −0.13 |
| April | 360 | 1136 | 0.180 | 0.097 | 11.6 | 0.02 |
| May | 350 | 1104 | 0.196 | 0.121 | 20.0 | 0.06 |
| June | 345 | 1088 | 0.205 | 0.134 | 23.45 | −0.02 |
| July | 344 | 1085 | 0.207 | 0.136 | 20.6 | −0.10 |
| August | 351 | 1107 | 0.201 | 0.122 | 12.3 | −0.04 |
| September | 365 | 1151 | 0.177 | 0.092 | 0 | 0.13 |
| October | 378 | 1192 | 0.160 | 0.073 | −10.5 | 0.26 |
| November | 387 | 1221 | 0.149 | 0.063 | −19.8 | 0.23 |
| December | 391 | 1233 | 0.142 | 0.057 | −23.45 | 0.03 |

### A.2.2. ATWATER&BALL correlations:

$$It2 = I_0(\cos(z))(T_M - a_W) \times T_A /(1 - r_g r_s) \tag{A.10}$$

Where,

$$I_d = I_0(\cos(z)) \times (T_{Md} - a_W) \times T_A \tag{A.11}$$

And,

$$T_{Md} = 1.041 - 0.16[M(949 \times 10^{-6}\, p + 0.051)]^{0.5} \tag{A.12}$$

$$T_M = 1.021 - 0.0824(M(949 \times 10^{-6}\, p + 0.051))^{0.5} \tag{A.13}$$

$$a_W = 0.077(U_W M)^{0.3} \tag{A.14}$$

$$T_A = \exp(-\tau_A M') \tag{A.15}$$

$$M = 35/((1224 \times \cos^2(z)) + 1)^{0.5} \tag{A.16}$$

$$M' = PM/1013 \tag{A.17}$$

### A.2.3. BIRD correlations:

$$It3 = (I_d + I_{as})/(I - r_g r_s) \tag{A.18}$$

Where,

$$I_d = I_0(\cos(z))(0.9662)T_R T_0 T_{UM} T_W T_A \tag{A.19}$$

$$I_{as} = I_0(\cos(z))(0.79)T_0 T_W T_{UM} T_{AA} \times [0.5(1-T_R) + B_a(1-T_{AS})]/[1-M+(M)^{1.02}] \tag{A.20}$$

$$T_R = \exp\{-0.0903(M^\cdot)^{0.84}[1+M^\cdot - (M^\cdot)^{1.01}]\} \tag{A.21}$$

$$T_0 = 1 - 0.1611 \times X_0(1+139.48 \times X_0)^{-0.3035} \times -0.002715 \times$$
$$X_0(1+0.044 \times X_0 + 0.0003 \times X_0^2)^{-1} \tag{A.22}$$

$$X_0 = U_0 M \tag{A.23}$$

$$T_{UM} = \exp[-0.0127(M^\cdot)^{0.26}] \tag{A.24}$$

$$T_W = 1 - 2.4959 \times X_W[(1+79.034 \times X_W)^{0.6828} + 6.385 \times X_W]^{-1} \tag{A.25}$$

$$X_W = U_W M \tag{A.26}$$

$$T_A = \exp[-\tau_A^{0.873}(1+\tau_A - \tau_A^{0.7088})M^{0.9108}] \tag{A.27}$$

$$\tau_A = 0.2758 \times \tau_{A,0.38} + \tau_{A,0.5} \tag{A.28}$$

$$T_{AA} = 1 - K_1(1-M+M^{1.06})(1-T_A) \tag{A.29}$$

$$T_{AS} = T_A/T_{AA} \tag{A.30}$$

$$r_s = 0.0685 + (1-B_a)(1.0-T_{as}) \tag{A.31}$$

$$M = [\cos(z) + 0.15(93.885-z)^{-1.25}]^{-1} \tag{A.32}$$

$$M^\cdot = MP/1013 \tag{A.33}$$

And,

$$B_a = 0.5(1+ <\cos\theta>) \tag{A.34}$$


### A.2.4. DAVIES&HAY correlations:

$$It4 = I_d + I_{as} + I_G \tag{A.35}$$

Where,

$$I_d = I_0(\cos(z))(T_0 T_R - a_W)T_A \tag{A.36}$$

$$I_{as} = I_0(\cos(z))[T_0(1-T_R)T_A(0.5) + (T_0 T_R - a_W)(1-T_A)W_0 B_a] \tag{A.37}$$

$$I_G = r_g r_s(I_d + I_{as})/(1-r_g r_s) \tag{A.38}$$

And,

$$T_0 = 1 - 0.02118 \times X_0/(1+0.042 \times X_0 + 0.000323 \times X_0^2)$$
$$\times -1.082 \times X_0/(1+138.6 \times X_0)^{0.805} - 0.0658 \times X_0/[1+(103.6 \times X_0)^3] \tag{A.39}$$

$$X_0 = U_0 M \tag{A.40}$$

$$a_W = 2.9 \times X_W/[(1+141.5 \times X_W)^{0.635} + 5.925 \times X_W] \tag{A.41}$$

$$X_W = U_W M \tag{A.42}$$

$$T_A = K^M \tag{A.43}$$

$$r_s = 0.0685 + (1-B_a)(1-T_A)W_0 \tag{A.44}$$

### A.2.5. HOYT Correlations:

$$It5 = I_d + I_{as} + I_G \tag{A.45}$$

And,

$$I_d = I_0 (\cos(z)) \left(1 - \sum_{i=1}^{5} a_i \right) T_{AS} T_R \tag{A.46}$$

$$I_{as} = I_0 (\cos(z)) \left(1 - \sum_{i=1}^{5} a_i \right) [(1 - T_R)0.5 + (1 - T_{AS})0.75] \tag{A.47}$$

$$I_G = (I_d + I_{as}) r_g \left(1 - \sum_{i=1}^{5} a_i{}' \right) [(1 - T_R{}')0.5 + (1 - T_{AS}{}')0.25] \tag{A.48}$$

Where,

$$a_1 = a_W = 0.110(0.75 \times U_W M + 6.31 \times 10^{-4})^{0.3} - 0.0121 \tag{A.49}$$

$$a_2 = a_{co} = 0.00235(126 \times M{}' + 0.0129)^{0.26} - 7.5 \times 10^{-4} \tag{A.50}$$

$$a_3 = (1 - T_0) = 0.045(U_0 M + 8.34 \times 10^{-4})^{0.38} - 3.1 \times 10^{-3} \tag{A.51}$$

$$a_4 = a_{0X} = 7.5 \times 10^{-3} (M{}')^{0.875} \tag{A.52}$$

$$a_5 = 0.05 \times T_{AS} \tag{A.53}$$

$$M{}' = MP / 1013.25 \tag{A.54}$$

### A.2.6. LACIS&HANSEN correlations:

$$It6 = I_0 (\cos(z)) [(0.647 - r_s{}' - a_0) / (1 - 0.0685 \times r_g) + 0.353 - a_W] \tag{A.55}$$

Where,

$$r_s{}' = 0.28 / (1 + 6.43 \times \cos(z)) \tag{A.56}$$

$$a_0 = 1 - T_0 \tag{A.57}$$

$$a_W = X_W \tag{A.58}$$

$$X_W = X_W (P / 1013)^{0.75} \times (273 / T)^{0.5} \tag{A.59}$$

### A.2.7. SPECTRAL2 correlations:

$$I_{d\lambda} = H_{o\lambda} D T_{r\lambda} T_{a\lambda} T_{w\lambda} T_{o\lambda} T_{u\lambda} \tag{A.60}$$

$$D = 1.00011 + 0.034221 \cos\varphi + 0.00128 \sin\varphi + \\ 0.000719 \cos 2\varphi + 0.000077 \sin 2\varphi \tag{A.61}$$

$$\varphi = 2\pi(n-1) / 365 \tag{A.62}$$

And the Rayleigh scattering is:

$$T_{r\lambda} = EXP\left\{ -M{}' / \left[ \lambda^4 \left(115.6406 - 1335 / \lambda^2 \right) \right] \right\} \tag{A.63}$$

Where M' is the pressure-corrected air mass. The relative air mass as given as:

$$M = \left[ \cos Z + 0.15(93.885 - Z)^{-1.253} \right]^{-1} \tag{A.64}$$

$$T_{a\lambda} = EXP\left(-\beta_{n\lambda}^{-\alpha a_{1,2}}\right) \tag{A.65}$$

Two $\alpha$ values were used for this aerosol model: $\alpha_1 = 1.0274$ for wavelengths $<0.5$ μm, and $\alpha_2 = 1.2060$ for wavelengths $\leq 0.5$ μm. The value of $\beta_n$ was chosen appropriately for each wavelength interval to produce accurate turbidity values (aerosol optical depth in a vertical path) at 0.5 μm wavelength.

The turbidity is represented as:

$$\tau_{a\lambda} = \beta_n \lambda^{-\alpha_i} \tag{A.66}$$

The water vapor absorption is determined as following:

$$T_{w\lambda} = EXP\left[-0.2385a_{w\lambda}WM/(1+20.07a_{w\lambda}WM)^{0.45}\right] \tag{A.67}$$

$$T_{o\lambda} = EXP\left(-a_{o\lambda}o_3M_o\right) \tag{A.68}$$

$$M_o = (1+h_o/6370)/(\cos^2 Z + 2h_o/6370)^{0.5} \tag{A.69}$$

The parameter $h_o$ is the height of maximum ozone concentration, which is approximately 22 km.

The following correlation is made for mixed gas transmittance:

$$T_{u\lambda} = EXP\left[-1.41a_{u\lambda}M'/(1+118.3a_{u\lambda}M')^{0.45}\right] \tag{A.70}$$

### *A.2.8. S.C.S.G correlations:*

The new suggested correlation S.C.S.G (Solar Correlation in Suez Gulf) is presented as following;

$$It8 = (A \times I_o \cos(z)) - C_{season} \tag{A.71}$$

Table (A-2) shows the different values of the $C_{season}$.

Table (A-3) The desired values of the S.C.S.G model constant ($C_{season}$) for different seasons

| Seasons and Julian days (n): | Dec, Jan, Feb: (winter) n=334:59 | Mar, Apr, May: (spring) n=60:150 | Jun, Jul, Aug: (summer) n=151:242 | Sep, Oct, Nov: (autumn) n=243:333 |
|---|---|---|---|---|
| A | 0.709 | | | |
| $C_{season}$: | 100.2 | 84.13 | 50.031 | 78.178 |

# APPENDIX (B)

## Flat plate solar collector correlations

The energy balance equation of the solar collector can be written as follows;

$$I_S \times A_c = Q_{loss} + Q_u + Q_{stg} \tag{B.1}$$

The heat loss is expressed by Frederick as;

$$Q_{loss} = A_c U_l F'(\overline{T}_f - T_{amb}) \tag{B.2}$$

The overall heat loss of the collector $U_l$ is the summation of three components; the top loss $U_t$, the bottom loss $U_b$, and the edge loss $U_e$:

$$U_l = U_t + U_b + U_e \tag{B.3}$$

Where, the bottom and edge losses are calculated respectively as following:

$$U_b = k_b / l_b \tag{B.4}$$

$$U_e = (k_e / l_e) \times \frac{2(C_L + C_W)C_h}{C_L \times C_W} \tag{B.5}$$

An empirical equation for the top losses $U_t$ for both hand and computer calculations was developed by Klein (1975) [13].

$$U_t = \left[ \frac{NG}{\frac{C}{T_{mp}}\left[\frac{(T_{mp} - T_{amb})}{(NG + f)}\right]^e} + \frac{1}{h_w} \right]^{-1} + \frac{\sigma(T_{mp} + T_{amb})(T_{mp}^2 + T_{amb}^2)}{(\varepsilon_p + 0.00591NG \times h_w)^{-1} + \frac{2NG + f - 1 + 0.133 \times \varepsilon_p}{\varepsilon_g} - NG} \tag{B.6}$$

Where,

$NG$ is the number of glass covers, $f = (1 + 0.089h_w - 0.1166h_w\varepsilon_p)(1 + 0.07866NG)$, $C = 520 \times (1 - 0.000051\beta^2)$ for $0° < \beta < 70°$, $e = 0.43(1 - 100/T_{pm})$ where $\beta$ is the collector tilt angle in degree and $h_w$ is the wind heat transfer coefficient and given as;

$$h_w = 5.7 + 3.8 \times V_w \tag{B.7}$$

Efficiency factor $F'$ can be calculated as follows;

$$F' = \frac{\frac{1}{U_t}}{s\left(\frac{1}{U_t[(s_t - d)F + d]} + \frac{1}{\frac{kb}{l}} + \frac{1}{h_f \pi d_i}\right)} \tag{B.8}$$

The fin efficiency $F$ is given as;

$$F = \frac{\tanh\left[\sqrt{\frac{U_t}{k\delta}\left(\frac{s_t - d}{2}\right)}\right]}{\sqrt{\frac{U_t}{k\delta}\left(\frac{s_t - d}{2}\right)}}$$ (B.9)

The heat removal factor is calculated from;

$$F_R = F' \times \frac{GC_p}{U_t F'}\left(1 - \exp-\left(\frac{U_t F'}{GC_p}\right)\right)$$ (B.10)

Where $G = m/A_c$. Once $F_R$ is calculated, the useful energy from the collector can be calculated from the following equation;

$$Q_u = F_R A_c [I_s - U_l(T_{icol} - T_{amb})]$$ (B.11)

The energy stored is expressed by Frederick as;

$$Q_{stg} = A_c C_c \frac{d\overline{T}_{col}}{dt}$$ (B.12)

The collector heat removal factor times this maximum possible useful energy gain is equal to the actual useful energy gain $Q_u$:

$$Q_u = A_c F_R \left[S - U_t(T_{fi} - T_{amb})\right]$$ (B.13)

The thermal efficiency equation becomes,

$$\eta_{thc} = F_R(\tau\alpha) - F_R U_t\left(\frac{T_{fi} - T_{amb}}{S}\right)$$ (B.14)

In a flat plate collector the heat transfer occurs between the absorber plate and the cooling fluid. J. C. Francken expressed the effectiveness correlation as a function of efficiency factor.

$$\varepsilon_c = \frac{1 - \exp(-NTU_c(1 - F'))}{1 - F' \exp(-NTU_c(1 - F'))}$$ (B.15)

$NTU_c$ is the number of transferring units of the collector heat exchanger and equal to $U_t A_c / m C_p$ (B.16)

It may be noted that the effectiveness, $E$ is defined by Edwards and Phillips is quite different from $\varepsilon_c$, as defined above in equation (B.15)

$$E_c = 1 - \exp(-NTU_c(1 - F'))$$ (B.17)

For simplification, the term $NTU_c(1 - F')$ may be considered as flow parameter $\phi_c$ of the collector.

$$\phi_c = NTU_c(1 - F')$$ (B.18)

The collector effectiveness may be expressed as a function of the collector tube effectiveness. The tube effectiveness equation presented as following;

$$\varepsilon_t = SNTU(1 - \exp(-1/SNTU))$$ (B.19)

Where $SNTU$ is the solar number of transfer units, $m C_p / F^* U_t A_t$ where $F^*$ is the collector parameter and is equal to;

$$F^* = \frac{W_e C_b h_f}{\pi d_i (C_b h_f + W_e U_t h_f) + W_e U_t C_b} \tag{B.20}$$

Where the effective tube spacing is

$$W_e = (s - d_o)F + d_o \tag{B.21}$$

*SNTU* is presenting the ratio of the potential for the fluid to absorb energy to the loss potential for the solar collector. The relationship for the collector effectiveness as a function of *SNTU* parameter is determined as following;

$$E_c = \psi(SNTU(1 - \exp(-1/SNTU))) \tag{B.22}$$

Where,

$$\psi = N_{tubes} F^* A_p / A_r \tag{B.23}$$

The collector heat capacity equation derived as following as;

$$C_c = \frac{\left(F'U_t + \dfrac{GC_p}{K}\right)(T_{fo} - T_{fi})}{\ln\left[\dfrac{T_o(t_1) - T_{amb}}{T_o(t_1) - T_{amb}}\right]} \tag{B.24}$$

Where

$$K = \frac{GC_p}{F'U_t}\left(\frac{F'}{F_R} - 1\right) \tag{B.25}$$

The collector time constant in may be calculated as;

$$t_c = \frac{C_c}{F'U_t + \dfrac{GC_p}{K}} \times \ln 100 \tag{B.26}$$

# APPENDIX (C)

## The flash chamber and condenser unit equations and correlations

The energy balance for the flashing brine is expressed as follows,

$$B_o^\cdot h_o(T_{bo}, x_{bo}) = B_1^\cdot h_{b1}(T_{b1}, x_{b1}) + [(B_o^\cdot - B_1^\cdot)H_{V1}(T_{b1}, P(T_o))] \tag{C.1}$$

Where,

$$B_1^\cdot = W_{b1} + X_{b1} \tag{C.2}$$

The two equations below shows the overall mass balance for both flash and condenser units,

$$B_o^\cdot = D_1^\cdot + B_1^\cdot \tag{C.3}$$

$$F_i^\cdot = F_o^\cdot \tag{C.4}$$

And the flash unit enthalpy balance is;

$$B_o^\cdot h_o + F_i^\cdot h_{Fi} = B_1^\cdot h_{b1} + D_1^\cdot h_{D1} + F_o^\cdot h_{Fo} + Q_{loss} \tag{C.5}$$

While the overall heat transfer coefficient is represented by the following equation,

$$U_1 = f(\phi, T_{Fi}, T_{Fo}, T_{D1}, ID_1, OD_o, FF, R_F) \tag{C.6}$$

The amount of heat exchanges across the condenser heat transfer surface $Q_1$ is calculated as;

$$Q_1 = m_{Fi,o}^\cdot c_p (T_{Fo} - T_{Fi}) = U_1 A_1 \times \Delta T_{lm1} \tag{C.7}$$

From equation (C.7),

$$\frac{U_1 \times A_1}{m_{Fi,o}^\cdot c_p} = \ln\frac{T_{D1} - T_{Fi}}{T_{D1} - T_{F0}} = -\ln\frac{T_{D1} - T_{F0}}{T_{D1} - T_{Fi}} \tag{C.8}$$

From equation (C.8), the following equation is obtained:

$$(1 - E) \times T_{Fi} + E \times T_{D1} - T_{Fo} = 0 \tag{C.9}$$

Where $E = 1 - e^{-NTU_1}$ and $NTU_1 = U_1 \times A_1 / m_{Fi,o}^\cdot c_p$ (C.10)

$$T_{D1} = T_{b1} - NEA - BPR \tag{C.11}$$

The non-equilibrium allowance *NEA* and *BPR* are calculated by the following equations;
Where,

$$NEA = A + B \times T_{b1} + C \times T_{b1}^2 + D \times T_{b1}^3 \tag{C.12}$$

$$BPR = (B + C \times X) \times X \tag{C.13}$$

Where,

$$10^3 \times B = 6.71 + 6.43 \times 10^{-2} \times T_{b1} + 9.74 \times 10^{-5} \times T_{b1}^2$$

$$10^5 \times C = 2.38 + 9.59 \times 10^{-3} \times T_{b1} + 9.42 \times 10^{-5} \times T_{b1}^2 \tag{C.14}$$

The performance ratio can be estimated as follows:

$$PR_n = \frac{\sum_{1...n} D_{tn}^\cdot \times Hv_n}{I_S \times Ac} \tag{C.15}$$

# APPENDIX (D)

## The error analysis of the experimental work

### D.1. The error analysis of the experimental work:

The measured experimental data includes some errors due to the uncertainty of the measuring process and the limited precision of the experimental instruments. For the examination of the validity of the experimental work; the following fractional error ($Fr$) equation is used:

$$\% Fr = \frac{Calculated - Measured}{Calculated} \times 100$$

The average $Fr$ percentage for the measuring of the solar radiation was about 1%-2%. For the TBT; the $Fr$ error; was not exceeding about 6%-7%. Also for the wasted brine and outlet feed water temperatures; the percentage was about 9% and 8% respectively. The percentage for the system performance ratio PR is about 4% and 9% for the system productivity DP.

Table (D-1)
The $Fr$ error percentage of the measured data

| Parameter: | $Fr$ Percentage%: |
|---|---|
| $I_S$ | 2% |
| $TBT$ | 6%-7% |
| $T_{b1}$ | 9% |
| $T_{icol}$ | 8% |
| $DP$ | 7% |
| $PR$ | 4% |

# APPENDIX (E)

## Exergy analysis correlations

### E.1. Exergy analysis definitions:

The general form of the availability method is defined as;

$$A_2 - A_1 = A_q + A_w + A_{f_i} - A_{f_e} - I \tag{E.1}$$

Where $A_2 - A_1 = 0$ is the nonflow availability change in steady state condition,

The availability transfer due to the heat transfer between the controls is;

$$A_q = \sum_J (1 - \frac{T_0}{Tj}) Q_j$$

The work produced by the control volume is;

$$A_w = -W_{cv} + P_0 (V_2 - V_1)$$

And, $I = T_0 \times Sgen$ is the availability destruction in the process. The flow availability expressed as $A_{f_{i,e}} = \sum_{i,e} m_{i,e} a_{f_{i,e}}$.

So the general form in steady state condition would become

$$A_q + A_w + A_{f_i} - A_{f_e} = I \tag{E.2}$$

### E.2. Flat plate collector exergy analysis:

Thus the entropy generation production equation for the solar collector is obtained as;

$$Sgen_{col} = \frac{1}{T_0} (Q^* (1 - \frac{T_0}{T^*}) - \dot{m}_{wi,e} c_{pm} (T_{we} - T_{wi} - T_0 \ln \frac{T_{we}}{T_{wi}})) . \tag{E.3}$$

### E.3. Flash unit and condenser exergy analysis:

The internal irreversibility for one chamber should become,

$$I_{fch} = I_{fu} + I_{cw} \tag{E.4}$$

For flashing part,

$$I_{fu} = A_{fbi} - A_{fbe} - A_{fde} \tag{E.5}$$

And for cooling water streams passing through the condenser,

$$I_{cw} = A_{fcwi} - A_{fcwe} \tag{E.6}$$

The final state for the flashing part;

$$I_{fu} = B_i(C_{pbi}(T_{bi} - T_o) - T_o(C_{pbi} \ln(T_{bi}/T_o) - V_w(P_{bi} - P_o)/T_o)) -$$
$$B_e(C_{pbe}(T_{be} - T_o) - T_o(C_{pbe} \ln(T_{be}/T_o) - V_w(P_{be} - P_o)/T_o)) - \tag{E.7}$$
$$D_e(C_{pde}(T_{de} - T_o) - T_o(C_{pde} \ln(T_{de}/T_o) - V_w(P_{de} - P_o)/T_o))$$

For cooling water stream in the condenser, the internal irreversibility should be exists like this,

$$I_{cw} = F_{cw}(C_{pl}(T_{cwi} - T_{cwe}) - T_o(C_{pl} \ln(T_{cwi}/T_{cwe}) - V_w(P_{cwi} - P_{cwe})/T_o)) \tag{E.8}$$

The total entropy generation for the flashing part (flash chamber and condenser) becomes,

$$Sgen_{fch} = \frac{1}{T_o} \times I_{fch} \tag{E.9}$$

For mixer and splitter units that are shown the analysis becomes as;

$$I_{mix} = B_{mi1} \times a_{f,bmi1} + F_{mi2} \times a_{f,Fmi2} - R \times a_{fme} \tag{E.10}$$

$$I_{spl} = B_{spi} \times a_{f,spi} - B_{sp,e1} \times a_{f,spe1} - B_{sp,e2} \times a_{f,spe2} \tag{E.11}$$


## E.4. The exergetic efficiency of the system:


For any given system when achieving the required task;

$$\eta_{ex} = \frac{\sum E_{xout}}{\sum E_{xin}} . \tag{E.12}$$

So, the exergy efficiency for solar water heater should become

$$\eta_{ex\,col} = \frac{\dot{m}_{we} c_{pl}(T_{we} - T_{wi} - T_0 \ln \frac{T_{we}}{T_{wi}})}{Q^*(1 - \frac{T_0}{T^*})} \tag{E.13}$$

And for the flashing unit, the exergy efficiency becomes;

$$\eta_{exfch} = \frac{B_e a_{fbe} + F_{cwe} a_{fcwe} + D_e a_{fde}}{(B_i a_{fbi} + F_{cwi} a_{fcwi})} \tag{E.14}$$

The overall exergy efficiency becomes;

$$\eta_{overall1} = \frac{D_e a_{fde}}{F_{cwi} a_{fcwi} + Q^*(1 - \frac{T_0}{T^*})} \tag{E.15}$$

### E.5. Exergy destruction analysis:

The exergy destruction term $E_d$ for brine heater is;

$$E_{dcol} = \frac{1}{\eta_{excol}} - 1 \qquad\qquad (E.16)$$

So for the brine heater section, the exergy destruction term becomes,

$$E_{dcol} = \frac{Q^*(1 - \frac{T_0}{T^*})}{m_{we} c_{pm}(T_{we} - T_{wi} - T_0 \ln \frac{T_{we}}{T_{wi}})} - 1 \qquad\qquad (E.17)$$

The exergy destruction term for flashing units also defined as;

$$E_{dfch} = \frac{exergyloss}{\dot{D}_t} = \frac{I_{fch}}{\dot{D}_t} \qquad\qquad (E.18)$$

The minimum number of entropy generation for the solar collector can be estimated as presented as;

$$Ns = \frac{\dot{S}_{gen} T_o}{Q^* A_c (\tau\alpha)} \qquad\qquad (E.19)$$

# APPENDIX (F)

## Physical & thermodynamic and heat transfer coefficient correlations

### F.1. Density of saltwater:

The equation is applicable in the temperature range of 10 to 180 ºC and for salinity from 0 to 160 g/kg.

$$\rho = 0.5 \times a_o + a_1 \times Y + a_2 \times (2 \times Y^2 - 1) + a_3 \times (4 \times Y^3 - 3 \times Y)$$

Where:

$$a_o = 2.016110 + 0.115313 \times \sigma + 0.000326 \times (2 \times \sigma^2 - 1)$$

$$a_1 = -0.0541 + 0.01571 \times \sigma - 0.000423 \times (2 \times \sigma^2 - 1)$$

$$a_2 = -0.006124 + 0.00174 \times \sigma - 0.000009 \times (2 \times \sigma^2 - 1)$$

$$a_3 = 0.000346 + 0.000087 \times \sigma - 0.000053 \times (2 \times \sigma^2 - 1)$$

$$Y = \frac{2t - 200}{160}$$

$$\sigma = \frac{2X - 150}{150}$$

### F.2. Dynamic viscosity:

The Validity range of this correlation is 10-150 ºC and 0-130 g/kg salt concentration.

$$\mu = \mu_w \times \mu_R$$

$\mu_w$: Viscosity of pure water.

$\mu_R$: Relative viscosity and =1 for pure water & > 1 for salt solution.

$$\ln \mu_w = -3.79418 + \frac{604.129}{139.18 + t}$$

$t$: Temperature in ºC.

$$\mu_R = 1 + a_1 \times X + a_2 \times X^2$$

Where,

$$a_1 = 1.474 \times 10^{-3} + 1.5 \times 10^{-5} \times t - 3.927 \times 10^{-8} \times t^2$$

$$a_1 = 1.0734 \times 10^{-5} + 8.5 \times 10^{-8} \times t - 2.23 \times 10^{-10} \times t^2$$

### F.3. Boiling point elevation:

This equation is valid for $X$ (salt concentration) from 20 to 160 g/kg for $t$ (temperature) from 20 to 180 ºC.

$$BPR = (B + C \times X) \times X$$

Where:

$$10^3 \times B = 6.71 + 6.43 \times 10^{-2} \times t + 9.74 \times 10^{-5} \times t^2$$
$$10^5 \times C = 2.38 + 9.59 \times 10^{-3} \times t + 9.42 \times 10^{-5} \times t^2$$

### F.4. Specific heat capacity:

$$C_P = A + B \times t + C \times t^2 + D \times t^3$$

Where:

$$A = 4206.8 - 6.6197 \times X + 1.2288 \times 10^{-2} \times X^2$$
$$B = -1.1262 + 5.4178 \times 10^{-2} \times X - 2.2719 \times 10^{-4} \times X^2$$
$$C = 1.2026 \times 10^{-2} - 5.3566 \times 10^{-4} \times X + 1.8906 \times 10^{-6} \times X^2$$
$$D = 6.8774 \times 10^{-7} + 1.517 \times 10^{-6} \times X - 4.4268 \times 10^{-9} \times X^2$$

### F.5. Thermal conductivity of saltwater:

$$k = A + B \times t + C \times t^2$$
$$A = 576.6 - 34.64 \times CA + 7.286 \times CA^2$$
$$B = 10^{-3} \times (1526 + 466.2 \times CA - 226.8 \times CA^2 + 28.67 \times CA^3)$$
$$C = -10^{-5} \times (581 + 2055 \times CA - 991.6 \times CA^2 + 146.4 \times CA^3)$$

And,

$$CA = \frac{28.17 \times X}{1000 - X}$$

### F.6. Latent heat of vaporization of saltwater as a function of boiling temperature:

$$\lambda = 597.49 - 5.6624 \times 10^{-1} \times t + 1.5082 \times 10^{-4} \times t^2 - 3.2764 \times 10^{-6} \times t^3$$

## F.7. Pressure drop due to friction loss:

$$\Delta P = \Im \frac{L}{ID} \bullet \frac{\rho V^2 m}{2}$$

$\Im = 64/\text{Re}$ For laminar flow (Re<2000).

$\Im = (1.82 \log \text{Re} - 1.64)^{-2}$ For Re>4000.

## F.8. Overall heat transfer coefficient:

The following correlations are used to calculate the overall heat transfer coefficients for the flash evaporator and the condenser unit.

$$U = 1/\sum R = [R_{ci} + R_{fi} + R_w + R_{fo} + R_{nc} + R_{co}]^{-1}$$

### F.8.1. Tube wall resistance:

$$R_w = \frac{OD}{2k_m} \times \log_e \frac{OD}{ID}$$

Where: $k_m$ is the thermal conductivity of the tube wall.

### F.8.2. Inside convection resistance:

$$R_{ci} = \frac{1}{h_i} \times \{OD/ID\}$$

Where: $h_i$ is the heat transfer coefficient for the inside flow in W/m²K and obtained from the following equation:

$$Nu = 0.027 \times (\text{Re})^{0.8} \times (\text{Pr})^{1/3} \times (\frac{\mu_w}{\mu_b})^{0.14}$$

Where:

*Nu* is the Nusselt number and *Re* is the Reynolds number and *Pr* is the Prandtl number.

$\mu$ is the absolute brine viscosity kg/hr.m, $\mu_b$ evaluated at stream bulk temperature.

### F.8.3. outside convection resistance:

$$R_{co} = 1/h_o$$

$$h_o = 0.725 \times CR \times \left[\frac{k_f^3 \times \rho_f^2 \times \lambda \times g}{N \times OD \times \mu_f \times \Delta t_f}\right]^{1/4}$$

Where:

$h_o$          Mean condensing coefficient for N tubes in a vertical row.

$CR$          Practical correction factor to account for experimentally observed deviation from Nusselt equation.

$k_f$          Thermal conductivity.

$\rho_f$          Density kg/m$^3$.

$g$          Acceleration of gravity m/hr

$\lambda$          Latent heat of condensation.

$\mu_f$          Viscosity.

$OD$          Tube outside diameter.

$\Delta t_f$          Temperature drop across condensate film.

The subscript $f$ refers to the condensation film.

For $N \leq 10$

$$Cr = 1.23795 + 0.0353608N - 0.00157035N^2$$

For $N > 10$

$$CR = 1.434523$$

Where $N$ is the number of tubes in a vertical row of the rectangular cross section bundle of tubes.

# APPENDIX (G)

## Average measured data of the system obtained from 8/2004 to 7/2005

**N=1**   **1-1-2005**   *FEED=0.0183 KG/S*

| Tfs | Tco | Tbo | Tb1 | Is | Tamb | Tg | Tins | Vw | Hr | product |
|---|---|---|---|---|---|---|---|---|---|---|
| 15 | 22 | 38 | 25 | 380 | 17 | 22 | 20 | 2.1 | 9 | |
| 16 | 25 | 39 | 27 | 455 | 18 | 23 | 20 | 1.2 | 10 | |
| 18 | 26 | 40 | 29 | 535 | 20 | 25 | 21 | 1.2 | 11 | |
| 19 | 27 | 42 | 31 | 562 | 22 | 25 | 23 | 2.3 | 12 | |
| 21 | 26 | 41 | 31 | 488 | 22 | 23 | 23 | 2.1 | 13 | |
| 21 | 26 | 41 | 30 | 436 | 21 | 23 | 22 | 3.1 | 14 | |
| 20 | 25 | 40 | 30 | 342 | 20 | 22 | 21 | 2.8 | 15 | |
| 19 | 24 | 39 | 29 | 271 | 19 | 21 | 20 | 3.2 | 16 | |
| **18.625** | **25.125** | **40** | **29** | **3469** | **19.875** | **23** | **21.25** | **2.25** | **8** | **2.5** |

**N=48**   **17-2-2005**   *FEED=0.0183 KG/S*

| Tfs | Tco | Tbo | Tb1 | Is | Tamb | Tg | Tins | Vw | Hr | product |
|---|---|---|---|---|---|---|---|---|---|---|
| 16 | 22 | 39 | 22 | 395 | 19 | 26 | 20 | 1.2 | 9 | |
| 17 | 23 | 40 | 23 | 467 | 21 | 29 | 22 | 1.1 | 10 | |
| 18 | 25 | 45 | 27 | 532 | 24 | 33 | 25 | 1.1 | 11 | |
| 20 | 28 | 48 | 30 | 610 | 27 | 33 | 30 | 0.8 | 12 | |
| 20 | 28 | 47 | 29 | 497 | 25 | 32 | 30 | 0.9 | 13 | |
| 19 | 27 | 46 | 28 | 389 | 24 | 31 | 29 | 1.2 | 14 | |
| 18 | 26 | 45 | 27 | 255 | 23 | 30 | 28 | 2.1 | 15 | |
| 18 | 24 | 44 | 26 | 177 | 22 | 30 | 27 | 2.3 | 16 | |
| **18.25** | **25.375** | **44.25** | **26.5** | **3322** | **23.125** | **30.5** | **26.375** | **1.3375** | **8** | **4.5** |

**N=74**   **15-3-2005**   *FEED=0.0183 KG/S*

| Tfs | Tco | Tbo | Tb1 | Is | Tamb | Tg | Tins | Vw | Hr | product |
|---|---|---|---|---|---|---|---|---|---|---|
| 18 | 23 | 47 | 31 | 418 | 23 | 26 | 25 | 1.2 | 9 | |
| 19 | 25 | 49 | 32 | 534 | 24 | 29 | 26 | 1.1 | 10 | |
| 20 | 27 | 49 | 36 | 608 | 25 | 33 | 27 | 1.1 | 11 | |
| 22 | 31 | 50 | 37 | 634 | 27 | 33 | 30 | 0.8 | 12 | |
| 22 | 31 | 49 | 36 | 611 | 25 | 32 | 30 | 0.9 | 13 | |
| 21 | 30 | 48 | 36 | 540 | 24 | 31 | 29 | 1.2 | 14 | |
| 20 | 29 | 47 | 35 | 426 | 23 | 30 | 27 | 2.1 | 15 | |
| 20 | 29 | 45 | 34 | 278 | 22 | 30 | 27 | 2.3 | 16 | |
| **20.25** | **28.125** | **48** | **34.625** | **4049** | **24.125** | **30.5** | **27.625** | **1.3375** | **8** | **6.5** |

| N=106 | 15-4-2005 | FEED=0.0183 KG/S | | | | | | | | |
|---|---|---|---|---|---|---|---|---|---|---|
| Tfs | Tco | Tbo | Tb1 | Is | Tamb | Tg | Tins | Vw | Hr | product |
| 21 | 27 | 46 | 34 | 498 | 24 | 27 | 26 | 3 | 9 | |
| 22 | 30 | 49 | 35 | 588 | 25 | 30 | 27 | 2 | 10 | |
| 23 | 32 | 50 | 36 | 634 | 26 | 32 | 28 | 2 | 11 | |
| 24 | 35 | 51 | 38 | 651 | 27 | 34 | 31 | 1 | 12 | |
| 24 | 35 | 51 | 37 | 630 | 26 | 33 | 30 | 0.9 | 13 | |
| 23 | 34 | 49 | 36 | 589 | 25 | 32 | 29 | 1.2 | 14 | |
| 22 | 33 | 49 | 35 | 470 | 24 | 31 | 28 | 3 | 15 | |
| 22 | 30 | 47 | 34 | 402 | 23 | 30 | 27 | 3 | 16 | |
| **22.625** | **32** | **49** | **35.625** | **4462** | **25** | **31.125** | **28.25** | **2.0125** | **8** | **8** |

| N=135 | 15-5-2005 | FEED=0.0183 KG/S | | | | | | | | |
|---|---|---|---|---|---|---|---|---|---|---|
| Tfs | Tco | Tbo | Tb1 | Is | Tamb | Tg | Tins | Vw | Hr | product |
| 23 | 30 | 47 | 35 | 432 | 24 | 30 | 27 | 1.2 | 9 | |
| 24 | 33 | 49 | 37 | 553 | 26 | 31 | 29 | 0.5 | 10 | |
| 24.5 | 35 | 51 | 37 | 664 | 27 | 36 | 30 | 0.4 | 11 | |
| 26 | 37 | 52 | 38 | 688 | 28 | 37 | 30 | 1.2 | 12 | |
| 25 | 36 | 51 | 38 | 671 | 29 | 36 | 33 | 1.8 | 13 | |
| 24 | 35 | 51 | 37 | 605 | 30 | 36 | 31 | 0.8 | 14 | |
| 23 | 34 | 50 | 36 | 489 | 29 | 34 | 30 | 0.5 | 15 | |
| 23 | 32 | 49 | 34 | 393 | 27 | 32 | 29 | 2 | 16 | |
| **24.0625** | **34** | **50** | **36.5** | **4495** | **27.5** | **34** | **29.875** | **1.05** | **8** | **8.5** |

| N=160 | 9/6/2005 | FEED=0.0183 KG/S | | | | | | | | |
|---|---|---|---|---|---|---|---|---|---|---|
| Tfs | Tco | Tbo | Tb1 | Is | Tamb | Tg | Tins | Vw | Hr | product |
| 26 | 31 | 50 | 37 | 450 | 26 | 33 | 28 | 2 | 9 | |
| 26 | 36 | 52 | 39 | 562 | 27 | 33 | 29 | 2.5 | 10 | |
| 26 | 38 | 54 | 41 | 650 | 28 | 34 | 30 | 3 | 11 | |
| 27 | 39 | 56 | 42 | 680 | 29 | 34 | 31 | 4 | 12 | |
| 28 | 37 | 52 | 40 | 648 | 30 | 33 | 31 | 1.5 | 13 | |
| 29 | 36 | 50 | 39 | 571 | 30 | 35 | 31 | 2 | 14 | |
| 28 | 36 | 50 | 39 | 474 | 31 | 34 | 31 | 3 | 15 | |
| 28 | 36 | 49 | 37 | 415 | 30 | 33 | 31 | 2.5 | 16 | |
| **27.25** | **36.125** | **51.625** | **39.25** | **4450** | **28.875** | **33.625** | **30.25** | **2.5625** | **8** | **11** |

| N=197 | 15-7-2005 | FEED=0.0183 KG/S | | | | | | | | |
|---|---|---|---|---|---|---|---|---|---|---|
| Tfs | Tco | Tbo | Tb1 | Is | Tamb | Tg | Tins | Vw | Hr | product |
| 27 | 33 | 52 | 42 | 533 | 28 | 34 | 30 | 1 | 9 | |
| 27 | 37 | 54 | 43 | 627 | 29 | 35 | 31 | 1.5 | 10 | |
| 28 | 39 | 57 | 44 | 686 | 31 | 35 | 32 | 2 | 11 | |
| 29 | 40 | 60 | 46 | 710 | 32 | 36 | 34 | 0.5 | 12 | |
| 28 | 40 | 60 | 45 | 680 | 33 | 36 | 34 | 0.5 | 13 | |
| 28 | 39 | 59 | 45 | 623 | 32 | 35 | 33 | 1.2 | 14 | |
| 27 | 38 | 59 | 44 | 520 | 31 | 35 | 33 | 2.2 | 15 | |
| 27 | 37 | 58 | 43 | 488 | 31 | 34 | 32 | 1.8 | 16 | |
| **27.625** | **37.875** | **57.375** | **44** | **4867** | **30.875** | **35** | **32.375** | **1.3375** | **8** | **14** |

*N=227*    *15/8/2004*    *FEED=0.0183 KG/S*

| Tfs | Tco | Tbo | Tb1 | Is | Tamb | Tg | Tins | Vw | Hr | product |
|---|---|---|---|---|---|---|---|---|---|---|
| 28 | 36 | 59 | 42 | 560 | 29 | 33 | 31 | 1.5 | 9 | |
| 28 | 38 | 61 | 43 | 652 | 30 | 36 | 32 | 0 | 10 | |
| 29 | 40 | 64 | 45 | 704 | 32 | 37 | 34 | 0.1 | 11 | |
| 30 | 42 | 67 | 46 | 773 | 35 | 38 | 36 | 0 | 12 | |
| 30 | 41 | 67 | 45 | 710 | 36 | 38 | 37 | 1.1 | 13 | |
| 29 | 39 | 66 | 44 | 654 | 35 | 37 | 36 | 0.2 | 14 | |
| 28 | 39 | 65 | 43 | 575 | 34 | 37 | 35 | 0.8 | 15 | |
| 28 | 38 | 63 | 42 | 492 | 34 | 36 | 35 | 0.9 | 16 | |
| **28.75** | **39.125** | **64** | **43.75** | **5120** | **33.125** | **36.5** | **34.5** | **0.575** | **8** | **16.5** |

<br>

*N=259*    *15-9-2004*    *FEED=0.0183 KG/S*

| Tfs | Tco | Tbo | Tb1 | Is | Tamb | Tg | Tins | Vw | Hr | product |
|---|---|---|---|---|---|---|---|---|---|---|
| 27 | 33 | 50 | 40 | 485 | 27 | 30 | 29 | 8.1 | 9 | |
| 27 | 35 | 53 | 41 | 596 | 28 | 32 | 30 | 4.5 | 10 | |
| 27 | 37 | 55 | 42 | 654 | 29 | 34 | 31 | 3.5 | 11 | |
| 28 | 39 | 58 | 43 | 660 | 30 | 40 | 32 | 2.1 | 12 | |
| 27 | 38 | 56 | 43 | 599 | 31 | 40 | 32 | 1.7 | 13 | |
| 26 | 38 | 52 | 42 | 485 | 30 | 39 | 31 | 0.2 | 14 | |
| 26 | 37 | 50 | 41 | 400 | 29 | 38 | 31 | 2.8 | 15 | |
| 26 | 35 | 49 | 41 | 322 | 28 | 38 | 30 | 3.1 | 16 | |
| **26.75** | **36.5** | **52.875** | **41.625** | **4201** | **29** | **36.375** | **30.75** | **3.25** | **8** | **12** |

<br>

*N=298*    *24-10-2004*    *FEED=0.0183 KG/S*

| Tfs | Tco | Tbo | Tb1 | Is | Tamb | Tg | Tins | Vw | Hr | product |
|---|---|---|---|---|---|---|---|---|---|---|
| 26 | 31 | 44 | 33 | 385 | 26 | 31 | 30 | 5 | 9 | |
| 26 | 33 | 49 | 36 | 491 | 27 | 34 | 32 | 1.8 | 10 | |
| 27 | 36 | 53 | 39 | 593 | 28 | 38 | 33 | 3.5 | 11 | |
| 28 | 39 | 56 | 41 | 630 | 30 | 39 | 34 | 4.8 | 12 | |
| 28 | 38 | 54 | 39 | 570 | 29 | 38 | 31 | 3.5 | 13 | |
| 27 | 37 | 51 | 38 | 488 | 28 | 37 | 30 | 3.4 | 14 | |
| 26 | 35 | 48 | 38 | 386 | 27 | 36 | 30 | 4.2 | 15 | |
| 24 | 33 | 44 | 35 | 315 | 26 | 34 | 29 | 4.2 | 16 | |
| **26.5** | **35.25** | **49.875** | **37.375** | **3858** | **27.625** | **35.875** | **31.125** | **3.8** | **8** | **9** |

<br>

*N=320*    *15-11-2004*    *FEED=0.0183 KG/S*

| Tfs | Tco | Tbo | Tb1 | Is | Tamb | Tg | Tins | Vw | Hr | product |
|---|---|---|---|---|---|---|---|---|---|---|
| 19 | 30 | 39 | 33 | 331 | 22 | 31 | 30 | 5 | 9 | |
| 20 | 32 | 43 | 34 | 430 | 23 | 32 | 32 | 1.8 | 10 | |
| 21 | 35 | 48 | 36 | 482 | 24 | 33 | 33 | 3.5 | 11 | |
| 22 | 38 | 50 | 38 | 490 | 25 | 34 | 31 | 4.8 | 12 | |
| 21 | 37 | 48 | 37 | 444 | 24 | 34 | 30 | 3.5 | 13 | |
| 21 | 36 | 43 | 35 | 361 | 23 | 33 | 29 | 3.4 | 14 | |
| 20 | 35 | 42 | 33 | 240 | 21 | 32 | 28 | 4.2 | 15 | |
| 19 | 30 | 39 | 30 | 110 | 20 | 30 | 27 | 4.2 | 16 | |
| **20.375** | **34.125** | **44** | **34.5** | **2888** | **22.75** | **32.375** | **30** | **3.8** | **8** | **5** |

| N=350 | 15-12-2004 | FEED=0.0183 KG/S | | | | | | | | |
|---|---|---|---|---|---|---|---|---|---|---|
| Tfs | Tco | Tbo | Tb1 | Is | Tamb | Tg | Tins | Vw | Hr | product |
| 16 | 30 | 38 | 30 | 266 | 18 | 28 | 23 | 1.2 | 9 | |
| 17 | 32 | 42 | 33 | 370 | 19 | 29 | 24 | 2 | 10 | |
| 17 | 33 | 44 | 36 | 432 | 20 | 30 | 25 | 1.5 | 11 | |
| 19 | 35 | 48 | 37 | 447 | 21 | 32 | 26 | 2.3 | 12 | |
| 18 | 34 | 47 | 35 | 415 | 19 | 30 | 24 | 1.2 | 13 | |
| 17 | 32 | 40 | 33 | 341 | 18 | 28 | 23 | 0.8 | 14 | |
| 17 | 31 | 39 | 32 | 230 | 17 | 26 | 22 | 0.5 | 15 | |
| 16 | 29 | 39 | 30 | 90 | 17 | 24 | 21 | 3.5 | 16 | |
| **17.125** | **32** | **42.125** | **34.5** | **2591** | **18.625** | **28.375** | **23.5** | **1.625** | **8** | **3.5** |

| Tfs | Tco | Tbo | Tb1 | Tstage | Is | Tamb | Tg | Tins | Vw | month | Product |
|---|---|---|---|---|---|---|---|---|---|---|---|
| 18 | 25.125 | 40 | 26 | 14 | 3344 | 20 | 24 | 22 | 2.25 | 1 | 2.5 |
| 19 | 25.357 | 44.25 | 28 | 16.25 | 3469 | 23 | 30 | 26 | 1.3 | 2 | 4.5 |
| 20.25 | 28.125 | 48 | 34.5 | 13.5 | 4049 | 24 | 30.5 | 27 | 4.2 | 3 | 6.5 |
| 22.6 | 32 | 49 | 35.5 | 13.5 | 4462 | 25 | 31 | 28.25 | 3.7 | 4 | 8 |
| 24 | 34 | 51 | 36.5 | 14 | 4495 | 27.5 | 30 | 30 | 1.05 | 5 | 8.5 |
| 27.25 | 36.125 | 52 | 40 | 12 | 4450 | 29 | 34 | 30.25 | 2.5 | 6 | 11 |
| 27.6 | 38 | 58 | 44 | 14 | 4867 | 31 | 35 | 32.357 | 1.5 | 7 | 14 |
| 28.75 | 39 | 65 | 43.75 | 20 | 5120 | 33 | 36.5 | 34.5 | 0.8 | 8 | 16.5 |
| 26.75 | 36.5 | 52 | 42 | 10 | 4201 | 29 | 36.5 | 30.75 | 3.25 | 9 | 12 |
| 26.5 | 35.25 | 49 | 37 | 12 | 3858 | 28 | 35.6 | 31 | 3.7 | 10 | 9 |
| 20.375 | 34 | 44 | 35 | 9 | 2888 | 23 | 32 | 30 | 3.8 | 11 | 5 |
| **17.125** | **32** | **42** | **34.5** | **7.5** | **2591** | **19** | **28.5** | **23.5** | **1.625** | **12** | **3.5** |

# APPENDIX (H)

## Measured data points obtained for the solar flux from 1998 to 2005

| Measured points of solar radiation: | $I_o \cos(z)$: |
|---|---|
| 281.00 | 293.29 |
| 422.00 | 541.71 |
| 500.00 | 737.19 |
| 545.00 | 866.41 |
| 510.00 | 920.55 |
| 426.00 | 895.92 |
| 298.00 | 794.21 |
| 140.00 | 622.35 |
| 400.00 | 719.70 |
| 590.00 | 958.00 |
| 650.00 | 1140.30 |
| 802.00 | 1254.10 |
| 856.00 | 1291.70 |
| 810.00 | 1250.40 |
| 698.00 | 1133.20 |
| 497.00 | 948.00 |
| 320.00 | 707.40 |
| 545.00 | 740.40 |
| 688.00 | 970.10 |
| 830.00 | 1148.80 |
| 897.00 | 1264.30 |
| 903.00 | 1308.80 |
| 884.00 | 1279.30 |
| 775.00 | 1177.70 |
| 650.00 | 1011.00 |
| 479.00 | 790.60 |
| 379.00 | 520.86 |
| 522.00 | 752.12 |
| 630.00 | 922.55 |
| 655.00 | 1020.50 |
| 667.00 | 1039.40 |
| 510.00 | 977.81 |
| 422.00 | 840.03 |
| 333.00 | 635.42 |
| 142.00 | 377.93 |
| 458.00 | 623.91 |
| 577.00 | 863.44 |
| 730.00 | 1043.70 |
| 790.00 | 1152.30 |
| 800.00 | 1181.90 |
| 760.00 | 1130.50 |
| 643.00 | 1001.60 |
| 488.00 | 803.94 |
| 294.00 | 551.03 |
| 360.00 | 740.40 |
| 630.00 | 970.10 |
| 770.00 | 1148.80 |
| 850.00 | 1264.30 |
| 900.00 | 1308.80 |
| 825.00 | 1279.30 |
| 700.00 | 1177.70 |
| 560.00 | 1011.00 |
| 400.00 | 790.60 |
| 350.00 | 691.04 |
| 600.00 | 930.71 |

| | |
|---|---|
| 750.00 | 1115.70 |
| 820.00 | 1233.40 |
| 885.00 | 1275.80 |
| 800.00 | 1240.00 |
| 700.00 | 1128.40 |
| 570.00 | 948.67 |
| 400.00 | 713.04 |
| 252.00 | 415.10 |
| 331.00 | 641.94 |
| 430.00 | 809.69 |
| 482.00 | 906.93 |
| 490.00 | 927.02 |
| 444.00 | 868.59 |
| 361.00 | 735.64 |
| 240.00 | 537.21 |
| 111.00 | 286.83 |
| 467.00 | 597.32 |
| 544.00 | 834.74 |
| 662.00 | 1012.00 |
| 721.00 | 1116.90 |
| 735.00 | 1142.40 |
| 691.00 | 1086.70 |
| 543.00 | 953.66 |
| 463.00 | 752.30 |
| 384.00 | 496.35 |
| 432.00 | 573.97 |
| 506.00 | 809.40 |
| 637.00 | 984.17 |
| 690.00 | 1086.40 |
| 710.00 | 1109.10 |
| 640.00 | 1050.70 |
| 528.00 | 915.18 |
| 396.00 | 711.83 |
| 212.00 | 454.48 |
| 421.00 | 788.10 |
| 500.00 | 1008.40 |
| 622.00 | 1177.10 |
| 712.00 | 1282.60 |
| 741.00 | 1317.80 |
| 706.00 | 1280.20 |
| 623.00 | 1172.40 |
| 544.00 | 1001.80 |
| 467.00 | 780.01 |
| 264.00 | 572.66 |
| 595.00 | 773.16 |
| 686.00 | 906.99 |
| 743.00 | 965.04 |
| 735.00 | 943.35 |
| 645.00 | 843.39 |
| 532.00 | 671.98 |
| 460.00 | 440.80 |
| 430.00 | 640.27 |
| 650.00 | 845.12 |
| 760.00 | 982.29 |
| 802.00 | 1042.40 |
| 693.00 | 1021.50 |
| 626.00 | 920.77 |
| 495.00 | 747.26 |
| 357.00 | 512.74 |
| 582.00 | 913.59 |
| 750.00 | 1098.30 |
| 780.00 | 1214.20 |

| | |
|---|---|
| 825.00 | 1253.20 |
| 700.00 | 1212.90 |
| 650.00 | 1095.80 |
| 612.00 | 910.09 |
| 470.00 | 668.30 |
| 620.00 | 909.72 |
| 730.00 | 1094.20 |
| 815.00 | 1209.60 |
| 840.00 | 1247.80 |
| 790.00 | 1206.50 |
| 632.00 | 1088.30 |
| 488.00 | 901.32 |
| 300.00 | 658.31 |
| 400.00 | 885.19 |
| 560.00 | 1067.70 |
| 580.00 | 1179.40 |
| 760.00 | 1212.80 |
| 750.00 | 1165.70 |
| 720.00 | 1041.10 |
| 622.00 | 847.60 |
| 450.00 | 598.40 |
| 500.00 | 860.48 |
| 750.00 | 1040.40 |
| 790.00 | 1148.60 |
| 800.00 | 1177.70 |
| 760.00 | 1125.80 |
| 580.00 | 996.41 |
| 420.00 | 798.30 |
| 270.00 | 544.00 |
| 375.00 | 857.46 |
| 460.00 | 1037.00 |
| 650.00 | 1144.80 |
| 740.00 | 1173.50 |
| 670.00 | 1121.10 |
| 434.00 | 991.19 |
| 352.00 | 792.62 |
| 239.00 | 538.92 |
| 400.00 | 851.24 |
| 550.00 | 1030.20 |
| 650.00 | 1137.20 |
| 736.00 | 1164.90 |
| 730.00 | 1111.50 |
| 690.00 | 980.63 |
| 560.00 | 781.19 |
| 400.00 | 526.76 |
| 570.00 | 848.05 |
| 670.00 | 1026.60 |
| 725.00 | 1133.20 |
| 730.00 | 1160.50 |
| 650.00 | 1106.60 |
| 560.00 | 975.30 |
| 380.00 | 775.44 |
| 230.00 | 520.67 |
| 650.00 | 927.55 |
| 780.00 | 1112.60 |
| 830.00 | 1230.00 |
| 890.00 | 1271.80 |
| 760.00 | 1235.20 |
| 630.00 | 1122.60 |
| 500.00 | 941.69 |
| 350.00 | 704.82 |
| 640.00 | 929.15 |

| | |
|---|---|
| 760.00 | 1114.20 |
| 800.00 | 1231.70 |
| 820.00 | 1273.80 |
| 740.00 | 1237.60 |
| 610.00 | 1125.50 |
| 490.00 | 945.23 |
| 330.00 | 708.98 |
| 620.00 | 930.71 |
| 790.00 | 1115.70 |
| 820.00 | 1233.40 |
| 830.00 | 1275.80 |
| 790.00 | 1240.00 |
| 660.00 | 1128.40 |
| 505.00 | 948.67 |
| 335.00 | 713.04 |
| 600.00 | 932.25 |
| 750.00 | 1117.20 |
| 820.00 | 1235.00 |
| 880.00 | 1277.70 |
| 800.00 | 1242.20 |
| 700.00 | 1131.20 |
| 570.00 | 952.03 |
| 400.00 | 717.00 |
| 610.00 | 933.76 |
| 730.00 | 1118.60 |
| 790.00 | 1236.60 |
| 820.00 | 1279.50 |
| 800.00 | 1244.40 |
| 700.00 | 1133.90 |
| 520.00 | 955.29 |
| 320.00 | 720.87 |
| 600.00 | 935.24 |
| 770.00 | 1120.10 |
| 800.00 | 1238.00 |
| 820.00 | 1281.20 |
| 800.00 | 1246.50 |
| 640.00 | 1136.50 |
| 500.00 | 958.45 |
| 350.00 | 724.64 |
| 300.00 | 936.70 |
| 630.00 | 1121.40 |
| 700.00 | 1239.50 |
| 800.00 | 1282.90 |
| 780.00 | 1248.60 |
| 760.00 | 1139.00 |
| 610.00 | 961.53 |
| 450.00 | 728.32 |
| 617.00 | 938.13 |
| 740.00 | 1122.80 |
| 820.00 | 1240.90 |
| 830.00 | 1284.50 |
| 770.00 | 1250.50 |
| 660.00 | 1141.40 |
| 542.00 | 964.50 |
| 330.00 | 731.89 |
| 560.00 | 940.94 |
| 740.00 | 1125.30 |
| 780.00 | 1243.50 |
| 785.00 | 1287.50 |
| 735.00 | 1254.20 |
| 640.00 | 1146.00 |
| 500.00 | 970.18 |

| | |
|---|---|
| 360.00 | 738.74 |
| 632.00 | 950.15 |
| 745.00 | 1133.40 |
| 805.00 | 1251.50 |
| 830.00 | 1296.40 |
| 750.00 | 1265.00 |
| 620.00 | 1159.50 |
| 450.00 | 987.14 |
| 360.00 | 759.57 |
| 600.00 | 951.40 |
| 710.00 | 1134.40 |
| 780.00 | 1252.40 |
| 795.00 | 1297.40 |
| 775.00 | 1266.30 |
| 610.00 | 1161.20 |
| 475.00 | 989.20 |
| 300.00 | 762.15 |
| 620.00 | 953.87 |
| 780.00 | 1136.40 |
| 790.00 | 1254.30 |
| 800.00 | 1299.40 |
| 750.00 | 1268.60 |
| 600.00 | 1164.20 |
| 500.00 | 993.07 |
| 350.00 | 767.01 |
| 480.00 | 959.84 |
| 670.00 | 1141.20 |
| 830.00 | 1258.40 |
| 930.00 | 1303.60 |
| 900.00 | 1273.60 |
| 890.00 | 1170.40 |
| 800.00 | 1001.20 |
| 580.00 | 777.49 |
| 400.00 | 961.01 |
| 680.00 | 1142.10 |
| 830.00 | 1259.10 |
| 930.00 | 1304.30 |
| 900.00 | 1274.40 |
| 880.00 | 1171.50 |
| 850.00 | 1002.60 |
| 600.00 | 779.30 |
| 635.00 | 963.32 |
| 780.00 | 1143.80 |
| 855.00 | 1260.50 |
| 925.00 | 1305.60 |
| 860.00 | 1275.90 |
| 730.00 | 1173.40 |
| 578.00 | 1005.20 |
| 402.00 | 782.65 |
| 650.00 | 964.46 |
| 790.00 | 1144.70 |
| 860.00 | 1261.20 |
| 920.00 | 1306.20 |
| 850.00 | 1276.50 |
| 720.00 | 1174.30 |
| 580.00 | 1006.30 |
| 400.00 | 784.19 |
| 630.00 | 966.73 |
| 770.00 | 1146.30 |
| 850.00 | 1262.50 |
| 900.00 | 1307.30 |
| 825.00 | 1277.80 |

| | |
|---|---|
| 700.00 | 1175.80 |
| 560.00 | 1008.40 |
| 370.00 | 787.01 |
| 617.00 | 967.85 |
| 740.00 | 1147.20 |
| 820.00 | 1263.10 |
| 830.00 | 1307.90 |
| 770.00 | 1278.30 |
| 660.00 | 1176.50 |
| 542.00 | 1009.40 |

# APPENDIX (I)

## The simulation program for different system configurations

### I.1. Two stages:

The simulation program for two stages (Two flashing chambers with one FPC) is built as the same considerations and assumptions as presented in one stage (Single flash chamber with one FPC). Figure (I.1) shows a schematic diagram for two stages.



Figure (I.1) The schematic diagram for two stages

The list of the solved equations below is rearranged and put in the matrixes. The coefficients, desired variables and constants are put in the coefficients matrix, desired variable matrix and constant variable matrix respectively. By using the Mat-Lab program V.7.0.1, the desired variables matrix=coefficients matrix\constants matrix.

$F_S$=Feed flow rate           (I.1)

$F_2 - F_S = 0$           (I.2)

$F_3 - F_2 = 0$           (I.3)

$F_4 - F_3 = 0$           (I.4)

$B_o - F_4 = 0$           (I.5)

$B_o - B_1 - D_1 = 0$           (I.6)

$B_1 - B_2 - D_2 = 0$           (I.7)

$T_{f2}$=Inlet feed water temperature           (I.8)

$T_{f3} - E2T_{d2} - (1-E2)T_{f2} = 0$           (I.9)

$T_{b2} - T_{d2} = NEA2 + BPR2$           (I.10)

$B_1(Cp_{b1}T_{b1} - H_{v2}) + B_2(H_{v2} - Cp_{b2}T_{b2}) = 0$           (I.11)

$T_{f4} - ET_{d1} - (1-E)T_{f3} = 0$           (I.12)

$T_{b1} - T_{d1} = NEA + BPR$           (I.13)

$B_o(Cp_{bo}T_{bo} - H_{v1}) + B_1(H_{v1} - Cp_{b1}T_{b1}) = 0$           (I.14)

$$F_2(Cp_{f2}*T_{f2})+B_1(Cp_{b1}*T_{b1})-B_2(Cp_{b2}*T_{b2})-(F_3Cp_{f3})*T_{f3}-D_2(Cp_{d2}*T_{d2})=0 \qquad (I.15)$$

$$F_3*Cp_{f3}*T_{f3}+B_o(Cp_{bo}*T_{bo})-B_1(Cp_{b1}*T_{b1})-(F_4Cp_{f4})*T_{f4}-D_1(Cp_{d1}*T_{d1})=0 \qquad (I.16)$$

$$B_o*Cp_{bo}*T_{bo}-F_4*Cp_{f4}*T_{f4}=Is*Ac \qquad (I.17)$$

Figure (I.2) shows the schematic diagram of different matrixes.

**Desired variables matrix** (column vector):

$F_1$, $F_2$, $F_3$, $F_4$, $B_o$, $B_1$, $D_1$, $B_2$, $D_2$, $T_{f2}$, $T_{f3}$, $T_{d2}$, $T_{b2}$, $T_{f4}$, $T_{d1}$, $T_{b1}$, $TBT$

**Coefficients matrix** (17×17):

| 1 | 0 | 0 | 0 | 0 | 0 | 0 | 0 | 0 | 0 | 0 | 0 | 0 | 0 | 0 | 0 | 0 |
|---|---|---|---|---|---|---|---|---|---|---|---|---|---|---|---|---|
| -1 | 1 | 0 | 0 | 0 | 0 | 0 | 0 | 0 | 0 | 0 | 0 | 0 | 0 | 0 | 0 | 0 |
| 0 | -1 | 1 | 0 | 0 | 0 | 0 | 0 | 0 | 0 | 0 | 0 | 0 | 0 | 0 | 0 | 0 |
| 0 | 0 | -1 | 1 | 0 | 0 | 0 | 0 | 0 | 0 | 0 | 0 | 0 | 0 | 0 | 0 | 0 |
| 0 | 0 | 0 | -1 | 1 | 0 | 0 | 0 | 0 | 0 | 0 | 0 | 0 | 0 | 0 | 0 | 0 |
| 0 | 0 | 0 | 0 | 1 | -1 | -1 | 0 | 0 | 0 | 0 | 0 | 0 | 0 | 0 | 0 | 0 |
| 0 | 0 | 0 | 0 | 0 | 1 | 0 | -1 | -1 | 0 | 0 | 0 | 0 | 0 | 0 | 0 | 0 |
| 0 | 0 | 0 | 0 | 0 | 0 | 0 | 0 | 0 | 1 | 0 | 0 | 0 | 0 | 0 | 0 | 0 |
| 0 | 0 | 0 | 0 | 0 | 0 | 0 | 0 | 0 | $-(1-E2)$ | 1 | $-E2$ | 0 | 0 | 0 | 0 | 0 |
| 0 | 0 | 0 | 0 | 0 | 0 | 0 | 0 | 0 | 0 | 0 | -1 | 1 | 0 | 0 | 0 | 0 |
| 0 | 0 | 0 | 0 | 0 | $\frac{H_{vr}}{Cp_{b4}T_M}$ | 0 | $\frac{Cp_{b4}}{T_{br}H_{v2}}$ | 0 | 0 | 0 | 0 | 0 | 0 | 0 | 0 | 0 |
| 0 | 0 | 0 | 0 | 0 | 0 | 0 | 0 | 0 | 0 | $-(1-E)$ | 0 | 0 | 1 | $-E$ | 0 | 0 |
| 0 | 0 | 0 | 0 | 0 | 0 | 0 | 0 | 0 | 0 | 0 | 0 | 0 | 0 | -1 | 1 | 0 |
| 0 | 0 | 0 | 0 | $\frac{H_{v1}-}{Cp_{b1}T_{b1}}$ | $\frac{Cp_{br}}{T_{br}H_{v1}}$ | 0 | 0 | 0 | 0 | 0 | 0 | 0 | 0 | 0 | 0 | 0 |
| 0 | $\frac{Cp_{f2}}{T_{f2}}$ | 0 | 0 | 0 | $\frac{Cp_{b4}}{T_M}$ | 0 | $\frac{Cp_{b2}}{T_{b2}}$ | $\frac{-F_S}{Cp_{F5}}$ | 0 | $\frac{Cp_{d1}}{T_{d1}}$ | 0 | 0 | 0 | 0 | 0 | 0 |
| 0 | 0 | 0 | 0 | $\frac{Cp_{bo}}{T_{bo}}$ | $\frac{Cp_{b4}}{T_M}$ | $\frac{Cp_{b1}}{T_{d1}}$ | 0 | 0 | 0 | $\frac{F_S}{Cp_{F5}}$ | 0 | 0 | $\frac{-F_4}{Cp_{b4}}$ | 0 | 0 | 0 |
| 0 | 0 | 0 | 0 | 0 | 0 | 0 | 0 | 0 | 0 | 0 | 0 | 0 | $\frac{-F_4}{Cp_{b4}}$ | 0 | 0 | $\frac{B_o}{Cp_{bo}}$ |

**Constants matrix** (column vector):

$F_S$, 0, 0, 0, 0, 0, 0, $T_{f2}$, 0, $NEA2+BPR2$, 0, 0, $NEA+BPR$, 0, 0, 0, $Is*Ac-Q_{loss}$

Figure (I.2) The schematic diagram of different matrixes for two stages: Desired variables matrix, Coefficients matrix and Constants matrix

157

## I.2. Three stages:

The simulation program for three stages (Three flashing chambers with one FPC) is built as the same considerations and assumptions as presented in one stage (Single flash chamber with one FPC). Figure (I.3) shows a schematic diagram for three stages.
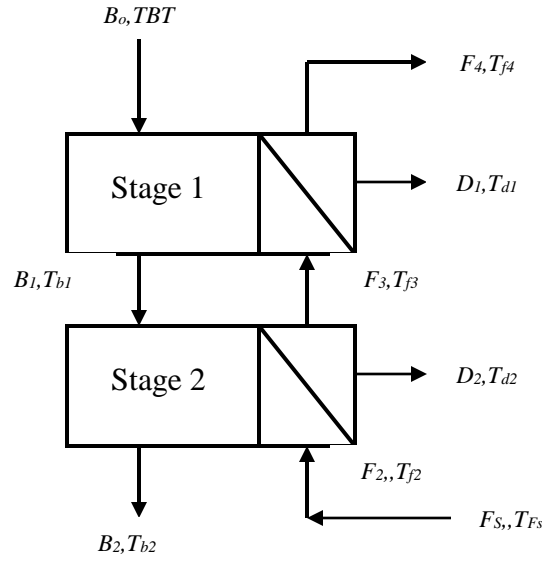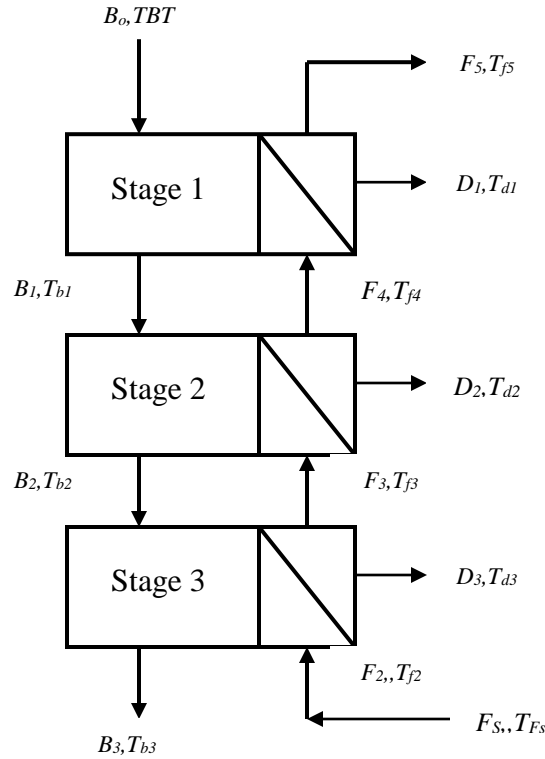


Figure (I.3) The schematic diagram for three stages

The list of the solved equations below is rearranged and put in the matrixes. The coefficients, desired variables and constants are put in the coefficients matrix, desired variable matrix and constant variable matrix respectively. By using the Mat-Lab program V.7.0.1, the desired variables matrix=coefficients matrix\constants matrix.

$F_S$=Feed water flow rate  (I.18)

$F_2 - F_S = 0$  (I.19)

$F_3 - F_2 = 0$  (I.20)

$F_4 - F_3 = 0$  (I.21)

$F_5 - F_4 = 0$  (I.22)

$B_o - F_5 = 0$  (I.23)

$B_o - B_1 - D_1 = 0$  (I.24)

$B_1 - B_2 - D_2 = 0$  (I.25)

$B_2 - B_3 - D_3 = 0$  (I.26)

$T_{f3} - E3 * T_{d3} - (1 - E3)T_{f2} = 0$  (I.27)

$T_{b3} - T_{d3} = NEA3 + BPR3$  (I.28)

$B_2(Cp_{b2}T_{b2} - H_{v3}) + B_3(H_{v3} - Cpb3T_{b3}) = 0$  (I.29)

$T_{f4}-E2*T_{d2}-(1-E2)T_{f3}=0$         (I.30)

$T_{b2}-T_{d2}=NEA2+NEA2$         (I.31)

$B_1(Cp_{b1}T_{b1}-H_{v2})+B_2(H_{v2}-Cpb2T_{b2})=0$         (I.31)

$T_{f5}-E*T_{d1}-(1-E)T_{f4}=0$         (I.32)

$T_{b1}-T_{d1}=NEA+NEA$         (I.33)

$B_o(Cp_{bo}T_{bo}-H_{v1})+B_1(H_{v1}-Cpb1T_{b1})=0$         (I.34)

$F_2(Cp_{f2}*T_{f2})+B_2(Cp_{b2}*T_{b2})-B_3(Cp_{b3}*T_{b3})-(F_3Cp_{f3})*T_{f3}-D_3(Cp_{d3}*T_{d3})=0$         (I.35)

$(F_3Cp_{f3})*T_{f3}+B_1(Cp_{b1}*T_{b1})-B_2(Cp_{b2}*T_{b2})-(F_4Cp_{f4})*T_{f4}-D_2(Cp_{d2}*T_{d2})=0$         (I.36)

$(F_4Cp_{f4})*T_{f4}+(B_o*Cp_{bo})*T_{bo}-B_1(Cp_{b1}*T_{b1})-(F_5Cp_{f5})*T_{f5}-D_1(Cp_{d1}*T_{d1})=0$         (I.37)

$T_{f2}=$ Inlet feed water temperature         (I.38)

$B_o*Cp_{bo}*T_{bo}-F_5*Cp_{f5}*T_{f5}=Is*Ac-Q_{loss}$         (I.39)

Figure (I.4) shows the schematic diagram of the different matrixes (desired variables matrix, coefficients matrix and constants matrix) for three stages.
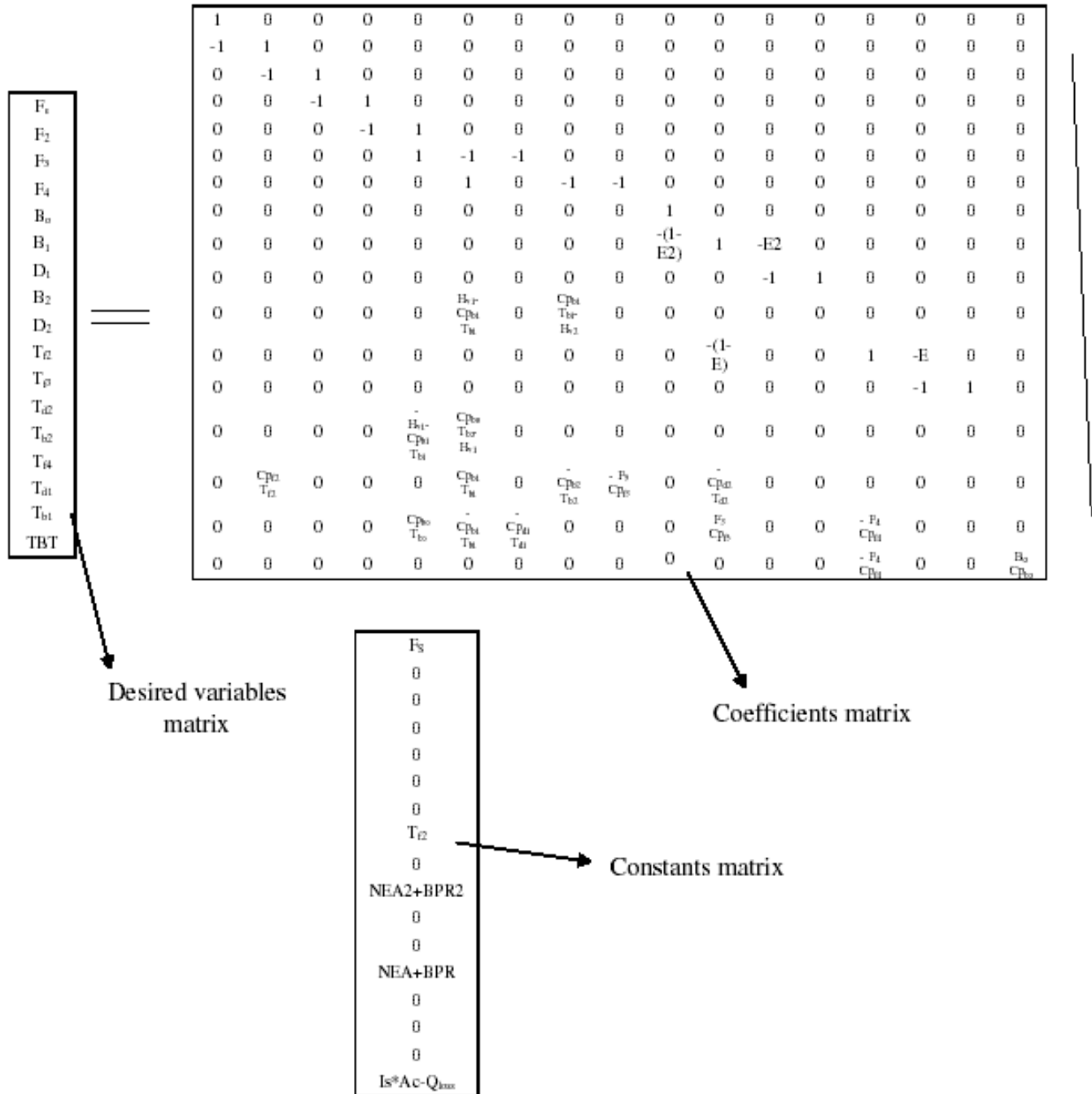
Desired variables matrix

Coefficient matrix

Constants matrix

Figure (I.4) The schematic diagram of different matrixes: Desired variables matrix, Coefficients matrix and Constants matrix

## I.3. Configuration #2:

The configuration description is introduced in Chapters 2 and 5. Figure (I.5) shows the schematic diagram of configuration # 2. Figure (I.6) shows the schematic diagram of the different matrixes (desired variables matrix, coefficients matrix and constants matrix) for configuration # 2.



Figure (I.5) The schematic diagram of configuration # 2

| | |
|---|---|
| $F_S$=Feed flow rate | (I.40) |
| $F_4-F_3=0$ | (I.41) |
| $B_o-F_4=0$ | (I.42) |
| $B_o-B_1-D_1=0$ | (I.43) |
| $B_1-B_2-D_2=0$ | (I.44) |
| $T_{f2}$=Inlet feed water temperature | (I.45) |
| $T_{f3}-E2T_{d2}-(1-E2)T_{f2}=0$ | (I.46) |
| $T_{b2}-T_{d2}=NEA2+BPR2$ | (I.47) |
| $B_1(Cp_{b1}T_{b1}-H_{v2})+B_2(H_{v2}-Cp_{b2}T_{b2})=0$ | (I.48) |
| $T_{f4}-ET_{d1}-(1-E)T_{f3}=0$ | (I.49) |
| $T_{b1}-T_{d1}=NEA+BPR$ | (I.50) |
| $B_o(Cp_{bo}T_{bo}-H_{v1})+B_1(H_{v1}-Cp_{b1}T_{b1})=0$ | (I.51) |
| $F_2(Cp_{f2}*T_{f2})+B_1(Cp_{b1}*T_{b1})-B_2(Cp_{b2}*T_{b2})-(F_3Cp_{f3})*T_{f3}-D_2(Cp_{d2}*T_{d2})=0$ | (I.52) |
| $F_3*Cp_{f3}*T_{f3}+B_o(Cp_{bo}*T_{bo})-B_1(Cp_{b1}*T_{b1})-(F_4Cp_{f4})*T_{f4}-D_1(Cp_{d1}*T_{d1})=0$ | (I.53) |
| $B_o*Cp_{bo}*T_{bo}-F_4*Cp_{f4}*T_{f4}=Is*Ac$ | (I.54) |
| Tb1-Tb2=0 | (I.55) |
| Tb1-Tb3=0 | (I.56) |
| B2-(1-SPL)*B1=0 | (I.57) |
| B3-SPL*B1=0 | (I.58) |

161

| Tf4 |
|---|
| Tb1 |
| Tb2 |
| Tb3 |
| Td1 |
| Tbo |
| Tf3 |
| Tfs |
| Fs |
| F3 |
| F4 |
| Bo |
| B1 |
| B2 |
| B3 |
| D1 |

=

| | | | | | | | | | | | | | | | |
|---|---|---|---|---|---|---|---|---|---|---|---|---|---|---|---|
| 1 | 0 | 0 | 0 | -1 | 0 | -2.15e-08 | 0 | 0 | 0 | 0 | 0 | 0 | 0 | 0 | 0 |
| 0 | 1 | 0 | 0 | -1 | 0 | 0 | 0 | 0 | 0 | 0 | 0 | 0 | 0 | 0 | 0 |
| 0 | 0 | 0 | 0 | 0 | 0 | 0 | 0 | 0 | 0 | 0 | 1 | -1 | 0 | 0 | -1 |
| -0.109 | 0 | 0 | 0 | 0 | 0 | 0.10982 | 0 | 0 | 0 | 0 | 210.75 | -177.2 | 0 | 0 | -170 |
| 0 | 0 | 0 | 0 | 0 | 0 | 0 | 0 | 0 | 0 | 0 | -2381 | 2415.2 | 0 | 0 | 0 |
| 0 | 0 | 0 | 0 | 0 | 0 | 0 | 0 | 1 | 0 | 0 | 0 | 0 | 0 | 0 | 0 |
| 0 | 0 | 0 | 0 | 0 | 0 | 0 | 0 | -1 | 1 | 0 | 0 | 0 | 0 | -1 | 0 |
| 0 | 0 | 0 | 0 | 0 | 0 | 0 | 0 | 0 | -1 | 1 | 0 | 0 | 0 | 0 | 0 |
| 0 | 0 | 0 | 0 | 0 | 0 | 0 | 0 | 0 | 0 | -1 | 1 | 0 | 0 | 0 | 0 |
| 0 | 0 | 0 | 0 | 0 | 0 | 0 | 1 | 0 | 0 | 0 | 0 | 0 | 0 | 0 | 0 |
| -0.1097 | 0 | 0 | 0 | 0 | 0.10977 | 0 | 0 | 0 | 0 | 0 | 0 | 0 | 0 | 0 | 0 |
| 0 | 0 | 0 | 0 | 0 | 0 | 0.10982 | -0.07 | 0 | 0 | 0 | 0 | 0 | 0 | -177.1 | 0 |
| 0 | 1 | -1 | 0 | 0 | 0 | 0 | 0 | 0 | 0 | 0 | 0 | 0 | 0 | 0 | 0 |
| 0 | 1 | 0 | -1 | 0 | 0 | 0 | 0 | 0 | 0 | 0 | 0 | 0 | 0 | 0 | 0 |
| 0 | 0 | 0 | 0 | 0 | 0 | 0 | 0 | 0 | 0 | 0 | 0 | -0.7 | 1 | 0 | 0 |
| 0 | 0 | 0 | 0 | 0 | 0 | 0 | 0 | 0 | 0 | 0 | 0 | -0.3 | 0 | 1 | 0 |

| |
|---|
| 0 |
| 1.5535 |
| 0 |
| 0 |
| 0 |
| 0.0185 |
| 0 |
| 0 |
| 0 |
| 28.75 |
| 1.0517 |
| 0 |
| 0 |
| 0 |
| 0 |
| 0 |

Desired variables matrix

Coefficients matrix

Constants matrix

Figure (I.6) shows the schematic diagram of the different matrixes (desired variables matrix, coefficients matrix and constants matrix) for configuration # 2
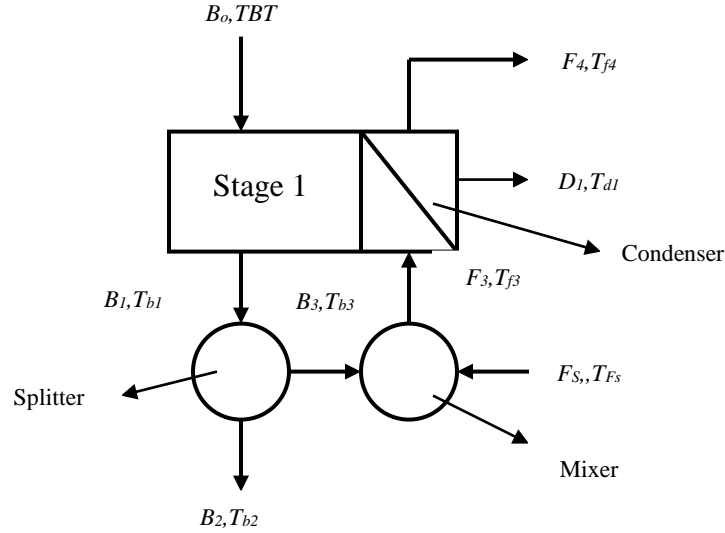
## I.4. Configuration #3:

The configuration description is introduced in Chapters 2 and 5. Figure (I.7) shows the schematic diagram of configuration # 3. Figure (I.8) shows the schematic diagram of the different matrixes (desired variables matrix, coefficients matrix and constants matrix) for configuration # 3.
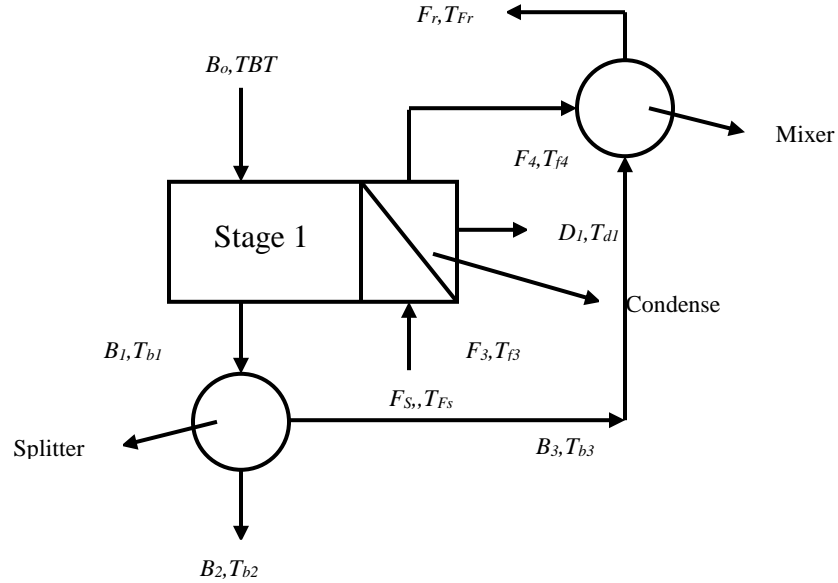


Figure (I.7) The schematic diagram of configuration # 3

| | |
|---|---|
| $F_S$=Feed flow rate | (I.59) |
| $F_4-F_3=0$ | (I.60) |
| $Fr-F4-B3=0$ | (I.61) |
| $B_o-F_r=0$ | (I.62) |
| $B_o-B_1-D_1=0$ | (I.63) |
| $B_1-B_2-D_2=0$ | (I.64) |
| $T_{f2}$=Inlet feed water temperature | (I.65) |
| $T_{f3}-E2T_{d2}-(1-E2)T_{f2}=0$ | (I.66) |
| $T_{b2}-T_{d2}=NEA2+BPR2$ | (I.67) |
| $B_1(Cp_{b1}T_{b1}-H_{v2})+B_2(H_{v2}-Cp_{b2}T_{b2})=0$ | (I.68) |
| $T_{f4}-ET_{d1}-(1-E)T_{f3}=0$ | (I.69) |
| $T_{b1}-T_{d1}=NEA+BPR$ | (I.70) |
| $B_o(Cp_{bo}T_{bo}-H_{v1})+B_1(H_{v1}-Cp_{b1}T_{b1})=0$ | (I.71) |
| $F_2(Cp_{f2}*T_{f2})+B_1(Cp_{b1}*T_{b1})-B_2(Cp_{b2}*T_{b2})-(F_3Cp_{f3})*T_{f3}-D_2(Cp_{d2}*T_{d2})=0$ | (I.72) |
| $F_3*Cp_{f3}*T_{f3}+B_o(Cp_{bo}*T_{bo})-B_1(Cp_{b1}*T_{b1})-(F_4Cp_{f4})*T_{f4}-D_1(Cp_{d1}*T_{d1})=0$ | (I.73) |
| $Bo*Cpbo*Tbo-Fr*Cpfr*Tfr=Is*Ac-Qloss$ | (I.74) |
| $Fr*Cpfr*Tfr-B3*Cpb3*Tb3-F4*Cpf4*Tf4=0$ | (I.75) |
| $Tb1-Tb2=0$ | (I.76) |
| $Tb1-Tb3=0$ | (I.77) |
| $B2-(1-SPL)*B1=0$ | (I.78) |
| $B3-SPL*B1=0$ | (I.79) |

Desired variables matrix (column vector):

| Variable |
|----------|
| Tf4 |
| Tb1 |
| Tb2 |
| Th3 |
| Td1 |
| Tbo |
| Tf3 |
| Tfr |
| Fs |
| F3 |
| F4 |
| Fr |
| Bo |
| B1 |
| B2 |
| B3 |
| D1 |

$$=$$

Coefficients matrix:

| | | | | | | | | | | | | | | | | |
|---|---|---|---|---|---|---|---|---|---|---|---|---|---|---|---|---|
| 1 | 0 | 0 | 0 | -1 | 0 | -3.028e-01 | 0 | 0 | 0 | 0 | 0 | 0 | 0 | 0 | 0 | 0 |
| 0 | 1 | 0 | 0 | -1 | 0 | 0 | 0 | 0 | 0 | 0 | 0 | 0 | 0 | 0 | 0 | 0 |
| 0 | 0 | 0 | 0 | 0 | 0 | 0 | 0 | 0 | 0 | 0 | 0 | 1 | -1 | 0 | 0 | -1 |
| -0.077299 | 0 | 0 | 0 | 0 | 0 | 0.07736 | 0 | 0 | 0 | 0 | 0 | 212.38 | -177.04 | 0 | 0 | -170.55 |
| 0 | 0 | 0 | 0 | 0 | 0 | 0 | 0 | 0 | 0 | 0 | 0 | -2384. | 2420.2 | 0 | 0 | 0 |
| 0 | 0 | 0 | 0 | 0 | 0 | 0 | 0 | 1 | 0 | 0 | 0 | 0 | 0 | 0 | 0 | 0 |
| 0 | 0 | 0 | 0 | 0 | 0 | 0 | 0 | -1 | 1 | 0 | 0 | 0 | 0 | 0 | 0 | 0 |
| 0 | 0 | 0 | 0 | 0 | 0 | 0 | 0 | 0 | -1 | 1 | 0 | 0 | 0 | 0 | 0 | 0 |
| 0 | 0 | 0 | 0 | 0 | 0 | 0 | 0 | 0 | 0 | 0 | -1 | 1 | 0 | 0 | 0 | 0 |
| 0 | 0 | 0 | 0 | 0 | 0 | 1 | 0 | 0 | 0 | 0 | 0 | 0 | 0 | 0 | 0 | 0 |
| 0 | 0 | 0 | 0 | 0 | 0.10974 | 0 | -0.109 | 0 | 0 | 0 | 0 | 0 | 0 | 0 | 0 | 0 |
| -0.07729 | 0 | 0 | 0 | 0 | 0 | 0 | 0.1094 | 0 | 0 | 0 | 0 | 0 | 0 | 0 | -177 | 0 |
| 0 | 1 | -1 | 0 | 0 | 0 | 0 | 0 | 0 | 0 | 0 | 0 | 0 | 0 | 0 | 0 | 0 |
| 0 | 1 | 0 | -1 | 0 | 0 | 0 | 0 | 0 | 0 | 0 | 0 | 0 | 0 | 0 | 0 | 0 |
| 0 | 0 | 0 | 0 | 0 | 0 | 0 | 0 | 0 | 0 | 0 | 0 | 0 | -0.7 | 1 | 0 | 0 |
| 0 | 0 | 0 | 0 | 0 | 0 | 0 | 0 | 0 | 0 | 0 | 0 | 0 | -0.3 | 0 | 1 | 0 |
| 0 | 0 | 0 | 0 | 0 | 0 | 0 | 0 | 0 | 0 | -1 | 1 | 0 | 0 | 0 | -1 | 0 |

Constants matrix (column vector):

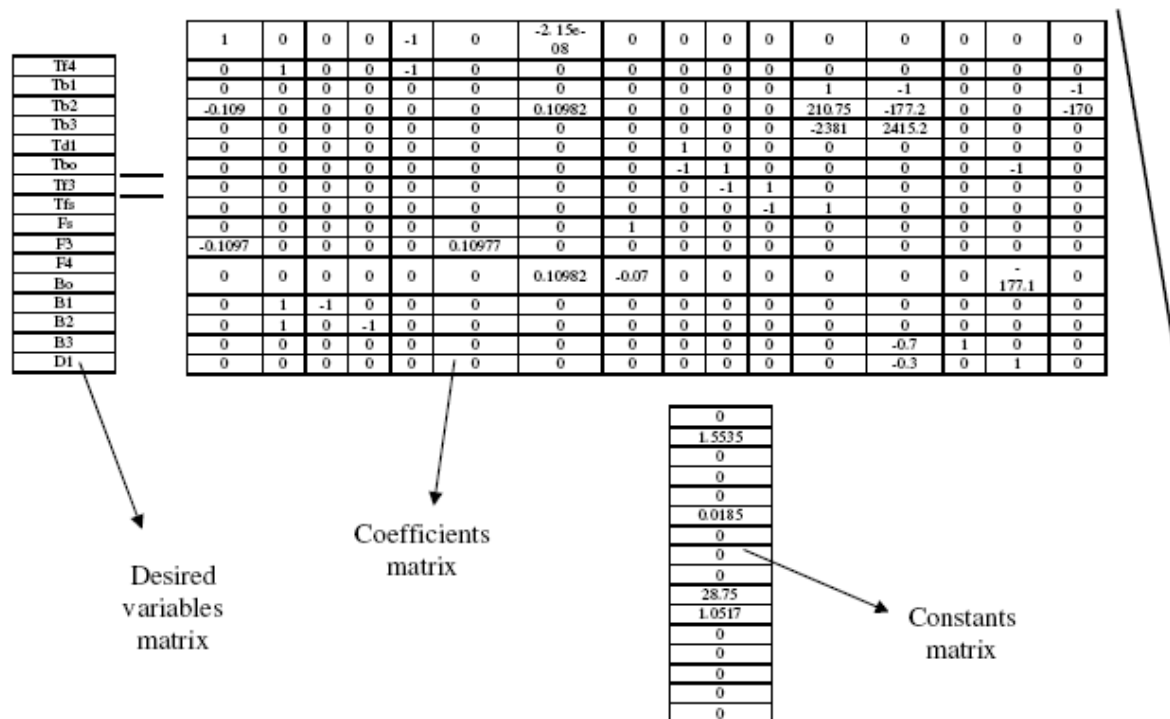| Value |
|-------|
| 0 |
| 1.5545 |
| 0 |
| 0 |
| 0 |
| 0.0185 |
| 0 |
| 0 |
| 0 |
| 28.75 |
| 1.0483 |
| 0 |
| 0 |
| 0 |
| 0 |
| 0 |
| 0 |

Figure (I.8) shows the schematic diagram of the different matrixes (desired variables matrix, coefficients matrix and constants matrix) for configuration # 3
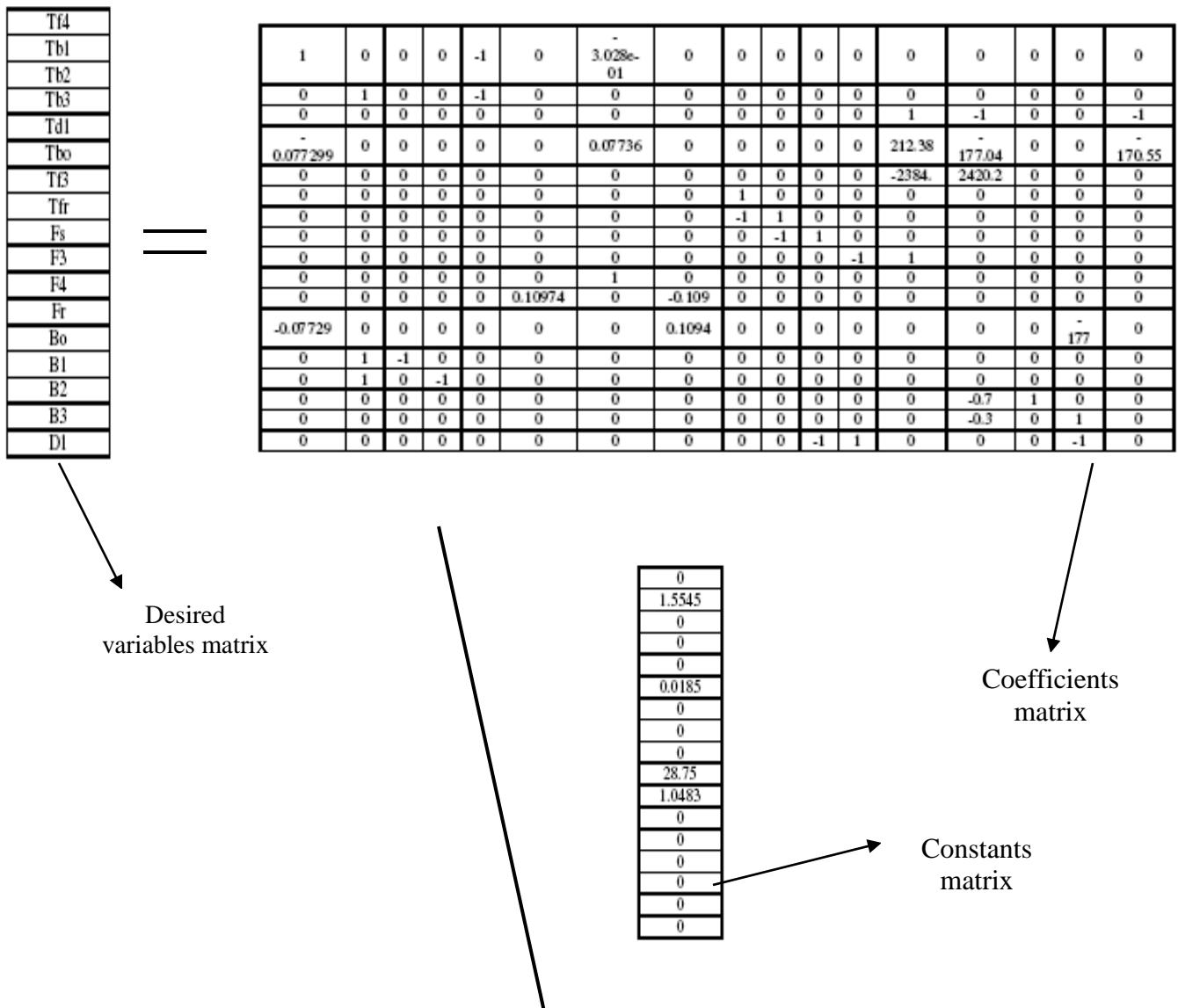
جامعة قناه السويس
كلية هندسة البترول والتعدين
قسم العلوم الهندســية

# دراسـة تحليـة الميـاه عن طريق الطـاقة الشمسية باستخدام عمليـة الوميـض متعدد المـراحل

**رسالة مقدمة من المهندس:**
محمد عبدالوهاب شرف الدين

للحصول على درجه الماجستير في هندسة الطاقة

**تحت اشراف**

**أ.د. منصور عوض محمد**       **د. سيد عثمان الحليبي**
قسم الطاقة الشمسية ـ المركز القومي للبحوث القاهرة       رئيس قسم العلوم الهندسية ـ كلية هندسة البترول
والتعدين جامعة قناة السويس

**د. أحمد صفوت محمد طه**
مدرس بقسم العلوم الهندسية ــ كلية هندسة البترول و التعدين
جامعة قناة السويس

2007